THE UNIVERSITY *of* EDINBURGH

Structure-dependent Quantum Electrodynamics in Heavy Meson Physics

Matthew Rowe

Doctor of Philosophy
The University of Edinburgh
August 2024

Abstract

The presence of electromagnetism in heavy meson systems cannot be neglected in the era of precision physics. While Quantum Electrodynamic (QED) effects are generally smaller than strong force contributions, factorisation properties are lost as photons may couple to light charged leptons. This can lead to mass-regulated collinear logarithms which, if left uncancelled, may lead to percent level corrections to decay rates.

In this thesis we explore QED effects in two settings. The main work of this thesis is a dispersive sum rule calculation of the leptonic B decay $B^- \to l^- \bar{\nu}(\gamma)$ to $\mathcal{O}(\alpha_{\text{QED}})$ in a new manifestly gauge-invariant framework. Particular attention is paid to the non-cancellation of collinear-type logarithms and structure-dependent effects beyond scalar QED. Virtual structure-dependent corrections are found to be $+4.6(6)\%$ and $+2.9(2)\%$ in the muon and tau channels respectively. Real structure-dependence lifts the helicity suppression found in the non-radiative decay and dominates in the electron and muon case.

The second setting in which QED effects are important is the mass difference between charged and neutral pseudoscalar mesons. While this is a well-studied problem we attack it for the first time using a double dispersion relation calculating the QED and linear quark mass shifts in a model independent way. This is a leading order 'proof-of-principle' calculation which we apply to the B, D and K systems giving good agreement with experiment albeit with large uncertainties.

Lay Summary

17 particles. Is that too many or not enough? That, depending on how you count them, is the number of fundamental particles that make up everything in the universe. At least as far as we know. How these particles interact with each other and combine to form larger particles has broadly been understood since the 1970s. This mathematical description is known as the Standard Model (SM) of particle physics and it has been extensively tested with increasingly precise experiments over the last 50 years.

Atoms are not fundamental: they are made up of protons, neutrons and electrons. Electrons *are* fundamental - they are part of a class of six matter particles called leptons. Protons and neutrons however are made of smaller fundamental particles known as quarks. These fundamental quarks and leptons interact with each other by exchanging force-carrying particles known as bosons. Light, for example, is made up of massless bosons called photons that carry electromagnetic force. How photons interact with quarks and leptons is described mathematically through a field theory known as Quantum Electrodynamics (QED).

This thesis concerns QED in heavy meson systems. Mesons are composite particles of a quark and an antiquark that are strongly bound together. Arguably the most exciting are the B-mesons, ones that contain a heavy b-type quark. Lots of modern physics research involves looking for new (non-SM) physics and so experiments such as the Large Hadron Collider at CERN are searching for tiny deviations from SM predictions. Correspondingly this requires extremely precise theoretical predictions of, for example, how light interacts with mesons. By treating mesons as point-like particles one can make some progress but really internally mesons are very complicated objects. Going beyond this point-like approximation, probing *structure-dependent* QED is the aim of this work.

Perhaps in time we will discover new physics, perhaps we won't. Maybe 17 is correct, maybe it's turtles all the way down.

Declaration

I declare that this thesis was composed by myself, that the work contained herein is my own except where explicitly stated otherwise in the text, and that this work has not been submitted for any other degree or professional qualification except as specified.

Parts of this work have been published in [1, 2].

(*Matthew Rowe, August 2024*)

Acknowledgements

There are innumerable people who have helped and supported me over both the last few years and in life in general who sadly I cannot thank individually. To those unnamed but not unappreciated: *thank you*.

On the academic side I must firstly thank my supervisor Roman Zwicky for his wisdom. In particular for his ability to know which path to take when the road ahead is unclear. I am also indebted to Saad Nabeebaccus for his helping hand and advice in the early stages of this project. Lastly, it has been a pleasure sharing 5301, initially with Toby and André, then with Emmet and Niamh M and finally ending with Sam, Maegan and Amedeo.

My time in Edinburgh has been shaped for the better by my wonderful friends: Sophie, Dan, Erin, Lia, Hazel, Jenni, Pippa and Linda, to name but a few. Special mentions go to Joe, my PhD companion, who has been there through rain or shine, or more accurately thin clag and thick clag, and especially to Niamh for her constant support and kindness. The last three years would have been considerably less fun without you.

And finally to my family. To Katherine, for putting up with me, to my grandad Hanson, for his quiet example, but most importantly to my parents for their encouragement and love. It is impossible to adequately express my gratitude for two and a half decades of sacrifice. Certainly I would not be in this position without you.

Contents

List of Figures

List of Tables

Chapter 1

Introduction

Much of the difficulty of theoretical particle physics lies in the disconnect between the composite bound states we observe and the quarks and gluons that make them up. The description of the dynamics and interactions of fundamental fermions in terms of a gauge field theory is one of the triumphs of twentieth century physics. Nevertheless there remains considerable difficulty in understanding the behaviour of hadrons due to their strongly coupled nature.

These difficulties are intertwined with the development of the Standard Model (SM), our current best theory of nature. By the early 1960s a multitude of particle states of varying spins and masses had been discovered, some fast decaying, others strangely slowly. It was not until Gell-Mann's 'Eightfold Way' in 1961 [3, 4] that some semblance of classification appeared. This was based on a flavour $\mathrm{SU}(3)_{\mathrm{F}}$ symmetry and paved the way for the development of the quark model [5–7].

Still however, descriptions in terms of a Quantum Field Theory (QFT) were limited. There was success in a quantum theory of electromagnetism, Quantum Electrodynamics (QED), pioneered by Schwinger, Dyson, Tomonaga and Feynman [8–14] however acceptance of the renormalisation procedure was tentative. Its utility lay in perturbative expansions in its small coupling, the fine-structure constant $\alpha = e^2/4\pi \approx 1/137$. Conversely the non-perturbative nature of the strong force meant that considerable effort in this era went into developing an alternative to QFT known as the S-matrix program [15–17]. The S-matrix program was based on dispersion relations and invoked fundamental properties such as unitarity, analyticity and causality. Current algebras based on symmetry were constructed and analyticity in angular momentum led to Regge theory [18].

Our current theory of the strong force, Quantum Chromodynamics (QCD) was finally constructed in the early 1970s based on $\mathrm{SU}(3)_{\mathrm{C}}$ colour symmetry. Crucially Gross, Wilczek and Politzer [19, 20] demonstrated the property of asymptotic freedom: that the strong coupling becomes weaker at high energies. This explained the experimentally observed Bjorken scaling [21] and with the discovery of the J/ψ led to the full acceptance of the quark model. Formally, QCD is a Yang-Mills theory [22] based on the principle of local gauge invariance. This idea pervades the rest of the SM with the electroweak sector being based on the gauge symmetries of weak isospin and weak hypercharge, $\mathrm{SU}(2)_{\mathrm{L}} \times \mathrm{U}(1)_{\mathrm{Y}}$. The final ingredient is spontaneous symmetry breaking that gives rise to fermion and weak boson masses via the Higgs mechanism [23–25]. Electromagnetism arises as a linear combination of the electroweak neutral bosons.

In summary, the full Standard Model of particle physics is a quantum field theory based on the symmetry group

$$\mathrm{SU}(3)_{\mathrm{C}} \times \mathrm{SU}(2)_{\mathrm{L}} \times \mathrm{U}(1)_{\mathrm{Y}} \,. \tag{1.1}$$

It has 25 free parameters: 12 fermion masses, 3 coupling constants, 2 Higgs parameters and 8 mixing angles. The large amount of parameters perhaps indicates that the SM is the low-energy limit of a more fundamental theory. Such a theory would hopefully incorporate gravity and cure some of the imperfections in the SM such as non-zero neutrino masses [26]. That being said, the SM has been extensively tested over the last 50 years with little sign of trouble. The current focus of experimental particle physics is in extremely precise measurements looking for tiny deviations that might signal physics beyond the SM.

This thesis goes a small way to aid that effort. Theoretical descriptions of hadron structure and decays are still difficult due to the non-perturbative nature of the strong force. Heavy meson decays in particular help to shed light on the intricacies of the flavour sector. We study the effects of electromagnetism in B-meson systems and in particular analyse QED structure-dependence. Concretely, we study the rare leptonic decay $B^- \to \ell^- \bar{\nu}(\gamma)$, $\ell = e, \mu, \tau$, using a new manifestly gauge invariant framework. While often dismissed as small, QED effects are enhanced in this setting and we further perform a numerical study which emphasises their phenomenological relevance in the era of precision physics. Using the same sort of techniques we also consider the role of QED in inducing a mass difference between charged and neutral pseudoscalar mesons. While this is a well-studied problem for which we cannot hope to be competitive numerically,

our dispersive approach is elegant in that it is model independent, coming directly from pure QED and QCD.

The rest of the thesis is structured as follows. In the remainder of this chapter we give a more mathematical tour of the SM as well as introducing some of the formalism used to model hadrons. In particular, rare B decays are discussed including the main features of the aforementioned pure leptonic decay. Next in Chapter 2 we are more specific, discussing QED and structure-dependence. The technique that forms the basis of our computations, Shifman-Vainshtein-Zakharov (SVZ) sum rules [27, 28], are introduced as well as some calculations in scalar QED. We review other methods of investigating QED structure dependence before finally setting up the gauge-invariant sum rules formalism used in our computation.

In Chapters 3 and 4 the main calculation of structure-dependent QED in the $B^- \to \ell^- \bar{\nu}(\gamma)$ decay is presented. Chapter 3 details the computation itself with the corresponding numerical results given in Chapter 4. These results are put into their phenomenological context, with some discussion of the strengths and limitations of the work. Chapter 5 covers the dispersive calculation of the charged-neutral mass difference in heavy mesons. After introducing the relevant theory, the calculation and results are presented with comparison to previous work. Finally we end in Chapter 6 with some concluding remarks.

1.1 The Standard Model

The Standard Model is a quantum field theory based on colour and electroweak symmetry specified by the gauge group SU(3) × SU(2) × U(1). Its dynamics follows from the Lagrangian $\mathcal{L}_{\text{SM}}$ in Minkowski spacetime with metric $g_{\mu\nu} = \text{diag}(1, -1, -1, -1)$. For a more comprehensive review see [29–33].

Consider first a photon field A_μ and a fermion field ψ which do not interact. These are governed by the free Lagrangian

$$\mathcal{L}_{\text{free}} = -\frac{1}{4} F_{\mu\nu} F^{\mu\nu} + \bar{\psi}(i\not{\partial} - m)\psi \,, \tag{1.2}$$

where $\not{\partial} = \gamma^\mu \partial_\mu$ and the electromagnetic field strength tensor F is defined as $F_{\mu\nu} = \partial_\mu A_\nu - \partial_\nu A_\mu$. The classical equations of motion arise from minimising the

action $S = \int \mathcal{L}\, \mathrm{d}^4x$ and lead to the Dirac equation for a free spin-1/2 particle

$$(i\partial\!\!\!/ - m)\psi = 0\,. \tag{1.3}$$

Electromagnetic interactions with matter can be found through minimal substitution, promoting the partial derivative to a covariant one, $\partial_\mu \to D_\mu$ in (1.2). For a fermion with electric charge eQ_f with $e > 0$ this reads

$$D_\mu = \partial_\mu + ies_eQ_fA_\mu\,. \tag{1.4}$$

The sign $s_e = \pm 1$ is convention dependent and in this work we keep it general. Analogously to its gravitational counterpart, the covariant derivative makes the notion of a derivative meaningful in a theory with local U(1) (phase) symmetry. Geometrically the presence of the photon field acts to connect phase transformations at infinitesimally separated points. More formally, under a local phase and gauge transformation

$$\psi(x) \to e^{i\alpha(x)}\psi(x)\,, \qquad A_\mu(x) \to A_\mu(x) - (es_eQ_f)^{-1}\partial_\mu\alpha(x)\,, \tag{1.5}$$

the interaction term $i\bar{\psi}D\!\!\!\!/\,\psi$ in the Lagrangian is invariant. Having coupled the electromagnetic field to matter in such a way we have arrived at the full theory of quantum electrodynamics, with equation of motion

$$\partial_\mu F^{\mu\nu} = es_ej^\nu\,, \qquad j^\nu = Q_f\bar{\psi}\gamma^\mu\psi \tag{1.6}$$

and Feynman rules

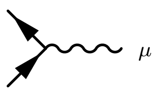

$$= -\,ies_eQ_f\gamma^\mu$$

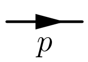

$$= \frac{i(p\!\!\!/ + m)}{p^2 - m^2 + i\varepsilon} \tag{1.7}$$

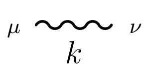

$$= \frac{-i}{k^2 + i\varepsilon}\left(g_{\mu\nu} - (1-\xi)\frac{k_\mu k_\nu}{k^2}\right).$$

This last expression for the photon propagator hides various subtleties arising from gauge freedom in the electromagnetic 4-potential A_μ, for example negative norm states. Physically this freedom can be traced back to the massless photon

only having two polarisation states. Indeed a naive (non-Higgs) mass term $m_\gamma^2 A_\mu A^\mu$ is not gauge-invariant. Formally integration over inequivalent gauge orbits in the path integral is done via the Faddeev-Popov procedure [34]. This corresponds to the addition of a gauge-fixing term $-(\partial_\mu A^\mu)^2/2\xi$ to the Lagrangian (1.2). Pragmatically results should be independent of the 'gauge-parameter' ξ and its value may be chosen for convenience.

At a classical level the conservation of electric charge arises from the global U(1) symmetry of the Lagrangian, leading to the conserved current $\partial_\mu j^\mu = 0$ via Noether's theorem. The analogue in the quantum theory is the famous Ward-Takahashi identity [35, 36]. In its most simple form this states that for a process with amplitude $\mathcal{A} = \epsilon_\mu^*(k)\mathcal{A}^\mu$, involving an external photon of polarisation $\epsilon^*(k)$, one has

$$k_\mu \mathcal{A}^\mu = 0\,. \tag{1.8}$$

We now turn to the theory of strong interactions, quantum chromodynamics. This is a richer theory than QED owing to its non-Abelian nature. The six quark flavours live in the fundamental representation of the SU(3) gauge group, while the eight gluons (which we shall also denote by A_μ) belong to the adjoint representation. The QCD Lagrangian is given by

$$\mathcal{L}_{\mathrm{QCD}} = -\frac{1}{4} G^a_{\mu\nu} G^{a\,\mu\nu} + \sum_f \bar{q}_f \Big(i\partial\!\!\!/ - g s_g A\!\!\!/^a \frac{\lambda^a}{2} - m_{q_f} \Big) q_f\,, \tag{1.9}$$

where the sum runs over the quark flavours and λ^a are the conventionally chosen Gell-Mann matrices. In QCD the field strength $G_{\mu\nu} = G^a_{\mu\nu}\frac{\lambda^a}{2}$ is quadratic in the gluon fields $A_\mu = A^a_\mu \frac{\lambda^a}{2}$,

$$G_{\mu\nu} \;\equiv\; \frac{1}{i g s_g}[D_\mu, D_\nu] \;=\; \partial_\mu A_\nu - \partial_\nu A_\mu + i g s_g [A_\mu, A_\nu]\,, \tag{1.10}$$

as $[\lambda^a, \lambda^b] \neq 0$. This leads to triple and quartic gauge boson self-interactions in addition to the quark-gluon vertex. For completeness we note that gauge fixing in non-Abelian Yang-Mills theories leads to unphysical ghost fields which must be taken into account. As this thesis only uses QCD at a surface level we will not go into detail.

In the calculation of loop diagrams in quantum field theories one encounters ultraviolet (UV) divergences which are removed through renormalisation. In this work all UV divergences will be regulated via Dimensional Regularisation

(DimReg) in $d = 4 - 2\epsilon$. Divergences then appear as powers of $1/\epsilon$ in the limit $\epsilon \to 0$. Counterterm renormalisation removes these poles in ϵ_{UV} at the cost of parameters developing energy scale dependence. Freedom in the choice of counterterm means we have a choice of renormalisation scheme. In general for external particles we employ the On-Shell (OS) scheme while elsewhere we will use modified Minimal Subtraction ($\overline{\text{MS}}$). For later convenience we define

$$\frac{1}{\hat{\epsilon}} = \frac{1}{\epsilon} - \gamma_E + \ln 4\pi \,, \tag{1.11}$$

where γ_E is the Euler-Mascheroni constant. From a modern viewpoint divergences and scale dependence are understood in a Wilsonian manner and come from separating high and low momentum degrees of freedom. One can consider the SM as a low energy effective theory, valid only up to some cut-off, beyond which a more fundamental theory emerges.

In particular coupling constants such as α_{QED} and α_s run with renormalisation scale μ. While the QED coupling constant $\alpha_{\text{QED}}(\mu^2 \to 0) \ll 1$ and remains so at hadronic scales, the QCD coupling instead decreases with energy. At high energies therefore, QCD is asymptotically free and perturbative expansions can be performed. Conversely at low energy scales $\mu \sim \Lambda_{\text{QCD}} \sim \mathcal{O}(200\,\text{MeV})$ the strong coupling $\alpha_s \gg 1$ and physics is non-perturbative. Quarks are confined within hadrons, constantly strongly interacting with gluons. It is this messy environment that makes linking the fundamental QCD Lagrangian with hadronic properties so difficult. Even when working in perturbative QED one has to deal with, one way or another, the fact that quarks are fundamentally non-perturbative objects.

Finally we complete the SM with a discussion of the electroweak sector. Again, this sector will play little role in our work and so we will only give a brief survey. The electroweak sector is the gauge theory of $\text{SU}(2)_{\text{L}} \times \text{U}(1)_{\text{Y}}$ which gets spontaneously broken by the Higgs mechanism to leave our original $\text{U}(1)_{\text{EM}}$ symmetry with a massless photon. Along with a scalar Higgs particle this also leaves three massive bosons conveying the weak force: the W^+, W^- and Z. Unlike QED and QCD the $W^\pm$ is parity violating coupling only to left handed (LH) fermions through V-A type interactions. Weak interactions with quarks may change their flavour and are further complicated by quark mixing, parameterised

through the Cabibbo-Kobayashi-Maskawa (CKM) matrix

$$
\begin{aligned}
|V_{\mathrm{CKM}}| &= \begin{pmatrix} |V_{\mathrm{ud}}| & |V_{\mathrm{us}}| & |V_{\mathrm{ub}}| \\ |V_{\mathrm{cd}}| & |V_{\mathrm{cs}}| & |V_{\mathrm{cb}}| \\ |V_{\mathrm{td}}| & |V_{\mathrm{ts}}| & |V_{\mathrm{tb}}| \end{pmatrix} \\
&= \begin{pmatrix} 0.97373 \pm 0.00031 & 0.2243 \pm 0.0008 & 0.00382 \pm 0.00020 \\ 0.221 \pm 0.004 & 0.975 \pm 0.006 & 0.0408 \pm 0.0014 \\ 0.0086 \pm 0.0002 & 0.0415 \pm 0.0009 & 1.014 \pm 0.029 \end{pmatrix},
\end{aligned}
\tag{1.12}
$$

using (non-fitted) values from the Particle Data Group (PDG) [37]. The CKM hierachy makes transitions across quark generations less likely, so called Cabibbo or CKM-suppression. For three generations of quarks this matrix may acquire a complex phase bringing about charge-parity (CP) violation in the theory. Decays of heavy flavoured mesons in particular provide a valuable setting in which to study CKM matrix elements and considerable research is being done in this area.

Experimentally the SM is now extremely well tested. Electroweak properties were extensively studied at the Large Electron-Positron collider (LEP) at the end of the twentieth century [38]. Similarly, in high energy QCD, multi-loop calculations are now the norm rather than the cutting edge. With the discovery of the Higgs boson in 2012 we are now truly in the era of precision physics. New Physics (NP) is hoped to be discovered in rare decays or in tiny deviations from the SM. As part of this effort, the High-Luminosity upgrade to the Large Hadron Collider (HL-LHC) will increase the collected dataset by roughly ten-times [39] and is expected to become operational in 2029. Further the Belle-II experiment at the SuperKEKB accelerator in Japan will run asymmetrically at the $\Upsilon(4s)$ resonance to continue to study the B-sector in detail. This will probe CP violation, the CKM matrix elements and provide a wealth of data on the flavour sector.

1.2 Hadronic Physics

Colour confinement in QCD means that we only ever observe bound combinations of quarks carrying no colour. To understand the hadronic spectrum at low energies it is helpful to turn to symmetry. Approximating[1] the light $q = u, d, s$

[1]This of course requires turning off electromagnetism and taking their masses to be equal. Certainly such an isospin symmetry is valid for the u, d quarks however this is very much an approximation for the strange quark as $m_s \sim 30\, m_{\mathrm{u(d)}}$ [37].

quarks as identical leads to an $\mathrm{SU(3)_F}$ flavour symmetry. Combining a quark and an antiquark gives Gell-Mann's famous octet of light meson states - the pions and kaons (and an η). Playing the same game with three quarks one gets an octet and decuplet of light baryons. To be specific the pions and kaons are the lowest lying states with zero spin or orbital angular momentum ($S = 0, L = 0$) and odd parity. These are the lightest pseudoscalar mesons having quantum numbers $J^P = 0^-$. Including the heavier charm and bottom quarks we get the D- and B- pseudoscalar mesons respectively. Note that conventionally a B-meson contains a b antiquark, while the $\bar{B}$ contains a b quark. Higher spin mesons are typically heavier than their pseudoscalar counterparts. For example the vector ($J^P = 1^-$) equivalent of the Kaon, the K^*, has mass $m_{K^*} \approx 900\,\mathrm{MeV}$ compared to $m_K \approx 500\,\mathrm{MeV}$ [37].

As discussed previously, the decay of a meson into the vacuum state is very hard to derive from the fundamental QCD Lagrangian due to its non-perturbative nature. More pragmatically, we can instead parameterise the decay in terms of a decay constant that bundles together the difficult to calculate QCD interactions. For pseudoscalar mesons, taking the B^- meson ($q = u$) as an example, the decay constant $f_{B^-} \approx 200\,\mathrm{MeV}$ [40] is defined from the matrix element

$$\langle 0|\bar{q}\gamma_\mu\gamma_5 b|B^-(p_B)\rangle = i f_{B^-}(p_B)_\mu\,, \tag{1.13}$$

where q and b are quark fields. Note that the vector part of the V-A current vanishes by parity conservation. Taking the divergence of this current and conjugating leads us to the standard interpolating operator for a B_q-meson

$$J_B = m_+\,\bar{b}i\gamma_5 q\,, \qquad m_\pm = m_b \pm m_q\,, \qquad \langle\bar{B}|J_B|0\rangle = m_B^2 f_B\,. \tag{1.14}$$

The pseudoscalar operator J_B in some sense 'creates' a $\bar{B}_q$-meson. More properly it 'interpolates' states with the correct quantum numbers in a given correlator. A similar idea is employed for hadronic transitions, where QCD effects are described by form factors. For example (e.g. [41]) the $\bar{B} \to \bar{K}\ell\bar{\ell}$ decay is governed by the the functions $f_\pm(q^2)$

$$\langle\bar{K}(p_K)|\bar{q}\gamma_\mu(1-\gamma_5)b|\bar{B}(p_B)\rangle = f_+(q^2)(p_B+p_K)_\mu + f_-(q^2)(p_B-p_K)_\mu\,, \tag{1.15}$$

with $q = p_B - p_K$.

As it is hard to impossible to describe low energy QCD analytically from its Lagrangian, instead we can make progress in hadronic physics by considering various effective or simplified theories. For light mesons we can exploit the above described flavour symmetry which leads to the famous Chiral Perturbation Theory (χPT) of Gasser and Leutwyler [42, 43]. This is essentially a low-energy expansion with the $\mathcal{O}(E^2)$ effective Lagrangian taking the form

$$\mathcal{L}^{(2)}_{\chi\mathrm{PT}} = \frac{F_\pi^2}{4}\Big(\mathrm{Tr}\big[\partial_\mu U \partial^\mu U^\dagger\big] + 2B_0\,\mathrm{Tr}\big[MU^\dagger + UM^\dagger\big]\Big) + \cdots . \tag{1.16}$$

This Lagrangian leads to a theory of π, K, η meson interactions contained in $U = \exp i\lambda\cdot\phi/F_\pi$ with quark mass matrix $M = \mathrm{diag}(m_u, m_d, m_s)$ and

$$\frac{1}{\sqrt{2}}\sum_{a=1}^{8}\lambda^a\phi^a = \begin{pmatrix} \frac{1}{\sqrt{2}}\pi^0 + \frac{1}{\sqrt{6}}\eta_8 & \pi^+ & K^+ \\ \pi^- & -\frac{1}{\sqrt{2}}\pi^0 + \frac{1}{\sqrt{6}}\eta_8 & K^0 \\ K^- & \bar{K}^0 & -\frac{2}{\sqrt{6}}\eta_8 \end{pmatrix}. \tag{1.17}$$

The quantities F_π and B_0 are low energy constants with $\sqrt{2}F_\pi$ being the pion decay constant. The χPT Lagragian is constructed to mirror the symmetries of the QCD Lagrangian. If we had a theory of three identical massive quarks we would have a theory with global vectorial (isospin) symmetry. Further making the quarks massless $m_{u,d,s} = 0$ there is exact global chiral symmetry $\mathrm{SU}(3)_\mathrm{L} \times \mathrm{SU}(3)_\mathrm{R}$ of the Lagrangian. However in nature chiral symmetry is explicitly broken by non-zero quark masses and also dynamically by quantum effects. The dynamical breaking

$$\mathrm{SU}(3)_\mathrm{L} \times \mathrm{SU}(3)_\mathrm{R} \longrightarrow \mathrm{SU}(3)_\mathrm{V} \tag{1.18}$$

would in theory produce eight massless Goldstones but of course really pions and kaons have non-zero masses due to $m_{u,d,s} > 0$. The heavy strange quark means that $\mathrm{SU}(3)_\mathrm{V}$ symmetry is only approximate and any analysis based on this can only be expected to hold to $\mathcal{O}(20-30\%)$. A signal of the breakdown of chiral symmetry in QCD comes from the non-vanishing of the *chiral condensate*

$$\langle 0|\bar{q}q|0\rangle \neq 0\,. \tag{1.19}$$

This object (which is scale dependent) has the empirical value $\langle\bar{q}q\rangle = -(269(2))^3$ MeV^3 at $\mu = 2\,\mathrm{GeV}$ [44] for $q = u, d$. Chiral perturbation theory in its full form includes couplings to currents by promoting the derivatives in (1.16) to covariant ones. As of 2024 the chiral Lagrangian is now known completely to $\mathcal{O}(E^8)$ [45, 46].

For heavier mesons such as the B and D, χPT is unsuitable. An alternate technique is given by Heavy-Quark Effective Theory (HQET) [47–50] which makes predictions as expansions in the small parameter $\Lambda_{\rm QCD}/m_{b(c)}$. For example consider the mass of the $B^{(*)}$ meson. One expects it to be dominated by the b-quark mass m_b, with some dynamical power corrections $\mathcal{O}(1/m_b^n)$ and a contribution $\bar{\Lambda} = \mathcal{O}(\Lambda_{\rm QCD})$ from the light quarks. A systematic expansion gives

$$m_B = m_b + \bar{\Lambda} - \frac{\mu_\pi^2 + 3\mu_G^2}{2m_b} + \mathcal{O}\left(\frac{1}{m_b^2}\right) \tag{1.20}$$

$$m_{B^*} = m_b + \bar{\Lambda} - \frac{\mu_\pi^2 - \mu_G^2}{2m_b} + \mathcal{O}\left(\frac{1}{m_b^2}\right), \tag{1.21}$$

where μ_π^2 and μ_G^2 are the expectation values of the kinetic and chromatic operators[2]

$$\mu_\pi^2 = \frac{1}{2m_B}\langle B|\bar{b}_v iD_\mu iD^\mu b_v|B\rangle \tag{1.22}$$

$$\mu_G^2 = \frac{-1}{12m_B}\langle B|\bar{b}_v g s_g \sigma_{\mu\nu} G^{\mu\nu} b_v|B\rangle\,, \tag{1.23}$$

where $\sigma_{\mu\nu} = \frac{i}{2}[\gamma_\mu, \gamma_\nu]$. As one goes to higher powers of m_b^{-1} in the HQET expansion more and more operators appear. As $\mu_G^2 > 0$, (1.20) implies that the B^* is heavier than the B and that they become equal as $m_b \to \infty$.

A similar effective theory is Soft-Collinear Effective Theory (SCET) [51–57] which expands instead in $\Lambda_{\rm QCD}/Q$ for some hard energy scale Q. All these effective theories involve the idea of matching and the related Operator Product Expansion (OPE).

Wilson's OPE [58] concerns products of fields at the same spacetime point. For two local operators O_A and O_B evaluated at a short distance x apart, the OPE allows us to replace their product with an expansion over local operators in the limit $x \to 0$

$$\lim_{x\to 0} O_A(x)O_B(0) = \sum_i C_i(x)O_i(0)\,. \tag{1.24}$$

This is an expansion at the level of operators not matrix elements, meaning the Wilson coefficients C_i are process independent. In hadronic physics at energy

[2] At this order in m_b^{-1} one does not need to worry about the difference between the physical $|B\rangle$ state and the state defined in the $m_b \to \infty$ limit. Indeed strictly speaking (1.20) and (1.21) should involve the 'static' versions of μ_π^2 and μ_G^2 with the m_b dependence removed. Similarly the field b_v is really only the true quark field whe $m_b \to \infty$. The HQET Lagrangian comes from systematically integrating out the m_b^{-1} power suppressed part of the spinor.

scales of a few GeV ($\ll M_W$) we typically integrate out the heavy W-boson, contracting two fermion currents to a point. That is we essentially work in 4-Fermi theory when dealing with weak decays. Via the OPE any amplitude for a weak decay can be written as

$$\mathcal{A} = \sum_i C_i(\mu, M_W)\langle O_i(\mu)\rangle\,, \tag{1.25}$$

where the operators O_i must respect the symmetries and quantum numbers of the decay. The Wilson coefficients run with scale and parameterise short distance physics calculable in perturbation theory[3]. Conversely the operator hadronic matrix elements describe the hard to calculate long distance effects. For the $B^- \to \ell^-\bar{\nu}$ decay in 4-Fermi theory the W-propagator $1/(q^2 - M_W^2) \to -1/M_W^2$ as $q^2 \ll M_W^2$ and the relevant operator is

$$O_{\bar{B}\to\ell\bar{\nu}} = -\frac{G_F}{\sqrt{2}} V_{\rm ub}\, \cdot \bar{u}\gamma_\mu(1-\gamma_5)b \cdot \bar{\ell}\gamma^\mu(1-\gamma_5)\nu\,, \tag{1.26}$$

which does not run in QCD. Thus in a world without QED[4] the Fermi constant G_F is indeed a constant and takes the value $G_F = 1.166 \times 10^{-5}\,\text{GeV}^{-2}$ [37].

There are numerous other techniques and models based on effective theories or simplifications of QCD. For example letting the number of colours $N_c \to \infty$ [59] or assuming quarks are non-relativistic within hadrons [60]. However to conclude this section we will discuss two final methods: lattice QCD and sum rules techniques. These are perhaps more special as they still use the fundamental QCD Lagrangian.

Firstly, while the idea of a sum rule was certainly around in the pre-QCD era, in this thesis we are concerned with QCD (SVZ) sum rules. These link a perturbative QCD calculation with a non-perturbative hadronic property (like a decay constant or a hadron mass for example) using a dispersion relation and a judiciously chosen correlator. As this technique is the basis for the $B^- \to \ell^-\bar{\nu}(\gamma)$ calculation in Chapters 3 and 4 we give a comprehensive introduction in 2.1.

Lattice QCD [61–64] however is a completely non-perturbative method. It is based on Monte-Carlo sampling of the path integral with fields defined on a finite

[3]The strong coupling is still small down to $\mu \sim 1\,\text{GeV}$ and can be used as an expansion parameter. However large logarithms $\ln(M_W/\mu)$ generated by the large separation of scales can complicate matters and must be dealt with via renormalisation group methods.

[4]This operator renormalises non-trivially in QED, cf. Section 3.2.5 and the subtleties involved in the definition of G_F.

Euclidean spacetime lattice. Numerical simulations are hugely computationally expensive and historically various approximations have been employed. For example the quenched approximation (no fermion loops), assuming isospin symmetry and working at non-physical quark masses. Indeed heavy b-quarks are very difficult to simulate on the lattice due to the tiny lattice spacings required to resolve them. That being said, lattice QCD is now highly competitive with many quantities now calculated to sub-1% precision [40].

1.3 B Decays

Analysis of systems involving a heavy b quark occupy a disproportionately large portion of modern physics research. This is because B decays provide an excellent laboratory for probing NP. As b-quarks are the heaviest hadronising quarks there is a large scope for exotic and varied decay products. Consequently considerable information can be gleaned regarding CKM matrix elements and CP violation.

By far the most common transition is $b \to c$ meaning that D-mesons are produced copiously at B-factories such as BaBar and Belle. All but a few percent of decays are of other types, which can mostly be traced back to the relative sizes of the CKM matrix elements $|V_{\text{ub}}| \ll |V_{\text{cb}}|$. In general a *rare* B decay refers to any decay suppressed or non-existent at tree level and these are often especially sensitive to NP. One large class of rare decays are the Flavour-Changing Neutral Currents (FCNCs). These change a quark's flavour but not its charge and thus only exist at loop level in the SM via box or penguin diagrams. Indeed decays such as $\bar{B}_s \to \mu^+\mu^-$, $\bar{B} \to \bar{K}^{(*)}\ell^+\ell^-$ and neutral $B - \bar{B}$ oscillations have been extensively studied, e.g. [65–72]. The latter is of special interest in studying CP violation while $\bar{B} \to \bar{K}^{(*)}\ell^+\ell^-$ has drawn considerable attention in recent years due to Lepton Flavour Universality (LFU) anomalies (see [73] and references therein). Deviations from one in the so-called R_K and R_{K^*} ratios describe differences in the weak force couplings to muons and electrons [74]. While these ratios at one point exhibited as much as a 3.1σ deviation from the SM [75–78], a recent LHCb re-analysis has mostly removed this anomaly [79, 80].

Chapters 3 and 4 of this thesis concern the rare decay $B^- \to \ell^-\bar{\nu}$ and its radiative counterpart $B^- \to \ell^-\bar{\nu}\gamma$, with $\ell = e, \mu, \tau$. The B^- has valence quarks $b\bar{u}$ and for the rest of this work we shall abbreviate the decay using the shorthand $\bar{B} \to \ell\bar{\nu}(\gamma)$. While not loop suppressed the charged-current leptonic $\bar{B} \to \ell\bar{\nu}$ decay is both

CKM suppressed and helicity suppressed for light leptons $\ell = e, \mu$. The CKM suppression comes from $V_{\rm ub} = \mathcal{O}(10^{-3})$ contained in the V-A operator (1.26) mediating the weak decay while helicity suppression refers to the amplitude being proportional to the (light) lepton mass. The neutrino mass is taken to be zero.

Physically this is understood via spin conservation. The anti-neutrino must be in a right-handed (RH) chiral eigenstate which coincides with the RH helicity eigenstate as the neutrino mass is zero. To conserve spin, in the rest frame of the decaying (spin-0) $\bar{B}$, the lepton must also be in a RH helicity state as the decay products are back-to-back. Leptons cannot be in a RH chiral state and so it is the small difference between helicity and chiral eigenstates, proportional to the lepton mass, that allows this decay to occur.

Neglecting QED corrections, the decay amplitude is proportional to the decay constant

$$\mathcal{A}_{\bar{B}\to\ell\bar{\nu}} = \frac{iG_F V_{\rm ub} f_B}{\sqrt{2}} \cdot \bar{u}\not{p}_B(1-\gamma_5)v\,, \tag{1.27}$$

with the p_B in the spinor structure being the $\bar{B}$-meson 4-momentum and using amplitude convention $\mathcal{A} = \langle \ell\bar{\nu}| - \mathcal{L}|\bar{B}\rangle$. In pure QCD the amplitude factorises as gluons are only contained in the meson whose decay to the vacuum is described by f_B. In the presence of electromagnetism photons connect the meson and the leptonic final state, meaning the factorisation is lost and f_B becomes ill-defined. The decay rate is found by squaring the amplitude, summing over final state spins and integrating over the 2-body phase space. In the rest frame of the meson the decay products are back-to-back and so the integration is trivial. This leads to the theoretical branching ratio

$$\mathcal{B}(\bar{B}\to\ell\bar{\nu}) = \frac{G_F^2\, m_B}{8\pi}\, m_\ell^2 \left(1 - \frac{m_\ell^2}{m_B^2}\right)^2 f_B^2\, |V_{\rm ub}|^2\, \tau_B\,, \tag{1.28}$$

where $\tau_B = 1.638(4) \times 10^{-12} s$ is the $B^\pm$ lifetime [37]. Note that helicity suppression is manifest in the factor of m_ℓ^2 in (1.28). This leads to the hierarchy in the SM theory predictions (e.g. [81])

$$\begin{aligned} \mathcal{B}(\bar{B}\to e\bar{\nu}) &= 8.1(6)\cdot 10^{-12} \\ \mathcal{B}(\bar{B}\to \mu\bar{\nu}) &= 3.5(3)\cdot 10^{-7} \\ \mathcal{B}(\bar{B}\to \tau\bar{\nu}) &= 7.7(6)\cdot 10^{-5}\,, \end{aligned} \tag{1.29}$$

with the dominant uncertainties being from f_B and $|V_{\rm ub}|$. Helicity suppression

only really exists for the light electron and muon cases. In the tau case, with $m_\tau = 1.777\,\text{GeV}$ [37], there is no longer such a suppression.

Finally, while in the SM this decay is mediated by a V-A type interaction, it is interesting to consider a scenario where instead there is an S-P interaction. That is an operator of the form

$$O^{\text{S-P}}_{\bar{B}\to\ell\bar{\nu}} = -\frac{G_F}{\sqrt{2}} C_{\text{S-P}} \cdot \bar{u}(1-\gamma_5)b \cdot \bar{\ell}(1-\gamma_5)\nu\,, \tag{1.30}$$

where $C_{\text{S-P}} = 0$ in the SM. Such an operator does not lead to helicity suppression and this feature makes it a useful testing ground. Further, S-P NP contributions would potentially be quite large compared to the SM V-A prediction.

Let us now turn to the radiative decay $\bar{B} \to \ell\bar{\nu}\gamma$. The characteristic features of this decay depends strongly on whether the emitted photon is *soft* (low-energy) or *hard* (high-energy). For large photon energies the radiative rate is completely dominated by structure-dependent effects (emissions from the $\bar{B}$-meson). This lifts the helicity suppression: the radiative rate is not m_ℓ^2 suppressed (as it is no longer proportional to the tree level). Consequently the radiative rate dominates over the non-radiative rate when the photon energy $E_\gamma \gg m_\ell$. This is an important consideration in the electron and muon channels.

The leptonic decay can be studied for any pseudoscalar meson, e.g. $(\pi^-, K) \to \ell\bar{\nu}(\gamma)$ and even exotica like B_c. For the lighter mesons the sum rules techniques we employ to study this decay become unsuitable and lattice results are competitive, e.g. [82–87]. The leptonic decay is of interest as it is theoretically clean (in pure QCD) and so a good environment for looking for NP. For example NP with a different chiral structure or even modifications to (1.28) in a charged Higgs model [88, 89].

Chapter 2

QED and Heavy Mesons

In this chapter we discuss some of the differences and subtleties in QED that do not appear in QCD. While QED is a simpler gauge-theory, being non-Abelian in nature, QCD bound states are colourless. Conversely, QED bound states can and do carry electric charge to the far-future and far-past. Using sum rules (SR) techniques (introduced in Section 2.1), this causes problems with Infrared (IR) divergences (Section 2.2) and gauge-invariance (Section 2.4).

Historically, QED corrections have been overshadowed by their QCD counterparts due to the relative sizes of their coupling constants, $\alpha_s(m_b)/\alpha_{\rm QED} \approx 30$, with QED corrections expected as an $\mathcal{O}(1\%)$ effect. However QED is now of increasing relevance in the precision calculation of observables (with many quantities now approaching or below percent precision) and in certain situations QED effects can be considerably larger than 1%. For example at the differential level, in certain regions of phase space, QED effects in $B \to K e^+ e^-$ have been found to be as much as 10–20% [73, 90]. When fully inclusive such effects are usually dampened though corrections of a few percent often still exist.

Many of these large QED corrections can be traced back to the loss of factorisation between initial and final states. Taking $\bar{B} \to \ell\bar{\nu}$ as an example, all QCD effects are contained in the initial $\bar{B}$-meson, with f_B encompassing all orders in QCD. As the final state lepton carries electric charge, virtual photons can connect the initial and final states. This is particularly relevant for the light leptons as it can lead to so-called large 'hard-collinear' logarithms $\frac{\alpha}{\pi}\ln(m_\ell/m_B)$. These logs, discussed further in Section 2.2, can be structure-dependent and we will pay special attention to them. These logs exist in the point-like approximation and

so we study $\bar{B} \to \bar{K}^{(*)}\ell\bar{\ell}(\gamma)$ and $\bar{B} \to \ell\bar{\nu}(\gamma)$ in scalar QED in Section 2.3.

2.1 Sum Rules and Analyticity

While true physics may be considered to exist on the real axis, considerable constraints come from analyticity and causality in the full complex plane; see for example [91–93] for a more thorough review. This was the idea of the S-matrix program in the pre-QCD era. The S-matrix relates asymptotic in and out states

$$ {}_{\text{out}}\langle p_1', p_2', \cdots | p_1, p_2, \cdots \rangle_{\text{in}} \;=\; {}_{\text{in}}\langle p_1', p_2', \cdots | S | p_1, p_2, \cdots \rangle_{\text{in}} \,, \tag{2.1} $$

and is related to time-ordered correlators via the celebrated Lehmann-Symanzik-Zimmermann (LSZ) formula [94]. Promoting momenta and masses to be complex valued variables $p^2 \in \mathbb{C}$, one can investigate the positions of poles or branch cuts in the complex plane. Indeed, dispersion relations have their origins in classical electromagnetism in the Kramers-Kronig [95, 96] relations which exhibit the deep links between analytic structure and causality. Response functions that are causal have no poles in the upper half-plane and vice versa (Titchmarsh's theorem [97]).

In the quantum theory branch cuts immediately manifest themselves as the Schrödinger equation is linear not quadratic in the time derivative. The natural variable is now $E = \frac{p^2}{2m}$ rather than p itself. This relative square-root means $S(E)$ is defined over *two* complex planes referred to as the physical and unphysical sheets, glued together at a branch cut conventionally chosen as the positive real axis. Bound states (which don't exist in perturbation theory) appear as poles in the S-matrix located on the negative real axis of the physical sheet while resonances live on the unphysical sheet. Roughly speaking, one can relate causality to analyticity in the energy while analyticity in angular variables is related to the locality of interactions.

Another important tenet of the S-matrix is unitarity, $S^\dagger S = \mathbb{1}$. Decomposing the S-matrix into an interacting and non-interacting part

$$ S = \mathbb{1} + iT \,, \tag{2.2} $$

and applying the unitarity condition $(\mathbb{1} - iT^\dagger)(\mathbb{1} + iT) = \mathbb{1}$, one gets

$$ i(T^\dagger - T) = 2\,\text{Im}\,T = T^\dagger T \,. \tag{2.3} $$

Sandwiching this between initial and final states, $T_{fi} = \langle f|T|i\rangle$, and using the completeness relation $\mathbb{1} = \sum_n |n\rangle\langle n|$ gives the (generalised) optical theorem

$$2\,\mathrm{Im}\,T_{fi} = \sum_n T^\dagger_{fn} T_{ni}\,. \tag{2.4}$$

This relates the imaginary part of an amplitude to scattering into a set of on-shell intermediate states $|n\rangle$ (which must be kinematically allowed and have the right quantum numbers). Diagrammatically, this can be represented by

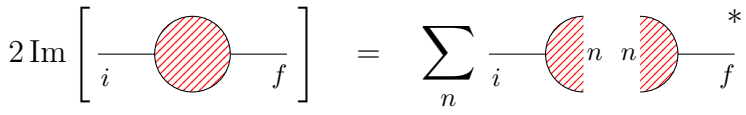

(2.5)

and in the case of forward scattering, $|i\rangle = |f\rangle$, the result is particularly simple. We see that the imaginary part of the amplitude can be found by *cutting* the diagram in two. Only when a threshold energy is reached, corresponding to being able to generate on-shell intermediate states on the RHS, does the amplitude acquire an imaginary part. Above threshold a branch cut forms along the real axis for $E > E_{\text{threshold}}$. The imaginary part of the amplitude is linked to the discontinuity across the branch cut via $\mathrm{disc}[f(E)] = 2i\,\mathrm{Im}[f(E+i\varepsilon)]$ guaranteed by Schwartz's reflection principle[1].

The cutting procedure can be made more formal through the Cutkosky rules [99]. These state that the discontinuity of a Feynman diagram can be found by cutting through the diagram in all possible ways, putting all intermediate particles on shell. This corresponds to replacing all cut propagators with delta functions

$$\frac{1}{p^2 - m^2 + i\varepsilon} \longrightarrow -2\pi i\,\delta^+(p^2 - m^2)\,, \tag{2.6}$$

where $\delta^+(p^2-m^2) \equiv \theta(p^0)\delta(p^2-m^2)$ and $\theta(x)$ is the Heaviside step function. The $\theta(p^0)$ selects the positive root and is important in ensuring correct energy flow through diagrams. This can be motivated by the Sokhotski-Plemelj Theorem, noting that the $i\varepsilon$ prescription is only relevant when $p^2 = m^2$

$$\frac{1}{p^2 - m^2 + i\varepsilon} = \mathcal{P}\frac{1}{p^2 - m^2} - i\pi\delta(p^2 - m^2)\,, \tag{2.7}$$

with $\mathcal{P}$ being the Cauchy principle value. While cutting rules make it easier to

[1]For an analytic function $f(z)$, real on some interval of the real line, the analytic continuation of $f(z^*)^* = f(z)$ to the whole complex plane exists [98]. Thus for $s \in \mathbb{R}$ one has $\mathrm{disc}[f(s)] \equiv f(s+i\varepsilon) - f(s-i\varepsilon) = f(s+i\varepsilon) - f^*(s+i\varepsilon) = 2i\,\mathrm{Im}\,f(s+i\varepsilon)$.

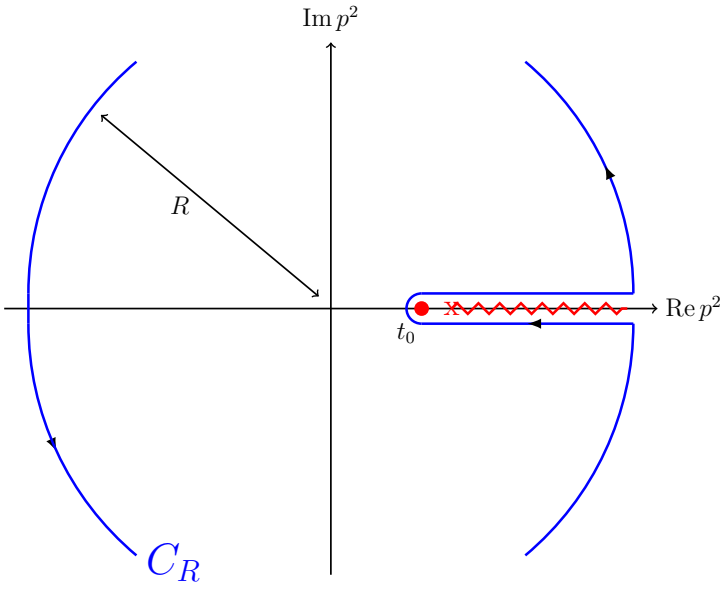

Figure 2.1 *The contour C_R in the complex plane $\mathbb{C}_{p^2}$ (physical sheet) used to derive the dispersion relation (2.9). The contour (of radius R) is taken anti-clockwise and is shown in blue, while the singularities of $\Pi(p^2)$ are shown in red. Along the real axis there is typically a pole (red circle) and a branch cut (red zigzag line) extending to infinity. The onset of these singularities is the threshold t_0.*

find the imaginary part of Feynman integrals, this is only really useful if one can reconstruct the rest of the function. This is where dispersion relations become useful.

Consider a two-point correlator $\Pi(p^2)$, as drawn in (2.5). At physical energies $s = 4E^2 > 0$, the correlator in general contains poles and a branch cut above threshold t_0 as drawn in Figure 2.1. This is guaranteed by the Källén-Lehmann spectral representation [100] and its physical interpretation will be discussed in the next section. In the rest of the complex plane $\Pi(p^2)$ is analytic, so choosing the contour C_R (Figure 2.1) we have

$$\Pi(p^2) = \frac{1}{2\pi i} \oint_{C_R} \mathrm{d}z \, \frac{\Pi(z)}{z - p^2} \,, \tag{2.8}$$

by Cauchy's theorem. Assuming the function decays fast enough (see comments below), we may take the contour arc to infinity giving

$$\begin{aligned} \Pi(p^2) &= \frac{1}{2\pi i} \int_{t_0}^{\infty} \mathrm{d}s \, \frac{\Pi(s + i\varepsilon) - \Pi(s - i\varepsilon)}{s - p^2} = \frac{1}{2\pi i} \int_{t_0}^{\infty} \mathrm{d}s \, \frac{\mathrm{disc}[\Pi(s)]}{s - p^2 - i\varepsilon} \\ &= \frac{1}{\pi} \int_{t_0}^{\infty} \mathrm{d}s \, \frac{\mathrm{Im}[\Pi(s)]}{s - p^2 - i\varepsilon} \,, \end{aligned} \tag{2.9}$$

with the only contributions coming from the real line. This is the dispersion relation which links a correlator to an integral over the spectral density $\rho(s) \equiv \text{Im}[\Pi(s)]/\pi = \text{disc}[\Pi(s)]/2\pi i$. If the integral diverges as $s \to \infty$ convergence can be improved by instead using a *subtracted* dispersion relation. For a density that grows as s^N, we can subtract off the first N-terms in the Taylor expansion around zero to kill off the divergence.

$$\Pi(p^2) = \frac{(p^2)^N}{\pi} \int_{t_0}^{\infty} \mathrm{d}s \, \frac{\text{Im}[\Pi(s)]}{s^N(s - p^2 - i\varepsilon)} + \sum_{n=0}^{N-1} \frac{\Pi^{(n)}(0)}{n!}(p^2)^n \tag{2.10}$$

This is exactly the dispersion analogue of renormalisation. Our ignorance of high-energy (UV) behaviour requires us to introduce subtraction constants that either come from experiment or are scheme-dependent.

While for two-point functions singularities on the physical sheet are well-understood via the Källén-Lehmann spectral representation, much less is known for higher point functions. Anomalous thresholds (which may live on the physical sheet) can develop which corresponds to cutting diagrams into more than two pieces (generalised unitarity). These will play no role in this work. Lastly, Landau equations [101] are a useful general tool to locate singularities of multi-loop Feynman integrals, though again these are not used in this thesis.

The dream of the dispersion program is to remove the need for a relativistic wave equation by iteratively gluing together lower order contributions to get higher order imaginary parts via unitarity/optical theorem arguments (cf. (2.5)) and then reconstructing the full function via a dispersion. However even in $2 \to 2$ scattering the relevant dispersion relation (Mandelstam representation [102, 103]) has never been proven.

2.1.1 SVZ Sum Rules

SVZ sum rules, rather than fighting QCD in its non-perturbative regime, instead embrace it. Pioneered by Shifman, Vainshtein and Zakharov in 1979 [27, 28] and often referred to as QCD sum rules, they parameterise non-perturbative effects through quantities known as *vacuum condensates*. The fundamental idea is to calculate a correlator in two different ways. On one hand relate it to a non-perturbative hadronic quantity, like a decay constant or a mass, that needs to be calculated. On the other hand exploit asymptotic freedom at high

energies to calculate it perturbatively (plus condensate improvements) from the fundamental quark and gluon fields. These two regimes are then linked together via a dispersion relation to allow extraction of the hadronic quantity from the QCD computation. To illustrate the procedure we will consider the sum rules calculation of the B-meson decay constant f_B (1.13) [104].

First, define a correlator using the interpolating operator J_B (1.14)

$$\Pi(p^2) = i \int \mathrm{d}^4x \, e^{ip\cdot x} \langle 0|T J_B^\dagger(x) J_B(0)|0\rangle \,. \tag{2.11}$$

As before, this two-point function has hadronic poles and branch cuts at positive p^2 as guaranteed by the Källén-Lehmann spectral representation. Conversely at large negative p^2 (t-channel) the momenta transferred to the quark fields b and q is large and the integral is dominated by short distance (perturbative) physics. At intermediate negative p^2, this is supplemented by the condensates that include longer distance non-perturbative vacuum fluctuations. In any case, the negative p^2 region can be linked to the positive p^2 region via a dispersion

$$\Pi(p^2) = \frac{1}{\pi} \int_{t_0}^{\infty} \mathrm{d}s \, \frac{\mathrm{Im}\,\Pi(s)}{s - p^2 - i\varepsilon} \, + \text{ subtractions}\,, \tag{2.12}$$

as in Figure 2.1.

Let us now extract the hadronic content from (2.11). Begin by inserting the identity $\mathbb{1}$, written as a complete set of *hadronic* states

$$\mathbb{1} = |0\rangle\langle 0| + \int \frac{\mathrm{d}^3\boldsymbol{k}}{(2\pi)^3} \frac{1}{2E_{\boldsymbol{k}}} |\bar{B}(\boldsymbol{k})\rangle\langle\bar{B}(\boldsymbol{k})| \, + \text{ higher states}\,. \tag{2.13}$$

with $E_{\boldsymbol{k}} = \sqrt{|\boldsymbol{k}|^2 + m_B^2}$ and bold-type indicating 3-momenta. This includes the vacuum state, single-particle hadronic states and multi-particle states. Only states with the correct quantum numbers are relevant, the lowest lying of which are the (on-shell) $\bar{B}$ states. At higher energies there are excited states and multi-hadron contributions which we will aim to suppress. Inserting this into the matrix element (2.11), the vacuum state vanishes and one gets

$$\Pi(p^2) = i \int \mathrm{d}^4x \, \frac{\mathrm{d}^3\boldsymbol{k}}{(2\pi)^3} \frac{e^{ip\cdot x}}{2E_{\boldsymbol{k}}} \underbrace{\langle 0|J_B^\dagger(x)|\bar{B}(\boldsymbol{k})\rangle}_{m_B^2 f_B e^{-ik\cdot x}} \underbrace{\langle\bar{B}(\boldsymbol{k})|J_B(0)|0\rangle}_{m_B^2 f_B} \theta(x^0) + \cdots \,, \tag{2.14}$$

where we have used the translation $\langle 0|J_B^\dagger(x)|\bar{B}(\boldsymbol{k})\rangle = \langle 0|J_B^\dagger(0)|\bar{B}(\boldsymbol{k})\rangle e^{-ik\cdot x}$ and

with $+\cdots$ including the $\theta(-x^0)$ time-ordering[2] as well as the higher energy states. We end up with

$$\Pi(p^2) = i \int \mathrm{d}^4x \, \frac{\mathrm{d}^3\boldsymbol{k}}{(2\pi)^3} \frac{e^{ip\cdot x}}{2E_{\boldsymbol{k}}} \Big(\theta(x^0) e^{-ik\cdot x} + \theta(-x^0) e^{+ik\cdot x} \Big) m_B^4 f_B^2 \, + \, \cdots \, . \tag{2.15}$$

We could represent $2\pi i \, \theta(\pm x^0) = \int_{\mathbb{R}} \mathrm{d}w \, e^{\pm iwx^0}/(w - i\varepsilon)$ and take the discontinuity of (2.15) directly, however it is easier to instead recognise the appearance of the Feynman propagator.

$$\Pi(p^2) = i \, m_B^4 f_B^2 \int \mathrm{d}^4x \, e^{ip\cdot x} \int \frac{\mathrm{d}^4k}{(2\pi)^4} \frac{i \, e^{-ik\cdot x}}{k^2 - m_B^2 + i\varepsilon} \, + \, \text{higher states} \, . \tag{2.16}$$

The integration over d^4x can be performed generating a $\delta^{(4)}(p-k)$ which in turn collapses the d^4k integral. Once the dust settles, we end up with

$$\Pi(p^2) = \frac{m_B^4 f_B^2}{m_B^2 - p^2} \, + \, \text{continuum} \, , \tag{2.17}$$

or equivalently

$$\frac{1}{\pi} \operatorname{Im} \Pi(p^2) = m_B^4 f_B^2 \, \delta(p^2 - m_B^2) \, + \, \text{continuum} \, , \tag{2.18}$$

where we drop the $i\varepsilon$ in (2.17) and hereafter for brevity. The higher multi-particle states that we ignored give a continuous imaginary part above some threshold. The 'pole + continuum' hadronic representation of $\Pi(p^2)$ in (2.17) is exact with the quantity of interest, f_B, appearing as the residue of the lowest-lying pole with pollution from a continuum of higher-energy states.

Turning now to the partonic (perturbative) calculation, the leading order (LO) result comes from Wick contracting the quark fields in the correlator

$$\Pi(p^2)|_{\mathrm{LO}} = \, - i m_b^2 \int \mathrm{d}^4x \, e^{ip\cdot x} \langle 0| \overbrace{\bar{q}(x) \gamma_5 \, \underbrace{b(x) \bar{b}(0)}_{} \gamma_5 q(0)}^{} |0\rangle \tag{2.19}$$

$$= \, - i m_b^2 N_c \int \frac{\mathrm{d}^4l}{(2\pi)^4} \frac{\operatorname{Tr}\big[\gamma_5(-\not{l} + m_q)\gamma_5(\not{p} - \not{l} + m_b)\big]}{[(p-l)^2 - m_b^2][l^2 - m_q^2]} \, , \tag{2.20}$$

where $N_c = 3$ is the number of colours. This is simply a bubble graph whose discontinuity can be found via cutting rules. Taking the light quark mass $m_q \to 0$

[2]With the $\theta(-x^0)$ ordering the relevant insertion is $|B\rangle\langle B|$ rather than $\bar{B}$.

for simplicity we have

$$\text{disc}\left[i \right. \quad \left. \right] \;=\; -im_b^2 N_c(-2\pi i)^2 \int \frac{\mathrm{d}^4 l}{(2\pi)^4}\delta^+(l^2)\delta^+((p-l)^2-m_b^2) \times \mathrm{Tr}\big[\gamma_5(-\not{l})\gamma_5(\not{p}-\not{l}+m_b)\big]\,, \qquad (2.21)$$

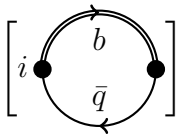

where the black circle denotes the J_B operator and l is the loop momenta. Both the b-quark propagator (carrying momentum $p-l$) and the $\bar{q}$-propagator (carrying momentum l) are cut generating two delta functions. This is the only way of cutting this diagram. Note that conventionally heavy b quark propagators are drawn with a double line. The trace evaluates to $4p\cdot l$ as the $\delta(l^2)$ enforces $l^2=0$. The two delta functions collapse two of the four integrals with the remaining angular integrals trivial in the $\boldsymbol{p}=\mathbf{0}$ frame. Performing the calculation[3] gives

$$\frac{\text{disc}\,\Pi(p^2)}{2\pi i} = \frac{m_b^2 N_c}{8\pi^2}\frac{(p^2-m_b^2)^2}{p^2}\,, \quad p^2 \geq m_b^2\,, \qquad (2.22)$$

where on the partonic side the correlator acquires an imaginary part for all p^2 above m_b^2. Finally now we can equate the hadronic and partonic calculations of $\Pi(p^2)$ to arrive at our sum rule

$$\frac{m_B^4 f_B^2}{m_B^2-p^2} \,+\, \text{cont.} \,=\, \frac{m_b^2 N_c}{8\pi^2}\int_{m_b^2}^{\infty}\frac{\mathrm{d}s}{s-p^2}\frac{(s-m_b^2)^2}{s} \,+\, \text{subtr.} \qquad (2.23)$$

Barring some practicalities involving removing the continuum (cont.) contributions and the subtractions (subtr.), discussed in 2.1.2, this equation can be used to extract f_B. Of course in its present form it will not do this very well. Higher order corrections in α_s should be added to the perturbative calculation (RHS of (2.23)) and we can add in non-perturbative effects systematically through a condensate expansion. For example, at the level of diagrams the chiral condensate $\langle\bar{q}q\rangle$ (in this context referred to as the quark condensate) arises from not Wick contracting a pair of quark fields

$$\Pi(p^2)|_{\text{LO}}^{\langle\bar{q}q\rangle} = -im_b^2\int \mathrm{d}^4x\, e^{ip\cdot x}\langle 0|\bar{q}(x)\gamma_5 \overbrace{b(x)\bar{b}}(0)\gamma_5 q(0)|0\rangle \qquad (2.24)$$

$$= m_b^2 N_c \int \mathrm{d}^4x\, e^{ip\cdot x}(\gamma_5 S_F^{(b)}(x)\gamma_5)_{\alpha\beta}\langle 0|\bar{q}_\alpha(x)q_\beta(0)|0\rangle\,. \qquad (2.25)$$

[3]Such integrals form the basis of the $\bar{B}\to\ell\bar{\nu}(\gamma)$ sum rules calculation and so we postpone the details to Section 3.2.2.

The heavy quark fields combine to form a fermion b-propagator

$$iS_F^{(b)}(x-y)_{\alpha\beta} = \int \frac{\mathrm{d}^4k}{(2\pi)^4} \frac{i(\not{k}+m_b)_{\alpha\beta}}{k^2-m_b^2} e^{-ik\cdot(x-y)}\,, \tag{2.26}$$

where α, β are spinor indices, while the uncontracted q-quark fields form a non-vanishing matrix element via a Taylor expansion

$$\langle 0|\bar{q}_\alpha(x) q_\beta(0)|0\rangle = \frac{\langle\bar{q}q\rangle}{4N_c}\delta_{\alpha\beta} + \mathcal{O}(x)\,. \tag{2.27}$$

This matrix element would vanish in perturbation theory and so the expansion in terms of condensates parameterises genuine non-perturbative interactions with the QCD vacuum. Further terms in the Taylor expansion are discussed in Section 5.3.1 however these are $\mathcal{O}(m_q)$ and so can generally be neglected as small. The normalisation factor of $4N_c$ in (2.27) comes from contracting the spinor and (suppressed) colour indices. Diagrammatically, the quark condensate is conventionally drawn as a pair of crosses, with Feynman rule

$$= \frac{\langle\bar{q}q\rangle}{4N_c}\,\mathbb{1} + \mathcal{O}(m_q)\,. \tag{2.28}$$

No momenta enters the condensate and so condensate calculations are one loop less than the corresponding perturbative ones. Via (2.24), or from the Feynman rules, the LO quark condensate diagram is

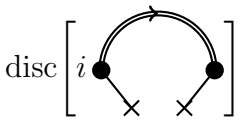

$$\begin{aligned} &= \mathrm{disc}\left[\frac{1}{4}m_b^2\langle\bar{q}q\rangle \frac{\mathrm{Tr}\left[\gamma_5\mathbb{1}\gamma_5(\not{p}+m_b)\right]}{p^2-m_b^2}\right] \\ &= -2\pi i\, m_b^3\langle\bar{q}q\rangle\delta^+(p^2-m_b^2)\,. \end{aligned} \tag{2.29}$$

Only the b-quark propagator can be cut and the result is particularly simple. Note that heavy quarks do not form condensates $\langle\bar{b}b\rangle = 0$, being highly virtual at Λ_{QCD}.

The quark condensate is not the only condensate however. The condensate expansion can be made more formal via the OPE

$$\Pi(p^2) = i\sum_j \langle 0|O_j(0)|0\rangle \int \mathrm{d}^4x\, e^{ip\cdot x} C_j(x)\,, \tag{2.30}$$

strictly valid only for $p \to 0$ with $p^2 < 0$. The (Fourier-transformed) Wilson coefficients scale as $\tilde{C}_j(p^2) \sim (p^2)^{(4-d_j)/2}$ for an operator O_j of dimension d_j.

Thus there is a natural ordering with the most relevant contributions from the low dimension operators while high dimensional operators are suppressed. Up to dimension-5 we have

O_j	$\mathbb{1}$	$\bar{q}q$	$G^a_{\mu\nu}G^{a\,\mu\nu}$	$\bar{q}\sigma_{\mu\nu}G^{\mu\nu}q$
d_j	0	3	4	5
name	perturbative	quark	gluon	mixed

In this notation the perturbative contribution is the $\mathbb{1}$ operator. Higher-dimensional contributions like four-quark and 3-gluon condensates are sufficiently small to rarely be relevant and will not play a role in the rest of this thesis. Further, in pure QED really only the $\mathbb{1}$ and $\langle\bar{q}q\rangle$ terms are needed as there are no gluons involved.

2.1.2 Practicalities

The final obstacles to calculating f_B from (2.23) is dealing with the continuum of higher energy multi-particle states that contaminate the pole at $p^2 = m_B^2$ as well as possible subtractions. Letting the onset of the higher energy states be s_0^{cont}, we can parameterise their continuous imaginary part above s_0^{cont} with an (unknown) spectral density $\rho^{\text{cont}}(s)$. That is, for convenience we may write

$$\frac{m_B^4 f_B^2}{m_B^2 - p^2} + \int_{s_0^{\text{cont}}}^{\infty} \frac{\rho^{\text{cont}}(s)}{s - p^2}\,\mathrm{d}s \;=\; \int_{m_b^2}^{\infty} \frac{\rho^{\text{pert}}(s)}{s - p^2}\,\mathrm{d}s \;+\; \text{subtr.}\,, \tag{2.31}$$

where as we have calculated, in a slight abuse of the label 'pert'

$$\rho^{\text{pert}}(s) \;=\; \frac{m_b^2 N_c}{8\pi^2}\frac{(s - m_b^2)^2}{s} \;-\; m_b^3\langle\bar{q}q\rangle\,\delta(p^2 - m_b^2) + \mathcal{O}\big(\alpha_s, \langle G^2\rangle\big)\,. \tag{2.32}$$

To make progress we estimate the unknown contribution of ρ^{cont} on the LHS by making use of 'quark-hadron duality'. If we had a perfect[4] all orders (in α_s and condensates) computation of $\rho^{\text{pert}}(s)$, it would exactly reconstruct the hadronic side, e.g. ρ^{cont}. There would be a *local* duality between the quark computation and the hadron one, $\rho^{\text{pert}}(s) = \rho^{\text{cont}}(s)$. This however is too bold a statement as typically we only manage the first few terms in the perturbative and condensate

[4]Much discussion of *duality violations* and their importance can be found in [105]. Practically the Borel transformation (2.36) suppresses the importance of any violations.

expansions. Instead one can consider an averaged version over some interval $s \in [s_1, s_2]$, possibly with some weight function $\omega(s)$

$$\int_{s_1}^{s_2} \omega(s)\rho^{\rm pert}(s)\,{\rm d}s \;\approx\; \int_{s_1}^{s_2} \omega(s)\rho^{\rm cont}(s)\,{\rm d}s\;, \tag{2.33}$$

referred to as *global* quark-hadron duality. Standardly in the literature (see for example the review [106]) one takes

$$\int_{s_0}^{\infty} \frac{\rho^{\rm pert}(s)}{s-p^2}\,{\rm d}s \;=\; \int_{s_0^{\rm cont}}^{\infty} \frac{\rho^{\rm cont}(s)}{s-p^2}\,{\rm d}s\;, \tag{2.34}$$

where s_0 is an effective threshold which we fit. Then our sum rule takes the more manageable form

$$\frac{m_B^4 f_B^2}{m_B^2-p^2} \;=\; \int_{m_b^2}^{s_0} \frac{\rho^{\rm pert}(s)}{s-p^2}\,{\rm d}s \;+\; \text{subtr.}\,. \tag{2.35}$$

The final improvement to (2.35) is to perform a Borel transform from p^2 to a new variable M^2. Formally the Borel transform $\mathcal{B}_{M^2}$ of $\Pi(p^2)$ is the distinguished limit

$$\big(\mathcal{B}_{M^2}\Pi(p^2)\big)(M^2) \;=\; \lim_{\substack{-p^2,n\to\infty \\ -p^2/n=M^2}} \frac{(-p^2)^{n+1}}{n!}\left(\frac{\rm d}{{\rm d}p^2}\right)^n \Pi(p^2)\,, \tag{2.36}$$

though practically we need only the results ($k>0$)

$$\mathcal{B}_{M^2}\left[\frac{1}{(m^2-p^2)^k}\right] \;=\; \frac{1}{(k-1)!}\frac{e^{-m^2/M^2}}{(M^2)^{k-1}} \tag{2.37}$$

$$\mathcal{B}_{M^2}\big[(p^2)^k\big] \;=\; 0\,. \tag{2.38}$$

The second of these means the Borel transform identically kills the subtraction terms. Further the Borel transform provides a factorial improvement in the convergence of the condensate expansion. This leads to the final form for our sum rule

$$m_B^4 f_B^2\, e^{-m_B^2/M^2} \;=\; \int_{m_b^2}^{s_0} \rho^{\rm pert}(s) e^{-s/M^2}\,{\rm d}s\;, \tag{2.39}$$

and so f_B can be extracted by evaluating

$$f_B^2 \;=\; \frac{m_b^2}{m_B^4}\left[\frac{3}{8\pi^2}\int_{m_b^2}^{s_0} \frac{(s-m_b^2)^2}{s} e^{-s/M^2}\,{\rm d}s\right.$$

$$- m_b\langle\bar{q}q\rangle e^{-m_b^2/M^2}\Big] e^{m_B^2/M^2} + \mathcal{O}\big(\alpha_s, \langle G^2\rangle\big)\,. \quad (2.40)$$

The Borel transform exponentially suppresses higher-s (higher energy) contributions. Indeed, in place of the subtractions the exponential remedies any divergence as $s \to \infty$ in the integrand (though of course it is cut-off at s_0). The other advantage is that the unknown higher energy continuum contributions, which we are estimating via quark-hadron duality, are also suppressed relative to the pole.

The only[5] remaining issue is what values to choose for s_0 and M^2. The effective threshold s_0 should be near the onset of multi-particle states, around $(m_B + 2m_\pi)^2$ (or $(m_B + m_\rho)^2$). However really this parameter is fitted, usually using the Daughter (or derivative) Sum Rule (DSR). The idea is that by taking the derivative of (2.39) with respect to $-1/M^2$

$$m_B^2 \cdot m_B^4 f_B^2\, e^{-m_B^2/M^2} \;=\; \int_{m_b^2}^{s_0} s\,\rho^{\rm pert}(s) e^{-s/M^2}\,{\rm d}s\;, \quad (2.41)$$

we can generate a consistency condition. Taking the ratio of (2.41) to (2.39) the decay constant drops out

$$m_B^2 \;=\; \left(\int_{m_b^2}^{s_0} s\,\rho^{\rm pert}(s) e^{-s/M^2}\,{\rm d}s\right) \Big/ \left(\int_{m_b^2}^{s_0} \rho^{\rm pert}(s) e^{-s/M^2}\,{\rm d}s\right), \quad (2.42)$$

and we can use this to fix s_0 provided we know M^2. The latter is fixed by balancing two competing factors. Higher dimensional condensates enter the SR (2.40) suppressed by powers of the Borel mass, e.g. the mixed condensate enters as $\langle\bar{q}\sigma\cdot Gq\rangle/M^2$. This is the Borel analogue of the Wilson coefficient scaling mentioned earlier. At too-low M^2 neglected higher dimensional condensates will not be adequately suppressed. On the other hand at too-high M^2 the exponential e^{-s/M^2} does not sufficiently suppress the higher energy continuum and the quark-hadron duality approximation becomes unreliable.

Ideally there is a *Borel window*, a range of intermediate M^2 where both demands can be satisfied. In this window f_B should be approximately flat with M^2, with the flatness serving as a measure of the quality of the sum rule. Practically we content ourselves to suppressing the condensates to $\lesssim 20$ - 30% of the perturbative

[5]There is also some ambiguity over the b-quark mass as quarks are confined and so do not have a physical mass. Corresponding scheme choices will be discussed in Section 4.1 and so we do not elaborate here.

(𝟙) result while also requiring the continuum contribution to be $\lesssim 30\%$ of the total dispersive integral. To be specific we ideally require

$$\int_{s_0}^{\infty} \rho^{\text{pert}}(s) e^{-s/M^2}\,\mathrm{d}s \lesssim \frac{3}{10}\int_{m_b^2}^{\infty} \rho^{\text{pert}}(s) e^{-s/M^2}\,\mathrm{d}s\ . \tag{2.43}$$

Of course including corrections in α_s we also require a scheme such that these converge as well. A more complete numerical study, including $\mathcal{O}(\alpha_s^2)$ perturbative corrections, partial m_q dependence and condensates up to dimension-5 in the sum rule leads to the extraction $f_B = 210 \pm 19\,\text{MeV}$ [107].

As well as decay constants, SVZ sum rules have been used to extract quark masses, form factors and even exotic hadron spectroscopy [106, 108, 109]. While they have enjoyed great success, there are certain drawbacks. Higher dimensional condensates are not well known and, like α_s^n corrections, are difficult to calculate. Achieving better than a 10% accuracy is generally difficult. Additionally certain sum rules are unfeasible (e.g. the light pseudoscalar channel) due to being plagued with extra non-perturbative difficulties known as instantons [105, 110, 111]. While we shall not go into detail, these are often signalled by a lack of a Borel window in the sum rule.

In the calculation of 3-point functions the method of Light-Cone Sum Rules (LCSR) [112–115] has evolved in place of SVZ sum rules which can become unsuitable due to issues with OPE convergence [116]. In LCSR products of currents are expanded on the light cone $x^2 = 0$, with *distribution amplitudes* being the analogue of vacuum condensates. In our calculations we require only 2-point correlators and thus SVZ sum rules are sufficient.

2.2 Infrared Divergences

The existence of infrared (IR) divergences in quantum field theory was recognised right from its inception. These come in two types: soft and collinear[6]. Both of these arise due to the presence of massless particles (like photons and gluons) in the theory. Roughly speaking, soft divergences appear when an on-shell particle emits a massless particle of vanishing energy while collinear divergences occur

[6]Historically the label 'infrared' referred specifically to the soft divergence, with the collinear divergence being known as the 'mass singularity'. We use the term infrared to refer to both types.

when a massless particle emits another massless particle travelling in the same direction. If both conditions are met, the resulting divergence is called soft-collinear. Because of this distinction collinear divergences are often specifically known as hard-collinear divergences.

In contrast to UV (high energy) divergences, IR divergences involve low energy behaviour. While UV divergences only appear in virtual diagrams and are renormalised away, IR divergences appear in both real and virtual. Indeed this is crucial as cancellation occurs between virtual loops and real emissions.

In the SM photons and gluons cause soft divergences in their coupling with quarks and leptons. As all fundamental fermions are massive there are no true collinear divergences in these interactions, however as the fermions can be light there can be numerically large effects. In QCD gluon self interactions can cause complications though of course experimentally gluons appear as jets.

To illustrate the nature of IR divergences first consider a real photon emission from a lepton of mass m_ℓ. If the photon has momentum k and the lepton has momentum l then in the diagram there will be a propagator with momentum $k+l$.

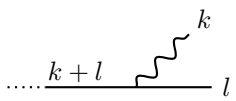

$$\sim \quad \frac{1}{(k+l)^2 - m_\ell^2} \quad \xrightarrow{\substack{k^2=0,\\ l^2=m_\ell^2}} \quad \frac{1}{2k\cdot l}$$

To generate an IR divergence, both the photon and lepton must be on-shell. Crucially the photon is massless $k^2 = 0$ (and $l^2 = m_\ell^2$), and so the propagator $(k^2 + 2k\cdot l + l^2 - m_\ell^2)^{-1}$ becomes $(2k\cdot l)^{-1}$. Parameterising $k^\mu = E_\gamma(1, \hat{\boldsymbol{k}})$ and $l^\mu = (l^0, \boldsymbol{l})$ with $l^0 = \sqrt{|\boldsymbol{l}|^2 + m_\ell^2}$ and $\hat{\boldsymbol{k}}$ being a unit vector then

$$\frac{1}{2k\cdot l} = \frac{1}{2E_\gamma\big(\sqrt{|\boldsymbol{l}|^2 + m_\ell^2} - |\boldsymbol{l}|\cos\theta\big)}\,, \tag{2.44}$$

where θ is the angle between the photon and lepton. As we let the photon become soft $E_\gamma \to 0$ there is a divergence. Of course really we should analyse at the level of cross sections. The above diagram is squared (giving a $1/E_\gamma^2$ divergence) and then integrated over the photon phase space. This involves a photon energy integral $\mathrm{d}E_\gamma$ as well as an angular integral $\mathrm{d}\Omega_{d-1}$ ($\Omega_3 = 4\pi$). The energy integral is

$$\int \underbrace{(E_\gamma)^{d-3}}_{\text{phase space}} \times \frac{1}{E_\gamma^2}\,\mathrm{d}E_\gamma \xrightarrow{d=4} \int \frac{\mathrm{d}E_\gamma}{E_\gamma}\,, \tag{2.45}$$

which in $d = 4$ diverges logarithmically at its lower limit. If we regulated this soft divergence by giving the photon a small mass m_γ, the divergence would appear as $\ln m_\gamma$ terms in the result. Alternatively we can use dimensional regularisation to regulate the IR as well as the UV. In $d = 4-2\epsilon$ the integral becomes $\int \mathrm{d}E_\gamma \, / E_\gamma^{1+2\epsilon}$ which does not diverge for finite $\epsilon < 0$. Like with the UV the divergence appears as poles in ϵ and we distinguish these types of poles with labels ϵ_{IR} and ϵ_{UV}.

The collinear divergence on the other hand arises from the angular integration in the limit of a massless lepton. The propagator (2.44) becomes $(1 - \cos\theta)^{-1}$ and diverges when the photon and lepton become *collinear* to each other, $\theta \to 0$. Keeping the lepton mass non-zero to regulate this divergence we encounter integrals like

$$\int \frac{\mathrm{d}\Omega_{d-1}}{(l^0 - |\boldsymbol{l}|\cos\theta)^n} \xrightarrow{d=4} 2\pi \int_0^\pi \frac{\sin\theta \, \mathrm{d}\theta}{(l^0 - |\boldsymbol{l}|\cos\theta)^n} \,, \tag{2.46}$$

where typically $n = 1, 2$. For $n = 1$ we generate a logarithmic dependence on the lepton mass

$$2\pi \int_0^\pi \frac{\sin\theta \, \mathrm{d}\theta}{l^0 - |\boldsymbol{l}|\cos\theta} \;=\; \frac{2\pi}{|\boldsymbol{l}|} \ln\!\left(\frac{l^0 + |\boldsymbol{l}|}{l^0 - |\boldsymbol{l}|}\right) \;=\; -\frac{2\pi}{|\boldsymbol{l}|} \log m_\ell^2 + \cdots \,, \tag{2.47}$$

which diverges as $m_\ell \to 0$. Such terms are known as hard-collinear (HC) logs. The electron mass m_e is very light compared to a B-meson and so a hard-collinear log of the form $\ln(m_e/m_B)$ is potentially a large important effect. In DimReg any soft-collinear divergences appear as $\epsilon_{\mathrm{IR}}^{-1} \ln m_\ell^2$ terms, which become double poles $1/\epsilon_{\mathrm{IR}}^2$ in the massless limit.

For virtual diagrams IR divergences are generated in loop integrations in regions of low photon momentum. For example consider the triangle graph

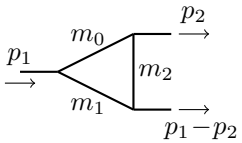

$$\begin{aligned} &= C_0\big(p_1^2, (p_1 - p_2)^2, p_2^2, m_0^2, m_1^2, m_2^2\big) \\ &= \frac{(2\pi\mu)^{2\epsilon}}{i\pi^2} \int \frac{\mathrm{d}^d k}{[k^2 - m_0^2][(k + p_1)^2 - m_1^2][(k + p_2)^2 - m_2^2]} \,. \end{aligned} \tag{2.48}$$

This three-point scalar integral is the Passarino-Veltman function C_0 with FeynCalc [117, 118] conventions and normalisation $(2\pi\mu)^{2\epsilon} \int \frac{\mathrm{d}^d k}{i\pi^2}$. Similar 1- (tadpole), 2- (bubble) and 4- (box) propagator integrals are known as A_0, B_0 and

D_0 functions respectively[7]. The Passarino-Veltman functions [119] are a useful basis for one-loop integrals and a brief summary of them is given in Appendix A.1.

If the external momenta are on-shell $p_1^2 = m_1^2$, $p_2^2 = m_2^2$ and they exchange a massless photon, $m_0 = 0$, then the integral becomes

$$\frac{(2\pi\mu)^{2\epsilon}}{i\pi^2}\int \frac{\mathrm{d}^d k}{k^2[k^2+2k\cdot p_1][k^2+2k\cdot p_2]} \overset{\text{small k}}{\sim} \int \frac{k^3\,\mathrm{d}k}{k^2 k k} \sim \int \frac{\mathrm{d}k}{k}\,. \tag{2.49}$$

This gives a logarithmic soft divergence at small k as k^2 can be neglected compared to $k\cdot p_{1,2}$ in the denominators. More properly we can perform the k^0 integral via residues, picking up the pole at $k^0 = |\boldsymbol{k}| - i\varepsilon'$ which forces the photon on-shell.

$$\frac{(2\pi\mu)^{2\epsilon}}{2\pi}\int \frac{\mathrm{d}^{d-1}\boldsymbol{k}}{2|\boldsymbol{k}|}\frac{1}{(p_1^0|\boldsymbol{k}| - \boldsymbol{p_1}\cdot\boldsymbol{k})(p_2^0|\boldsymbol{k}| - \boldsymbol{p_2}\cdot\boldsymbol{k})} = \frac{(2\pi\mu)^{2\epsilon}}{4\pi}\int |\boldsymbol{k}|^{-1-2\epsilon}\,\mathrm{d}|\boldsymbol{k}|\int \frac{\mathrm{d}\Omega_{3-2\epsilon}}{(p_1^0 - \boldsymbol{p_1}\cdot\hat{\boldsymbol{k}})(p_2^0 - \boldsymbol{p_2}\cdot\hat{\boldsymbol{k}})}\,. \tag{2.50}$$

Integrating the photon energy $|\boldsymbol{k}|$ from 0 to some cut-off Λ the soft divergence appears as poles in ϵ_{IR}

$$\int_0^\Lambda \frac{\mathrm{d}|\boldsymbol{k}|}{|\boldsymbol{k}|^{1+2\epsilon}} = \frac{\Lambda^{-2\epsilon}}{-2\epsilon} = \frac{-1}{2\epsilon_{\mathrm{IR}}} + \ln\Lambda\,. \tag{2.51}$$

As before collinear divergences are generated from the angular integration when the photon is parallel to $\boldsymbol{p_1}$ or $\boldsymbol{p_2}$. In general virtual soft divergences appear when a massless particle is exchanged between two on-shell particles while virtual collinear divergences appear when a massless on-shell particle couples to two massless propagators. At one-loop the IR divergences of any N-point function can be written in terms of 3-point functions (C_0's) by the Dittmaier algorithm [120].

There are considerable similarities between the real and virtual calculations which really is not surprising in view of the optical theorem. This similarity enables IR divergences to cancel between real and virtual diagrams in sufficiently inclusive quantities.

[7]Power counting arguments imply A_0 and B_0 are UV divergent, while C_0 and higher point functions are IR divergent.

2.2.1 Cancellation

In any sensible theory, measurable quantities should not contain IR divergences. Observables free of IR divergences are called *infrared safe*. In QED, cancellation of the soft divergence order by order in α is guaranteed by the Bloch-Nordsieck theorem[8] [124]. Unlike UV divergences, IR divergences cancel at the cross-section level not in Green's functions. The idea is that any detector will have a small but finite energy resolution ΔE, below which photons cannot be detected. The cross section for a process $i \to f$ is indistinguishable from one for the same process with the addition of a very soft photon and so these cross sections must be added.

$$\sigma(i \to f) + \sigma(i \to f\gamma)_{E_\gamma < \Delta E} \tag{2.52}$$

Soft divergences from $\mathcal{O}(\alpha)$ virtual diagrams in $\sigma(i \to f)$ are exactly cancelled by the $\mathcal{O}(\alpha)$ real soft divergence in $\sigma(i \to f\gamma)$ leaving a IR finite result. The logarithmic soft divergence is replaced by a $\ln \Delta E$ dependence in the result. Only the sum of the radiative and non-radiative cross-sections is a sensible observable. A similar argument, invoking finite angular resolution, can be made for collinear divergences. At higher orders soft divergences *exponentiate*, that is $\mathcal{O}(\alpha^n)$ corrections take the form $(\alpha \ln \Delta E)^n$ [125].

While practical, citing finite detector efficiency is a little unsatisfactory from a field theory viewpoint. Really in theories with massless particles the idea of exactly what we mean by a particle state gets called into question. Physically massless charged particles are always accompanied by a cloud of photons with an electric field perpendicular to the plane of their motion. If the charged particle had a mass we could go to its rest frame which would separate off the collinear photons. However in the limit of vanishing mass this separation becomes impossible. In QED we are forced to abandon the idea of a one-particle Fock space in favour of a coherent state formulation, as done originally by Faddeev and Kulish[9] [130].

Similar issues appear with radiation in and out of *initial* state particles. An

[8] Originally proved in 1937, with improvements by Pauli and Fierz [121] and Jauch and Rohrlich [122]. A more comprehensive analysis was later done using modern field theoretic methods by Yennie et al. [123].

[9] They (and others [126–129]) showed how a non-vanishing S-matrix can be ascertained by building a physical charged electron (say) out of linear combinations of $|e^-; \gamma_1, \gamma_2, \ldots \gamma_n\rangle_{E_\gamma^i < \Delta E}$ states like as with the simple harmonic oscillator in quantum mechanics. Reminiscent of renormalisation, IR divergences are essentially absorbed into the definition of the states.

analogous and more familiar situation is that of QCD. For example in proton-proton scattering the incoming states are valence uud quarks that live in a sea of quarks and gluons. This mix necessitates the introduction of Parton Distribution Functions (PDFs), $f_i(x)$, which characterise the probability that a parton i inside a proton carries a fraction x of the proton's momentum. IR divergences can be absorbed into these functions, inducing scale dependence described by the DGLAP equations [131–133]. Universal objects known as splitting functions P_{ij} describe the collinear splitting of two partons i and j. There are QED counterparts to PDFs known as electron distribution (or Weizsäcker-Williams [134, 135]) functions though these are rarely used[10] as α is small.

While Bloch-Nordsieck guarantees the cancellation of soft divergences, the more general Kinoshita-Lee-Naeunberg (KLN) theorem [136, 137] assures all IR divergences cancel in any unitary quantum field theory provided one is careful to sum over all degenerate states. For example a massless electron is collinear degenerate from an electron accompanied by a parallel photon and so both states should be treated on equal footing. Hard-collinear logs $\ln m_\ell$ (which diverge as the regulator $m_\ell \to 0$) generated from lepton-photon interactions should therefore cancel if one suitably sums over the whole collinear region. This means we must include collinear photons of all (kinematically allowed) energies, that is be fully inclusive in the photon. However in practise we often prematurely cut-off the photon energy and so HC logs can appear. In general these can be predicted from splitting functions (unitarity) however in certain important cases the KLN theorem does not apply.

The leptonic $\bar{B} \to \ell\bar{\nu}(\gamma)$ decay we care about in this thesis is an important example of this due to its helicity suppression. Let $\Gamma^{(n)}$ denote the $\mathcal{O}(e^n)$ contribution to the decay rate, then the tree and $\mathcal{O}(\alpha)$ results are schematically

$$\begin{aligned} \Gamma^{(0)} &\propto m_\ell^2 \\ \Gamma^{(2)} &\propto \alpha\, C_{\text{V-A}}(E_\gamma^{\text{cut}})\, m_\ell^2 \ln m_\ell + \text{non-HC}\,, \end{aligned} \tag{2.53}$$

with $C_{\text{V-A}}(E_\gamma^{\text{cut}})$ a function of the maximum photon energy that is included in the integration, $E_\gamma < E_\gamma^{\text{cut}}$. *Relative* to the tree level, the $\mathcal{O}(\alpha)$ HC logs are numerically important as the factor of m_ℓ^2 suppressing them cancels. However it is precisely this m_ℓ^2 that allows the decay to circumvent the KLN theorem. As $m_\ell^2 \ln m_\ell \to 0$ as $m_\ell \to 0$ there is actually no divergence. As this is not a true

[10] In our case, $\bar{B} \to \ell\bar{\nu}(\gamma)$, they are definitely not necessary as m_B is certainly not small.

collinear divergence the KLN theorem does not apply and so the HC logs[11] need not cancel when fully inclusive. That is $C_{\text{V-A}}(E_\gamma^{\text{cut}} \to \frac{1}{2}m_B) \neq 0$. Further the HC logs can no longer be predicted from the splitting function meaning there can be structure-dependent effects. Conversely, with an S-P (non-SM) type interaction the decay is no longer helicity supressed. The KLN theorem then does apply and S-P HC logs must cancel, $C_{\text{S-P}}(E_\gamma^{\text{cut}} \to \frac{1}{2}m_B) = 0$. This property makes the S-P decay a useful testing ground when looking at structure-dependent logs.

Helicity suppression is not the only way the KLN theorem may be bypassed. It does not apply to logs of composite particles, e.g. $\ln m_K$, or if one works at the differential level [138]. The latter case will be discussed further in Section 2.3.1. Numerical calculations in quantum field theory are only feasible if IR sensitive terms are properly dealt with. In this thesis we shall slice out soft and collinear regions, dealing with them separately to the rest of the integrand. Common alternate techniques are subtraction methods where difficult integrals are tamed by adding and subtracting an analytically calculable part.

2.2.2 Low's Theorem

Low's theorem [139–142] formalises the idea that long wavelength photons cannot resolve the structure of a composite particle. In the soft photon limit the spin of the particle is not resolved. For a transition $i \to f\gamma$ with photon momentum k and polarisation $\epsilon^*(k)$

$$\langle f\gamma|S|i\rangle = es_e \sum_j \hat{Q}_j \left[\frac{\epsilon^* \cdot \hat{p}_j}{k \cdot \hat{p}_j} - i\epsilon_\mu^* k_\nu \frac{J_j^{\mu\nu}}{k \cdot \hat{p}_j}\right] \langle f|S|i\rangle + \mathcal{O}(E_\gamma)\,, \tag{2.54}$$

where $J_j^{\mu\nu}$ is the total angular momentum operator[12] for the j^{th} particle involved in the interaction. We employ the hat notation for the particle momenta p_j and charge Q_j where $\hat{p}_j = \pm p_j$ and $\hat{Q}_j = \pm Q_j$ depending on whether the particle in ingoing $(-)$ or outgoing $(+)$, with $\hat{Q}_{\bar{j}} = -\hat{Q}_j$. This has the advantage that charge conservation takes the conveniently simple form $\sum_j \hat{Q}_j = 0$.

Equation (2.54) is ordered in powers of the photon energy E_γ. The first two terms in this expansion, the E_γ^{-1} and E_γ^0 terms, are universal with structure-dependence

[11] While as discussed these are technically not true collinear logs, they are generated from collinear physics and we shall still refer to them as thus for brevity.

[12] For scalars this takes the form $J_j^{\mu\nu} = i(\hat{p}_j^\mu \partial_{\hat{p}_j}^\nu - \hat{p}_j^\nu \partial_{\hat{p}_j}^\mu)$. For generalisation to Yang-Mills, higher spin etc., see e.g. [143].

only appearing in the $\mathcal{O}(E_\gamma^1)$ term. The particle's spin appears in the E_γ^0 term through the angular momentum operator while the E_γ^{-1} term (which leads to the soft divergence) is independent even of that. This simplicity leads to the previously mentioned exponentiation of soft divergences sometimes referred to as 'Weinberg's universal form' after the exposition of the IR behaviour of photons and gravitons in [144]. This reads

$$\Gamma(i \to f)_{\Delta E} \;=\; \Gamma^{(0)}(i \to f) e^{-A \ln(\Delta E/\Lambda)}\,, \tag{2.55}$$

where on the LHS $\Gamma(i \to f)_{\Delta E}$ is shorthand for the transition $i \to f$ at all orders in α with the accompaniment of any number of soft photons provided their total energy is less than ΔE. Again Λ is some hard cut off and A is defined as

$$A \;=\; \frac{\alpha}{2\pi} \sum_{jk} \hat{Q}_j \hat{Q}_k \frac{1}{\beta_{jk}} \ln\!\left(\frac{1+\beta_{jk}}{1-\beta_{jk}}\right), \qquad \beta_{jk} = \frac{\beta_j + \beta_k}{1+\beta_j\beta_k}\,, \tag{2.56}$$

with β_{jk} being the relative velocities of the particles j, k in the j-k rest frame. We note the general feature that in the soft limit the radiative rate becomes proportional to the tree level result, $\Gamma^{(0)}$.

2.3 Scalar QED

While there are no fundamental charged scalar particles in the SM there are innumerable scalar hadrons. Treating these as point-like, their electromagnetic interaction can be found via minimal coupling with Lagrangian[13]

$$\mathcal{L}_{\text{SQED}} = (D_\mu \phi)^* (D^\mu \phi) - m^2 |\phi|^2\,, \tag{2.57}$$

with ϕ a scalar field. Somewhat confusingly the term 'scalar QED' is commonly used more generally to refer to treating hadrons as point-like, even if the actual hadron in question is not a scalar. Scalar QED has a 3-point and a 4-point vertex, with the 3-point vertex carrying momentum dependence. For a point-like scalar particle of charge eQ_s this reads

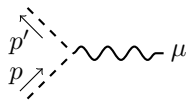

$$= \; -ies_e Q_s (p + p')^\mu\,, \tag{2.58}$$

[13]Properly of course one should also include a quartic $|\phi|^4$ interaction in (2.57) to render the theory renormalisable.

with dashed lines denoting the scalar. The weak decay of a scalar $\bar{B}$-meson can be modelled in an EFT by matching a $\bar{B}$ field to the axial quark current $J_5^\mu = \bar{q}\gamma^\mu\gamma_5 b$ to reproduce $\langle 0|J_5^\mu|\bar{B}(p_B)\rangle = if_B(p_B)^\mu$. While not an effective theory in the traditional sense, this matching neglects short distance (high energy) structure and so is often referred to as a mesonic EFT [90]. The correct prescription is

$$J_{5\,\mu} \longrightarrow -f_B D_\mu \bar{B} = -f_B\big(\partial_\mu \bar{B} + ies_e Q_{\bar{B}} A_\mu \bar{B}\big)\,, \tag{2.59}$$

where for gauge-invariance we must use the covariant derivative. Thus in the EFT there are photon emissions from the weak vertex itself, usually referred to as the contact term contribution.

Experimentally QED effects are modelled using Monte-Carlo generators such as PHOTOS [145–148], or the PHOTONS++ module [149] of Sherpa [150]. In general these work well for assessing QED effects in experimental measurements, for example in the well-studied $R_{K^{(*)}}$ [151], however they can be limited by their use of scalar QED to model hadron interactions. The programs are based on resumming leading log QED corrections using the soft exponentiation (2.55) and using splitting functions to capture HC logs. Virtual corrections are ascertained from their real counterparts by exploiting KLN cancellations. Thus these packages can fall down if (a) the HC logs cannot be predicted from the splitting function (KLN does not apply) and/or (b) structure-dependent effects are relevant. Both of these are pertinent to the $\bar{B} \to \ell\bar{\nu}(\gamma)$ decay where a scalar QED based Monte-Carlo may struggle to capture all QED effects.

In this thesis we aim to go beyond the point-like approximation, capturing structure-dependence which could be used in future to inform a purpose built Monte-Carlo for the decay. The aim of this present chapter is to discuss calculations in scalar QED, using $\bar{B} \to \bar{K}^{(*)}\ell\bar{\ell}(\gamma)$ as an example before studying the $\bar{B} \to \ell\bar{\nu}(\gamma)$ decay in detail.

2.3.1 $\bar{B} \to \bar{K}\ell\bar{\ell}(\gamma)$

A comprehensive analysis of QED in the semi-leptonic $\bar{B} \to \bar{K}\ell\bar{\ell}(\gamma)$ decay in scalar QED was performed in [90] based on earlier work [73, 152–154]. In this work it was demonstrated how HC logs do not cancel, even when fully inclusive in the photon, in some differential variables. In this decay momentum conservation

takes the form

$$p_B = p_K + l_1 + l_2 \quad (+k)\,, \tag{2.60}$$

and so when the photon is present, one can be differential in *either* $q_\ell^2 = (l_1 + l_2)^2$ *or* $q_0^2 = (p_B - p_K)^2$ with $q_\ell = q_0 - k$. The former is the standard choice at hadron colliders where the $\bar{B}$ momentum is unknown while the latter are referred to as 'B-factory' variables. The $\bar{B} \to \bar{K}$ transition is modelled by the form factors $f_\pm$ defined in (1.15). These can be incorporated into an effective mesonic weak Lagrangian via an expansion

$$\mathcal{L}_{\rm EFT} \propto \bar{\ell}_1 \Gamma^\mu \ell_2 \sum_{n\geq 0} \frac{f_+^{(n)}(0)}{n!} (-D^2)^n [(D_\mu B^\dagger) K \mp B^\dagger (D_\mu K)] + \text{h.c.}\,, \tag{2.61}$$

with $\Gamma^\mu \equiv \gamma^\mu (C_V - C_A \gamma_5)$ and $C_{V(A)}$ vector (axial) coefficients. The derivative expansion allows a consistent and gauge-invariant treatment of the $q^2_{(0,\ell)}$ dependence of the form factors beyond LO in QED. While there is structure-dependence contained in the form factors (FF), the meson-photon interaction is still treated in the point-like approximation and so this is still fundamentally a scalar QED calculation. Working in this effective field theory (EFT) means ambiguity over counterterms which can only really be resolved via a full matching to QCD. The calculation [90] was performed at $\mathcal{O}(\alpha)$ (here 1-loop) with real IR divergences handled via two cut-off phase space slicing [155, 156] (with masses).

Nothing unusual was found with the cancellation of soft divergences at the double differential level, however HC logs only cancel in the fully photon inclusive case when differential in q_0^2 and not in q_ℓ^2. Roughly speaking this can be understood by considering that the decay of a scalar particle $X \to \ell\bar{\ell}$ is infrared safe (non-differential). In q_0 variables the $\bar{B}$ and $\bar{K}$ can be treated as a single particle of momentum $q_0 = p_B - p_K$ and so by the KLN theorem collinear divergences must cancel. Numerically when fully inclusive in the photon, QED effects at the double differential level are found to be $< 2\%$ in q_0^2 variables while as much as 10% in q^2 variables (at low q^2) for the electron channel. Note that non-cancelling $\ln m_K$ terms can cause a $\mathcal{O}(2\%)$ effect.

With instead a tight photon energy cut-off, HC logs exist in any variable and large effects can be found. This led to the dedicated Monte-Carlo [151] for R_K analysis. From [90] the QED R_K theory prediction is a correction of +1.7% (cf. +3% in earlier work [73]). These QED effects are smaller because R_K is integrated over q^2 (not differential). Potentially structure-dependent effects could modify this,

though these are generally precluded on gauge invariance arguments in [90]. We stress again that such arguments do not apply to $\bar{B} \to \ell\bar{\nu}(\gamma)$.

2.3.2 $\bar{B} \to \bar{K}^*\ell\bar{\ell}(\gamma)$

In this section we briefly present the extension of 2.3.1 to vector K^* mesons. This is for pedagogical purposes only to illustrate some of the ideas of Section 2.2. In particular we consider the real amplitude to demonstrate gauge invariance, Low's theorem and the appearance of the splitting function. Given that the LHCb results for R_{K^*} are now broadly consistent with the SM [79, 80] and that HC logs are expected to match [90] with little structure-dependent effects, we did not perform a full calculation.

The K^* is a massive vector (but not gauge) boson described by the Proca Lagrangian[14] with minimal coupling

$$\mathcal{L}_{K^*} = -\frac{1}{2}\big(D_{[\mu}K^*_{\nu]}\big)^\dagger\big(D^{[\mu}(K^*)^{\nu]}\big) + m^2_{K^*}(K^*_\mu)^\dagger K^{*\mu}\,, \tag{2.62}$$

where $[\mu\cdots\nu]$ denotes antisymmetrisation in the indices μ,ν. From now on we drop the * superscript on the K^*_μ field. Being massive the K^* has 3 polarisation vectors $\eta(p_K)$ which by the equation of motion automatically satisfy $\eta(p_K)\cdot p_K = 0$. This is not to be confused with the photon polarisation vectors $\epsilon(k)$ which satisfy $\epsilon(k)\cdot k = 0$ by a gauge choice (Lorenz gauge). Like with the scalar field (2.62) leads to 3- and 4-point vertices with the 3-point vertex having momentum dependence. Denoting vector fields with a dotted line a vector particle of charge eQ_V has 3-point vertex and propagator

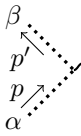

$$= \; -\,ies_eQ_V\big(p'_\alpha g_{\mu\beta} + p_\beta g_{\mu\alpha} - (p+p')_\mu g_{\alpha\beta}\big) \tag{2.63}$$

$$= \; \frac{i\mathcal{P}^*_{\alpha\beta}(p)}{p^2 - m^2_{K^*}}\,, \qquad \mathcal{P}^*_{\alpha\beta}(p) = -g_{\alpha\beta} + \frac{p_\alpha p_\beta}{m^2_{K^*}}\,. \tag{2.64}$$

[14] This is essentially just $-\frac{1}{4}F^2 + \frac{1}{2}m^2_\gamma A^2$ as for the gauge field with a factor of 2 as K^* is complex. Like the photon field the timelike component K^*_0 is non-dynamical ($\dot{K}^*_0$ drops out of the Lagrangian) and the + sign in (2.62) means the spacelike components have the correct sign. Unlike the photon field the condition $\partial^\mu K^*_\mu = 0$ is a direct consequence of the equation of motion $\partial^\mu F_{\mu\nu} + m^2 K^*_\nu = 0$ for $m^2 \neq 0$. As is well-known the $m \to 0$ limit is not smooth.

The $\bar{B} \to \bar{K}^* \ell^+ \ell^-$ transition is described by the form factors[15]

$$\langle \bar{K}^*(p_K,\eta)|\bar{s}\gamma^\mu(1\mp\gamma_5)b|\bar{B}(p_B)\rangle = \pm\, P_P^\mu\, \mathcal{V}_P(q^2) \pm \sum_{i=1}^{3} P_i^\mu \mathcal{V}_i(q^2)\,, \tag{2.65}$$

with $q = p_B - p_K$, $\epsilon_{0123} = +1$ and the Lorentz structures

$$\begin{aligned} P_P^\mu &= i(\eta^*\cdot q)q^\mu\,, \qquad P_1^\mu \;=\; 2\epsilon^\mu{}_{\alpha\beta\gamma}\eta^{*\alpha}p_K^\beta q^\gamma \\ P_2^\mu &= i\Big((m_B^2 - m_{K^*}^2)\eta^{*\mu} - (\eta^*\cdot q)(p_B+p_K)^\mu\Big) \\ P_3^\mu &= i(\eta^*\cdot q)\Big(q^\mu - \frac{q^2}{m_B^2-m_{K^*}^2}(p_B+p_K)^\mu\Big)\,. \end{aligned} \tag{2.66}$$

Defining the tensor structure

$$\begin{aligned} T^{\alpha\beta\rho\mu} \;=\; &\epsilon^{\mu\alpha\beta\rho}\,\mathcal{V}_1 + ig^{\alpha\beta}g^{\rho\mu}\,\mathcal{V}_2 + ig^{\alpha\rho}g^{\beta\mu}\big(\mathcal{V}_3+\mathcal{V}_P\big) \\ &- ig^{\alpha\mu}g^{\beta\rho}\bigg(\mathcal{V}_2 + \frac{q^2}{m_B^2-m_{K^*}^2}\mathcal{V}_3\bigg)\,, \end{aligned} \tag{2.67}$$

one recovers the correct LO amplitude

$$\begin{aligned} \mathcal{A}^{(0)} &\equiv \langle \bar{K}^*(p_K)\ell_1(l_1)\bar{\ell}_2(l_2)| - \mathcal{L}_{\rm EFT}^{K^*}|\bar{B}(p_B)\rangle \\ &= -\,g_{\rm eff}\,(p_B+p_K)_\alpha(p_B-p_K)_\beta\eta_\rho^*\,T^{\alpha\beta\rho\mu}\,\bar{u}(l_1)\Gamma_\mu v(l_2)\,, \end{aligned} \tag{2.68}$$

from the Lagrangian

$$\begin{aligned} \mathcal{L}_{\rm EFT}^{K^*} \;=\; g_{\rm eff}\bar{\ell}_1\Gamma_\mu\ell_2\Big(&B^\dagger\partial_\beta\partial_\alpha K_\rho - (\partial_\alpha\partial_\beta B)^\dagger K_\rho \\ &+ (\partial_\beta B)^\dagger\partial_\alpha K_\rho - (\partial_\alpha B)^\dagger\partial_\beta K_\rho\Big)T^{\alpha\beta\rho\mu} \;+\; \text{h.c.}\,. \end{aligned} \tag{2.69}$$

Above $g_{\rm eff}$ is an effective coupling constant and the external K^* (polarisation λ) satisfies $\langle \bar{K}^*(p_K,\lambda)|K_\mu(x)|0\rangle = \eta^*(p_K,\lambda)_\mu e^{ip_K\cdot x}$. We take the form factors as constant to justify them appearing in the Lagrangian. More properly one would have to add the tower of derivative operators like in (2.61). Gauge invariance[16]

[15] See [157, 158] for the relation to the more traditional FFs $A_{0-3}(q^2)$. This parameterisation is useful if one is to include the chromomagnetic matrix element $\langle \bar{K}^*|\bar{s}iq_\nu\sigma^{\mu\nu}(1\pm\gamma_5)b|\bar{B}\rangle$.

[16] In this case minimal coupling does not constrain us to a unique Lagrangian. The two derivatives $D_\alpha D_\beta$ in (2.69) commute at $\mathcal{O}(e^0)$ but not at $\mathcal{O}(e)$ as $[D_\alpha, D_\beta] = ies_eF_{\alpha\beta}$. The ordering of derivatives is not fixed at this level and this leads to a (gauge-invariant) ambiguity in the contact terms, cf. [159]. In the main text the contact terms are given using the ordering (2.69) (with $\partial \to D$). The three other options can be parameterised with an extra term $-ies_e\tilde{Q}F_{\alpha\beta}B^\dagger K_\rho$ in the bracket where $\tilde{Q} \in \{\hat{Q}_{\bar{B}}, \hat{Q}_{\bar{K}}, \hat{Q}_{\bar{B}} + \hat{Q}_{\bar{K}}\}$.

of the Lagrangian is restored by minimal coupling, allowing determination of the $\mathcal{O}(e)$ real amplitude

$$\begin{aligned}
\frac{-\mathcal{A}^{\bar{B}\to\bar{K}^*\ell\bar{\ell}\gamma}}{g_{\rm eff}es_e} &= \bar{u}(l_1)\left[\hat{Q}_{\ell_1}\frac{2l_1\cdot\epsilon^*+\not{\epsilon}^*\not{k}}{2l_1\cdot k}\Gamma\cdot H_0+\hat{Q}_{\bar{\ell}_2}\Gamma\cdot H_0\frac{2l_2\cdot\epsilon^*+\not{k}\not{\epsilon}^*}{2l_2\cdot k}\right]v(l_2)\\
&+ \hat{Q}_{\bar{B}}\frac{p_B\cdot\epsilon^*}{p_B\cdot k}L_0\cdot H_0|_{p_B\to p_B-k}\\
&+ \hat{Q}_{\bar{K}}\frac{p_K^\nu\epsilon^*\cdot\eta^*+\epsilon^{*\nu}k\cdot\eta^*-2\eta^{*\nu}p_K\cdot\epsilon^*}{2p_K\cdot k}[\mathcal{P}^*_{\nu\rho}L_0\cdot H_0^\rho]_{p_K\to p_K+k}\\
&+ \Big((\hat{Q}_{\bar{B}}+\hat{Q}_{\bar{K}})(p_B+p_K)_\alpha\epsilon^*_\beta+(\hat{Q}_{\bar{B}}-\hat{Q}_{\bar{K}})(p_B-p_K)_\beta\epsilon^*_\alpha\\
&\qquad +\hat{Q}_{\bar{K}}k_\beta\epsilon^*_\alpha-\hat{Q}_{\bar{B}}k_\alpha\epsilon^*_\beta\Big)L_{0\mu}\eta^*_\rho T^{\alpha\beta\rho\mu}\,, \qquad (2.70)
\end{aligned}$$

where for notational convenience we define

$$H_0^{\mu\rho}\equiv(p_B+p_K)_\alpha(p_B-p_K)_\beta T^{\alpha\beta\rho\mu}\,,\quad L_0^\mu\equiv\bar{u}(l_1)\Gamma^\mu v(l_2)\,, \qquad (2.71)$$

and $H_0^\mu=\eta^*_\rho H_0^{\mu\rho}$ such that $\mathcal{A}^{(0)}=-g_{\rm eff}L_0\cdot H_0$. The first, second and third lines of (2.70) correspond to emissions from the leptons, $\bar{B}$ and $\bar{K}^*$ respectively. The final lines are contact term contributions. The extra index that the vector K^* brings means this amplitude is quite complicated even without a derivative expansion of the form factors. Nevertheless gauge invariance of the amplitude under $\epsilon^*\to\epsilon^*+k$ must hold. There is a remarkable cancellation

$$\frac{p_K^\nu\epsilon^*\cdot\eta^*+\epsilon^{*\nu}k\cdot\eta^*-2\eta^{*\nu}p_K\cdot\epsilon^*}{2p_K\cdot k}\mathcal{P}^*_{\nu\rho}(p_K+k)\xrightarrow{\epsilon^*\to k}\eta^*_\rho\,, \qquad (2.72)$$

for the K^* contribution, and so (with $k^2=0$) we get

$$\begin{aligned}
\frac{-\delta\mathcal{A}^{(1)}}{es_eg_{\rm eff}} &= \hat{Q}_{\ell_1}L_0\cdot H_0+\hat{Q}_{\bar{\ell}_2}L_0\cdot H_0 \qquad (2.73)\\
&+ \hat{Q}_{\bar{B}}L_0\cdot H_0|_{p_B\to p_B-k}+\hat{Q}_{\bar{K}}L_0\cdot H_0|_{p_K\to p_K+k}\quad+\\
&\Big((\hat{Q}_{\bar{B}}+\hat{Q}_{\bar{K}})(p_B+p_K)_\alpha k_\beta+(\hat{Q}_{\bar{B}}-\hat{Q}_{\bar{K}})(p_B-p_K-k)_\beta k_\alpha\Big)L_{0\mu}\eta^*_\rho T^{\alpha\beta\rho\mu}\,.
\end{aligned}$$

The contact terms form $L_0\cdot H_0-L_0\cdot H_0|_{p_i\to p_i\pm k}$ combinations to intricately cancel the emissions from the $\bar{B}$ and $\bar{K}^*$. The change in the amplitude becomes

$$\begin{aligned}
\delta\mathcal{A}^{(1)} &= -es_eg_{\rm eff}L_0\cdot H_0\,(\hat{Q}_{\ell_1}+\hat{Q}_{\bar{\ell}_2}+\hat{Q}_{\bar{B}}+\hat{Q}_{\bar{K}})\\
&= es_e\mathcal{A}^{(0)}\sum_i\hat{Q}_i\;=\;0\,, \qquad (2.74)
\end{aligned}$$

which vanishes by charge conservation $\sum_i \hat{Q}_i = 0$ thus satisfying the Ward-identity $k \cdot \mathcal{A} = 0$. This guarantees that in the photon polarisation sum one can take $\sum_\lambda \epsilon_\mu^* \epsilon_\nu \to -g_{\mu\nu}$ as any part proportional to k vanishes.

We learn three things from this exercise, all of which will also be true for $\bar{B} \to \ell\bar{\nu}\gamma$ decays. Firstly, contact terms are essential to the correct physics with intricate cancellations giving gauge-invariance. Indeed for the point-like $\bar{B} \to \ell\bar{\nu}\gamma$ decay the contact term is crucial for restoring helicity suppression. Secondly, note the appearance of the tree level amplitude in (2.74). Lastly charge conservation and gauge invariance follow from one another. In Section 2.4 we will discuss operators that do not conserve charge and therefore are not gauge-invariant.

Next consider the soft (or 'eikonal') limit of this amplitude. Neglect all subleading powers of E_γ in (2.70). That is, neglect any k appearing in numerators. In this limit the amplitude becomes

$$\frac{\mathcal{A}^{(1)}}{e s_e} = \mathcal{A}^{(0)} \left(\hat{Q}_{\ell_1} \frac{l_1 \cdot \epsilon^*}{l_1 \cdot k} + \hat{Q}_{\bar{\ell}_2} \frac{l_2 \cdot \epsilon^*}{l_2 \cdot k} + \hat{Q}_{\bar{B}} \frac{p_B \cdot \epsilon^*}{p_B \cdot k} + \hat{Q}_{\bar{K}} \frac{p_K \cdot \epsilon^*}{p_K \cdot k} \right) + \mathcal{O}(E_\gamma^0) \,. \quad (2.75)$$

All particles are treated equally irrespective of spin, recovering Low's theorem (2.54). Gauge-invariance of the amplitude is trivial in this limit. Again the tree level result appears; intuitively the photon is not really there when it has vanishing energy. Low's theorem and gauge invariance are useful sanity checks for any calculation.

Finally we will consider collinear behaviour. For simplicity take the $\bar{B}$ and $\bar{K}^*$ as neutral. Then the amplitude becomes

$$\frac{-\mathcal{A}^{(1)}}{g_{\text{eff}} e s_e} = \bar{u}(l_1) \left[\hat{Q}_{\ell_1} \frac{2 l_1 \cdot \epsilon^* + \not{\epsilon}^* \not{k}}{2 l_1 \cdot k} \Gamma_\mu + \hat{Q}_{\bar{\ell}_2} \Gamma_\mu \frac{2 l_2 \cdot \epsilon^* + \not{k} \not{\epsilon}^*}{2 l_2 \cdot k} \right] v(l_2) H_0^\mu \,. \quad (2.76)$$

The square of the LO amplitude is

$$\langle |\mathcal{A}^{(0)}|^2 \rangle = 8 g_{\text{eff}} \left(2\, l_1 \cdot H_0\, l_2 \cdot H_0 - H_0 \cdot H_0\, l_1 \cdot l_2 \right) , \quad (2.77)$$

where $\langle \cdots \rangle$ denotes spin and polarisation sums and we work in $d = 4$. Consider the collinear region where the photon is parallel to l_1, looking only for $\ln m_{\ell_1}$ terms. These arise from $1/k \cdot l_1$ dependence. With this in mind we can neglect any powers of $k \cdot l_1$ in the numerator, as well as m_ℓ^2 as these give subleading $m_\ell^2 \ln m_\ell$ (this decay is not helicity suppressed). In this region we use the traditional

collinear parameterisation

$$k = (1-z)l_\gamma\,, \qquad l_1 = z\,l_\gamma\,, \qquad l_\gamma = l_1 + k\,, \tag{2.78}$$

valid to $\mathcal{O}(m_\ell^2)$. The variable $1-z \in [0,1]$ takes on the role of a dimensionless photon energy. Squaring the amplitude (2.76), neglecting non-collinear terms[17], then

$$\begin{aligned}\langle|\mathcal{A}^{(1)}_{l_1\|\gamma}|^2\rangle &= \frac{8e^2g_{\text{eff}}^2}{k\cdot l_1}\left(\hat{Q}^2_{\ell_1}(1-z) - \hat{Q}_{\ell_1}\hat{Q}_{\bar{\ell}_2}\frac{2z}{1-z}\right)\left(2\,l_\gamma\cdot H_0\,l_2\cdot H_0 - H_0^2\,l_\gamma\cdot l_2\right)\\ &= \frac{e^2\hat{Q}_{\ell_1}}{k\cdot l_1}\left(\hat{Q}_{\ell_1}(1-z) - \hat{Q}_{\bar{\ell}_2}\frac{2z}{1-z}\right)\langle|\mathcal{A}^{(0)}|^2\rangle_{l_1\to l_\gamma}\,.\end{aligned} \tag{2.79}$$

The tree level result has again appeared, though here of course in the shifted kinematics $l_1 \to l_\gamma = l_1 + k$. Applying charge conservation, here $\hat{Q}_{\bar{\ell}_2} = -\hat{Q}_{\ell_1}$, one gets

$$\langle|\mathcal{A}^{(1)}_{l_1\|\gamma}|^2\rangle \;=\; \frac{e^2\hat{Q}^2_{\ell_1}}{k\cdot l_1}\tilde{P}_{f\to f\gamma}(z)\langle|\mathcal{A}^{(0)}|^2\rangle_{l_1\to l_\gamma}\,, \qquad \tilde{P}_{f\to f\gamma}(z) = \frac{1+z^2}{1-z}\,, \tag{2.80}$$

where $\tilde{P}_{f\to f\gamma}(z)$ is the collinear emission part of the fermion splitting function. The splitting function in this form exhibits a soft divergence as $z \to 1$. The full fermion splitting function with virtual contributions included (which cancels the soft divergence) reads

$$P_{f\to f\gamma}(z) = \frac{1+z^2}{(1-z)_+} + \frac{3}{2}\delta(1-z)\,, \tag{2.81}$$

where $1/(1-z)_+$ is the plus distribution, defined under the integral as $\int_0^1 \mathrm{d}z\, f(z)/(1-z)_+ \equiv \int_0^1 \mathrm{d}z\,(f(z)-f(1))/(1-z)$, which is finite as $z \to 1$. Integration over all collinear phase space involves such an integral over z. The KLN theorem manifests itself as $\int_0^1 P_{f\to f\gamma}(z)\,\mathrm{d}z = 0$.

Scalar QED can be considered as the monopole approximation to $\bar{B}$ and $\bar{K}^{(*)}$ electromagnetic interactions. One could start to include higher multipole terms in the EFT approach, though a more natural method is to use LCSR techniques. These truly probe structure-dependence though can struggle to be fully inclusive in the photon.

[17]There are also terms of the form $m_\ell^2/(k\cdot l_1)^2$ that appear. While these do not give rise to collinear logs they are important in the collinear slicing procedure as they lead to an inverse power of the collinear cut-off.

2.3.3 $\bar{B} \to \ell\bar{\nu}(\gamma)$

Lastly we turn to leptonic $\bar{B}$ decays in scalar QED, as a reference point for the structure-dependent calculation in Chapter 3. This calculation was originally carried out by Berman and Kinoshita [160, 161] (see also [162, 163]) over 60 years ago. More recently this was revisited using W-regularisation for the lattice calculation of the pseudoscalar decays $P \to \ell\bar{\nu}(\gamma)$, $P = \pi, K$ [164] giving the more general (non-fully inclusive) result. W-regularisation (W-reg) [165] is a commonly adopted method of UV regularisation where the photon propagator is effectively cut-off at the weak scale

$$\frac{1}{k^2} \quad \longrightarrow \quad \frac{M_W^2}{M_W^2 - k^2}\frac{1}{k^2}\,. \tag{2.82}$$

This is convenient as it is consistent with radiative corrections being absorbed into the very definition of G_F [166]. In Chapter 3 we regulate in DimReg and further comments are given in 3.2.5. We quote the result given in [164] for the scalar QED $\mathcal{O}(\alpha)$ calculation $P \to \ell\bar{\nu}(\gamma)$ applied to $P = \bar{B}$

$$\begin{aligned}\Gamma^{(2)}(r_E) = \frac{\alpha}{4\pi}\,\Gamma^{(0)}\Bigg[&3\ln\!\left(\frac{m_B^2}{M_W^2}\right) + \ln\!\big(\hat{m}_\ell^2\big) - 4\ln\!\big(r_E^2\big) + \frac{2-10\hat{m}_\ell^2}{1-\hat{m}_\ell^2}\ln\!\big(\hat{m}_\ell^2\big) \\ &- 2\frac{1+\hat{m}_\ell^2}{1-\hat{m}_\ell^2}\ln\!\big(r_E^2\big)\ln\!\big(\hat{m}_\ell^2\big) - 4\frac{1+\hat{m}_\ell^2}{1-\hat{m}_\ell^2}\,\mathrm{Li}_2(1-\hat{m}_\ell^2) - 3 \\ &+ \frac{3+r_E^2-6\hat{m}_\ell^2-4r_E(1-\hat{m}_\ell^2)}{(1-\hat{m}_\ell^2)^2}\ln(1-r_E) - 4\frac{1+\hat{m}_\ell^2}{1-\hat{m}_\ell^2}\,\mathrm{Li}_2(r_E) \\ &+ \frac{r_E(22-3r_E-28\hat{m}_\ell^2)}{2(1-\hat{m}_\ell^2)^2} + \frac{r_E(4-r_E-4\hat{m}_\ell^2)}{(1-\hat{m}_\ell^2)^2}\ln\!\big(\hat{m}_\ell^2\big)\Bigg]\,.\end{aligned} \tag{2.83}$$

Here r_E is the dimensionless photon energy cut-off, $E_\gamma < E_\gamma^{\rm cut}$, with

$$r_E \equiv \frac{2E_\gamma^{\rm cut}}{m_B} \in \big[0, 1-\hat{m}_\ell^2\big]\,, \tag{2.84}$$

and using the shorthand $\hat{m}_\ell \equiv m_\ell/m_B$. Equation (2.83) is arranged so that the first two lines are the eikonal contribution, with the final two lines vanishing as $r_E \to 0$. The function Li_2 is the usual dilogarithm

$$\mathrm{Li}_2(z) = -\int_0^z \frac{\ln(1-u)}{u}\,\mathrm{d}u\,, \quad z \in \mathbb{C}\,, \tag{2.85}$$

that satisfies $\mathrm{Li}_2(0) = 0$ and $\mathrm{Li}_2(1) = \pi^2/6$. In the fully photon inclusive case, $r_E \to 1 - \hat{m}_\ell^2$, then

$$\begin{aligned}\Gamma^{(2)}|_{\rm inc} = \frac{\alpha}{4\pi}\,\Gamma^{(0)}\Bigg[&3\ln\!\left(\frac{m_B^2}{M_W^2}\right) - 8\ln\!\big(1-\hat{m}_\ell^2\big) - \frac{3\hat{m}_\ell^4}{(1-\hat{m}_\ell^2)^2}\ln\!\big(\hat{m}_\ell^2\big)\\ &- 8\frac{1+\hat{m}_\ell^2}{1-\hat{m}_\ell^2}\,\mathrm{Li}_2(1-\hat{m}_\ell^2) - 4\frac{1+\hat{m}_\ell^2}{1-\hat{m}_\ell^2}\ln\!\big(1-\hat{m}_\ell^2\big)\ln\!\big(\hat{m}_\ell^2\big)\\ &+ \frac{13-19\hat{m}_\ell^2}{2(1-\hat{m}_\ell^2)} + \frac{6-14\hat{m}_\ell^2}{1-\hat{m}_\ell^2}\ln\!\big(\hat{m}_\ell^2\big)\Bigg]. \end{aligned} \tag{2.86}$$

To complement the above we give two new results: the virtual computation in DimReg rather than W-reg and the full calculation for S-P interactions. While straightforward these do not appear in the literature.

Firstly[18] we give the result for the virtual one-particle irreducible (1PI) diagrams in the standard V-A theory using DimReg to regulate both the UV and IR.

$$\begin{aligned}\Gamma^{(2)}|^{\rm Virt}_{\rm 1PI} = \frac{\alpha}{4\pi}\Gamma^{(0)}\Bigg[&-2\left(\frac{1}{\hat{\epsilon}_{\rm IR}} + \ln\frac{\mu^2}{m_B^2}\right)\frac{1+\hat{m}_\ell^2}{1-\hat{m}_\ell^2}\ln\!\big(\hat{m}_\ell^2\big) - 4\left(\frac{1}{\hat{\epsilon}_{\rm UV}} + \ln\frac{\mu^2}{m_B^2} + 1\right)\\ &+ \frac{1+\hat{m}_\ell^2}{1-\hat{m}_\ell^2}\ln^2\!\big(\hat{m}_\ell^2\big) + 2\frac{1-3\hat{m}_\ell^2}{1-\hat{m}_\ell^2}\ln\!\big(\hat{m}_\ell^2\big)\Bigg] \end{aligned} \tag{2.87}$$

The result where the IR is regulated by a photon mass follows from the replacement $(\hat{\epsilon}_{\rm IR})^{-1} \to \ln\!\big(m_\gamma^2/\mu^2\big)$. Notice there is a soft-collinear term $(\hat{\epsilon}_{\rm IR})^{-1}\ln\hat{m}_\ell^2$ in the result as well as a $\ln^2\hat{m}_\ell^2$ term. This latter term is also of soft-collinear origin and cancels with an identical term in the real contribution.

For the S-P case, the equivalent of (2.59) requires the matching

$$m_+\langle 0|J_5|\bar{B}\rangle = m_B^2 f_B\,, \qquad J_5 = \bar{q}i\gamma_5 b \longrightarrow m_+^{-1}m_B^2 f_B\bar{B}\,, \tag{2.88}$$

which note contains no derivatives. This means that no momentum enters the vertex and thus there is no contact term (arising from the A_μ part of the covariant derivative) in the S-P case. The 1PI diagrams give the result

[18]The virtual calculation is easily performed as it is 1-loop. For completeness' sake the Feynman rules are $ig_{\rm eff}(p_B)_\mu\gamma^\mu(1-\gamma_5)$ and $-ies_eQ_{\bar{B}}g_{\rm eff}g_{\mu\nu}\gamma^\nu(1-\gamma_5)$, with here $\sqrt{2}g_{\rm eff} = f_B G_F V_{\rm qb}$, for the $\bar{B}\ell\bar{\nu}$ and $\bar{B}\ell\bar{\nu}\gamma$ (contact) vertex respectively.

$$\Gamma^{(2)}_{\text{S-P}}|^{\text{Virt}}_{\text{1PI}} = \frac{\alpha}{4\pi}\Gamma^{(0)}_{\text{S-P}}\Bigg[-2\bigg(\frac{1}{\hat{\epsilon}_{\text{IR}}} + \ln\frac{\mu^2}{m_B^2}\bigg)\frac{1+\hat{m}_\ell^2}{1-\hat{m}_\ell^2}\ln\big(\hat{m}_\ell^2\big) + 2\bigg(\frac{1}{\hat{\epsilon}_{\text{UV}}} + \ln\frac{\mu^2}{m_B^2} + 2\bigg) + \frac{1+\hat{m}_\ell^2}{1-\hat{m}_\ell^2}\ln^2(\hat{m}_\ell^2) - \frac{4}{1-\hat{m}_\ell^2}\ln\big(\hat{m}_\ell^2\big)\Bigg], \quad (2.89)$$

in DimReg, with the same substitution as in the V-A case for the case of a photon mass regulator. To instead regularise with the W mass, send $(\hat{\epsilon}_{\text{UV}})^{-1} \to \ln(m_W^2/\mu^2) - 1$. As expected the soft terms are identical for the V-A and S-P case. The self energy contributions are also the same.

The real computation involves phase-space integrations over the photon and lepton energies. Unlike in the virtual computation, all particles are external and on-shell (at $\mathcal{O}(e)$). On these physical states the equation of motion holds

$$-iD_\mu\,\bar{\ell}\gamma^\mu = m_\ell\,\bar{\ell}\,. \quad (2.90)$$

Taking the effective Lagrangian

$$\sqrt{2}\,\mathcal{L}_{\text{V-A}} = -G_F V_{\text{qb}} J_5^\mu\,\bar{\ell}\,\Gamma_\mu\nu \;\longrightarrow\; G_F V_{\text{qb}} f_B (D_\mu \bar{B})\,\bar{\ell}\,\Gamma^\mu\nu\,, \quad (2.91)$$

integrating by parts and using (2.90) then

$$\mathcal{L}^{\text{EFT}}_{\text{V-A}} = -\frac{iG_F V_{\text{qb}} f_B}{\sqrt{2}}\,\bar{B}\,m_\ell\,\bar{\ell}\,\Gamma\nu \;\propto\; m_\ell\,\mathcal{L}^{\text{EFT}}_{\text{S-P}} + \mathcal{O}(e^2)\,, \quad (2.92)$$

with $\Gamma = C_V - C_A\gamma_5$. That is the V-A and S-P rates are the same up to normalisation[19] for *real* photon emission. We have verified this by explicit calculation. Historically this caused confusion amongst the original calculators as this does not hold for virtual quanta, with Feynman and Kinoshita originally neglecting the $\mathcal{O}(e^2)$ mass renormalisation [167, 168]. It is the virtual rate which distinguishes the S-P and V-A calculations and gives different HC logs (discussed below). Fascinatingly it was exactly these (non-)cancellations of mass singularities in pion decay that led Kinoshita to develop the KLN theorem. We

[19] If we take the S-P Lagrangian as $\sqrt{2}\mathcal{L}_{\text{S-P}} = iG_F V_{\text{qb}} J_5 \bar{\ell}\Gamma\nu$ (i.e. the V-A one with $\Gamma_\mu \to \Gamma$, $J_{5\mu} \to J_5$ and an extra factor of $-i$), then the normalisation factor is $m_B^2\mathcal{L}^{\text{EFT}}_{\text{V-A}} = -m_\ell m_+ \mathcal{L}^{\text{EFT}}_{\text{S-P}}$.

give the equivalent of (2.83) for the full calculation in the S-P case[20]

$$\begin{aligned}\Gamma^{(2)}_{\text{S-P}}(r_E) = \frac{\alpha}{4\pi}\,\Gamma^{(0)}_{\text{S-P}}\Bigg[&3\ln\!\left(\frac{M_W^2}{m_B^2}\right) + \ln\!\big(\hat{m}_\ell^2\big) - 4\ln\!\big(r_E^2\big) - 4\frac{1+\hat{m}_\ell^2}{1-\hat{m}_\ell^2}\ln\!\big(\hat{m}_\ell^2\big)\\ &- 2\frac{1+\hat{m}_\ell^2}{1-\hat{m}_\ell^2}\ln\!\big(r_E^2\big)\ln\!\big(\hat{m}_\ell^2\big) - 4\frac{1+\hat{m}_\ell^2}{1-\hat{m}_\ell^2}\,\text{Li}_2(1-\hat{m}_\ell^2)\\ &+ \frac{3+r_E^2-6\hat{m}_\ell^2-4r_E(1-\hat{m}_\ell^2)}{(1-\hat{m}_\ell^2)^2}\ln(1-r_E) - 4\frac{1+\hat{m}_\ell^2}{1-\hat{m}_\ell^2}\,\text{Li}_2(r_E)\\ &+ \frac{r_E(22-3r_E-28\hat{m}_\ell^2)}{2(1-\hat{m}_\ell^2)^2} + \frac{r_E(4-r_E-4\hat{m}_\ell^2)}{(1-\hat{m}_\ell^2)^2}\ln\!\big(\hat{m}_\ell^2\big)\Bigg]. \end{aligned} \tag{2.93}$$

which includes the self energy (SE) contributions

$$\Gamma^{(2)}|^{\text{Virt}}_{\text{SE}} = \frac{\alpha}{4\pi}\,\Gamma^{(0)}\left(\ln\frac{M_W^2}{m_B^2} - 4\ln\frac{m_\gamma^2}{m_B^2} + 3\ln\frac{m_\ell^2}{m_B^2} - 6\right), \tag{2.94}$$

taken from [164]. When fully inclusive, this result becomes

$$\begin{aligned}\Gamma^{(2)}_{\text{S-P}}|_{\text{inc}} \;=\; \frac{\alpha}{4\pi}\,\Gamma^{(0)}_{\text{S-P}}\Bigg[&3\ln\!\left(\frac{M_W^2}{m_B^2}\right) - 8\ln\!\big(1-\hat{m}_\ell^2\big) - \frac{\hat{m}_\ell^2(8-5\hat{m}_\ell^2)}{(1-\hat{m}_\ell^2)^2}\ln\!\big(\hat{m}_\ell^2\big) + 3\\ &- 8\frac{1+\hat{m}_\ell^2}{1-\hat{m}_\ell^2}\,\text{Li}_2(1-\hat{m}_\ell^2) - 4\frac{1+\hat{m}_\ell^2}{1-\hat{m}_\ell^2}\ln\!\big(1-\hat{m}_\ell^2\big)\ln\!\big(\hat{m}_\ell^2\big) + \frac{13-19\hat{m}_\ell^2}{2(1-\hat{m}_\ell^2)}\Bigg]. \end{aligned} \tag{2.95}$$

Let us turn to the collinear logs contained in these equations. Inspecting (2.83) and (2.93), neglecting subleading $\hat{m}_\ell^2$ terms the HC logs are

$$\Gamma^{(2)}_{\text{V-A}}|_{\text{HC}} = \frac{\alpha}{\pi}\,\Gamma^{(0)}_{\text{V-A}}\left[+\frac{3}{2} + r_E(2-\frac{1}{2}r_E)\right]\ln\hat{m}_\ell\,, \tag{2.96}$$

$$\Gamma^{(2)}_{\text{S-P}}|_{\text{HC}} = \frac{\alpha}{\pi}\,\Gamma^{(0)}_{\text{S-P}}\left[-\frac{3}{2} + r_E(2-\frac{1}{2}r_E)\right]\ln\hat{m}_\ell\,, \tag{2.97}$$

so that in the fully-inclusive case (here $r_E \to 1$) the S-P logs cancel whereas the V-A logs do not

$$\Gamma^{(2)}_{\text{V-A}}|_{\text{HC}} \longrightarrow \frac{3\alpha}{\pi}\,\Gamma^{(0)}_{\text{V-A}}\,\ln\hat{m}_\ell\,, \qquad \Gamma^{(2)}_{\text{S-P}}|_{\text{HC}} \longrightarrow 0\cdot\Gamma^{(0)}_{\text{S-P}}\,\ln\hat{m}_\ell\,, \tag{2.98}$$

[20] In theory we could reverse engineer the result from the historical confusions, though these use Pauli-Villars regulators and further only consider the fully photon inclusive case. Our (2.95) matches equation (9) in [161]. We note also a slight inconsistency in the presentation given in [164], where equations (47) & (49) correspond to the S-P, not the V-A case. Of course this does not matter as the contributions are summed.

Contribution	S-P	V-A
Real	$-1 + r_E(2 - \frac{1}{2}r_E)$	$-1 + r_E(2 - \frac{1}{2}r_E)$
Virtual (1PI)	-2	1
Virtual (Z)	$\frac{3}{2}$	$\frac{3}{2}$

Table 2.1 *The table shows the coefficients of $\frac{\alpha}{\pi}\Gamma^0 \ln \hat{m}_\ell$ broken up into the real, virtual (1PI) and virtual (renormalisation) $\mathcal{O}(\alpha)$ contributions to $\bar{B} \to \ell\bar{\nu}(\gamma)$ in scalar QED. The overall collinear logs are given by summing the columns.*

in accordance with the KLN theorem. Of course the S-P result in (2.97) is really the splitting function (2.81) in disguise. A breakdown of these logs is given in Table 2.1. Numerically these logs give a sizeable correction to the decay rate for V-A interactions. When fully inclusive there is a $\{-6.4, -2.7, -0.8\}\%$ correction to the LO rate for the $\ell = \{e, \mu, \tau\}$ channels respectively. The correction is negative and the hierarchy follows from $m_e \ll m_\mu \ll m_\tau \approx m_B/3$.

In the language of the EFT, the difference in the virtual hard-collinear logs in the two cases can be traced back to the extra contact term diagram in the V-A case. The necessity of the contact term is even more extreme for the real radiation. The contact diagram

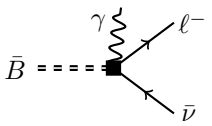

$$= \quad -ies_e Q_{\bar{B}} \frac{G_F V_{\rm qb} f_B}{\sqrt{2}} \epsilon^*_\rho(k)\, \bar{\ell}\, \Gamma^\rho \nu \tag{2.99}$$

is helicity un-suppressed and combines with the similarly un-suppressed lepton emission to restore helicity suppression to the amplitude. In the above, the double dashed line denotes the $\bar{B}$-meson with the back square denoting the weak vertex.

The point-like calculation of the real decay that we have discussed is referred to as *inner bremsstrahlung* (IB) and as emphasised is helicity suppressed. Going beyond scalar QED, structure-dependent contributions to the real decay are no longer helicity suppressed. This lifting of helicity suppression means structure-dependent effects dominate the real rate for the light leptons $\ell = e, \mu$. This can be described through axial and vector form factors. The structure-dependent calculation will be discussed in detail in Section 3.3.

2.4 Structure-dependent QED

To probe structure-dependent electromagnetic effects in hadrons a suitable non-perturbative framework is needed. While in this work we give the first QED calculation in a SR framework, considerable recent attention has been given to structure-dependent QED in methods like χPT, HQET and SCET.

In χPT, electromagnetic effects are easily built into the effective Lagrangian (1.16) through the covariant derivative, which here takes the form

$$D_\mu U = \partial_\mu U + ies_e A_\mu [Q, U] + il_\mu^{(\ell)} U + \dots \,, \tag{2.100}$$

where $Q = \text{diag}(2/3, -1/3, -1/3)$ is the quark charge matrix and $U = \exp i\lambda \cdot \phi / F_\pi$ as before. The coupling to leptons is added in similarly via the weak current $l_\mu^{(\ell)} \sim \bar{\ell}\,\Gamma_\mu \nu$. Loops involving photons and leptons lead to extra counterterms in addition to the QCD low energy constants L_i. QED effects (along with taking $m_u \neq m_d$) are referred to as isospin-breaking contributions.

When considering the leptonic decays $P = (\pi, K) \to \ell\bar{\nu}(\gamma)$, the ratio

$$R_{e/\mu}^{(P)} = \frac{\Gamma(P^- \to e^- \bar{\nu}(\gamma))}{\Gamma(P^- \to \mu^- \bar{\nu}(\gamma))} = \frac{m_e^2}{m_\mu^2} \left(\frac{m_{P^-}^2 - m_e^2}{m_{P^-}^2 - m_\mu^2} \right)^2 + \mathcal{O}(e^2) \,, \tag{2.101}$$

(from (1.28)) is often considered as the decay constant and CKM matrix elements drop out at LO. Numerically $R_{e/\mu}^{(\pi)} = 1.284 \times 10^{-4}$ and $R_{e/\mu}^{(K)} = 2.567 \times 10^{-5}$ before we add isospin-breaking terms. Electromagnetic corrections in leptonic decays were worked out in [169] at $\mathcal{O}(e^2E^2)$ and then pushed to $\mathcal{O}(e^2E^4)$ in [170]. At $\mathcal{O}(e^2E^2)$ the χPT result matches the scalar QED result of Section 2.3, with structure-dependent effects only entering at $\mathcal{O}(e^2E^4)$. These effects give a negative QED correction, pushing down $R_{e/\mu}$ to $R_{e/\mu}^{(\pi)} = 1.2352(1) \times 10^{-4}$ and $R_{e/\mu}^{(K)} = 2.477(1) \times 10^{-5}$, consistent with experiment. Similarly, $\mathcal{O}(e^2E^2)$ χPT has been performed for semi-leptonic kaon decays [171, 172], pionic beta decay [173], and non-leptonic decays (e.g. [174, 175]) and may be considered a somewhat standard procedure by now.

For heavy mesons SCET approaches are more suitable. The FCNC decay $\bar{B}_{s,d} \to \mu^+\mu^-$ has drawn recent attention due to the presence of *power-enhanced* electromagnetic corrections $m_b/\Lambda_{\text{QCD}} \sim 20$ [176, 177]. These arise from virtual photons connecting the light quark to final state leptons. In practise

however, these enhanced terms are actually only a $-0.7(4)\%$ effect due to large cancellations between semi-leptonic (Q_9) and dipole (Q_7) operators. In the charged $B^- \to \ell^- \bar{\nu}$ case these power-enhanced terms have been shown not to exist at all. Structure-dependent effects are written in terms of non-perturbative Light-Cone Distribution Amplitudes (LCDA) whose moments are poorly known. This is the origin of the large uncertainty in the neutral case quoted above. In the charged case [178] a further unknown hadronic parameter $F(\mu)$ appears (a SCET generalisation of f_B in the presence of QED) and a numerical study has yet to appear. Note also that the analysis [178] applies only to the muon channel. In the radiative case the photon lifts the helicity suppression and structure-dependent effects contained in $\bar{B} \to \gamma$ form factors become very important [179]. One can even turn the tables and use hard photons in $\bar{B} \to \ell\bar{\nu}\gamma$ to constrain the inverse moment of the $\bar{B}$-meson LCDA, $\lambda_B(\mu)$ [180].

2.4.1 Lattice QED

Historically lattice simulations worked in an isospin symmetric $m_u = m_d$ universe with no electromagnetic effects and periodic boundary conditions (BC) in the finite box $L^3 \times T$. Adding in QED one immediately runs into the problem that even classically Gauss' law forbids charged particles in a box with periodic BCs.

$$Q = \int_V \mathrm{d}^3\boldsymbol{x}\, \rho = \int_V \mathrm{d}^3\boldsymbol{x}\, \partial_i \boldsymbol{E}_i \;=\; 0 \tag{2.102}$$

In the quantum theory this issue arises as problems with gauge fixing and the treatment of zero momentum modes. Various prescriptions have been considered to circumvent this such as changing the BCs ($\mathrm{QED_C}$) [181], invoking a massive photon ($\mathrm{QED_M}$) [182], removing the zero modes ($\mathrm{QED_L}$) [183], or even keeping the QED part in infinite volume ($\mathrm{QED_\infty}$) [184]. The latter is motivated by worsening finite volume effects in QED. As well as discretisation errors from the non-zero lattice spacing a, there are also errors introduced by working in a finite box, $L < \infty$. In QCD these finite volume (FV) errors are exponentially suppressed, $\mathcal{O}(e^{-m_P L})$, while in QED there is instead power law dependence

$$\Delta_{\mathrm{FV}} = c_0 + \tilde{c}_0 \ln(m_P L) + \frac{c_1}{m_P L} + \frac{c_2}{(m_P L)^2} + \cdots\,, \tag{2.103}$$

with the coefficients c_i process and prescription dependent. For example in the calculation of the pseudoscalar mass m_P in $\mathrm{QED_L}$ the coefficients $(c_0, \tilde{c}_0) = (0, 0)$

while the coefficients $c_{1,2}$ have been shown to be universal – independent of meson structure [185].

The QED_L prescription has been used for lattice QCD+QED in the leptonic decay $(\pi, K) \to \ell\bar{\nu}(\gamma)$. The long distance nature of IR divergences means they are naturally regulated by the finite spatial extent of the lattice, L. The 2015 paper [164] sets up a framework for handling soft divergences in leptonic decays via a Bloch-Nordsieck cancellation. Exploiting Low's theorem, the soft divergence is universal and can be calculated perturbatively. This divergence is added and subtracted separately in the real and virtual rates to render each IR finite. Using this framework numerical studies [186, 187] give isospin-breaking corrections of $+1.53(19)\%$ and $+0.24(10)\%$ for the pion and kaon channels respectively, agreeing with χPT predictions. Including hard photons in the radiative rate requires knowledge of structure-dependent vector and axial-vector form factors which have been calculated on the lattice in [188–190] (for π, K, D, D_s) and recently even extrapolated to B_s decays [191].

In lattice QED calculations, typically a gauge choice is made. The QED_C framework gives a more explicit gauge-invariant strategy based on the Dirac formulation [192]. Rather than using completely periodic BCs, so-called C^* BCs are used with fields periodic up to charge conjugation. This allows charge to flow in and out of the box as (2.102) no longer holds.

Following Dirac, we may dress a fermion field $\psi(x)$ with a compensating factor $\mathcal{U}_I$

$$\Psi_I(x) \equiv \mathcal{U}_I(x)\psi(x)\,, \tag{2.104}$$

with

$$\mathcal{U}_I(x) = \exp\left(-ies_eQ_f \int_{L^3\times T} \mathrm{d}^4y\, A_\mu(y) I^\mu(y-x)\right). \tag{2.105}$$

The factor $\mathcal{U}_I$ is a functional of a generic current I^μ which is required to satisfy the same BCs as A_μ as well as $\partial_\mu I^\mu = \delta^{(4)}(x)$. With these conditions the Ψ_I field is gauge-invariant as the $\mathcal{U}_I$ factor exactly compensates the gauge transformation of the ψ field. Explicitly, under a gauge transformation

$$\psi(x) \to e^{ies_eQ_f\alpha(x)}\psi(x)\,, \qquad A_\mu(x) \to A_\mu(x) - \partial_\mu\alpha(x) \tag{2.106}$$

then

$$\mathcal{U}_I(x) \longrightarrow \exp\left(ies_eQ_f \int \mathrm{d}^4y\, (\partial_\mu\alpha(y)) I^\mu(y-x)\right)\mathcal{U}_I(x)$$

$$= \exp\left(-ies_e Q_f \int \mathrm{d}^4y\, \alpha(y)\partial_\mu I^\mu(y-x)\right)\mathcal{U}_I(x)$$
$$= e^{-ies_e Q_f \alpha(x)}\mathcal{U}_I(x)\,, \tag{2.107}$$

where we integrate by parts. This construction is only useful if an appropriate current I^μ exists. Crucially it has been shown that such a current only exists with C^* BC and is not possible with periodic BCs [181, 193]. This construction also allows us to justify the common lattice procedure of using non-dressed, gauge-variant fermion fields when computing gauge-invariant physical quantities. By choosing I^μ carefully, we can *trivialise* the compensating factor $\mathcal{U}_I(x) \to 1$ so that $\Psi_I = \psi$. For example let

$$I_\mu(x) = \partial_\mu\varphi(x)\,, \qquad \partial_\mu\partial^\mu\varphi(x) = \delta^{(4)}(x)\,, \tag{2.108}$$

where φ is some function satisfying appropriate BCs. Then

$$\begin{aligned}\mathcal{U}_I(x) &= \exp\left(-ies_e Q_f \int \mathrm{d}^4y\, A^\mu(y)\partial_\mu\varphi(y-x)\right)\\ &= \exp\left(ies_e Q_f \int \mathrm{d}^4y\, \varphi(y-x)\partial_\mu A^\mu(y)\right)\\ &\to 1 \qquad \text{if} \quad \partial_\mu A^\mu = 0\,.\end{aligned} \tag{2.109}$$

Thus if we compute in the Lorenz/Landau gauge $\partial_\mu A^\mu = 0$, then the $\mathcal{U}_I$ factor is trivialised and $\Psi_I = \psi$. We may compute non-dressed correlators like $\langle\psi(x)\bar{\psi}(0)\rangle$ knowing that this is a consistent method for extracting physical quantities (as this equals $\langle\Psi_I(x)\bar{\Psi}_I(0)\rangle$) *provided* we work in a fixed gauge. What we save on one hand by trivialising the gauge factor we lose on the other hand with potential difficulties in calculating in a fixed gauge. Other gauges such as the Coulomb gauge or axial gauges can similarly be trivialised through different choices of I^μ.

2.4.2 Gauge-invariant Interpolating Operators

For heavy mesons it is natural to investigate structure-dependence using the sum rules techniques of Section 2.1. However traditional interpolating operators, like $J_B = m_+\bar{b}i\gamma_5 q$, are not QED gauge invariant. Under the gauge transformation (2.106)

$$J_B \longrightarrow e^{-ies_e(Q_b - Q_q)\alpha}J_B = e^{-ies_e Q_{\bar{B}}\alpha}J_B\,, \tag{2.110}$$

which is non-invariant for electrically charged mesons. The J_B operator carries electric charge as $Q_b = -1/3 \neq Q_q = 2/3$. In QCD bound states do not carry colour charge while in QED electrically charged states exist and carry charge in from infinity, as is the case for the B^- meson. A solution to this dilemma was proposed in [194] by introducing an auxiliary on-shell charged scalar field Φ_{B^-} that takes on the role of the on-shell B^- meson. By replacing J_B with a modified operator

$$\mathcal{J}_B \equiv \Phi_{B^-} J_B \,, \tag{2.111}$$

then gauge invariance is restored

$$\Phi_B J_B \longrightarrow e^{ies_e(Q_\Phi - Q_{\bar{B}})\alpha} \Phi_B J_B = \Phi_B J_B \,, \tag{2.112}$$

by virtue of $Q_\Phi \equiv Q_{\bar{B}} = -1$. The field Φ_B flows charge $Q_\Phi = -1$ into the vertex to restore charge conservation and thus gauge-invariance. For brevity we abbreviate the field Φ_{B^-} as Φ_B and its charge $Q_{\Phi_{B^-}}$ as Q_Φ. Charge conservation at the vertex takes the form

$$Q_{\mathcal{J}_B} \equiv Q_\Phi - Q_b + Q_q = 0 \,. \tag{2.113}$$

In the presence of QED the matrix element $\langle B^-|J_B|0\rangle = m_B^2 f_B$ must be generalised to

$$\mathcal{Z}_B \equiv \langle B^-|\mathcal{J}_B|\Phi_B\rangle \,, \tag{2.114}$$

which was argued in [194] to be IR safe. We will back this up in Section 3.2.6 with an explicit computation.

Intuitively the long distance on-shell Φ_B is a proxy for the $\bar{B}$-meson, bringing in charge from the far past to the $\mathcal{J}_B$ vertex where it splits into partons b and $\bar{q}$, allowing structure-dependence to be probed in the usual sum-rules framework. The auxiliary field Φ_B itself is treated as point-like. The Φ_B being on-shell is crucial as it allows universal soft divergences to appear (and cancel in a Bloch-Nordsieck manner) in charged processes. Such soft divergences cannot appear without it as the partons are not on-shell in sum-rules methods.

By using the Φ_B construction any observables we compute are manifestly gauge invariant. In any case the Φ_B field is not physical and must disappear from the final result in any calculation. The modification $\mathcal{J}_B = \Phi_B J_B$ is reminiscent of the dressing $\Psi_I = \mathcal{U}_I \psi$ discussed earlier. Indeed it was shown in [194] that at $\mathcal{O}(\alpha)$ the Φ_B construction can be interpreted as a (continuum) Dirac dressing

with current[21]

$$iI_\mu(x) = (\partial - 2ip_\Phi)_\mu \, e^{ip_\Phi \cdot x} \Delta_F(x) \,, \tag{2.115}$$

where $p_\Phi^2 = m_\Phi^2$ and $i\Delta_F(x)$ is the scalar Feynman propagator satisfying (with appropriate BCs)

$$(\partial_\mu \partial^\mu + m_\Phi^2)\Delta_F(x-y) = -\delta^{(4)}(x-y) \,. \tag{2.116}$$

This has compensating factor

$$\mathcal{U}_I(x) \,=\, \exp\!\left(-ies_e \int \mathrm{d}^4 y \, e^{ip_\Phi \cdot (x-y)} \Delta_F(x-y)(i\partial - 2p_\Phi)_\mu A^\mu \right), \tag{2.117}$$

and so can be trivialised in the slightly non-standard (axial type) gauge $(\partial + 2ip_\Phi) \cdot A = 0$. In this gauge the photon propagator assumes a quite complicated form which makes it unattractive for perturbative calculations. The benefit of working in the manifestly gauge-invariant framework is that gauge-invariance can be checked explicitly and then if required a particularly simple gauge like the Feynman gauge can be chosen. Interpretation as a Dirac dressing emphasises how Φ_B is not physical; it does not appear in the Lagrangian and does not interact with other particles beyond the operator insertion.

In chapters 3 and 4 of this thesis we provide the first implementation of this method using the concrete setting of leptonic $\bar{B}$ decays. We develop the framework of how to actually use these modified operators $\mathcal{J}_B$ to calculate decay rates, working out the practical details. In particular we analyse soft and hard-collinear logs, showing how these appear in the gauge-invariant framework, and explicitly prove some of the conjectures in [194]. Using this work we then perform a numerical study, showing the sizeable effect of QED structure-dependence on leptonic decay rates.

[21] At higher order an interpretation in terms of iterated integrals is given in [194]. Note also that this current is just the Feynman rule for a scalar (2.58) in disguise, with $p = p_\Phi$ and $p' = p_\Phi - k$.

Chapter 3

Structure-dependent QED in $\bar{B} \to \ell\bar{\nu}(\gamma)$

We now present the calculation of the leptonic decay $\bar{B} \to \ell\bar{\nu}(\gamma)$ using gauge-invariant interpolating operators. The corresponding numerical study is given in Chapter 4. We use a sum rules technique to calculate complete next-to-leading-order (NLO) QED corrections with full structure-dependence. To summarise the discussions in Chapter 2, we choose this decay for the following reasons:

- Structure-dependent QED effects may be large as photons connect the initial and final states. Helicity suppression allows this decay to circumvent the KLN theorem meaning hard-collinear logs do not need to cancel. The large scale separation between the $\bar{B}$-mass and the light lepton masses means these logs can be numerically sizeable. Further, our framework allows us to investigate the effect of the $\bar{B}$-meson's structure on such hard-collinear logs.

- In QCD this decay is theoretically clean with only small uncertainties coming from f_B and V_{ub}. This means QED effects are now an important consideration. Monte-Carlo programs like PHOTOS are fundamentally structure-less and so are unlikely to capture all QED effects. While this is a rare decay, experimental prospects (for the μ and τ channels at least) are good. It is of phenomenological relevance as a method for extracting V_{ub} and could also be considerably enhanced by new physics.

- The leading order amplitude and the kinematics are relatively straightforward which is useful for the first application of the gauge-invariant framework. Usefully the S-P mediated decay does obey the KLN theorem and provides a useful sanity check of the hard-collinear logs.

3.1 Gauge-invariant Formalism

The gauge-invariant formalism for calculating the leptonic decay $\bar{B} \to \ell\bar{\nu}(\gamma)$ involves, roughly speaking, computing $|\mathcal{Z}_B|^2$ and $|\mathcal{A}^{(\gamma)}|^2|\mathcal{Z}_B|^2$ separately, and then dividing the two to extract the amplitude. Invoking Bloch-Nordsieck cancellation, the virtual rate must be combined with the real rate to give an IR finite quantity

$$\Gamma(\bar{B} \to \ell\bar{\nu}) + \Gamma(\bar{B} \to \ell\bar{\nu}\gamma)_{E_\gamma < E_\gamma^{\rm cut}} = \tag{3.1}$$
$$\frac{1}{|\mathcal{Z}_B|^2} \int \Big[|\mathcal{Z}_B|^2 \langle |\mathcal{A}(\bar{B} \to \ell\bar{\nu})|^2 \rangle\Big] \, \mathrm{dPS}_2 \, + \, \Big[|\mathcal{Z}_B|^2 \langle |\mathcal{A}(\bar{B} \to \ell\bar{\nu}\gamma)|^2 \rangle\Big] \, \mathrm{dPS}_3 \, |_{E_\gamma^{\rm cut}} \, ,$$

where dPS_2 and dPS_3 are two- and three-particle phase space elements respectively. The large square brackets in (3.1) emphasise that the amplitude is not computed directly, but instead the combination $\big[|\mathcal{Z}_B|^2 \langle |\mathcal{A}^{(\gamma)}|^2 \rangle\big]$, with the $|\mathcal{Z}_B|^2$ divided out at the end. As we shall discuss shortly, this procedure is a consequence of requiring explicitly gauge-invariant correlators at every stage. In the radiative case the photon energy is cut-off at $E_\gamma^{\rm cut}$, defined in the rest frame of the decaying $\bar{B}$-meson. Following the notation of Chapter 2, powers of e are denoted by superscripts: the LO amplitude is $\mathcal{A}^{(0)}$, real radiation is $\mathcal{A}^{(1)}$ and so on. The 'LSZ factor', $|\mathcal{Z}_B|^2$ (defined in (2.114)), which appears in the *denominator* of (3.1), is calculated from the correlator $C(p_B^2)$ defined below. Separately the integrand in the *numerator* of (3.1) is calculated from two further correlators, Π^γ and Π for the radiative and non-radiative case respectively. For convenience we will often refer to the extraction of $|\mathcal{Z}_B|^2$ as the 'denominator' computation with the calculation of the integral in (3.1) being referred to as the 'numerator' or 'main process'.

3.1.1 Correlation Functions

The integrand in (3.1) can be extracted from the following correlation functions

$$\Pi^{(\gamma)}(p_B^2, p_\Phi^2) \, = \, i \int \mathrm{d}^d x \, e^{ix\cdot r} \langle \ell\bar{\nu}(\gamma)|T\mathcal{J}_B(x)(-i\mathcal{L}_W(0))|\Phi_B\rangle \, , \tag{3.2}$$

in $d = 4 - 2\epsilon$ dimensions, with $\mathcal{J}_B$ defined in (2.111) and $\mathcal{L}_W$ the electroweak Lagrangian

$$\mathcal{L}_W \;=\; -g_{\text{eff}}\,\bar{\ell}\Gamma^\mu\nu\,\bar{u}\hat{\Gamma}_\mu b\,, \qquad \Gamma_\mu = \gamma_\mu(C_V - C_A\gamma_5), \qquad \hat{\Gamma}_\mu = \gamma_\mu(1-\gamma_5), \quad (3.3)$$

where $(C_V, C_A) = (+1, +1)$ in the SM. The prefactor g_{eff} is an effective coupling proportional to to the Fermi constant G_F and the relevant CKM matrix element V_{ub}

$$g_{\text{eff}} \;\equiv\; -\frac{G_F}{\sqrt{2}}V_{\text{ub}}\,. \quad (3.4)$$

The external charged Φ_B particle carries in momentum p_Φ, meaning momentum conservation takes the form

$$p_\Phi|_{\text{virt}} = l_1 + l_2\,, \qquad p_\Phi|_{\text{real}} = l_1 + l_2 + k\,, \quad (3.5)$$

in the virtual and real cases respectively. The neutrino is taken as massless and all external particles are on-shell

$$l_1^2 = m_\ell^2\,, \qquad l_2^2 = 0\,, \qquad p_\Phi^2 = m_\Phi^2\,, \qquad k^2 = 0\,. \quad (3.6)$$

The Φ_B mass is naturally identified with the $\bar{B}$-meson mass, $m_\Phi = m_B$, though we justify this more formally in the next section. Further we define

$$p_\Phi = p_B + r\,, \qquad q = p_B - k\,, \quad (3.7)$$

where the momentum r is auxiliary and used to distinguish the on-shell external p_Φ and the off-shell p_B momentum used for the dispersion relation. By inserting a complete set of hadronic $|\bar{B}\rangle\langle\bar{B}|$ states in the matrix element (3.2) we can derive a dispersion relation exactly as in Section 2.1.1. However this time rather than $m_B^4 f_B^2$ appearing we get $\mathcal{Z}_B$ and $\mathcal{A}^{(\gamma)}$ instead

$$\begin{aligned}\Pi^{(\gamma)}(p_B^2, m_B^2) &= \int \frac{\mathrm{d}s}{2\pi i}\frac{\text{disc}_s[\Pi^{(\gamma)}(s, m_B^2)]}{s - p_B^2 - i\varepsilon} \\ &= \frac{\mathcal{Z}_B\, i\mathcal{A}(\bar{B}\to\ell\bar{\nu}(\gamma))}{m_B^2 - p_B^2} + \cdots\,. \end{aligned} \quad (3.8)$$

The amplitude $\mathcal{A}^{(\gamma)} \equiv \langle\ell\bar{\nu}(\gamma)|-\mathcal{L}_W|\bar{B}\rangle$ appears as the residue of the lowest lying state with $+\cdots$ denoting higher states in the spectrum that will be suppressed

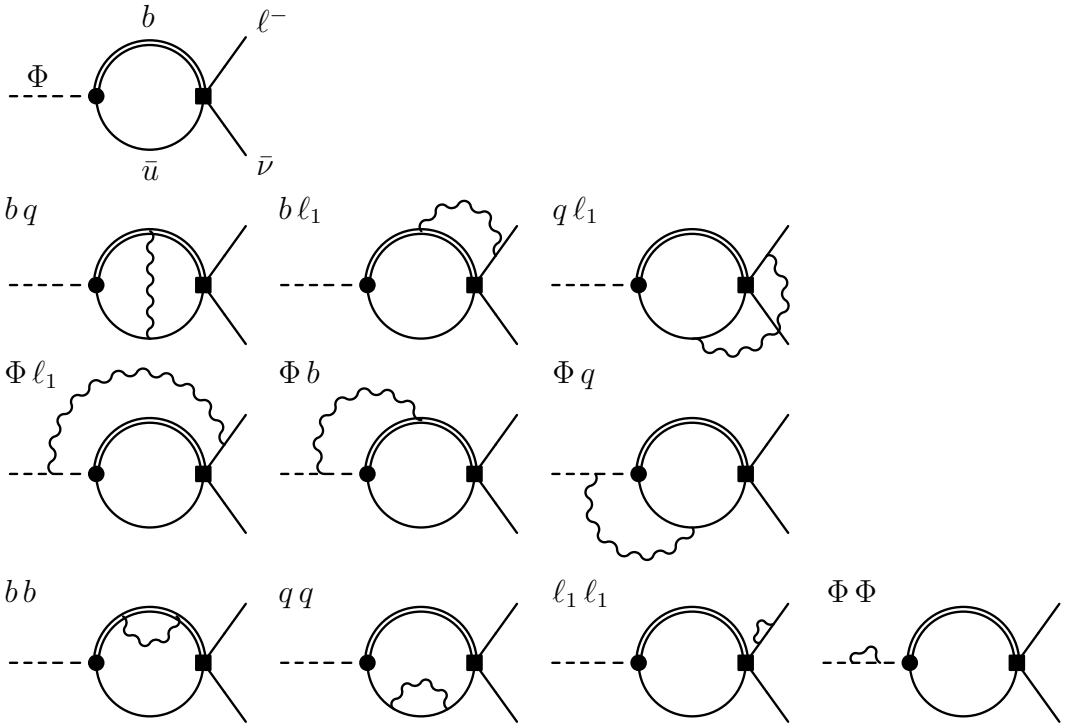

Figure 3.1 *Diagrams contributing to* $\Pi(p_B^2, p_\Phi^2)$ *in* (3.2) *(the non-radiative part). The black circle denotes the* $\mathcal{J}_B$ *operator, while the black square denotes the weak vertex* $\mathcal{L}_W$*. The top line is the LO diagram while the third line and last diagram are specific to the* Φ_B *framework.*

by Borel transformation. Defining the spectral density

$$2\pi i\,\rho_{\Pi^{(\gamma)}}(s) \;=\; 2i\,\mathrm{Im}\,\Pi^{(\gamma)}(s, m_B^2) \;=\; \mathrm{disc}_s[\Pi^{(\gamma)}(s, m_B^2)]\,, \tag{3.9}$$

then the amplitude is extracted by the usual sum rule procedure

$$\Big[i\mathcal{Z}_B\,\mathcal{A}(\bar{B}\to\ell\bar{\nu}(\gamma))\Big] \;=\; e^{\frac{m_B^2}{M^2}}\mathcal{B}_{M^2}\Pi^{(\gamma)}(p_B^2) \;\equiv\; \int_{m_+^2}^{s_0}\mathrm{d}s\,e^{\frac{m_B^2-s}{M^2}}\rho_{\Pi^{(\gamma)}}(s)\,, \tag{3.10}$$

where s_0 and M^2 are the continuum threshold and Borel mass respectively. The whole LHS of (3.10) is then squared and integrated over phase space to give the rate in the manner of (3.1). The calculation of the spectral density at $\mathcal{O}(\alpha)$ involves the calculation of the 11 virtual Feynman diagrams shown in Figure 3.1. Note that in QCD there would only be 4 such diagrams. The Φ_B particle is denoted by a dashed line which decomposes into a b and $\bar{q}$ quark at the $\mathcal{J}_B$ vertex (black circle) which themselves decay into a lepton and neutrino at the weak vertex (black square). Analogous diagrams exist for the S-P case, which follows from the substitution $\gamma_\mu \to \mathbb{1}$ in $\Gamma_\mu, \hat{\Gamma}_\mu$ (3.3). We do not perform the full computation for the S-P case, using it only to elucidate the nature of the collinear

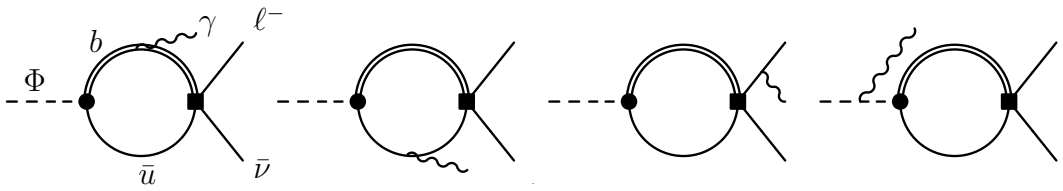

Figure 3.2 *Diagrams contributing to* $\Pi^\gamma(p_B^2, p_\Phi^2)$ *in* (3.2) *(the radiative part). The last diagram is unique to our framework. We stress that for the real structure-dependent part we take external form factors [195] which include many more contributions to the above diagrams (e.g.* $\mathcal{O}(\alpha_s)$ *and higher twist).*

logs in Section 3.4.

For the radiative correlator Π^γ the corresponding four $\mathcal{O}(e^1, \alpha_s^0)$ diagrams are given in Figure 3.2. The diagram with the emission from the Φ_B particle is unique to our framework and captures the soft divergence. Recall that the structure-dependent emissions from the b and $\bar{q}$ quarks lift the helicity suppression and thus dominate the radiative rate. Working only at LO in QCD, the b and $\bar{q}$ diagrams in Figure 3.2 do not adequately capture all structure-dependent effects. Instead we replace these two diagrams with the $\bar{B} \to \gamma$ form factors $V_{\parallel,\perp}(q^2)$ recently calculated via LCSR in [195]. This includes complete twist-$1, 2$ $\mathcal{O}(\alpha_s)$ corrections[1] as well as partial twist-$3, 4$ contributions and is valid for hard photons, $q^2 < 14\,\text{GeV}^2$. The paper includes the extrapolation to the soft photon region using the related computation [196]. The b and $\bar{q}$ diagrams of Figure 3.2 of course appear in the calculation of [195] as the LO contribution. While we take the real structure-dependent form factors externally, we give a comparison with the LO calculation (and other form factor computations) in Section 3.3.4.

The calculation of the denominator factor $|\mathcal{Z}_B|^2$ proceeds similarly, though is simpler as there are no leptons involved. We define a correlator $C(p_B^2, p_\Phi^2)$ which contains $|\mathcal{Z}_B|^2$ as the residue of the lowest lying pole.

$$\begin{aligned} C(p_B^2, p_\Phi^2) &= i \int \mathrm{d}^d x\, e^{ix\cdot r} \langle \Phi_B(p_\Phi)| T \mathcal{J}_B(x) \mathcal{J}_B^\dagger(0) |\Phi_B(p_\Phi)\rangle \\ &= \int \frac{\mathrm{d}s}{2\pi i} \frac{\mathrm{disc}_s[C(s, m_B^2)]}{s - p_B^2 - i\varepsilon} = \frac{|\mathcal{Z}_B|^2}{m_B^2 - p_B^2} + \cdots . \end{aligned} \tag{3.11}$$

The 11 relevant Feynman diagrams required to calculate the spectral density $\rho_C(s)$ are given in Figure 3.3. There is no radiative counterpart in this case. The correlation function is diagonal and so there is a symmetry between the in and out states as well as a $b \leftrightarrow q$ symmetry. By cutting these diagrams down the

[1] In LCSR methods the OPE is naturally ordered in terms of operator *twist* defined as the dimension of an operator minus its spin.

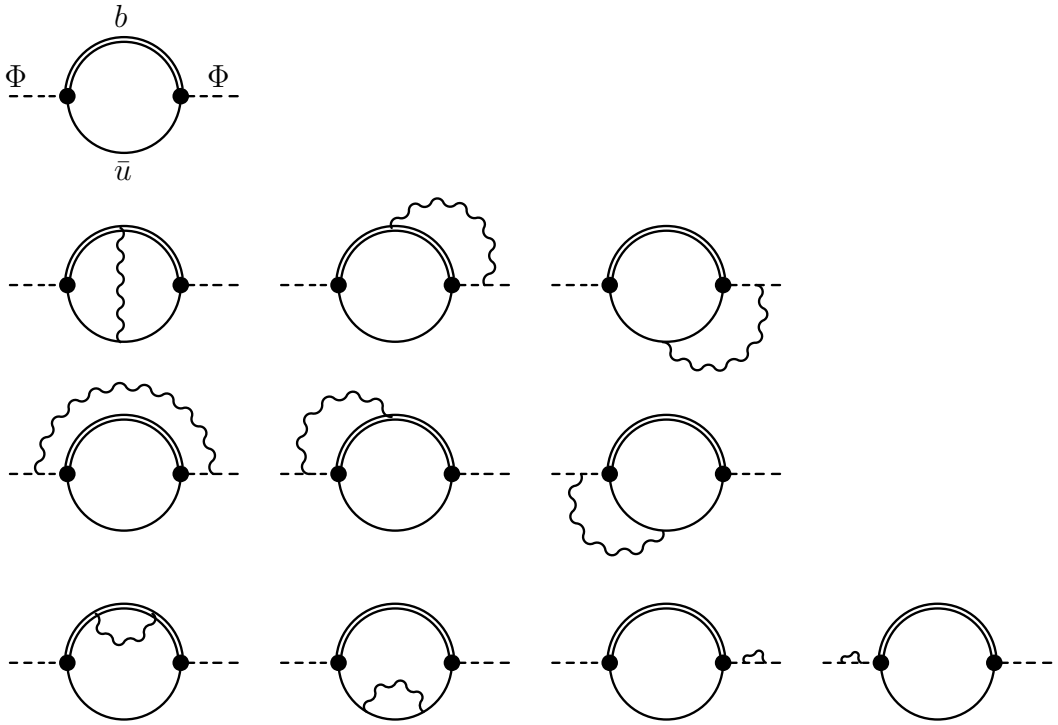

Figure 3.3 *Diagrams contributing to* $C(p_B^2, p_\Phi^2)$ (3.11)*, that is* $|\mathcal{Z}_B|^2$ (3.12)*. Again the top line is the LO contribution.*

middle they are equivalent to the hypothetical photon inclusive transition rate $\Phi_B \to b\bar{q}(\gamma)$ (decaying through the $\mathcal{J}_B$ vertex) via the optical theorem. Thus $|\mathcal{Z}_B|^2$ is guaranteed to be IR safe and we will show this explicitly in Section 3.2.6.

As there are no leptons involved in this correlator, there are no large collinear logs and QED effects are numerically small. Taking $\alpha \to 0$ and dropping the Φ_B particle, the correlator (3.11) reduces down to the correlator (2.11) used in the extraction of f_B. Indeed in this 'QCD limit' then the LSZ factor reduces as $|\mathcal{Z}_B|^2 \to m_B^4 f_B^2$. The full result is extracted through Borel transformation

$$|\mathcal{Z}_B|^2 \;=\; e^{\frac{m_B^2}{M^2}} \mathcal{B}_{M^2} C(p_B^2) \;\equiv\; \int_{m_+^2}^{s_0} \mathrm{d}s\, e^{\frac{m_B^2 - s}{M^2}} \rho_C(s)\,. \tag{3.12}$$

In addition to the Feynman diagrams drawn in Figures 3.1 to 3.3 there are condensate diagram contributions. Discussion of these is deferred to Section 3.2.7.

3.1.2 Kinematics

Before continuing we shall make some comments on the role of the auxiliary momentum $r = p_\Phi - p_B$, used to distinguish p_Φ (carried by the Φ_B) and p_B (the dispersion variable). The Φ_B particle must be on-shell, $p_\Phi^2 = m_B^2$, to give the correct IR physics, while $p_B^2 = s$ is integrated in the dispersion relation from m_+^2 to s_0. In a perfect world perturbative QCD would be exactly dual to the hadron spectrum and the spectral density taking the form $\rho(s) \propto \delta(s - m_B^2)$ would exactly enforce $p_B^2 = m_B^2$ in the dispersion relation. Of course this is never achieved in practise and so the dispersion relation enforces $p_B^2 \approx m_B^2$ only approximately. The auxiliary momentum r parameterises this difference. It is 'small' in the sense that it is $\mathcal{O}(p_B^2 - m_B^2)$ and really is crucial to the whole sum-rules idea: the whole concept of the sum rule technique hinges on $r \neq 0$.

Practically speaking the momentum r is injected at the $\mathcal{J}_B$ vertex so that p_B rather than p_Φ flows through the partons b and $\bar{q}$. The kinematics for the non-radiative decay takes the form

$$\begin{aligned} 2p_\Phi \cdot l_1 &= m_B^2 + m_\ell^2 \\ 2p_\Phi \cdot l_2 &= m_B^2 - m_\ell^2 \\ 2\, l_1 \cdot l_2 &= m_B^2 - m_\ell^2 \,, \end{aligned} \tag{3.13}$$

where recall $p_\Phi = l_1 + l_2$ and $m_\Phi = m_B$. This justifies the nature of m_Φ: if $m_\Phi \neq m_B$ then the fundamental kinematics of the decay would be incorrect. In the calculation r dependence appears through scalar products and extra Lorentz structures involving r. Extra Lorentz structures, like $\bar{u}\not{r}v$, $r \cdot \epsilon^*$ etc. (where $\bar{u} \equiv \bar{u}(l_1)$ and $v \equiv v(l_2)$), are considered extra unphysical information and are discarded. This is important as, for example, $\bar{u}\not{r}v$ does not have the required helicity suppression

$$\bar{u}\not{p}_B \Gamma v \;=\; m_\ell\, \bar{u}\Gamma v - \bar{u}\not{r}\Gamma v \,, \qquad \Gamma \equiv 1 - \gamma_5 \,. \tag{3.14}$$

Scalar products involving r are $\mathcal{O}(p_B^2 - m_B^2)$ and would vanish if we had a perfect LSZ procedure (perfect dispersion). There is some freedom[2] in how these are

[2]As momentum conservation takes the form $p_B + r = l_1 + l_2$ this is essentially a $2 \to 2$ process with 6 kinematic invariants. The physical leptonic decay is a $1 \to 2$ process with 3 fewer invariants. Fixing $p_\Phi^2 = m_B^2$ is one choice and the two conditions in (3.15) remove the remaining freedom. Note that assuming $r^2 = 0$ means the second choice must satisfy $2(l_1 \cdot r + l_2 \cdot r) = m_B^2 - p_B^2$.

chosen, we take

$$r^2 = 0\,, \qquad l_2 \cdot r = 0\,, \tag{3.15}$$

which fixes the remaining scalar products. This is the most sensible choice for a number of reasons. It is sensible to take the auxiliary r as massless to avoid introducing another scale, and the neutrino being massless allows us to set $l_2 \cdot r \to 0$. The choice $l_1 \cdot r = 0$ for example is prevented by the non-zero lepton mass. Further squaring (3.14) (essentially the LO amplitude) gives

$$\langle |\bar{u} \not{p}_B \Gamma v|^2 \rangle \;=\; 8 m_\ell^2\, l_1 \cdot l_2 + A\, l_2 \cdot r + B\, r^2\,, \tag{3.16}$$

where A and B are coefficients, meaning that the choices in (3.15) are consistent with the required helicity suppression. Physically the choice $l_2 \cdot r = 0$ is motivated by the fact that the neutrino is electrically neutral, does not interact and thus does not play a role in the sum rule calculation. A final argument, showing that this choice recovers the correct collinear logs in the scalar QED limit, will be given in the next section. Practically speaking we stress that such considerations are immaterial as these scalar products are suppressed under the dispersion where $p_B^2 \approx m_B^2$. These small effects are a consequence of working in a sum rules framework and enter the final sum rule uncertainty budget. With the choices (3.15), the remaining (non-radiative) scalar products are

$$\begin{aligned}
2p_B \cdot l_1 &= p_B^2 + m_\ell^2\,, & 2p_B \cdot r &= m_B^2 - p_B^2\,, \\
2p_B \cdot l_2 &= m_B^2 - m_\ell^2\,, & 2p_\Phi \cdot r &= m_B^2 - p_B^2\,, \\
2p_B \cdot p_\Phi &= p_B^2 + m_B^2\,, & 2l_1 \cdot r &= m_B^2 - p_B^2\,,
\end{aligned} \tag{3.17}$$

and we note that in the calculations one has to be wary of the sign change at $p_B^2 = m_B^2$. The extra scale m_B that now appears in the perturbative calculation adds to the complexity of the problem. To give an explicit parameterisation, in the $p_B = (\sqrt{s}, \mathbf{0})$ rest-frame (which we adopt for the calculation), the momenta are

$$\begin{aligned}
p_B &= \big(\sqrt{s}, 0, 0, 0\big) \\
p_\Phi &= \frac{1}{2\sqrt{s}}\Big(s + m_B^2, 0, 0, s - m_B^2\Big) \\
l_1 &= \frac{1}{2\sqrt{s}}\Big(s + m_\ell^2, 0, 0, s - m_\ell^2\Big) \\
l_2 &= \frac{m_B^2 - m_\ell^2}{2\sqrt{s}}\Big(1, 0, 0, -1\Big)\,,
\end{aligned} \tag{3.18}$$

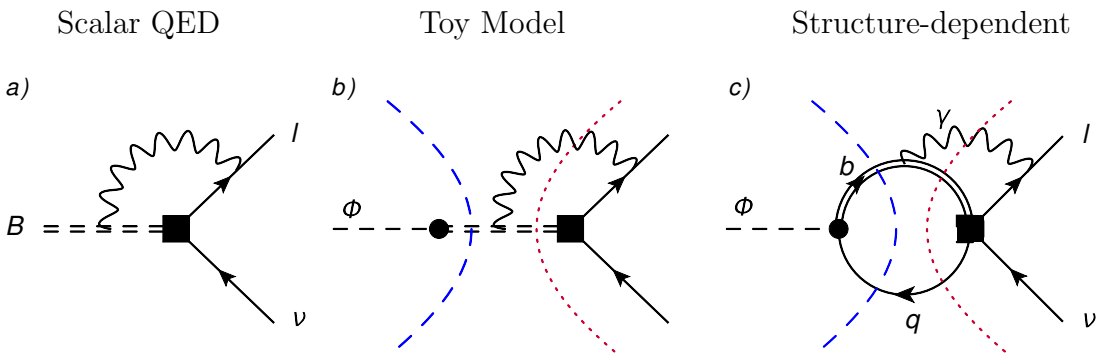

Figure 3.4 *Virtual diagrams for the decay of a $\bar{B}$-meson in increasing levels of complexity. Left (a): the decay in scalar QED where the meson is point-like, Section 2.3.3. In this case there are also contact diagrams (not drawn) where the photon emerges from the weak vertex (black square). Middle (b): a toy model where we make use of the $\mathcal{J}_B$ operator (black circle) but we keep the meson point-like. Right (c): the full calculation, i.e. the $b\,\ell_1$ contribution to $\Pi(p_B^2, p_\Phi^2)$. For (b) and (c) where there is a dispersion, the two classes of cuts in p_B^2 are shown. Those where the photon is not cut are what we refer to as blue cuts (dashed), while those where it is are called red cuts (dotted).*

where we choose the lepton momentum to be aligned with the $+z$ axis[3]. In the radiative case we employ external form factors and the calculation is most easily performed in Dalitz variables, discussed further in Section 3.3.

3.1.3 A Toy Model

Before embarking on the full structure-dependent calculation it is worthwhile to test these methods in a simplified toy model. We calculate the simplified diagrams where the b-$\bar{q}$ quark loop is replaced by a scalar $\bar{B}$-propagator as shown in Figure 3.4(b). Figure 3.4 illustrates how this toy model is the intermediate step between the scalar QED calculation (Fig. 3.4(a)) and the full structure-dependent calculation (Fig. 3.4(c)). The toy model is essentially a scalar QED calculation performed in a dispersive sum-rules framework.

As this simplified model is one loop we can calculate the exact result for the virtual numerator and denominator diagrams using FeynCalc. However we also compute the imaginary part of these diagrams using Cutkosky rules as an additional check. We distinguish two classes of cuts depending on whether the photon propagator is cut. Those where the photon is cut are referred to as 'red'

[3]Similarly the auxiliary momentum $r = ((m_B^2 - s)/(2\sqrt{s})) \cdot (1, 0, 0, -1)$ is in the $\pm z$ direction as it must be to not introduce a new unphysical angle into the kinematics.

cuts while 'blue' cuts do not involve the photon. For clarity these two types of cuts are displayed as red (dotted) and blue (dashed) lines in Figure 3.4 for both the toy model and the full computation. In the full structure-dependent case the red cuts involve cutting three propagators (b, $\bar{q}$ and γ) while the blue cuts cut just the b and $\bar{q}$. In all cases the quark loop is cut. The red cuts resemble a real decay as the photon is put on-shell in the cut, while the blue cuts are simplified as the photon loop factorises.

Returning to the toy model, we find for the 1PI collinear logs

$$\begin{aligned}\Pi^{(2)\,,\,\text{1PI}}_{\text{Toy, S-P}}\Big|_{\text{HC}} &= -\frac{\alpha}{\pi}\Pi^{(0)}_{\text{Toy,S-P}} \times \ln m_\ell \\ \Pi^{(2)\,,\,\text{1PI}}_{\text{Toy,V-A}}\Big|_{\text{HC}} &= +\frac{\alpha}{2\pi}\Big(1+\mathcal{O}(1)\, l_2\cdot r\Big)\Pi^{(0)}_{\text{Toy, V-A}} \times \ln m_\ell\,, \end{aligned} \tag{3.19}$$

which reassuringly matches the scalar QED calculation (Table 2.1) as it should do – no structure is being resolved here. In the V-A case we recover the scalar QED logs provided we set $l_2\cdot r = 0$ which, as discussed in previous section, is really the only sensible choice. The extra $\mathcal{O}(1)$ contribution arises from the red cuts[4] with the blue cuts giving the scalar QED logs. It may be tempting to consider taking just the blue cuts however this cannot be done. In a given diagram the individual red and blue cuts each contain an *unphysical* IR divergence which cancels only once red and blue cuts are combined. The *physical* IR divergences appear from diagrams that only have a *red* cut.

Including the self-energy corrections the physical virtual soft divergences appear as

$$\Pi^{(2)}_{\text{Toy}}(p_B^2) \;=\; -\frac{\alpha}{4\pi}\Pi^{(0)}_{\text{Toy}}(p_B^2)\left(2+\frac{m_\Phi^2-m_\ell^2}{m_\Phi^2-m_\ell^2}\ln\frac{m_\ell^2}{m_\Phi^2}\right)\frac{1}{\epsilon_{\text{IR}}}+\mathcal{O}(\epsilon^0)\,, \tag{3.20}$$

with the first term from the self-energies and the second from the $\Phi\,\ell_1$ diagram. The Φ_B particle is crucial for giving the correct soft divergence as it is on-shell. This matches the universal soft form (2.55) provided we identify $m_\Phi = m_B$, providing further justification for this procedure. This is mirrored by the real computation where emission from the Φ_B particle gives the physical soft divergence.

The denominator factor $|\mathcal{Z}_B|^2$ can also be investigated in the toy model, and it is explicitly found to be IR finite, with the IR divergence from the 1PI $\Phi\,\Phi$ graph

[4]To be specific, the extra term is proportional to $(l_2\cdot r)(\bar{u}\gamma_\alpha\Gamma v)(r_\beta)\mathcal{M}^{\alpha\beta}_{p_\Phi p_B l_1}(p_B;0,m_B)$ with the notation explained in equation (3.31).

being cancelled by the Φ_B self-energy contributions. The infrared structure is not affected by the Borel procedure as soft terms are still proportional to the tree result at the level of individual cuts.

Gauge dependence can be checked in the numerator and denominator correlators, with explicit gauge-invariance appearing. The gauge-parameter ξ vanishes as a consequence of charge conservation. For example in the numerator it enters as $\xi(Q_{\bar{B}} - Q_{\ell_1})(Q_{\bar{B}} - Q_{\Phi}) = 0$.

By computing the toy model using both cutting rules and the exact one-loop result we also verify our specific implementation of the two cut-off phase space slicing procedure (discussed in Section 3.2.6 and 3.4.1). An extra complication in the toy model is the appearance of box integrals. In these the IR parts can be extracted through Dittmaier's algorithm, for example

$$D_0(m_\ell^2, 0, 0, s, m_B^2, 0, 0, m_\ell^2, m_B^2, m_B^2)|_{\rm IR} = \\ \frac{1}{s - m_B^2}\Big(C_0(m_\ell^2, 0, m_B^2, 0, m_\ell^2, m_B^2) - \frac{s}{m_B^2} C_0(m_\ell^2, 0, s, 0, m_\ell^2, m_B^2)\Big)_{\rm IR}\,, \quad (3.21)$$

with the Passarino-Veltman functions described in Appendix A.1. The first C_0 function gives the soft divergence which also includes $\ln m_\ell^2$ soft-collinear terms. From a cutting rules perspective these correspond to the $1/\epsilon_{\rm IR}$ pole multiplying the $\mathcal{O}(\epsilon)$ part of an angular integral.

In summary, all important features (gauge-invariance, soft behaviour, HC logs) have been tested in the toy model which provides a useful check of the methodology.

3.1.4 Leading Order Result

In the full structure-dependent computation the tree level result for the V-A correlator reads

$$\mathrm{Im}\,\Pi^{(0)}(p_B^2) \;=\; \frac{m_+^2 N_c\, g_{\rm eff}}{8\pi} \frac{\sqrt{\lambda(p_B^2, m_b^2, m_q^2)}}{p_B^2}\left(1 - \frac{m_-^2}{p_B^2}\right)\mathcal{S}(\epsilon)\, m_\ell\, \bar{u}\Gamma v\,, \quad (3.22)$$

where at LO only the axial part contributes. The cutting of the quark propagators generates a Källén function

$$\lambda(x,y,z) \;\equiv\; x^2+y^2+z^2-2xy-2yz-2xz\,, \tag{3.23}$$

which as $m_b, m_q > 0$ can be written as (recall $m_\pm = m_b \pm m_q$)

$$\lambda(p_B^2, m_b^2, m_q^2) = \left(p_B^2 - m_+^2\right)\left(p_B^2 - m_-^2\right). \tag{3.24}$$

We will make use of the abbreviation $\lambda \equiv \lambda(p_B^2, m_b^2, m_q^2)$ and further denote $\lambda_q \equiv \lambda(q^2, m_b^2, m_q^2)$. The factor $\mathcal{S}(\epsilon)$ gives the $\mathcal{O}(\epsilon)$ correction which is

$$\mathcal{S}(\epsilon) \equiv 1 - \epsilon \ln\!\left(\frac{\lambda}{4\mu^2 p_B^2}\right) + \epsilon(2 - \gamma_E + \ln\pi) \tag{3.25}$$

where μ is the usual DimReg scale and γ_E the Euler-Mascheroni constant. For an S-P interaction, the corresponding result is

$$\mathrm{Im}\,\Pi^{(0)}_{\text{S-P}}(p_B^2) \;=\; -\frac{m_+ N_c\, g_{\text{eff}}}{8\pi}\sqrt{\lambda(p_B^2, m_b^2, m_q^2)}\left(1 - \frac{m_-^2}{p_B^2}\right)\mathcal{S}(\epsilon)\,\bar{u}\Gamma v\,, \tag{3.26}$$

though of course in this case the coupling g_{eff} is zero in the SM. The leading order denominator correlator takes a similar form

$$\mathrm{Im}\,C^{(0)}(p_B^2) \;=\; \frac{m_+^2 N_c}{8\pi}\sqrt{\lambda(p_B^2, m_b^2, m_q^2)}\left(1 - \frac{m_-^2}{p_B^2}\right)\mathcal{S}(\epsilon)\,, \tag{3.27}$$

which in the limit $m_q \to 0$ recovers the LO result for the f_B correlator given in (2.22) as $\lambda(p_B^2, m_b^2, 0) \to (p_B^2 - m_b^2)^2$. The LO results are all $m_b \leftrightarrow m_q$ symmetric as indeed they must be. The similarities between (3.22) and (3.27) are not by accident as at LO they are both just different ways of extracting f_B in a sum rules framework

$$\begin{aligned} e^{\frac{m_B^2}{M^2}}\mathcal{B}_{M^2} C^{(0)}(p_B^2) &= m_B^4 f_B^2 + \cdots \\ e^{\frac{m_B^2}{M^2}}\mathcal{B}_{M^2} \Pi^{(0)}(p_B^2) &= m_B^2 f_B^2\, g_{\text{eff}}\, m_\ell \bar{u}\Gamma v + \cdots . \end{aligned} \tag{3.28}$$

3.2 Virtual Computation

This section details the computation of the $\mathcal{O}(\alpha)$ virtual corrections to the numerator and denominator correlators, that is $\mathrm{Im}\,\Pi^{(2)}$ and $\mathrm{Im}\,C^{(2)}$. The virtual calculation is considerably more labour intensive than the real radiation.

3.2.1 Generalities

The diagrams of Figure 3.1 (numerator) and Figure 3.3 (denominator) are computed using Cutkosky cutting rules in $d = 4 - 2\epsilon$ dimensions to obtain the spectral densities ρ_Π and ρ_C. The calculation is two loop and involves a considerable number of scales: we calculate with full m_b, m_q, m_ℓ, m_B, s (and μ) dependence. For the B^- ($q = u$) decay the light quark m_q is indeed light so in principle could be neglected. However this would lead to artificial collinear divergences in individual cuts and so we keep this mass non-zero to act as a natural regulator $\ln m_q$. Of course once cuts are combined these $\ln m_q$ terms cancel as this is not a physical IR divergence as the light quark is not on-shell.

In the denominator correlator C there are no leptons and so the calculation is more simple. The numerator correlator Π is complicated by spinor structures and is where large QED effects are found. The methods of calculating Π and C are broadly similar and so we present these computations in parallel. Both correlators have the idea of red and blue cuts, depending on whether the photon is cut (red) or not cut (blue) in addition to the quark loop.

The red cuts resemble a real decay (albeit with different kinematics) as the photon is put on-shell in the cut. Correspondingly the photon energy is cut-off at a maximum value Λ and so no UV divergences are generated. This also means soft and collinear divergences can be handled in a manner similar to a real decay via a slicing procedure. We adapt the ideas of [156] to the virtual case, additionally including finite lepton masses into the framework. To the best of our knowledge this *virtual* two cut-off phase space slicing is new. In the slicing procedure we decompose the photon energy integral into a soft part, treated in $d = 4 - 2\epsilon$, and a hard part in $d = 4$

$$\int_0^\Lambda \mathrm{d}|\boldsymbol{k}| \int \mathrm{d}\Omega_{d-1} \to \int_0^{\Delta E_s} \mathrm{d}|\boldsymbol{k}| \int \mathrm{d}\Omega_{d-1} + \int_{\Delta E_s}^\Lambda \mathrm{d}|\boldsymbol{k}| \int \mathrm{d}\Omega_3 \ . \tag{3.29}$$

The boundary between the regions is ΔE_s which is chosen to be sufficiently small to allow us to drop subleading powers of $|\boldsymbol{k}|$ in the soft integrand. That is we *slice* out the soft region and treat it separately. The hard part is further broken down into collinear and non-collinear regions and this collinear slicing will be described in 3.4.1. We will also perform a slicing procedure for the real radiation (Section 3.3) though this is more standard, following [90].

In the blue cuts the photon loop is left untouched. The photon loop factorises and can be calculated using standard one-loop methods. The blue cuts are therefore where UV divergences appear and their renormalisation is discussed in Section 3.2.5. While all 1PI diagrams have a red cut, two diagrams do not have a blue cut. These are the 'rainbow' diagrams, $\Phi\,\ell_1$ (numerator) and $\Phi\,\Phi$ (denominator), drawn as the first diagram on the third line of Figure 3.1 and 3.3 respectively.

The three diagrams involving leptons are complicated by $\epsilon_{\mu\nu\rho\sigma}$ structures contracted with spinors. These can be removed via the Chisholm identity

$$\gamma_\mu \epsilon^{\mu\nu\rho\sigma} = i\big(\gamma^\nu\gamma^\rho\gamma^\sigma - g^{\nu\rho}\gamma^\sigma - g^{\rho\sigma}\gamma^\nu + g^{\nu\sigma}\gamma^\rho\big)\gamma_5\,, \tag{3.30}$$

valid in $d = 4$ only after we have removed all poles. To simplify the calculation we work in the p_B rest frame and evaluate all diagrams analytically up until a final single numerical integral. All the diagrams have been checked numerically to per mille precision using pySecDec [197] to $\mathcal{O}(\epsilon^0)$.

3.2.2 Delta Function and Angular Integrals

Integrals involving two delta functions occur repeatedly when using Cutkosky rules and take the general form

$$\mathcal{M}^{\alpha\beta\ldots}_{p_i p_j \ldots}(P; m_A, m_B) \equiv \int \mathrm{d}^d l\, \frac{\mu^{2\epsilon}\, l^\alpha l^\beta \cdots}{(p_i\cdot l)(p_j\cdot l)\cdots}\delta^+(l^2 - m_A^2)\delta^+((P-l)^2 - m_B^2)\,, \tag{3.31}$$

where l is a loop momentum and P an external momentum. Typically $P = p_B$ or $P = q \equiv p_B - k$ with k being the photon loop momentum. The delta functions collapse two of the four integrals with the difficulty of the remaining two angular integrals dependent on how many angles are in the problem. Consider first the simplest case

$$\mathcal{M}(p_B; m_q, m_b) = \mu^{2\epsilon}\int \mathrm{d}^d l\, \delta^+(l^2 - m_q^2)\delta^+((p_B - l)^2 - m_b^2)\,, \tag{3.32}$$

which is so ubiquitous that we will simply refer to it as $\mathcal{M}$ with the $(p_B; m_q, m_b)$ being implicit. This is the LO quark loop integral. It can be computed by introducing a second integral over $\mathrm{d}^d\tilde{l}$ with $\tilde{l} = p_B - l$

$$\mathcal{M} = \mu^{2\epsilon} \int \mathrm{d}^d l \, \mathrm{d}^d\tilde{l} \; \delta^{(d)}(\tilde{l} - (p_B - l)) \, \delta^+(l^2 - m_q^2) \delta^+(\tilde{l}^2 - m_b^2) \,, \tag{3.33}$$

which puts the delta functions in a more symmetric form. The original two delta functions can now easily be collapsed

$$\begin{aligned} \mathcal{M} &= \frac{\mu^{2\epsilon}}{4} \int \frac{\mathrm{d}^{d-1}\boldsymbol{l} \; \mathrm{d}^{d-1}\tilde{\boldsymbol{l}}}{(|\boldsymbol{l}|^2 + m_q^2)^{1/2} (|\tilde{\boldsymbol{l}}|^2 + m_b^2)^{1/2}} \delta^{(d)}(\tilde{l} + l - p_B) \\ &= \frac{\mu^{2\epsilon}}{4} \int \frac{\mathrm{d}^{d-1}\boldsymbol{l}}{(|\boldsymbol{l}|^2 + m_q^2)^{1/2} (|\boldsymbol{p_B} - \boldsymbol{l}|^2 + m_b^2)^{1/2}} \\ &\qquad \times \delta\big((|\boldsymbol{l}|^2 + m_q^2)^{1/2} + (|\boldsymbol{p_B} - \boldsymbol{l}|^2 + m_b^2)^{1/2} - p_B^0\big) \,, \end{aligned} \tag{3.34}$$

where in the second line we collapse $d-1$ delta functions which enforces 3-momentum conservation. The final delta function encodes energy conservation. Choosing the p_B rest frame for convenience we must solve

$$\sqrt{|\boldsymbol{l}|^2 + m_q^2} + \sqrt{|\boldsymbol{l}|^2 + m_b^2} = \sqrt{p_B^2} \,, \tag{3.35}$$

which has solution $|\boldsymbol{l}| = |\boldsymbol{l}^*|$ with

$$|\boldsymbol{l}^*| = \sqrt{\frac{\lambda(p_B^2, m_b^2, m_q^2)}{4p_B^2}} \,, \qquad p_B^2 \geq m_+^2 \,, \tag{3.36}$$

which is the origin of the Källén functions in the LO results in 3.1.4. Physically this arises from cutting the quark loop which puts the b- and $\bar{q}$-quark on-shell. By construction the momentum $\boldsymbol{p_B}$ flows through the quark loop and choosing this rest frame means the quarks are back-to-back. Equation (3.36) is just the momentum of each quark in the $1 \to 2$ decay of a particle of mass p_B^2. Consequently there is only a solution for $p_B^2 \geq m_+^2$. The result should be $b \leftrightarrow q$ symmetric which is reflected in the symmetry of the Källén function. Rewriting the remaining delta function in terms of its root

$$\begin{aligned} \mathcal{M} = \frac{\mu^{2\epsilon}}{4} \int & \frac{|\boldsymbol{l}|^{d-2} \, \mathrm{d}|\boldsymbol{l}| \, \mathrm{d}\Omega_{d-1}}{(|\boldsymbol{l}|^2 + m_q^2)^{1/2} (|\boldsymbol{l}|^2 + m_b^2)^{1/2}} \, \theta(p_B^2 - m_+^2) \\ & \times \frac{(|\boldsymbol{l}^*|^2 + m_q^2)^{1/2} (|\boldsymbol{l}^*|^2 + m_b^2)^{1/2}}{|\boldsymbol{l}^*| (p_B^2)^{1/2}} \delta(|\boldsymbol{l}| - |\boldsymbol{l}^*|) \end{aligned}$$

$$= \frac{\mu^{2\epsilon}}{4\sqrt{p_B^2}} |\boldsymbol{l}^*|^{d-3}\, \theta(p_B^2 - m_+^2) \int \mathrm{d}\Omega_{d-1}\ , \tag{3.37}$$

all that remains is the angular integration over the $3-2\epsilon$ dimensional solid angle $\mathrm{d}\Omega_{d-1}$. In this simple case there is no angular dependence in the integrand leading to the final result

$$\mathcal{M} \;=\; \frac{\mu^{2\epsilon}\,\Omega_{d-1}}{4\sqrt{p_B^2}} \left(\frac{\lambda(p_B^2, m_b^2, m_q^2)}{4p_B^2}\right)^{\frac{d-3}{2}} \theta(p_B^2 - m_+^2)\,. \tag{3.38}$$

Evaluating the cut this way means putting the quarks on-shell before enforcing momentum conservation. While loop momenta may generally be rerouted in integrals without issue, care must be taken when cutting to ensure correct energy flow through the diagram. This corresponds to being careful with the step functions contained in the δ^+ distribution. Beyond LO we encounter various integrals of this form which contain non-trivial angular dependence. The three most frequent are

$$\begin{aligned}
\mathcal{M}_k \;&= \mu^{2\epsilon} \int \mathrm{d}^d l\, \frac{1}{k\cdot l}\, \delta^+(l^2 - m_q^2)\delta^+((p_B - l)^2 - m_b^2) \\
\mathcal{M}_{kk} &= \mu^{2\epsilon} \int \mathrm{d}^d l\, \frac{1}{(k\cdot l)^2}\, \delta^+(l^2 - m_q^2)\delta^+((p_B - l)^2 - m_b^2) \\
\mathcal{M}_{\ell_1} &= \mu^{2\epsilon} \int \mathrm{d}^d l\, \frac{1}{l_1\cdot l}\, \delta^+(l^2 - m_q^2)\delta^+((p_B - l)^2 - m_b^2)\,,
\end{aligned} \tag{3.39}$$

where k is an on-shell photon momentum and as before the $(p_B; m_q, m_b)$ is assumed unless otherwise stated. Variants involving p_B (e.g. $\mathcal{M}_{p_B}$ and $\mathcal{M}_{p_B\, p_B}$) are trivial in the p_B rest frame while integrals involving denominator factors of $p_\Phi \cdot k$ are deferred to the discussion of IR physics in Section 3.2.6. Unlike at LO the above integrals are not $b \leftrightarrow q$ symmetric. Defining the counterpart

$$\mathcal{N}_k(p_B; m_q, m_b) \equiv \mu^{2\epsilon} \int \mathrm{d}^d l\, \frac{1}{k\cdot(p_B - l)} \delta^+(l^2 - m_q^2)\delta^+((p_B - l)^2 - m_b^2)\,, \tag{3.40}$$

then trivially

$$\mathcal{N}_k(p_B; m_q, m_b) = \mathcal{M}_k(p_B; m_b, m_q)\,, \tag{3.41}$$

and similarly for $\mathcal{M}_{kk}$ and $\mathcal{M}_{\ell_1}$. All integrals (including tensor ones like $\mathcal{M}_k^\alpha$, $\mathcal{M}_{\ell_1}^{\alpha\beta}$ etc.) must be calculated completely to $\mathcal{O}(\epsilon)$ due to the presence of poles in $1/\epsilon$ that multiply them. This means we require knowledge of angular integrals at $\mathcal{O}(\epsilon)$.

Angular integrals in $d-1$ dimensions have the recursive property

$$\int \mathrm{d}\Omega_{d-1} = \int_0^\pi (\sin\theta)^{d-3}\,\mathrm{d}\theta \int \mathrm{d}\Omega_{d-2}\ , \tag{3.42}$$

with the solid angle defined in terms of the Gamma function, $\Gamma(z)$

$$\int \mathrm{d}\Omega_{d-1} \ = \ \frac{2\pi^{\frac{d-1}{2}}}{\Gamma(\frac{d-1}{2})}\,, \qquad\qquad \Gamma(z)|_{\mathrm{Re}\,z>0} = \int_0^\infty t^{z-1}e^{-t}\,\mathrm{d}t\ , \tag{3.43}$$

such that $(\Omega_3, \Omega_2) = (4\pi, 2\pi)$. With our choice of kinematics we require

$$I^{(n,0)}|_{d=4-2\epsilon} \equiv 2^{2\epsilon}\pi \int_0^\pi \frac{(\sin\theta)^{d-3}\,\mathrm{d}\theta}{(a-b\cos\theta)^n}\,, \qquad \begin{array}{c} a\neq b \\ n=1,2 \end{array} \tag{3.44}$$

as integrals involving two denominators can be avoided. We give some comments on the full two denominator massive case which has been worked out in [90] (see also [198, 199]) in Section 3.2.6. The simpler cases can be found in [200–202], specifically these read

$$\begin{aligned} I^{(1,0)}|_{d=4-2\epsilon} &= \frac{\pi}{b}\left[\ln\left(\frac{a+b}{a-b}\right) + 2\epsilon\left(\mathrm{Li}_2\left(\frac{2b}{a+b}\right) + \frac{1}{4}\ln^2\left(\frac{a+b}{a-b}\right)\right)\right] + \mathcal{O}(\epsilon^2) \\ I^{(2,0)}|_{d=4-2\epsilon} &= \frac{2\pi}{a^2-b^2}\left[1 + \epsilon\frac{a}{b}\ln\left(\frac{a+b}{a-b}\right)\right] + \mathcal{O}(\epsilon^2)\,. \end{aligned} \tag{3.45}$$

Using these results one can derive (with $k^2=0$)

$$\begin{aligned} \mathcal{M}_k \ = \ \frac{\Omega_{d-2}}{4p_B\cdot k}\left(\frac{\lambda}{\mu^2 p_B^2}\right)^{-\epsilon}\theta(p_B^2-m_+^2)\Bigg[&\ln\frac{\left(\lambda^{\frac{1}{2}}+2p_B^2\mathbb{Y}\right)^2}{4p_B^2m_q^2} \\ &+\ 2\epsilon\left(\mathrm{Li}_2\frac{2\lambda^{\frac{1}{2}}}{\lambda^{\frac{1}{2}}+2p_B^2\mathbb{Y}} + \frac{1}{4}\ln^2\frac{(\lambda^{\frac{1}{2}}+2p_B^2\mathbb{Y})^2}{4p_B^2m_q^2}\right)\Bigg] + \mathcal{O}(\epsilon^2)\,, \end{aligned} \tag{3.46}$$

where we define the dimensionless $\mathbb{Y}(p_B^2, m_b^2, m_q^2)$

$$\mathbb{Y} \ \equiv \ \frac{p_B^2 - m_+m_-}{2p_B^2}\,, \qquad \mathbb{Y} + \mathbb{Y}|_{m_b\leftrightarrow m_q} = 1\,, \tag{3.47}$$

which physically corresponds to the energy of the cut $\bar{q}$-quark, $(l^*)^0 = \mathbb{Y}\sqrt{p_B^2}$. Note there is a collinear divergent $\ln m_q$ present in $\mathcal{M}_k$. Similarly

$$\mathcal{M}_{\ell_1} \;=\; \frac{1}{2}\frac{\Omega_{d-2}}{p_B^2-m_\ell^2}\left(\frac{\lambda}{\mu^2 p_B^2}\right)^{-\epsilon}\theta(p_B^2-m_+^2)\Big[\ln\Psi_1 \;+\; 2\epsilon\big(\mathrm{Li}_2\Psi_2+\tfrac{1}{4}\ln^2\Psi_1\big)\Big] \\ +\;\mathcal{O}(\epsilon^2)\,, \quad (3.48)$$

where

$$\begin{aligned}\Psi_1 &= \frac{2p_B^2\mathbb{Y}(p_B^2+m_\ell^2)+\lambda^{\frac{1}{2}}(p_B^2-m_\ell^2)}{2p_B^2\mathbb{Y}(p_B^2+m_\ell^2)-\lambda^{\frac{1}{2}}(p_B^2-m_\ell^2)}\\ \Psi_2 &= \frac{2\lambda^{\frac{1}{2}}(p_B^2-m_\ell^2)}{2p_B^2\mathbb{Y}(p_B^2+m_\ell^2)+\lambda^{\frac{1}{2}}(p_B^2-m_\ell^2)}\,,\end{aligned} \quad (3.49)$$

and finally

$$\mathcal{M}_{kk} \;=\; \frac{p_B^2}{m_q^2}\frac{(1-2\epsilon)}{(p_B\cdot k)^2}\left[1+2\epsilon\frac{p_B^2\mathbb{Y}}{\lambda^{\frac{1}{2}}}\ln\frac{\big(\lambda^{\frac{1}{2}}+2p_B^2\mathbb{Y}\big)^2}{4p_B^2m_q^2}\right]\mathcal{M}\;+\;\mathcal{O}(\epsilon^2)\,. \quad (3.50)$$

Tensor integrals are written in terms of scalar integrals via suitable projections, exploiting symmetry where convenient. Only a maximum of two-index integrals are needed for our purposes, for example

$$\begin{aligned}\mathcal{M}^\alpha &= \mathcal{M}\mathbb{Y}p_B^\alpha\\ \mathcal{M}^\alpha_{k^n} &= \frac{\mathcal{M}_{k^{n-1}}}{p_B\cdot k}\left[p_B^\alpha-\frac{p_B^2}{p_B\cdot k}k^\alpha\right]+\frac{p_B^2}{p_B\cdot k}\mathcal{M}_{k^n}\mathbb{Y}k^\alpha\\ \mathcal{M}^\alpha_{\ell_1^n} &= \frac{4}{(p_B^2-m_\ell^2)^2}\Big[\big(p_B\cdot l_1\,p_B^\alpha-p_B^2\,l_1^\alpha\big)\mathcal{M}_{\ell_1^{n-1}}-\big(m_\ell^2\,p_B^\alpha-p_B\cdot l_1\,l_1^\alpha\big)p_B^2\mathbb{Y}\mathcal{M}_{\ell_1^n}\Big],\end{aligned} \quad (3.51)$$

given in recursive form for $n\in\mathbb{Z}^+$ with the notation $\mathcal{M}_{k^n}=\mathcal{M}_{k\cdots k}$ (n times), $\mathcal{M}_{k^0}=\mathcal{M}$ and similarly for $\mathcal{M}_{\ell_1^n}$. Two index integrals require the inversion of 4×4 matrices, the simplest case is

$$\mathcal{M}^{\alpha\beta}=\mathcal{M}\left[\mathbb{Y}^2p_B^\alpha\,p_B^\beta+\frac{1}{1-d}\frac{\lambda}{4p_B^2}\Big(g^{\alpha\beta}-\frac{p_B^\alpha\,p_B^\beta}{p_B^2}\Big)\right], \quad (3.52)$$

while expressions for $\mathcal{M}^{\alpha\beta}_{k^n}$ and $\mathcal{M}^{\alpha\beta}_{\ell_1^n}$ are quite complicated.

3.2.3 Red Cuts

We now describe the calculation of the red cuts for the numerator and denominator diagrams. We illustrate the method using the numerator $b\,\ell_1$ graph

(Figure 3.4(c)) as an example. Other graphs are calculated in a similar fashion.

In the Feynman gauge $\xi = 1$ the integral representation of the $b\,\ell_1$ graph takes the form

$$\Pi^{(2)}_{b\,\ell_1} = \frac{-m_+ g_{\rm eff} e^2 Q_b Q_{l_1} N_c \mu^{4\epsilon}}{(2\pi)^{2d}} \int \mathrm{d}^d k\, \mathrm{d}^d l \qquad (3.53)$$
$$\frac{\mathrm{Tr}[\gamma_5(-\not{l} + m_q)\hat{\Gamma}^\mu(\not{q} - \not{l} + m_b)\gamma^\rho(\not{p}_B - \not{l} + m_b)]}{(l^2 - m_q^2)((p_B - l)^2 - m_b^2)((q - l)^2 - m_b^2)k^2} \frac{\bar{u}\gamma_\rho(\not{l}_1 - \not{k} + m_\ell)\Gamma_\mu v}{(l_1 - k)^2 - m_\ell^2},$$

where k is the photon loop momentum and l is the quark loop momentum. The red cut of this diagram involves putting the photon and both quarks on-shell, cutting the l, $q - l$ and k momentum propagators, giving imaginary part

$$\mathrm{Im}\,\Pi^{(2)}_{b\,\ell_1}|_{\rm red} = \frac{-4\pi^3 m_+ g_{\rm eff} e^2 Q_b Q_{l_1} N_c \mu^{4\epsilon}}{(2\pi)^{2d}} \int \mathrm{d}^d k\, \frac{\delta^+(k^2)}{(l_1 - k)^2 - m_\ell^2}$$
$$\times \int \mathrm{d}^d l\, \delta^+(l^2 - m_q^2)\delta^+((q - l)^2 - m_b^2) \frac{\mathrm{Tr}[\cdots]\bar{u}\cdots v}{(p_B - l)^2 - m_b^2}, \qquad (3.54)$$

where recall $q = p_B - k$ and the trace and spinor structures are dot-suppressed for brevity. These structures in general contain k and l dependence and are evaluated using FeynCalc. We perform the quark loop integral (over $\mathrm{d}^d l$) first, noting that the $\delta^+(k^2)$ plays no role here except to enforce $k^2 = 0$. The trace and spinor structures can be decomposed as

$$\mathrm{Tr}[\cdots]\bar{u}\cdots v \;=\; A + B_\alpha\, l^\alpha + C_{\alpha\beta}\, l^\alpha l^\beta\,, \qquad (3.55)$$

where A, B_α, $C_{\alpha\beta}$ do not depend on l. The remaining uncut quark propagator is fixed by the delta function constraint $(q - l)^2 = m_b^2$ to

$$\frac{1}{(p_B - l)^2 - m_b^2} \;=\; \frac{1}{2k\cdot(p_B - l)} \;=\; \frac{1}{2k\cdot l}\bigg|_{l\to p_B - l}, \qquad (3.56)$$

so that the denominator assumes the form of (3.31). The l integral can now be evaluated using the methods of Section 3.2.2. Tensor integrals are decomposed into scalar ones and eventually the result can be written in terms of $\mathcal{M}(q; m_q, m_b)$ and $\mathcal{M}_k(q; m_b, m_q)$.

A crucial difference however is the momentum shift $p_B \to q$ in these integrals. This arises because the cut photon carries off momentum k leaving the b-quark with momentum $p_B - k$. Consequently the theta functions generated by the l-

integral take the form $\theta(q^2 - m_+^2)$ rather than $\theta(p_B^2 - m_+^2)$ and act to cut-off the photon energy at

$$\Lambda \equiv \frac{p_B^2 - m_+^2}{2(p_B^2)^{\frac{1}{2}}} \,. \tag{3.57}$$

The red cuts really are equivalent to a real photon emission, with the $\delta^+(k^2)$ forcing the photon on-shell and the maximum photon energy corresponding to the radiative decay of a particle of mass p_B^2 into a $b, \bar{q}, \gamma$ final state. The cut happens after the photon is radiated from the quark loop as compared to the blue cuts where the cut is before. Thus, defining the result of the l-integral to be $\theta(q^2 - m_+^2) \cdot I_{b\,\ell_1}$ we obtain

$$\begin{aligned} \mathrm{Im}\,\Pi^{(2)}_{b\,\ell_1}|_{\mathrm{red}} &= \frac{\pi^3 m_+ g_{\mathrm{eff}} e^2 Q_b Q_{\ell_1} N_c \mu^{4\epsilon}}{(2\pi)^{2d}} \int \frac{\mathrm{d}^{d-1}\boldsymbol{k}}{|\boldsymbol{k}|} \frac{I_{b\,\ell_1}}{k \cdot l_1} \theta(q^2 - m_+^2) \\ &= \frac{\pi^3 m_+ g_{\mathrm{eff}} e^2 Q_b Q_{\ell_1} N_c \mu^{4\epsilon}}{(2\pi)^{2d}} \int_0^\Lambda \mathrm{d}|\boldsymbol{k}| \int \mathrm{d}\Omega_{d-1} \, \frac{|\boldsymbol{k}|^{d-3}}{k \cdot l_1} I_{b\,\ell_1} \,, \end{aligned} \tag{3.58}$$

where the $\delta^+(k^2)$ has collapsed the k^0 integral. Thus we are left with another angular integral and a photon energy integral. Upon angular integration the $k \cdot l_1$ denominator generates hard-collinear logs, $\ln m_\ell$, when $\boldsymbol{k}$ and $\boldsymbol{l_1}$ are parallel. There is also a soft divergence as $I_{b\,\ell_1} \sim 1/|\boldsymbol{k}|$ as $|\boldsymbol{k}| \to 0$. To handle these divergences we slice out the soft and collinear regions as follows

$$\mathrm{Im}\,\Pi^{(2)}_{b\,\ell_1}\big|^{\mathrm{HNC}}_{\mathrm{red}} = \frac{\alpha\, m_+ g_{\mathrm{eff}}}{16\pi^3} \int_{\Delta E_s}^{\Lambda} \mathrm{d}|\boldsymbol{k}| \int_{-1}^{1-u_c} \mathrm{d}u \, \frac{(p_B^2)^{\frac{1}{2}}\, I_{b\,\ell_1}(|\boldsymbol{k}|, u)}{(p_B^2 + m_\ell^2) - (p_B^2 - m_\ell^2)u} \,, \tag{3.59}$$

where $u = \cos\theta$ parameterises the angle between the photon and lepton in the p_B rest frame. The remaining integral is the hard non-collinear (HNC) contribution. The soft divergence is cut-off at ΔE_s (described in (3.29)) in the photon energy integral. Having removed the soft divergence we may take $d = 4$. The soft region is dealt with separately and is described in Section 3.2.6. The collinear divergence occurs as $u \to 1$, $m_\ell \to 0$ and is removed through a collinear cut $u_c \ll 1$. The calculation of the hard-collinear region is described in Section 3.4.1. These divergent regions are calculated separately and analytically to ensure numerical stability. For the τ channel, no collinear slicing is required due to its large mass.

The separation of the soft and hard regions is frame-dependent and so the same frame must be chosen when calculating the soft region in $d = 4 - 2\epsilon$ dimensions. The soft and hard regions each generate $\ln \Delta E_s$ terms which cancel once the regions are combined in the final result. It is convenient to define the

dimensionless cut-offs

$$\omega_s \equiv \frac{2\Delta E_s}{(p_B^2)^{\frac{1}{2}}}, \qquad \omega_c \equiv \frac{|\boldsymbol{k}|\, u_c}{2(p_B^2)^{\frac{1}{2}}} + \mathcal{O}(m_\ell^2), \tag{3.60}$$

and in practise in the slicing procedure ω_c is held fixed while u_c varies. Following [156] the hierarchy $\omega_c \ll \omega_s$ is required to resolve the soft-collinear overlap region. Both cut-offs must be chosen to be small, $\omega_s, \omega_c \ll 1$ as $\mathcal{O}(\omega_s)$ and $\mathcal{O}(\omega_c)$ terms are neglected.

The angular integral in (3.59) can be performed analytically[5] leaving the remaining energy integral that is done numerically. The function $I_{b\ell_1}$ contains non-trivial dependence on $|\boldsymbol{k}|$ and again, like with the l-loop integral, spinor structures like $\bar{u}\not{k}\Gamma v$ are dealt with via projections.

The red cuts of the other virtual diagrams proceed similarly though of course the master integrals involved are different. For example the bb and qq graphs, with the photon connecting twice to the quark, is written in terms of $\mathcal{M}_{kk}$ rather than $\mathcal{M}_k$. The non-lepton graphs are generally simpler as there are not enough independent momenta to generate non-vanishing $\epsilon_{\mu\nu\rho\sigma}$ terms. The $b\,q$ diagrams are special in that they have four cuts, two red and two blue. In the denominator graph the symmetry of the diagram means this simply corresponds to a multiplication by a factor two. This is not true of the numerator graph however. We exploit $b \leftrightarrow q$ symmetry where appropriate, for example the $\Phi\, b$ and $\Phi\, q$ graphs are related by $m_b \leftrightarrow m_q$ and $Q_b \to -Q_q$. These latter graphs are complicated by the extra scale m_B that appears in the perturbative calculation $m_+^2 < m_B^2 < s_0$. While $\boldsymbol{p_\Phi}$ changes direction at $s = m_B^2$ the spectral density remains continuous.

3.2.4 Blue Cuts

We now turn to the blue cuts, again taking the $b\,\ell_1$ diagram as an example. In this case the cut occurs before the photon is radiated from the quark loop. Only the $\bar{q}$ and b propagators are cut in (3.53), which carry momentum l and $p_B - l$

[5] As this integral can generally be performed analytically and we retain a finite lepton mass, in principle we could do away with collinear slicing altogether. However slicing leads to a considerable numerical speed-up which is especially important as the result is Borel transformed. We have checked that the results are identical in either case. Additionally the slicing procedure is illuminating in itself, showing how HC logs appear and connecting to previous literature. In the S-P case with massless leptons we would have no choice but to slice.

respectively. This gives

$$\begin{aligned}\mathrm{Im}\,\Pi^{(2)}_{b\,\ell_1}|_{\mathrm{blue}} = \frac{-2i\pi^2 m_+ g_{\mathrm{eff}} e^2 Q_b Q_{l_1} N_c \mu^{2\epsilon}}{(2\pi)^d} \int \mathrm{d}^d l\, \delta^+(l^2 - m_q^2)\delta^+((p_B - l)^2 - m_b^2) \\ \times \int \frac{\mathrm{d}^d k}{(2\pi)^d} \frac{\mu^{2\epsilon}\ \mathrm{Tr}[\cdots]\bar{u}\cdots v}{((q-l)^2 - m_b^2)k^2((l_1 - k)^2 - m_\ell^2)}\,. \quad (3.61)\end{aligned}$$

The advantage in this case is that the photon loop factorises and can be evaluated exactly using one-loop methods. We use FeynCalc and specifically the Package X [203] and FeynHelpers [204] packages. The presence of three denominators means that the result contains various C_0 functions. This result must then be integrated over $\mathrm{d}^d l$ taking into account the two delta functions, e.g. enforcing $l^2 = m_q^2$. Again the delta functions fix $l = l^*$, cf. (3.36) and so scalar products with external momenta become

$$\begin{aligned} l \cdot p_B &= \mathbb{Y} p_B^2 \\ l \cdot l_1 &= \frac{1}{4p_B^2}\Big[2p_B^2 \mathbb{Y}(p_B^2 + m_\ell^2) - \lambda^{\frac{1}{2}}(p_B^2 - m_\ell^2)\cos\theta\Big]\,, \end{aligned} \quad (3.62)$$

where in this case θ is the angle between $\boldsymbol{l}$ and $\boldsymbol{l_1}$, again in the p_B rest frame. The final remaining angular integral over $\mathrm{d}\Omega_{d-1}$ is performed numerically. There is of course again the challenge of various tensor structures (including $\epsilon_{\mu\nu\rho\sigma}$ terms) which are dealt with via projections. Letting the result of the photon loop integral in (3.61) be $J_{b\,\ell_1}$, then in analogy to (3.55) we can decompose this as

$$J_{b\,\ell_1} \;=\; P_i\Big(A_i + B_{ij} T_j^{\alpha} l_\alpha + C_{ij} T_j^{\alpha\beta} l_\alpha l_\beta\Big)\,, \quad (3.63)$$

where P_i and $T_j^{\alpha(\beta)}$ are lists of Passarino-Veltman and tensor structures respectively and A_i, B_{ij}, C_{ij} are coefficients. Contained in the Passarino-Veltman functions are soft divergences and hard-collinear logs. For example

$$\frac{A_0(m_\ell^2)}{m_\ell^2} + 1 \;=\; B_0(m_\ell^2, 0, m_\ell^2) \;=\; -2\ln m_\ell + \cdots\,, \quad (3.64)$$

with definitions of the Passarino-Veltman functions given in Appendix A.1. The total virtual hard collinear logs come from this, the collinear slicing of the red cuts, and self-energy corrections. Soft divergences generated in the blue cuts are not physical and cancel with soft divergences arising from the soft slicing of the red cuts.

The calculation of the blue cuts in all other virtual diagrams proceeds in a similar

fashion. A technical difficulty arises in the case of the bb and qq numerator and denominator diagrams due to the presence of double propagators, e.g. $1/(l^2 - m_q^2)^2$. When cut these formally generate derivatives[6] of delta functions, $+2\pi i\delta'(l^2 - m_q^2)$. For the qq graph one has for example

$$\Pi_{qq}^{(2)} = -m_+ g_{\rm eff} e^2 Q_q^2 N_c \, \mu^{2\epsilon} \int \frac{\mathrm{d}^d l}{(2\pi)^d} \frac{\bar{u}\Gamma^\mu v}{(l^2 - m_q^2)^2((p_B - l)^2 - m_b^2)} \Sigma_\mu \,, \tag{3.65}$$

where $\Sigma(l^2, m_b, m_q)$ is essentially the $\bar{q}$-quark self-energy

$$\Sigma_\mu(l^2, m_b, m_q) \equiv \mu^{2\epsilon} \int \frac{\mathrm{d}^d k}{(2\pi)^d} \frac{\mathrm{Tr}[\cdots]_\mu}{k^2((l-k)^2 - m_q^2)} \,. \tag{3.66}$$

It is easier to instead rewrite this as the derivative of a single propagator

$$\mathrm{Im} \int \frac{1}{(l^2 - m_q^2)^2} = \lim_{N^2 \to m_q^2} \frac{\mathrm{d}}{\mathrm{d}N^2} \mathrm{Im} \int \frac{1}{l^2 - N^2} \,, \tag{3.67}$$

so that (3.65) becomes when cut

$$\begin{aligned} \mathrm{Im}\, \Pi_{qq}^{(2)}|_{\rm blue} = &-2i\pi^2 m_+ g_{\rm eff} e^2 Q_q^2 N_c \, \mu^{2\epsilon} \, \bar{u}\Gamma^\mu v \\ &\times \lim_{N^2 \to m_q^2} \frac{\mathrm{d}}{\mathrm{d}N^2} \int \frac{\mathrm{d}^d l}{(2\pi)^d} \delta^+(l^2 - N^2) \delta^+((p_B - l)^2 - m_b^2) \Sigma_\mu \,. \end{aligned} \tag{3.68}$$

The integral can be done with the usual methods and then the derivative with respect to the auxiliary variable N^2 is taken. We distinguish N^2 from m_q^2 to avoid differentiating terms in the numerator. Note that the self-energy develops an N^2 dependence, $\Sigma(l^2) = \Sigma(N^2)$ under the integral. As is well known the (on-shell) derivative of the self energy, $\Sigma'(N^2)|_{N^2=m_q^2}$, contains an IR divergence. This soft divergence is artificial and cancels with the corresponding soft divergence of the red cut. It arises from taking derivatives of Passarino-Veltman functions, in particular the $DB_0(m_q^2, 0, m_q^2)$ function defined in Appendix A.1.

3.2.5 Self-energies and Renormalisation

As well as IR divergences there are UV divergences that are generated in the blue cuts. In QED there are some extra issues that do not arise in QCD. For example while the J_B operator is renormalisation group invariant in QCD it does run in

[6] If one considers the delta function as a functional acting on smooth functions, $\langle \delta, f \rangle = f(0)$ then its derivative is defined as $\langle \delta', f \rangle = -f'(0)$, cf. an integration by parts.

QED. Our new operator $\mathcal{J}_B$ renormalises as[7]

$$\begin{aligned} Z_{\Phi_B J_B} &= 1 + \frac{\alpha}{4\pi}\frac{1}{\hat{\epsilon}_{\rm UV}}\bigg(-(3+\xi)Q_bQ_q - \xi Q_\Phi(Q_b-Q_q) + \frac{1}{2}\xi(Q_b^2+Q_q^2) \\ &\qquad\qquad - \frac{1}{2}(3-\xi)Q_\Phi^2 + 3Q_b^2\bigg) \\ &= 1 + \frac{3\alpha}{8\pi}\frac{1}{\hat{\epsilon}_{\rm UV}}(Q_b^2-Q_q^2)\,, \end{aligned} \tag{3.69}$$

in $\overline{\rm MS}$, where for simplicity we set $m_q = 0$ and we use charge conservation $Q_\Phi = Q_b - Q_q$ to go from the first to the second line. The result is gauge-invariant and vanishes when $Q_b = Q_q$ (the QCD limit).

We perform all 1PI renormalisations in $\overline{\rm MS}$, except for the b-quark mass for which we consider several schemes. Two-loop diagrams generate non-local nested subdivergences in the real part of the correlator (as the tree level is UV divergent). Usefully however these do not plague the spectral density and from a cutting rules perspective the renormalisation is essentially just one-loop.

The self-energy corrections for the external particles (Φ and ℓ_1) are handled in the on-shell scheme

$$\begin{aligned} \operatorname{Im}\Pi^{(2)}_{\rm SE} &= \frac{\alpha}{2\pi}\bigg(Q_\Phi^2\delta Z_S + Q_{\ell_1}^2\delta Z_2\bigg)\operatorname{Im}\Pi^{(0)}(p_B^2) \\ \operatorname{Im}C^{(2)}_{\rm SE} &= \frac{\alpha}{\pi}Q_\Phi^2\delta Z_S \operatorname{Im}C^{(0)}(p_B^2)\,, \end{aligned} \tag{3.70}$$

using the scalar and fermion Z factors

$$\begin{aligned} 4\,\delta Z_S &= (3-\xi)\bigg(\frac{1}{\hat{\epsilon}_{\rm UV}} - \frac{1}{\hat{\epsilon}_{\rm IR}}\bigg) + 1 - \xi \\ 4\,\delta Z_2 &= -\xi\frac{1}{\hat{\epsilon}_{\rm UV}} - (3-\xi)\frac{1}{\hat{\epsilon}_{\rm IR}} + 3\ln\bigg(\frac{m_\ell^2}{\mu^2}\bigg) - (3+\xi)\,, \end{aligned} \tag{3.71}$$

which note contains a hard-collinear $\ln m_\ell$. Finally there is the issue of the running of the weak 4-Fermi operator (1.26) in QED. The value of G_F is taken experimentally from the muon lifetime τ_μ measured in the decay $\mu^- \to e^-\nu_\mu\bar{\nu}_e(\gamma)$

[7]We credit Saad Nabeebaccus for originally performing this calculation. Note that multiplicative renormalisation is spoiled when $m_q > 0$ as m_b and m_q renormalise differently in the m_+ prefactor due to their differing charges.

that *includes* radiative corrections [33]

$$\frac{1}{\tau_\mu} = \frac{G_F^2 m_\mu^5}{192\pi^3}\left(1 - \frac{8m_e^2}{m_\mu^2} + \mathcal{O}\Big(\frac{m_e^4}{m_\mu^4}\Big)\right)\left(1 + \frac{\alpha}{2\pi}\Big(\frac{25}{4} - \pi^2\Big)\right). \tag{3.72}$$

Thus when calculating QED decay rates some corrections are already absorbed into G_F and its running amounts to the replacement $G_F \to G_F C(\mu)$ with G_F being the measured experimental value. This is traditionally dealt with in W-regularisation (discussed previously) however we work in DimReg and so use the result given in [205–207]

$$C(\mu) = 1 + \frac{\alpha}{2\pi}\left(\ln\left(\frac{M_Z^2}{\mu^2}\right) - \frac{11}{6}\right), \tag{3.73}$$

where the rational term is scheme-dependent and has only recently been calculated (in Feynman gauge). For $\mu \sim m_b$ this electroweak correction leads to a $+0.5\%$ shift in the Wilson coefficient.

3.2.6 Soft Slicing and IR Divergences

We now turn to discussing in detail infrared sensitive terms. In this section we discuss soft and collinear $\ln m_q$ terms though collinear $\ln m_\ell$ terms are deferred to Section 3.4.

Each individual cut puts particles on-shell and so generates a soft divergence (and a collinear $\ln m_q$ if the photon connects to the light quark). Almost all the diagrams have both a red cut and blue cut and once combined these divergences cancel leaving the diagram infrared finite. Only the two rainbow diagrams ($\Phi\,\ell_1$ in the numerator and $\Phi\,\Phi$ in the denominator) have just a red cut and so a soft divergence remains. These are the physical soft divergences that are well described by scalar QED. This follows the principle that only diagrams where the photon connects two on-shell particles give soft divergences.

Let us now see explicitly how this works by again returning to the $b\,\ell_1$ example. Consider first the red cut. Recall that we slice out the soft region in equation (3.58), treating it properly in $d = 4 - 2\epsilon$ dimensions

$$\operatorname{Im}\Pi^{(2)}_{b\,\ell_1}\big|^{\text{soft}}_{\text{red}} = \frac{\pi^3 m_+ g_{\text{eff}} e^2 Q_b Q_{\ell_1} N_c \mu^{4\epsilon}}{(2\pi)^{2d}} \int_0^{\Delta E_s} \mathrm{d}|\boldsymbol{k}| \int \mathrm{d}\Omega_{d-1}\, \frac{|\boldsymbol{k}|^{d-3}}{k\cdot l_1} I_{b\,\ell_1}\,. \tag{3.74}$$

By choosing ΔE_s (or equivalently ω_s) sufficiently small we can neglect subleading powers of $|\boldsymbol{k}|$ in the integrand as these give $\mathcal{O}(\omega_s)$ contributions. This parallels the usual procedure when performing real soft slicing. Recalling that $I_{b\,\ell_1}$ is $\mathcal{O}(1/|\boldsymbol{k}|)$ then $|\boldsymbol{k}|I_{b\,\ell_1}$ only has angular dependence in this limit and we may write

$$\mathrm{Im}\,\Pi^{(2)}_{b\,\ell_1}\big|^{\text{soft}}_{\text{red}} = \frac{\alpha\, m_+ g_{\text{eff}} Q_b Q_{\ell_1} N_c}{64\pi^4}(2\pi\mu)^{4\epsilon}\int_0^{\Delta E_s} |\boldsymbol{k}|^{d-5}\,\mathrm{d}|\boldsymbol{k}| \times \int \mathrm{d}\Omega_{d-1}\,\frac{[|\boldsymbol{k}|I_{b\,\ell_1}]_{k\to 0}}{\hat{k}\cdot l_1} + \mathcal{O}(\omega_s)\,. \quad (3.75)$$

The energy integral can be evaluated in the manner of (2.51) giving the soft pole

$$\mathrm{Im}\,\Pi^{(2)}_{b\,\ell_1}\big|^{\text{soft}}_{\text{red}} = \frac{\alpha\, m_+ g_{\text{eff}} Q_b Q_{\ell_1} N_c}{64\pi^4}(2\pi\mu)^{2\epsilon}\left(\frac{-1}{2\epsilon_{\text{IR}}} + \ln\frac{\Delta E_s}{2\pi\mu}\right) \times \int \mathrm{d}\Omega_{d-1}\,\frac{[|\boldsymbol{k}|I_{b\,\ell_1}]_{k\to 0}}{\hat{k}\cdot l_1} + \mathcal{O}(\omega_s)\,, \quad (3.76)$$

while the angular integral must be computed to $\mathcal{O}(\epsilon)$ to capture all finite parts. This is complicated by the angle between the photon and lepton. The other example, the qq graph, is more simple. The soft region is

$$\mathrm{Im}\,\Pi^{(2)}_{qq}\big|^{\text{soft}}_{\text{red}} = -\frac{\alpha\, m_+^2 g_{\text{eff}} Q_q^2 N_c}{8\pi^4}(2\pi\mu)^{2\epsilon}\left(1-\frac{m_-^2}{p_B^2}\right) m_\ell\,\bar{u}\Gamma v \times m_q^2\,(2\pi)^{2\epsilon}\int_{|\boldsymbol{k}|<\Delta E_s}\mathrm{d}^d k\,\delta^+(k^2)\mathcal{M}_{kk} + \mathcal{O}(\omega_s)\,, \quad (3.77)$$

which using (3.50) and

$$(2\pi\mu)^{2\epsilon}\int_{|\boldsymbol{k}|<\Delta E_s}\mathrm{d}^d k\,\frac{\delta^+(k^2)}{(p_B\cdot k)^2} = \frac{2\pi}{p_B^2}\left(\frac{-1}{2\hat{\epsilon}_{\text{IR}}} + \ln\frac{2\Delta E_s}{\mu} - 1\right), \quad (3.78)$$

yields the simple result

$$\mathrm{Im}\,\Pi^{(2)}_{qq}\big|^{\text{soft}}_{\text{red}} = -\frac{\alpha}{\pi}Q_q^2\left(\frac{-1}{2\hat{\epsilon}_{\text{IR}}} + \ln\frac{2\Delta E_s}{\mu} - \frac{p_B^2\mathbb{Y}}{\lambda^{\frac{1}{2}}}\ln\frac{\left(\lambda^{\frac{1}{2}}+2p_B^2\mathbb{Y}\right)^2}{4p_B^2 m_q^2}\right)\mathrm{Im}\,\Pi^{(0)} + \mathcal{O}(\omega_s)\,. \quad (3.79)$$

Reassuringly the soft divergence is proportional to the tree level. As well as the pole there are finite contributions arising from the soft region which must not be neglected. Now consider the blue cuts. For the $b\,\ell_1$ diagram the IR divergence can be extracted from the photon loop integral in (3.61). Via Package X one

gets specifically

$$J_{b\,\ell_1} \;=\; \frac{i}{2\pi^2}\frac{1}{\epsilon_{\rm IR}}\left[\frac{l\cdot l_1}{\sqrt{(l\cdot l_1)^2-m_\ell^2 m_b^2}}\ln\frac{l\cdot l_1+\sqrt{(l\cdot l_1)^2-m_\ell^2 m_b^2}}{m_\ell\, m_b}\right]_{l\to p_B-l}$$
$$\times\left(m_q\, p_B^\mu+(m_b-m_q)l^\mu\right)\bar u\Gamma_\mu v \;+\; \mathcal{O}(\epsilon^0)\,, \quad (3.80)$$

where $J_{b\,\ell_1}$ was defined above (3.63). With some difficulty this can then be integrated over l and cancels the pole in (3.76). The same is true of the qq graph. Evaluating (3.68)

$$\mathrm{Im}\,\Pi^{(2)}_{qq}\big|^{\rm IR}_{\rm blue} \;=\; \frac{\alpha}{\pi}Q_q^2\cdot m_q^2\,\mathrm{D}B_0(m_q^2,0,m_q^2)|_{\rm IR}\cdot\mathrm{Im}\,\Pi^{(0)}\,, \quad (3.81)$$

this cancels the pole in (3.79) as $2m_q^2\,\mathrm{D}B_0(m_q^2,0,m_q^2)|_{\rm IR}=-1/\epsilon_{\rm IR}$, cf. (A.7).

The same cancellation occurs for all other diagrams except the rainbow diagrams. While such cancellations can be shown explicitly they can also be argued succinctly from Cauchy's theorem. Taking both the red and blue cuts together for a given diagram, in the soft limit their sum is proportional to

$$Q_iQ_j\int \mathrm{d}^dk\left(\frac{1}{k^2}+2\pi i\,\delta^+(k^2)\right)f(k,l,\cdots)\,, \qquad i\neq j \quad (3.82)$$

where the function f is diagram dependent but contains no poles in the lower half plane. The k^0 integral can be done by the residue theorem picking up the only contributing pole at $k^0=|\boldsymbol{k}|-i\varepsilon$ from the $1/k^2$ term (blue cut). This puts the photon on-shell and exactly cancels the effect of the $\delta^+(k^2)$ (red cut).

The other potentially worrying terms are the hard-collinear $\ln m_q$ that are generated in cuts when the photon connects to an on-shell light quark. However like with the soft terms these cancel between red and blue cuts in individual diagrams. Explicitly

$$\begin{aligned}\mathrm{Im}\,\Pi^{(2)}_{\rm blue} &= +\frac{\alpha}{\pi}Q_q\left(Q_{\ell_1}+Q_\Phi-2Q_b+\frac{5}{2}Q_q\right)\mathrm{Im}\,\Pi^{(0)}\times\ln m_q\;+\cdots\\ \mathrm{Im}\,\Pi^{(2)}_{\rm red} &= -\frac{\alpha}{\pi}Q_q\left(Q_{\ell_1}+Q_\Phi-2Q_b+\frac{5}{2}Q_q\right)\mathrm{Im}\,\Pi^{(0)}\times\ln m_q+\cdots\,, \end{aligned}\quad (3.83)$$

neglecting subleading $\mathcal{O}(m_q)$ terms. Both of these thus demonstrate the necessity of taking both red and blue cuts in the computation. While this is perhaps obvious in the virtual diagrams, on the real side there is a tradition of taking just blue

cuts for hard photons [194].

Finally let us turn to the two rainbow diagrams. These only have a red cut and are consequently soft divergent. The denominator $\Phi\,\Phi$ diagram reads

$$\operatorname{Im} C^{(2)}_{\Phi\Phi}(p_B^2) = -\frac{\alpha Q_\Phi^2}{2\pi^2}(2\pi\mu)^{2\epsilon}\int \mathrm{d}^d k\,\frac{\delta^+(k^2)\,(2p_\Phi - k)^2}{((p_\Phi-k)^2-m_B^2)^2}\operatorname{Im} C^{(0)}(q^2)\,, \tag{3.84}$$

where the LO correlator appears as the quark loop is left intact. The soft region is sliced out as

$$\begin{aligned}\operatorname{Im} C^{(2)}_{\Phi\Phi}\big|_{\text{soft}} \;=\; -\frac{\alpha Q_\Phi^2}{2\pi^2}(2\pi\mu)^{2\epsilon}\operatorname{Im} C^{(0)}(p_B^2)\int_{|\boldsymbol{k}|<\Delta E_s}\mathrm{d}^d k\,\delta^+(k^2)\frac{m_B^2}{(p_\Phi\cdot k)^2} \\ +\;\mathcal{O}(\omega_s)\,,\end{aligned} \tag{3.85}$$

which is most easily evaluated in the $p_\Phi = (m_B, \mathbf{0})$ frame. This gives the soft pole

$$\operatorname{Im} C^{(2)}_{\Phi\Phi}(p_B^2) \;=\; \frac{\alpha Q_\Phi^2}{2\pi}\frac{\operatorname{Im} C^{(0)}(p_B^2)}{\epsilon_{\text{IR}}} \;+\; \mathcal{O}(\epsilon^0)\,, \tag{3.86}$$

which is exactly cancelled by the Φ self-energy diagram given in (3.70). We have therefore shown explicitly that the denominator correlator C is infrared finite.

While the p_Φ rest frame is most convenient for capturing the pole, the finite terms are best evaluated in the p_B rest frame. In the slicing procedure one must always take the same frame for the soft and hard regions (as these are separately frame dependent) and in the actual calculation we always use the p_B frame.

Similarly the numerator rainbow, $\Phi\,\ell_1$, takes the form

$$\begin{aligned}\operatorname{Im}\Pi^{(2)}_{\Phi\,\ell_1}(p_B^2)\big|_{\text{soft}} \;=\; -\frac{\alpha}{4\pi^2}Q_\Phi Q_{\ell_1}\operatorname{Im}\Pi^{(0)}(p_B^2) \\ \times\,(m_B^2+m_\ell^2)\,(2\pi\mu)^{2\epsilon}\int_{|\boldsymbol{k}|<\Delta E_s}\mathrm{d}^d k\,\frac{\delta^+(k^2)}{l_1\cdot k\;p_\Phi\cdot k} \;+\; \mathcal{O}(\omega_s)\,,\end{aligned} \tag{3.87}$$

in the soft region. Soft integrals with multiple massive denominators can be difficult to compute analytically due to incomplete knowledge of angular integrals at $\mathcal{O}(\epsilon)$. Namely defining

$$\begin{aligned}\Omega(\beta_i,\beta_j,\tau_{ij}) = \int_0^\pi \mathrm{d}\theta\,(\sin\theta)^{1-2\epsilon}\int_0^\pi \mathrm{d}\phi\,(\sin\phi)^{-2\epsilon} \\ \frac{1}{(1-\beta_i\cos\theta)(1-\beta_j\cos\theta\cos\chi_{ij}-\beta_j\sin\theta\cos\phi\sin\chi_{ij})}\,,\end{aligned} \tag{3.88}$$

with $\cos\chi_{ij} = 2\tau_{ij} - 1$, the $\mathcal{O}(\epsilon)$ terms have only recently been found [90] in terms of generalised polylogarithms[8]. Such terms can be important in extracting hard-collinear logs (though not in this work). Our diagram can be recast as

$$\begin{aligned}\operatorname{Im}\Pi^{(2)}_{\Phi\,\ell_1}(p_B^2)\big|_{\text{soft}} \;=\; -\frac{\alpha}{\pi^2}Q_\Phi Q_{\ell_1}\frac{p_B^2(m_B^2+m_\ell^2)}{(p_B^2+m_B^2)(p_B^2+m_\ell^2)}\left(\frac{-1}{2\hat{\epsilon}_{\text{IR}}}+\ln\frac{2\Delta E_s}{\mu}\right)\\ \times\,\Omega\left(\frac{p_B^2-m_\ell^2}{p_B^2+m_\ell^2},\left|\frac{p_B^2-m_B^2}{p_B^2+m_B^2}\right|,\theta(p_B^2-m_B^2)\right)\operatorname{Im}\Pi^{(0)}(p_B^2)\;+\;\mathcal{O}(\omega_s)\,,\end{aligned}\tag{3.89}$$

where the angle between $\boldsymbol{l_1}$ and $\boldsymbol{p_\Phi}$, $\chi_{ij} = 0$ for $p_B^2 > m_B^2$ and $\chi_{ij} = \pi$ for $p_B^2 < m_B^2$. Really however our case does not need this full machinery as $\sin\chi_{ij} = 0\ \forall p_B^2$ (there is only actually one angle). Instead

$$\begin{aligned}&\Omega\left(\frac{p_B^2-m_\ell^2}{p_B^2+m_\ell^2},\left|\frac{p_B^2-m_B^2}{p_B^2+m_B^2}\right|,\theta(p_B^2-m_B^2)\right)\;=\\ &\frac{\pi}{\beta_i-\beta_j}\left\{\left[\ln\frac{1+\beta_i}{1-\beta_i}+2\epsilon\left(\operatorname{Li}_2\frac{2\beta_i}{1+\beta_i}+\frac{1}{4}\ln^2\frac{1+\beta_i}{1-\beta_i}\right)\right]-\operatorname{sgn}(\beta_j)\Big[\beta_i\to|\beta_j|\Big]\right\},\end{aligned}\tag{3.90}$$

where $\operatorname{sgn}(x)$ is the sign function and

$$\beta_i \;=\; \frac{p_B^2-m_\ell^2}{p_B^2+m_\ell^2}\,,\qquad \beta_j \;=\; \frac{p_B^2-m_B^2}{p_B^2+m_B^2}\,.\tag{3.91}$$

The soft-collinear behaviour arises from

$$\begin{aligned}\Omega\big(\beta_i,|\beta_j|,\theta(\beta_j)\big) \;=\; \frac{\pi}{2}\frac{(p_B^2+m_B^2)(p_B^2+m_\ell^2)}{p_B^2(m_B^2-m_\ell^2)}\left\{\ln\frac{p_B^2}{m_\ell^2}\;-\;\operatorname{sgn}(\beta_j)^2\ln\frac{p_B^2}{m_B^2}\right\}\\ +\;\mathcal{O}(\epsilon)\,,\end{aligned}\tag{3.92}$$

which combined with (3.89) gives

$$\operatorname{Im}\Pi^{(2)}_{\Phi\,\ell_1} = \frac{\alpha}{4\pi}Q_\Phi Q_{\ell_1}\frac{m_B^2+m_\ell^2}{m_B^2-m_\ell^2}\ln\left(\frac{m_B^2}{m_\ell^2}\right)\frac{\operatorname{Im}\Pi^{(0)}(p_B^2)}{\epsilon_{\text{IR}}}+\mathcal{O}(\epsilon^0)\,,\tag{3.93}$$

the required universal form [144] that cancels against the real radiation after Borel transformation has been performed. The finite part contains soft-collinear $\ln^2 m_\ell^2$ terms which cancel similarly with real counterparts. We see again how the Φ_B particle is crucial for recovering the correct soft physics.

[8]Note that $\Omega(\beta_i,\beta_j,\tau_{ij})$ is essentially $I^{(1,1)}|_{d=4-2\epsilon}$ in more traditional notation, cf. (3.44), though we follow the notation of [90].

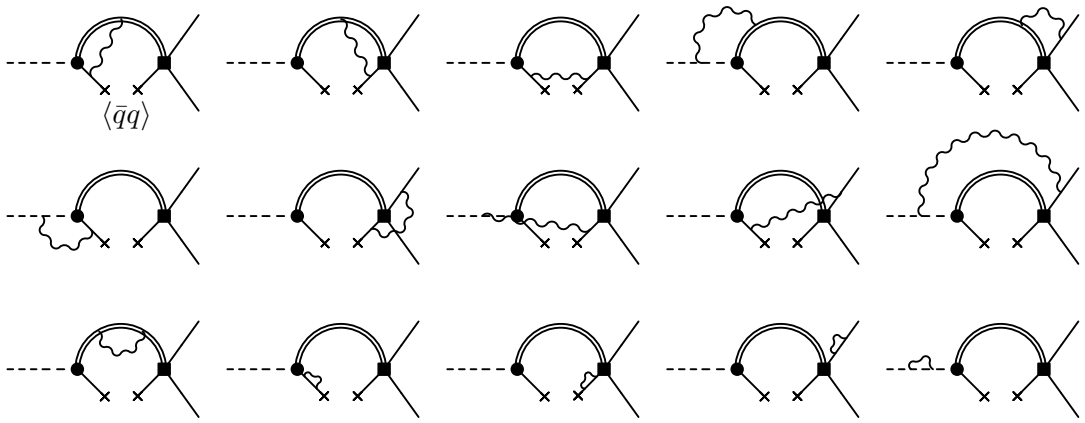

Figure 3.5 *Virtual quark condensate diagrams contributing to* $\Pi^{(2)}_{\langle\bar{q}q\rangle}$ *in* (3.2). *The two crosses denote the quark condensate* $\langle\bar{q}q\rangle$.

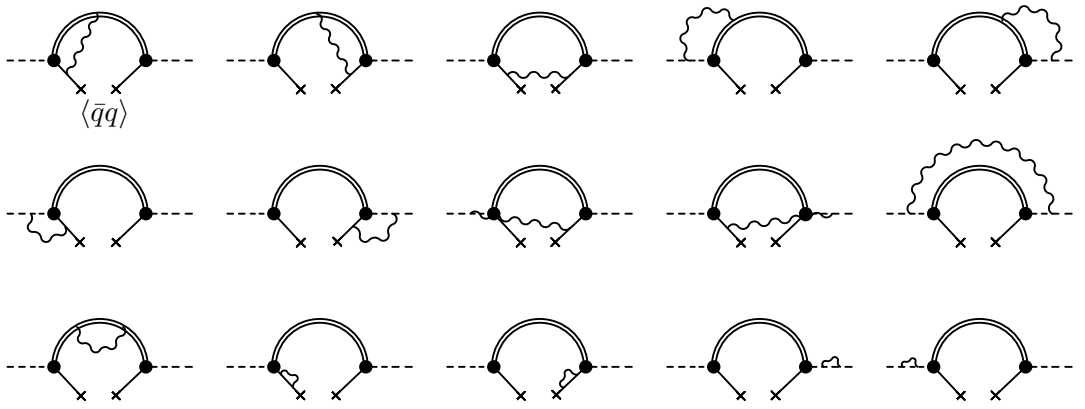

Figure 3.6 *Quark condensate diagrams contributing to the denominator correlator* $C^{(2)}_{\langle\bar{q}q\rangle}$ *given in* (3.11), *that is* $|\mathcal{Z}_B|^2$.

3.2.7 Condensate Contributions

Now we turn to the contribution of the quark condensate $\langle\bar{q}q\rangle$ diagrams. The LO results are

$$\begin{aligned}\operatorname{Im}\Pi^{(0)}_{\langle\bar{q}q\rangle} &= -\pi m_+ g_{\text{eff}}\langle\bar{q}q\rangle m_\ell \bar{u}\Gamma v\delta^+(p_B^2-m_b^2)\\ \operatorname{Im}C^{(0)}_{\langle\bar{q}q\rangle} &= -\pi m_+^2 m_b\langle\bar{q}q\rangle\delta^+(p_B^2-m_b^2)\,,\end{aligned} \tag{3.94}$$

where for the condensates we shall neglect the light quark mass $m_q = 0$, as this is a truly negligible effect. The $\mathcal{O}(\alpha)$ diagrams are in some ways simpler than the perturbative ($\mathbb{1}$) counterparts as they are only one-loop, however the cuts are quite non-standard and are trickier to handle. Due to the appearance of delta functions in the spectral density it is often easier to present results after Borel

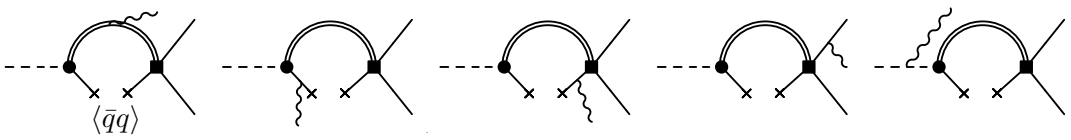

Figure 3.7 *Quark condensate diagrams contributing to* $\Pi^{\gamma}_{\langle\bar{q}q\rangle}$ *in* (3.2) *(i.e. the radiative correlator). We stress again that the diagrams where the photon connects to the quarks are subsumed by using external form factors [195].*

transformation. The virtual diagrams are given in Figures 3.5 (numerator) and 3.6 (denominator) while the real diagrams are given in Figure 3.7. Recall however that the structure-dependent part of the real radiation is given by external form factors [195].

In the condensates in general, and in particular in the triangle function $C_0(0, p_B^2, p_B^2, 0, 0, m_b^2)$, we encounter non-logarithmic (power) singularities at the endpoint $p_B^2 \to m_b^2$. This C_0 function has a double propagator $1/(k^2)^2$ and so we take the cut in the same manner as the bb and qq graphs via a derivative

$$\begin{aligned}\operatorname{Im} C_0(0, p_B^2, p_B^2, 0, 0, m_b^2) \;=\; & \\ & \frac{(2\pi\mu)^{2\epsilon}}{i\pi^2} \lim_{N^2\to 0} \frac{\mathrm{d}}{\mathrm{d}N^2} \operatorname{Im} \int \frac{\mathrm{d}^d k}{((p_B-k)^2 - m_b^2)(k^2 - N^2)} \\ & = -\pi\big(1 + \epsilon(-\gamma_E + \ln 4\pi\mu^2)\big) \frac{p_B^2 + m_b^2}{(p_B^2)^{1-\epsilon}(p_B^2 - m_b^2)^{1+2\epsilon}}\,,\end{aligned} \tag{3.95}$$

a form seen in [208]. The divergence at the endpoint is of IR type, regulated by taking $\epsilon < 0$. Conversely the $(p_B^2)^{1-\epsilon}$ part regulates the UV as $p_B^2 \to \infty$ (though practically this is exponentially suppressed by the Borel transform). The Borel transform can be performed via a subtraction method to separate out the divergent part of the integral. After this the IR divergence is clear

$$\mathcal{B}_{M^2} C_0 = e^{\frac{-m_b^2}{M^2}} \left(\frac{1}{\hat{\epsilon}_{\mathrm{IR}}} + \ln \frac{s_0 \mu^2}{(s_0 - m_b^2)^2} - \int_{m_b^2}^{s_0} \frac{s + m_b^2}{s(s - m_b^2)} \big(e^{\frac{m_b^2 - s}{M^2}} - 1\big)\, \mathrm{d}s \right). \tag{3.96}$$

These divergent cuts arise from terms of the form $\ln(m_b^2 - s)/(m_b^2 - s)$ which cancel in the QCD limit and so do not appear in previous work, e.g. [107, 209]. The integral in (3.96) can in theory be written as an infinite sum of Beta functions, though we work numerically.

We attack the diagrams via cutting rules as usual, again with a notion of red and blue cuts. NLO condensate diagrams are rarely computed using Cutkosky rules in the literature (if at all) and so we give some explicit details.

The blue cuts are mostly straightforward. For diagrams that do not involve the light quark the blue cuts simply generate a $\delta^{(\prime)}(p_B^2 - m_b^2)$ in the spectral density with the photon loop factorising as in the perturbative ($\mathbb{1}$) case. This is then decomposed as usual into Passarino-Veltman functions from which any soft or collinear terms can be extracted. For example consider the bb denominator condensate diagram

$$C_{bb}^{(2)}(p_B^2)\big|_{\langle\bar{q}q\rangle} = \frac{\alpha\, m_+^2 Q_b^2}{16i\pi^3}\langle\bar{q}q\rangle(2\pi\mu)^{2\epsilon} \times \int \mathrm{d}^d k\, \frac{\mathrm{Tr}\Big[\gamma_5 \mathbb{1}\gamma_5(\not{p}_B + m_b)\gamma^\rho(\not{q} + m_b)\gamma_\rho(\not{p}_B + m_b)\Big]}{(p_B^2 - m_b^2)^2(q^2 - m_b^2)k^2}\,. \quad (3.97)$$

The blue cut takes $1/(p_B^2 - m_b^2)^2 \to \pi\delta'(p_B^2 - m_b^2)$ (independent of k) and the remaining integral is straightforward. This is then Borel transformed

$$\mathcal{B}_{M^2} C_{bb}^{(2)}\big|_{\text{blue}}^{\langle\bar{q}q\rangle} = \frac{\alpha\, m_+^2 Q_b^2}{4\pi} m_b\langle\bar{q}q\rangle \int_{m_b^2}^{s_0} \mathrm{d}s\, \delta'(s - m_b^2) \times \Big((d-2)A_0(m_b^2) + 2(s + m_b^2)B_0(s, 0, m_b^2)\Big)e^{-s/M^2}\,, \quad (3.98)$$

and the derivative is shifted onto the second line. The delta functions can then be evaluated giving eventually

$$\mathcal{B}_{M^2} C_{bb}^{(2)}\big|_{\text{blue}}^{\langle\bar{q}q\rangle} = -\frac{\alpha\, m_+^2 Q_b^2}{2\pi} m_b\langle\bar{q}q\rangle e^{\frac{-m_b^2}{M^2}}\left[\frac{1}{\hat{\epsilon}_{\text{UV}}} - \frac{1}{\hat{\epsilon}_{\text{IR}}} - \frac{m_b^2}{M^2}\left(\frac{3}{\hat{\epsilon}_{\text{UV}}} + 4 + 3\ln\frac{\mu^2}{m_b^2}\right)\right]. \quad (3.99)$$

The UV poles are renormalised away while the IR cancels against the red cut, to which we now turn.

For the red cuts the soft slicing procedure takes a slightly different form. As there is one loop less than the perturbative ($\mathbb{1}$) contribution the red cuts now resemble a $1 \to 2$ real decay. The photon energy is fixed by the cut and not integrated over. Consider the bb graph again; the red cut of (3.97) is

$$\mathrm{Im}\, C_{bb}^{(2)}(p_B^2)\big|_{\text{red}}^{\langle\bar{q}q\rangle} = \frac{\alpha\, m_+^2 Q_b^2}{2\pi} m_b\langle\bar{q}q\rangle(2\pi\mu)^{2\epsilon} \times \int \mathrm{d}^d k\, \delta^+(k^2)\delta^+((p_B - k)^2 - m_b^2)\left(\frac{m_b^2}{(p_B\cdot k)^2} + \frac{1}{p_B\cdot k}\right). \quad (3.100)$$

Slicing out the soft region as usual, we let $k \to 0$ in the numerator

$$\begin{aligned}\operatorname{Im} C_{bb}^{(2)}(p_B^2)\big|_{\text{red, soft}}^{\langle\bar{q}q\rangle} \;=\; & \frac{\alpha\, m_+^2 Q_b^2}{2\pi} m_b^3 \langle\bar{q}q\rangle \delta^+(p_B^2 - m_b^2) \\ & \times (2\pi\mu)^{2\epsilon} \int_{|\boldsymbol{k}|<\Delta E_s} \mathrm{d}^d k\, \frac{\delta^+(k^2)}{(p_B\cdot k)^2} \;+\; \mathcal{O}(\omega_s)\,, \quad (3.101)\end{aligned}$$

giving

$$\mathcal{B}_{M^2} C_{bb}^{(2)}\big|_{\text{red, soft}}^{\langle\bar{q}q\rangle} \;=\; \frac{\alpha}{\pi} m_+^2 Q_b^2 m_b \langle\bar{q}q\rangle e^{\frac{-m_b^2}{M^2}} \left(\frac{-1}{2\hat{\epsilon}_{\text{IR}}} + \ln\frac{2\Delta E_s}{\mu} - 1\right) + \mathcal{O}(\omega_s), \quad (3.102)$$

which cancels the IR of (3.99). What about the hard region? This seems to be divergent[9] as $p_B^2 \to m_b^2$, that is evaluating (3.100) in $d = 4$ using the methods of Section 3.2.2 one finds curiously

$$\operatorname{Im} C_{bb}^{(2)}(p_B^2)\big|_{\text{red, hard}}^{\langle\bar{q}q\rangle} \;=\; \frac{\alpha\, m_+^2 Q_b^2}{2p_B^2} m_b \langle\bar{q}q\rangle \left(\frac{2m_b^2}{p_B^2 - m_b^2} + 1\right). \quad (3.103)$$

This can be understood however. For the condensates the photon energy is no longer free and is fixed at $|\boldsymbol{k}| = |\boldsymbol{k}^*|$ with

$$|\boldsymbol{k}^*| \;=\; \frac{p_B^2 - m_b^2}{2\sqrt{p_B^2}}\,, \quad (3.104)$$

in analogy to (3.36). The divergence is therefore really the soft divergence $\sim 1/|\boldsymbol{k}^*|$ appearing in the limit $p_B^2 \to m_b^2$. For the condensates the hard region is now defined by a cut in the dispersion variable $p_B^2 > m_b^2 + 2m_b\Delta E_s$ unlike in the perturbative case. Equation (3.103) should be modified to include an appropriate θ function enforcing this. Thus after Borel transforming the hard region is

$$\begin{aligned}&\mathcal{B}_{M^2} C_{bb}^{(2)}\big|_{\text{red, hard}}^{\langle\bar{q}q\rangle} \;= \\ &\qquad \frac{\alpha}{\pi} m_+^2 Q_b^2 m_b \langle\bar{q}q\rangle \int_{m_b^2(1+\omega_s)}^{s_0} \mathrm{d}s\, e^{-s/M^2} \left(\frac{1}{2s} + \frac{m_b^2}{s(s-m_b^2)}\right) \;+\; \mathcal{O}(\omega_s^2)\,, \quad (3.105)\end{aligned}$$

which is done numerically. The soft divergence is removed by the $\omega_s > 0$ in the lower integration limit. The only remaining issue is how the $\ln\Delta E_s$ (or equivalently $\ln\omega_s$) term in (3.102) cancels with the hard region (3.105). As $s \to$

[9] This problem also afflicts the toy model calculation.

m_b^2 the dominant term comes from the integral

$$\int_{m_b^2(1+\omega_s)}^{s_0} \frac{e^{-s/M^2}}{s-m_b^2}\,\mathrm{d}s \;=\; e^{-m_b^2/M^2}\left\{\Gamma\big(0,\frac{m_b^2\,\omega_s}{M^2}\big)-\Gamma\big(0,\frac{s_0-m_b^2}{M^2}\big)\right\}, \qquad (3.106)$$

written in terms of the (upper) incomplete Gamma function, $\Gamma(a,z)\equiv\int_z^\infty t^{a-1}e^{-t}\,\mathrm{d}t$. Asymptotically for small ω_s we have that

$$\Gamma\big(0,\frac{m_b^2\,\omega_s}{M^2}\big) \;=\; -\gamma_E-\ln\frac{m_b^2\,\omega_s}{M^2}\;+\;\mathcal{O}(\omega_s)\,, \qquad (3.107)$$

giving the required logarithmic dependence.

The 18 diagrams where the photon connects to the quark-condensate itself are particularly tricky as the light quark leg carries no momentum and behaves as if it is on-shell. It is precisely these diagrams that generate the endpoint divergences in the C_0 function discussed earlier. Applying charge conservation these endpoint IR divergences are proportional to Q_q^2 once summed. These can be traded for UV divergences by adding the contribution of the $\bar{q}$-quark leg self-energy diagrams which formally vanish in DimReg ($m_q=0$). Properly however they are proportional to $Q_q^2(\frac{1}{\epsilon_{\mathrm{UV}}}-\frac{1}{\epsilon_{\mathrm{IR}}})$ which exactly cancels the endpoint IR divergences and turns them into UV ones. Now as UV poles these are renormalised away and this is interpreted as a renormalisation of the condensate itself. As a sanity check of the procedure the counterterm $Z_{\langle\bar{q}q\rangle}$ matches the well-known results.

Other renormalisations proceed exactly as in the perturbative case in Section 3.2.5. For example we add in external self-energies as before with $\mathrm{Im}\,\Pi_{\mathbb{1}}^{(0)}\to\mathrm{Im}\,\Pi_{\langle\bar{q}q\rangle}^{(0)}$ and $\mathrm{Im}\,C_{\mathbb{1}}^{(0)}\to\mathrm{Im}\,C_{\langle\bar{q}q\rangle}^{(0)}$. The physical soft divergences behave in an identical manner as they must do as they are universal.

3.2.8 Gauge-invariance

In previous sections the Feynman gauge, $\xi=1$, has been assumed. Here we consider the remaining part of the photon propagator, tracking the $(\xi-1)k_\mu k_\nu/(k^2)^2$ terms. A priori such terms are troublesome to compute due to the presence of double propagators as in the bb and qq graphs. However as particles are put on-shell in the cuts, Ward identities simplify the rest of the amplitude meaning explicit gauge-invariance can be demonstrated analytically.

For example, for a photon connecting to an external lepton, one has explicitly

$$k^\mu \times \bar{u}(l_1)\gamma_\mu \frac{\not{l}_1 - \not{k} + m_\ell}{(l_1-k)^2 - m_\ell^2} \longrightarrow -\bar{u}(l_1)\,, \tag{3.108}$$

where the lepton propagator has been contracted to a point. Such contractions mean that the $\xi - 1$ 'gauge' contributions are expressible in terms of the LO correlator. In the case of the blue cuts, these gauge terms vanish separately for each diagram while the red cuts are gauge-invariant as a consequence of charge conservation.

Explicitly for the blue cuts one has

$$\mathrm{Im}\,\Pi^{(2)}_{\mathrm{blue}}\big|_{Q_iQ_j(\xi-1)} \propto \mathrm{Im}\,\Pi^{(0)} \int \frac{\mathrm{d}^d k}{(k^2)^2} = 0\,, \qquad (i \neq j) \tag{3.109}$$

as scale-less integrals vanish in DimReg. Identical behaviour is true of the denominator correlator C. The bb and qq graphs also vanish though this is more involved. In the red cuts one must cut the double $1/(k^2)^2$ propagator and so we use the derivative trick of Section 3.2.4. We find

$$\begin{aligned}\mathrm{Im}\,\Pi^{(2)}_{\mathrm{red}}|_{1-\xi} = {}& \frac{\alpha\, m_+^2 g_{\mathrm{eff}} N_c}{16\pi^3}(2\pi\mu)^{4\epsilon}\Big((Q_\Phi - Q_b + Q_q)(Q_{\ell_1} - Q_b + Q_q)\Big) \\ & \times \lim_{N^2\to 0}\frac{\mathrm{d}}{\mathrm{d}N^2}\int \mathrm{d}^d k\,\delta^+(k^2-N^2)\theta(q^2-m_+^2)\,\bar{u}\not{q}\Gamma v\,\frac{\lambda_q^{\frac{1}{2}}}{q^2}\left(1-\frac{m_-^2}{q^2}\right) \\ = {}& 0\,,\end{aligned} \tag{3.110}$$

which vanishes by virtue of conservation of charge at each vertex. Note again the LO structure appearing in the integral. Similarly for the denominator correlator

$$\begin{aligned}\mathrm{Im}\,C^{(2)}|_{1-\xi} = {}& \frac{\alpha}{2\pi^2}(2\pi\mu)^{2\epsilon}\big(Q_\Phi - Q_b + Q_q\big)^2 \\ & \times \lim_{N^2\to 0}\frac{\mathrm{d}}{\mathrm{d}N^2}\int \mathrm{d}^d k\,\delta^+(k^2-N^2)\theta(q^2-m_+^2)\,\mathrm{Im}\,C^{(0)}(q^2) \\ = {}& 0\,.\end{aligned} \tag{3.111}$$

Gauge-invariance of the condensate diagrams works out in a similar manner

$$\begin{aligned}\mathrm{Im}\,\Pi^{(2)}_{\langle\bar{q}q\rangle}|_{1-\xi} = {}& \alpha\, m_+ g_{\mathrm{eff}}\langle\bar{q}q\rangle\big(Q_\Phi - Q_b + Q_q\big)\big(Q_{\ell_1} - Q_b + Q_q\big)\frac{m_\ell \bar{u}\Gamma v}{8\pi p_B^2} \\ & \times \big(B_0(p_B^2,0,m_b^2) - (m_b^2+p_B^2)C_0(0,p_B^2,p_B^2,0,0,m_b^2)\big)\end{aligned}$$

$$= 0\,, \tag{3.112}$$

while for the denominator

$$\begin{aligned}\operatorname{Im} C^{(2)}_{\langle\bar{q}q\rangle}|_{1-\xi} &= -\frac{\alpha\, m_+^2}{4\pi} m_b \langle\bar{q}q\rangle \big(Q_\Phi - Q_b + Q_q\big)^2 C_0(0, p_B^2, p_B^2, 0, 0, m_b^2) \\ &= 0\,. \end{aligned} \tag{3.113}$$

These equations demonstrate the gauge invariance of the virtual 1PI diagrams. The Φ_B particle, which restores charge conservation to the vertices, is crucial to the whole procedure. Gauge-dependent terms in the Φ_B self-energies formally cancel between numerator and denominator correlators. Gauge-invariance in the renormalisation of the $\mathcal{J}_B$ and $\mathcal{L}_W$ vertices is discussed in Section 3.2.5.

3.2.9 Final Result

Having renormalised, the denominator correlator C is UV and IR finite. The final result for $|\mathcal{Z}_B|^2$ is then obtained by Borel transforming the spectral density $\rho_C(s)$ as given in (3.12).

The numerator correlator Π must first be squared and spin-summed to allow us to extract the virtual rate. For the virtual case the phase-space integration is trivial. Defining $\operatorname{Im}\Pi = \operatorname{Im}\overline{\Pi}\,\bar{u}\Gamma v$ and as before

$$\mathcal{B}_{M^2}\Pi \equiv \frac{1}{\pi}\int_{m_+^2}^{s_0} \operatorname{Im}\Pi(s) e^{-s/M^2}\,\mathrm{d}s\,, \tag{3.114}$$

then the virtual rate reads

$$\begin{aligned}\mu^{2\epsilon}\Big[|\mathcal{Z}_B|^2\Gamma_{\bar{B}\to\ell\bar{\nu}}\Big] = \frac{(m_B^2 - m_\ell^2)^2}{4\pi m_B^3} e^{\frac{2m_B^2}{M^2}} \Bigg(&\big(\mathcal{B}_{M^2}\overline{\Pi}^{(0)}\big)\big(\mathcal{B}_{M^2}\overline{\Pi}^{(0)}\big)^* \\ &+ 2\mathcal{K}(\epsilon)\operatorname{Re}\big(\mathcal{B}_{M^2}\overline{\Pi}^{(2)}\big)\big(\mathcal{B}_{M^2}\overline{\Pi}^{(0)}\big)^* + \mathcal{O}(\alpha^2)\Bigg)\,, \end{aligned} \tag{3.115}$$

and the final result follows from dividing by $|\mathcal{Z}_B|^2$. The first line and second line correspond to the LO and NLO result respectively. Note that the NLO result contains an IR divergence which cancels only when we add the real radiative contribution. The quantity $\mathcal{K}(\epsilon) \equiv 1 - 2\epsilon \ln\frac{m_B^2 - m_\ell^2}{2\mu m_B} + \epsilon(2 - \gamma_E + \ln\pi)$ encodes phase space corrections which similarly cancel with the real contribution and so in practise can be ignored.

Before concluding this section it is worthwhile to summarise the various checks that have been made to ensure the correctness of the calculation. On the methodology side the procedure has been thoroughly checked by using the toy model of Section 3.1.3. In this and in the full calculation the correct soft behaviour, explicit gauge invariance and the correct QCD limits have been shown. Additionally in Section 3.4 we will show how the framework recovers all universal hard-collinear logs. In terms of the actual calculation all diagrams have been numerically checked using pySecDec[10]. The three lepton diagrams (Φ, b, q)-ℓ_1 are the most computationally intensive and have been checked at the per mille level while all other diagrams have been checked to considerably higher precision.

3.3 Real Radiation

We now turn to the calculation of the real radiative rate, which follows from the correlator Π^γ. The correlator itself is relatively simple, being written in terms of form factors $V_{\parallel,\perp}(q^2)$ (to be defined shortly), with the integration over phase space now being slightly more involved.

3.3.1 Amplitude

The real amplitude $\mathcal{A}(\bar{B} \to \ell\bar{\nu}\gamma)$ is extracted from the correlator Π^γ (in the manner of (3.10)) which itself can be decomposed into three contributions

$$\Pi^\gamma_\rho(p_B^2, q^2) = \Pi^\gamma_\rho|_{\ell_1} + \Pi^\gamma_\rho|_{\Phi_B} + \Pi^\gamma_\rho|_{\bar{B}}\,, \tag{3.116}$$

where the index ρ is understood to be contracted with the photon polarisation vector $\epsilon^*_\rho(k)$. Recall that momentum conservation takes the form $p_\Phi|_{\text{real}} = l_1 + l_2 + k$ with $q \equiv p_B - k$ and $k^2 = 0$. The first term corresponds to emission from the charged lepton which is straightforward as it is point-like. The second term is unique to our framework and is the emission from the on-shell Φ_B particle. This is similarly straightforward as the Φ_B is treated as a point-like scalar and it is this term that gives the correct Low limit. Finally, all structure-dependence is contained in the form factors $V_{\parallel,\perp}(q^2)$ which enter the third term, $\Pi^\gamma_\rho|_{\bar{B}}$, that

[10] As pySecDec cannot handle spinor chains we check instead $\Pi^{(0)*}\Pi^{(2)}$ summed over fermion spins for the (renormalised) lepton diagrams. The rest of the diagrams need only a simple projection.

corresponds to emissions from the quarks.

For convenience we define $\Pi_{f_B}(p_B^2)$ as the LO result (including condensate contributions) with spinors and prefactors removed. That is

$$\Pi^{(0)}(p_B^2) \;=\; g_{\text{eff}}\, m_+ m_\ell\, \bar{u}\Gamma v\, \Pi_{f_B}(p_B^2)\,, \tag{3.117}$$

(without the m_ℓ in the S-P case) as well as the shorthand

$$\tilde{g} \equiv g_{\text{eff}}\, m_+ e s_e\,. \tag{3.118}$$

The real rate essentially can be considered as a LO process in its own right, especially for hard photon emissions. Thus unlike in the virtual computation (where the photon directly connects initial and final states) we may work with a sum-rules version of the decay constant. That is, in our framework we may define

$$F_B = F_B(M^2) \equiv \frac{m_+}{\mathcal{Z}_B} e^{\frac{m_B^2}{M^2}} \mathcal{B}_{M^2} \Pi_{f_B}(p_B^2)\,, \tag{3.119}$$

at $\mathcal{O}(\alpha^0)$. Following the virtual computation we drop all Lorentz structures involving r in the correlator. Structures like $r\cdot\epsilon^*$ do not appear in the amplitude and their coefficients are considered to be extra unphysical form factors. Further, the only place where we retain $r \neq 0$ is in the extraction of the *hadronic* quantities $F_B, V_\parallel, V_\perp$ and we set $r \to 0$ in all other structures. Essentially we should only use a dispersion to determine the unknown form factors and not where unnecessary.

While we discuss the first principles calculation of the form factors $V_{\parallel,\perp}(q^2)$ in Section 3.3.2, in the end the proximity of the $B^{*(1)}$ pole means our (LO in QCD) calculation is unsuitable and we instead take external form factors in the numerics. To be specific we utilise the NLO LCSR form factors [195] with the view that sum-rules calculations work better when combined with other sum-rules calculations.

In the Lorenz gauge, $\epsilon^*(k)\cdot k = 0$, one has

$$\Pi^\gamma_\rho|_{\ell_1} \;=\; +\,\tilde{g} Q_{\ell_1} \Pi_{f_B}(p_B^2)\bigg(\,\bar{u}\gamma_\rho\Gamma v + \frac{m_\ell}{2l_1\cdot k}\Big(\,\bar{u}\gamma_\rho \not{k}\Gamma v + 2(l_1)_\rho\,\bar{u}\Gamma v\Big)\bigg) \tag{3.120}$$

$$\Pi^\gamma_\rho|_{\Phi_B} = \;-\,\tilde{g} Q_\Phi \frac{(p_\Phi)_\rho}{p_\Phi\cdot k}\Pi_{f_B}(q^2) m_\ell\,\bar{u}\Gamma v$$

$$\Pi^\gamma_\rho|_{\bar{B}} \;=\; +\,\tilde{g} Q_\Phi\,\bar{u}\Gamma^\mu v\bigg(\frac{\Pi_{f_B}(q^2)-\Pi_{f_B}(p_B^2)}{p_B\cdot k}(p_B)_\rho(p_B)_\mu - \Pi_{f_B}(q^2) g_{\rho\mu}\bigg) + \Pi^\gamma_\rho|_{\text{struc}}\,,$$

where for $\Pi^\gamma_\rho|_{\bar{B}}$ we have separated out the true structure-dependence, $\Pi^\gamma_\rho|_{\rm struc}$, from the contact terms. Note the difference in the function arguments: $\Pi_{f_B}(p_B^2)$ versus $\Pi_{f_B}(q^2)$ for the lepton and Φ_B terms respectively due to emission after versus before the $\bar{B}$-meson is resolved. Again $\mathrm{Im}\,\Pi_{f_B}(q^2)$ contains a $\theta(q^2 - m_+^2)$ function which limits the allowed range of p_B^2 given a fixed photon energy E_γ.

Finally, true structure-dependence (i.e. a non-trivial dependence on the quark charges) is contained in the two form factors $V_{\parallel,\perp}$ defined from the matrix element

$$\begin{aligned}\langle\gamma|\bar{q}\hat{\Gamma}_\mu b|\bar{B}\rangle \;=\; \\ -\frac{s_e e}{m_B}\bigg(P^\perp_\mu V_\perp(q^2) - P^\parallel_\mu\Big(V_\parallel(q^2) + Q_{\bar{B}}\frac{m_B f_B}{k\cdot p_B}\Big) - P^{\rm Low}_\mu Q_{\bar{B}}\frac{m_B f_B}{k\cdot p_B}\bigg)\,,\end{aligned} \tag{3.121}$$

where in our case $Q_{\bar{B}} = -1$. We follow the notation and conventions of [195] where the charged form factors are of negative sign, $\epsilon_{0123} = +1$ and

$$\begin{aligned} P^\perp_{\mu\rho} &\equiv \epsilon_{\mu\rho\beta\gamma}(p_B)^\beta k^\gamma \\ P^\parallel_{\mu\rho} &\equiv i\left(k\cdot p_B\, g_{\mu\rho} - k_\mu\,(p_B)_\rho\right) \\ P^{\rm Low}_{\mu\rho} &\equiv i\,(p_B)_\mu(p_B)_\rho\,, \end{aligned} \tag{3.122}$$

with $P^\mu \equiv P^{\mu\rho}\epsilon^*_\rho(k)$. Assembling all parts, the amplitude follows from Borel transforming the correlator Π^γ, like in the virtual case (cf. (3.10)), and is expressible in terms of the hadronic quantities F_B, $V_\parallel$ and $V_\perp$

$$(m_+ m_B/\tilde{g})(\mathcal{A}^\gamma)^\rho \;=\; \bigg(P^{\mu\rho}_\parallel\Big[V_\parallel(q^2) + \frac{Q_\Phi m_B F_B}{k\cdot p_B}\Big] - P^{\mu\rho}_\perp V_\perp(q^2)\bigg)\bar{u}\Gamma_\mu v \tag{3.123}$$

$$-iQ_{\ell_1} m_B F_B\bigg(\bar{u}\gamma^\rho\Gamma v + \frac{m_\ell}{2l_1\cdot k}\Big(\,\bar{u}\gamma^\rho \not{k}\Gamma v + 2l_1^\rho\,\bar{u}\Gamma v\Big)\bigg) + \frac{Q_\Phi m_B F_B}{k\cdot p_B}P^{\mu\rho}_{\rm Low}\bar{u}\Gamma_\mu v\,.$$

This is the well known expression (e.g. [180]) for the radiative amplitude in terms of the form factors and $f_B \to F_B$. We must include the decay constant in this way to be consistent with the virtual computation. Note how F_B, rather than $\Pi_{f_B}(q^2)$, eventually appears in the Low term. Further note the conventional separation of the $P^{\mu\rho}_\parallel$ coefficient (square bracket in (3.123)) for charged mesons. The point-like term (proportional to F_B) is separated out from the parallel form factor $V_\parallel(q^2)$ [180]. The photon has maximum energy $E^{\rm inc}_\gamma = \frac{m_B}{2}(1 - \frac{m_\ell^2}{m_B^2})$ in the limit $q^2 \to m_\ell^2 \approx 0$, while the $q^2 \to m_B^2$ is the soft limit. While we take the functions $V_{\parallel,\perp}$ externally we give some comments on their relation to the

correlator $\Pi_\rho^\gamma|_{\text{struc}}$ in the next section.

3.3.2 Further Correlators

Calculating the form factors ourselves would mean calculating $\Pi_\rho^\gamma|_{\text{struc}}$ which is related to the functions $\Pi_{\parallel,\perp}^V(p_B^2, q^2)$ defined in the $\bar{B} \to \gamma$ LCSR calculation [195] via

$$is_e m_+ m_B \, \Pi_\rho^\gamma|_{\text{struc}} \;=\; \tilde{g}\, \bar{u}\Gamma^\mu v \big(\Pi_\perp^V P_{\mu\rho}^\perp - \Pi_\parallel^V P_{\mu\rho}^\parallel\big)\,, \tag{3.124}$$

which themselves follow from the Lorenz gauge correlation function

$$\begin{aligned}\Pi_{\mu\rho}^V &= -\, s_e m_B \int \mathrm{d}^d x\, \mathrm{d}^d y\, e^{-ip_B\cdot x} e^{ik\cdot y} \langle 0|T j_\rho(y) J_B(x) (\bar{q}\hat{\Gamma}_\mu b)(0)|0\rangle \\ &= s_e \bigg(P_{\mu\rho}^\perp \Pi_\perp^V - P_{\mu\rho}^\parallel \Pi_\parallel^V + (p_B)_\mu (p_B)_\rho X^V + k_\mu (p_B)_\rho Y^V + g_{\mu\rho} p_B\cdot k Z^V \bigg)\,,\end{aligned} \tag{3.125}$$

with $j_\rho = \sum_q Q_q \bar{\psi}_q \gamma_\rho \psi_q$. The X^V, Y^V, Z^V structures are contact terms which, to be consistent with [195], are chosen as

$$\begin{aligned} X^V &= \frac{iQ_\Phi m_B m_+}{p_B\cdot k}\Big(\Pi_{f_B}(q^2) - \Pi_{f_B}(p_B^2)\Big) \\ Y^V &= 0 \\ Z^V &= -\frac{iQ_\Phi m_B m_+}{p_B\cdot k}\Pi_{f_B}(q^2)\,, \end{aligned} \tag{3.126}$$

which matches $\Pi_\rho^\gamma|_{\bar{B}}$ in (3.120). As made clear in [159] the contact terms are not completely fixed by the Ward identity and depend on exactly what terms are absorbed into the definitions of the $\Pi_{\parallel,\perp}^V$ functions[11]. In the end, at the level of the form factors, the amplitude is nevertheless gauge-invariant.

In [195] the authors calculate $\operatorname{Im}\Pi_{\parallel,\perp}^V$ at NLO and beyond leading twist and then Borel transform to extract the form factors $V_{\parallel,\perp}$. Again there is the notion of red and blue cuts in the spectral density. Red cuts correspond to cutting after the photon is radiated, while blue cuts are cuts before the photon emission. Equivalently red cuts are cuts in the variable q^2 while blue cuts are in p_B^2. In our framework with the Φ_B particle we must take both red and blue cuts (as

[11] As a technical note, this also depends on whether the computation takes just blue cuts or red and blue cuts. In the spectral density for $\Pi_\parallel^V$ this corresponds to subtracting $\Pi_{f_B}(p_B^2)$ versus $\Pi_{f_B}(q^2)$, cf. equation (3.15) of [195]. To adapt to their notation use the relation $C^A(p_B^2) = im_+\Pi_{f_B}(p_B^2) + \mathcal{O}(\alpha_s)$.

emphasised in the virtual case) as the emission from the Φ_B (which is crucial for the correct soft physics) corresponds to a red cut. The calculation in [195] is only valid for hard photons[12], and so gets away with taking just blue cuts. This is understood by noting that the cuts start at

$$p_B^2|_{\text{blue}} > m_+^2\,, \quad p_B^2|_{\text{red}} > \left(E_\gamma + \sqrt{E_\gamma^2 + m_+^2}\right)^2, \tag{3.127}$$

and so for hard photons $q^2 \lesssim 14\,\text{GeV}^2$ (or $E_\gamma \gtrsim 1.25\,\text{GeV}$) the red cuts never actually contribute as the cut starts at $p_B^2 > s_0$. We of course certainly care about soft photons and so are required to take both red and blue cuts.

The form factors calculated in [195] are extrapolated from the hard region to the soft region in that paper, and it is that extrapolation that we use for our numerics in the end. It was hoped that by additionally including red cuts in the calculation one could calculate directly in the soft region and bypass the need for the extrapolation. However as will be shown in Section 3.3.4 this does not adequately resolve the hadronic $B^{*(1)}$ pole.

3.3.3 Low terms and Gauge-invariance

Let us now consider the real correlator in the soft limit. Recall from Low's theorem that structure-dependence only appears at $\mathcal{O}(E_\gamma)$ with the first two terms in the E_γ expansion being universal. Focus on the terms proportional to Q_Φ. We have

$$\begin{aligned}(\Pi^\gamma)^\rho \;=\; & -\tilde{g}Q_\Phi \frac{p_\Phi^\rho}{p_\Phi \cdot k}\Pi_{f_B}(q^2)\, m_\ell\, \bar{u}\Gamma v \\ & + \tilde{g}Q_\Phi\, \bar{u}\Gamma_\mu v\left(\frac{\Pi_{f_B}(q^2) - \Pi_{f_B}(p_B^2)}{p_B \cdot k}(p_B)^\rho (p_B)^\mu - \Pi_{f_B}(q^2) g^{\rho\mu}\right) + \dots\,,\end{aligned} \tag{3.128}$$

where $+\dots$ denotes lepton terms and structure-dependent terms that vanish in the soft limit. Taking all cuts, the first line (Φ_B emission) gives the leading Low term in the $k \to 0$ limit. The second line generates an $\mathcal{O}(1)$ contribution as the

[12]For hard photons it is acceptable to treat $|\bar{B}\rangle$ and $|\gamma\rangle$ as separate states, with p_B^2 and q^2 considered distinct variables, as one would do for $\bar{B} \to \rho$ form factors for example. For soft photons this becomes unfeasible as $p_B^2 \approx q^2$.

$\Pi_{f_B}(q^2)$ and $\Pi_{f_B}(p_B^2)$ combine to give $\Pi'_{f_B}(p_B^2)$ as $k \to 0$, i.e

$$\mathrm{Im}\,\Pi^\gamma|^\rho_{\rm soft} \;=\; -\tilde{g}Q_\Phi \frac{p_\Phi^\rho}{p_\Phi\cdot k}\,\mathrm{Im}\,\Pi_{f_B}(p_B^2)\,m_\ell\,\bar{u}\Gamma v \;+\; \mathcal{O}(1) \;+\; \ldots\,. \tag{3.129}$$

If instead we only took blue cuts then we would no longer have a Φ_B particle contribution in the first line. However in the second line one would not cut $\Pi_{f_B}(q^2)$ and thus

$$\mathrm{Im}\,\Pi^\gamma|^\rho_{\rm soft} \;=\; -\tilde{g}Q_\Phi\,\frac{\mathrm{Im}\,\Pi_{f_B}(p_B^2)}{p_B\cdot k}(p_B)^\rho(p_B)^\mu\,\bar{u}\Gamma_\mu v\,, \tag{3.130}$$

which is the same result (with $r \to 0$). That is, one can recover the correct Low behaviour in either the Φ_B formalism (3.129) or in the traditional formalism (3.130) without the Φ_B. However, as stressed in Section 3.3.2, for soft photons one should in general take all cuts. For completeness the eikonal form of the correlator is (including the lepton term)

$$\Pi^\gamma|^\rho_{\rm soft} \;=\; -\tilde{g}\,m_\ell\,\bar{u}\Gamma v\,\Pi_{f_B}(p_B^2)\bigg(Q_\Phi\frac{p_\Phi^\rho}{p_\Phi\cdot k} - Q_{l_1}\frac{l_1^\rho}{l_1\cdot k}\bigg)\,, \tag{3.131}$$

which is trivially gauge-invariant under $\epsilon^* \to \epsilon^* + k$.

Gauge-invariance of the full amplitude follows from noting that the structure-dependence disappears, $k_\rho P^{\mu\rho}_{\parallel,\perp} = 0$, and therefore

$$\begin{aligned}
k^\rho\Pi^\gamma_\rho|_{\ell_1} \;&=\; +\,\tilde{g}Q_{\ell_1}\Big(\bar{u}\not{k}\Gamma v + m_\ell\bar{u}\Gamma v\Big)\Pi_{f_B}(p_B^2) \qquad (3.132)\\
k^\rho\Pi^\gamma_\rho|_{\Phi_B} \;&=\; -\,\tilde{g}Q_\Phi\,m_\ell\,\bar{u}\Gamma v\,\Pi_{f_B}(q^2)\\
k^\rho\Pi^\gamma_\rho|_{\bar{B}} \;&=\; +\,\tilde{g}Q_\Phi\,\bar{u}\Gamma^\mu v\bigg(\big(\Pi_{f_B}(q^2)-\Pi_{f_B}(p_B^2)\big)(p_B)_\mu - \Pi_{f_B}(q^2)k_\mu\bigg)\,.
\end{aligned}$$

After some intricate cancellations the final result $k^\rho\Pi^\gamma_\rho = 0$ follows as a consequence of charge conservation $Q_\Phi = Q_{\ell_1}$.

$$k^\rho\Pi^\gamma_\rho \;=\; \tilde{g}\big(Q_{\ell_1}-Q_\Phi\big)\Big(\bar{u}\not{k}\Gamma v + m_\ell\bar{u}\Gamma v\Big)\Pi_{f_B}(p_B^2) \;=\; 0\,. \tag{3.133}$$

3.3.4 Form Factors

The fundamental difficulty in trying to compute the form factors[13] $V_{\parallel,\perp}(q^2)$ in $m_\ell^2 < q^2 < m_B^2$ using perturbation theory is the presence of hadronic poles at $q^2 = m_{B^1}^2$ (parallel FF) and $q^2 = m_{B^*}^2$ (perpendicular FF). These axial (1^+, m_{B^1}) and vector (1^-, m_{B^*}) excited states of the $\bar{B}$-meson are correspondingly heavier and so lie just above the physical q^2 range, $q^2 < m_B^2$. The poles do not directly enter the form factors, but the proximity of the $B^{*(1)}$ mass to the endpoint means there is a substantial blow-up in the FF as $q^2 \to m_B^2$, i.e in the soft photon region. The masses are [37]

$$m_B = 5.279\,\text{GeV}\,, \qquad m_{B^*} = 5.325\,\text{GeV}\,, \qquad m_{B^1} = 5.726\,\text{GeV}\,, \tag{3.134}$$

where the uncertainties are negligible. The rise towards the pole is more extreme for the perpendicular (vector) form factor as the B^* pole lies closer to m_B^2 than the B^1 pole. This rise is more pronounced for heavier mesons as the mass splittings vanish in the heavy quark limit, cf. (1.20) and (1.21).

Physically the pole arises from the hadronic transitions $B^* \to B\gamma$ (vector channel) and $B^1 \to B\gamma$ (axial channel). These are governed by the couplings $g_{BB^*\gamma}$ and $g_{BB^1\gamma}$ and the decay constants f_{B^*} and f_{B^1}. Following [179] and assuming *pole-dominance* the form factors can be written as

$$V_{\perp(\parallel)} = \frac{r^V_{\perp(\parallel)}}{1 - q^2/m^2_{B^{*(1)}}}\,, \qquad r^V_{\perp(\parallel)} = \frac{m_B}{m_{B^{*(1)}}} f_{B^{*(1)}} g_{BB^{*(1)}\gamma}\,, \tag{3.135}$$

where their magnitude depends on the pole residues $r^V_{\perp(\parallel)}$. These residues have been recently calculated via LCSR in [196] which can be compared to the older estimates in [179]

$$\begin{aligned} r^V_\perp|_{[196]} &= -0.30(4)\,, \quad r^V_\parallel|_{[196]} = -0.16(3)\,, \quad r^V_\perp/r^V_\parallel \approx 1.9\,, \\ r^V_\perp|_{[179]} &= -0.24(4)\,, \quad r^V_\parallel|_{[179]} = -0.20(5)\,, \quad r^V_\perp/r^V_\parallel \approx 1.2\,, \end{aligned} \tag{3.136}$$

giving a more extreme ratio between the perpendicular and parallel FFs. It is exactly these residues [196] that was used in the LCSR form factor calculation [195] to extrapolate the hard photon computation $q^2 \lesssim 14\,\text{GeV}^2$ to the soft photon

[13] Note the alternate notation for the form factors $F_V = V_\perp$ and $F_A = V_\parallel$. In the S-P case these form factors vanish by helicity conservation. Further, in the S-P case all red cut contributions actually cancel identically and so the amplitude is very simple.

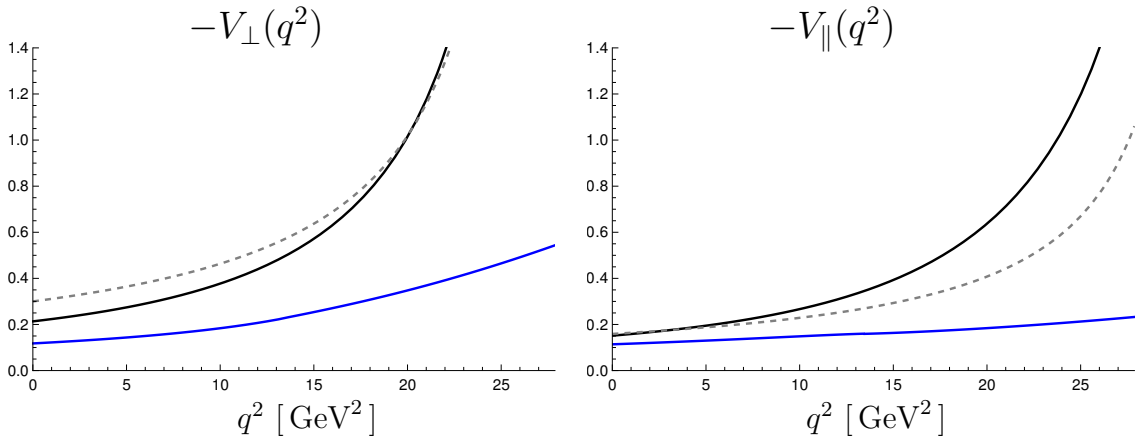

Figure 3.8 *A comparison of three different $B^- \to \gamma$ form factors $V_\perp$ (left) and $V_\parallel$ (right), where $q^2 = m_B^2 - 2m_B E_\gamma$. The black line is the LCSR computation [195] which takes a hard-photon computation (blue cuts only) and extrapolates to the soft region using the residues of [196]. For comparison we give the nearest pole-dominance form factors (using these residues) in grey (dashed). Finally the blue line is our LO in QCD calculation which does not manage to resolve this pole. Note that in our conventions the form factors are negative.*

region $14\,\text{GeV}^2 \lesssim q^2 < m_B^2$.

As discussed in Section 3.3.2, in principle we should be able to compute in the soft photon region directly by taking both red and blue cuts. However working at LO in QCD (i.e. calculating the diagrams in Figures 3.2 and 3.7) this does not in any way manage to capture the hadronic pole. To allow us to make sensible numerical predictions we take the form factors given in [195] for our computation. In Figure 3.8 we plot these form factors (black line) against the LO computation (blue line) with the pole-dominance approximation given in grey (dashed). The LCSR computation does not diverge too much from the pole approximation, especially for the vector form factor which is the most important numerically.

First principles lattice QCD predictions of these charged form factors have not yet been computed. However in the neutral ($\bar{B}_s$) case results have been given in [191] which make use of an extrapolation from unphysical values $m_{B_s} \in [m_{D_s}, 2m_{D_s}]$ to the physical point $m_{B_s} \approx 2.7 m_{D_s}$ using HQET relations. These predictions are in general smaller than the corresponding neutral form factors in [195].

3.3.5 Radiative Rate

The amplitude given in (3.123) must be squared and integrated over three-body phase space in order to infer the rate $\Gamma_{\bar{B}\to\ell\bar{\nu}\gamma}$. That is

$$\Big[|\mathcal{Z}_B|^2\Gamma_{\bar{B}\to\ell\bar{\nu}\gamma}\Big] = \frac{(2\pi)^d}{2m_B}\int\Big[\langle|\mathcal{A}^\gamma|^2\rangle|\mathcal{Z}_B|^2\Big]\delta^{(d)}(p_B-l_1-l_2-k) \times\frac{\mathrm{d}^{d-1}\boldsymbol{l_1}}{(2\pi)^{d-1}2E_{\ell_1}}\frac{\mathrm{d}^{d-1}\boldsymbol{l_2}}{(2\pi)^{d-1}2E_{l_2}}\frac{\mathrm{d}^{d-1}\boldsymbol{k}}{(2\pi)^{d-1}2E_\gamma}\,, \tag{3.137}$$

where again we work in the p_B rest frame and $\langle\cdots\rangle$ indicates spin and polarisation sums. We slice out the soft part of this integral using a soft cut-off $\omega_s^\gamma \ll 1$ to separate the $\epsilon_{\rm IR}$ pole at the cost of $\mathcal{O}(\omega_s^\gamma)$ terms. The result is

$$\begin{aligned}\Big[|\mathcal{Z}_B|^2\Gamma_{\bar{B}\to\ell\bar{\nu}\gamma}\Big]_{\rm soft} = &-\frac{\tilde{g}^2m_B^3}{16\pi^3}\Big(e^{\frac{m_B^2}{M^2}}\mathcal{B}_{M^2}\Pi_{f_B}(p_B^2)\Big)^2\mathcal{K}(\epsilon)\,\hat{m}_\ell^2(1-\hat{m}_\ell^2)^2\\ &\times\Bigg\{\left(\frac{-1}{2\hat{\epsilon}_{\rm IR}}+\ln\frac{m_B\omega_s^\gamma}{\mu}\right)\left(Q_\Phi^2+Q_{\ell_1}^2+Q_\Phi Q_{\ell_1}\frac{1+\hat{m}_\ell^2}{1-\hat{m}_\ell^2}\ln\hat{m}_\ell^2\right)\\ &+Q_\Phi Q_{\ell_1}\frac{1+\hat{m}_\ell^2}{1-\hat{m}_\ell^2}\left(\mathrm{Li}_2(1-\hat{m}_\ell^2)+\frac{1}{4}\ln^2\hat{m}_\ell^2\right)\\ &-Q_\Phi^2+\frac{1}{2}Q_{\ell_1}^2\frac{1+\hat{m}_\ell^2}{1-\hat{m}_\ell^2}\ln\hat{m}_\ell^2\Bigg\}+\mathcal{O}(\omega_s^\gamma)\,,\end{aligned} \tag{3.138}$$

where recall $\hat{m}_\ell \equiv m_\ell/m_B$. This is essentially just the result with the eikonal approximation to the amplitude. The pole and soft-collinear terms cancel exactly with (3.93) as they must. Notice that the final term in (3.138) is a finite collinear $\ln m_\ell$ term (not a soft-collinear term) that is generated from this soft region. The soft cut-off cancels against logarithmic ω_s^γ dependence in the remaining hard region.

The hard region is most easily calculated in Dalitz variables

$$x = 1-\frac{(p_B-k)^2}{m_B^2}\,,\qquad y = 1-\frac{(p_B-l_1)^2}{m_B^2}\,, \tag{3.139}$$

where we may take $d=4$ safely. These variables are essentially just the photon and lepton energies (in the meson rest frame) respectively

$$x=\frac{2E_\gamma}{m_B}\,,\qquad y=\frac{2E_{\ell_1}}{m_B}-\hat{m}_\ell^2\,. \tag{3.140}$$

In such dimensionless variables the hard region is

$$\omega_s^\gamma < x < r_E\,, \qquad r_E \in \left[0, 1-\hat{m}_\ell^2\right], \tag{3.141}$$

where r_E is the dimensionless photon energy cut-off, cf. (2.84). The phase space integral (3.137) can be rewritten in terms of Dalitz variables as

$$\left[|\mathcal{Z}_B|^2\Gamma_{\bar{B}\to\ell\bar{\nu}\gamma}\right]_{\text{hard}} = \frac{m_B}{256\pi^3}\int_{\omega_s^\gamma}^{r_E}\mathrm{d}x\int_{1-x+\frac{x}{1-x}\hat{m}_\ell^2}^{1}\mathrm{d}y\left[\langle|\mathcal{A}^\gamma|^2\rangle|\mathcal{Z}_B|^2\right], \tag{3.142}$$

with the integral over y performed analytically. The final energy integral has to be done numerically due to the x dependence in the form factors, $q^2 = m_B^2(1-x)$.

As stressed previously, structure-dependent terms in the real rate lift the tree-level helicity suppression. For hard photons, $E_\gamma \sim \frac{1}{2}m_B$, the real rate is enhanced by a factor of $(m_B/m_\ell)^2$ compared to the tree level. For the electron and muon channels this is an enhancement by a factor of approximately 10^8 and 2500 respectively. This means that for the real contribution to not completely overwhelm the virtual a very soft photon cut must be chosen, $E_\gamma^{\text{cut}} \sim m_\ell$. The large tau mass means the helicity suppression is effectively not there in the first place and we may consider a wide range of photon energy cuts for this channel.

With the light lepton channels in mind we can drop $\mathcal{O}(m_\ell^2)$ terms and recover the well-known form for the differential rate, valid for $E_\gamma \gg m_\ell$

$$\left.\frac{\mathrm{d}\Gamma_{\bar{B}\to\ell\bar{\nu}\gamma}}{\mathrm{d}E_\gamma}\right|_{m_\ell\to 0} = \frac{\alpha\,G_F^2|V_{\text{ub}}|^2}{6\pi^2}m_B E_\gamma^3\left(1-\frac{2E_\gamma}{m_B}\right)\left(|V_\parallel|^2+|V_\perp|^2\right), \tag{3.143}$$

which is entirely structure-dependent. The scalar QED real result in Section 2.3.3 of course does not capture this enhancement and vanishes in the $m_\ell \to 0$ limit. For later convenience (as we shall use it in plots and it does not appear in [164]) we give the scalar QED result at the double-differential level

$$\begin{aligned}\frac{1}{\Gamma^{(0)}_{\text{SQED}}}\frac{\partial^2\Gamma^{(2)}_{\text{SQED}}}{\partial x\partial y} &= \frac{\alpha}{2\pi}\frac{1}{(1-\hat{m}_\ell^2)^2}\left[\frac{(2-x)(\hat{m}_\ell^2+x-1)}{x^2}-\frac{1+\hat{m}_\ell^2}{x}\right.\\ &\quad\left.+\frac{2(1-\hat{m}_\ell^4)}{x(x+y-1)}+\frac{2\hat{m}_\ell^2+x-2}{x+y-1}+\frac{2\hat{m}_\ell^2(\hat{m}_\ell^2-1)}{(x+y-1)^2}\right]\\ &= \frac{\alpha}{2\pi}\frac{(x^2-2x+2)(1-y)}{x^2(x+y-1)}+\mathcal{O}(m_\ell^2)\,,\end{aligned} \tag{3.144}$$

which is particularly simple upon neglecting subleading $\mathcal{O}(m_\ell^2)$ terms on the RHS.

3.4 Collinear Logs

This final section discusses one of the central conceptual points of the work: the non-cancellation of collinear logs, $\ln m_\ell$. As emphasised in Chapter 2, such logs are sizeable and appear only for vector and axial interactions due to the helicity suppression of the tree level amplitude. In theories with S-P interactions the KLN theorem applies and hard-collinear logs must cancel between real and virtual rates when fully inclusive.

The KLN theorem itself is based on unitarity and implies that all collinear logs can be reproduced from the LO rate and the splitting function, $P_{f\to f\gamma}$ (2.81) in the S-P case. We must get [138]

$$\begin{aligned}\Gamma^{(2)}_{\text{S-P}}\big|_{\text{HC}} &= -\frac{\alpha}{\pi}Q_{\ell_1}^2 \ln m_\ell \int_{1-r_E}^{1} \mathrm{d}z\, P_{f\to f\gamma}(z)\, \Gamma^{(0)}_{\text{S-P}} \\ &= -\frac{\alpha}{\pi}Q_{\ell_1}^2 \ln m_\ell \left(\frac{3}{2} - r_E\big(2-\frac{1}{2}r_E\big)\right)\Gamma^{(0)}_{\text{S-P}}\,, \end{aligned} \tag{3.145}$$

where the traditional collinear variable z in these kinematics is simply the complement of the Dalitz variable $z \equiv 1-x$. As x is interpreted as a dimensionless photon energy the soft region is therefore the limit $z \to 1$. Note that the LO rate does not depend on z, unlike for example in $\bar{B} \to \bar{K}\ell\bar{\ell}$ at the double differential level (in q^2 variables) [90]. In the collinear region we neglect subleading m_ℓ^2 terms and so the fully photon inclusive limit is $r_E \to 1$, for which the RHS of (3.145) vanishes. In other words the collinear logs cancel once integrated over the entire photon energy range.

We will use the S-P result as an important check of our methodology. Structure-dependent logs are forbidden by the KLN theorem and we will verify this explicitly. On the other hand structure-dependent logs may appear for V±A interactions, as found for example in the SCET analysis of $\bar{B}_s \to \mu^+\mu^-$ [176]. Investigating how our logs differ from the naive scalar QED logs (Table 2.1) is the main aim of this section. The virtual logs are described in Section 3.4.1 (methods) and 3.4.2 (results) while real hard-collinear logs are given in Section 3.4.3.

3.4.1 Virtual Collinear Slicing

In general, hard-collinear logs are generated from both red and blue cuts in the virtual computation. Extracting hard-collinear logs from the blue cuts is relatively straightforward. They appear directly in the Passarino-Veltman functions as explained around (3.64) in Section 3.2.4. To put it another way, in the blue cuts the photon loop factorises and one-loop collinear logs are well-known. The extraction of hard-collinear logs arising from the red cuts is less standard and is the topic to which we now turn.

As explained in Section 3.2, the red cuts resemble a real decay with modified kinematics. Once we have integrated out the quark loop momenta we are left with an integral over the virtual photon phase space $\int \mathrm{d}^d k\, \delta^+(k^2)$ where the delta function forces the photon on-shell. Having sliced out the soft part of this integral, the hard part is decomposed into collinear and non-collinear sectors. The treatment of the collinear sector is a modification of the collinear slicing technique [156] from real to virtual and is new to the best of our knowledge. Again this procedure has been checked in the toy model.

Traditionally *real* collinear phase space is parameterised by an 'energy variable' z and the collinear variable $k \cdot l_1$, as discussed in Section 2.3.2. The collinear divergence appears due to terms in the integrand of $\mathcal{O}(1/(k\cdot l_1)^{1+\epsilon})$ as $k \cdot l_1 \to 0$. The collinear region is parameterised by a collinear cut-off ω_c which is chosen to be sufficiently small to allow us to drop subleading powers of $k \cdot l_1$ and m_ℓ^2 in the integrand at the cost of $\mathcal{O}(\omega_c)$ terms. The collinear divergence comes from

$$\int_0^{\omega_c m_B^2} \frac{\mathrm{d}(k\cdot l_1)}{(k\cdot l_1)^{1+\epsilon}} \;=\; \frac{-1}{\epsilon_{\mathrm{IR}}} + \ln\!\big(\omega_c m_B^2\big)\,, \tag{3.146}$$

in the limit where the lepton is massless. We retain a finite lepton mass and so $k\cdot l_1$ is cut off at its $\mathcal{O}(m_\ell^2)$ lower limit thus generating collinear logs $1/\epsilon_{\mathrm{IR}} \to \ln m_\ell^2$. The 'energy variable' z is traditionally defined as

$$k = (1-z)\, l_\gamma\,, \qquad l_\gamma \equiv l_1 + k\,, \tag{3.147}$$

which for our kinematics can also be defined as $z = 1 - x$ as discussed earlier. Implicit in the definition (3.147) is the fact that in the collinear region one may take k parallel to l_1 up to neglected terms of order m_ℓ^2. The quantity l_γ naturally appears as the momentum carried by the lepton before it emits the collinear

photon.

In the virtual case however the object l_γ is no longer the natural variable and the definition (3.147) is not optimal. For the virtual phase space in the red cuts we instead parameterise the collinear region with $\{z_v, k \cdot l_1\}$ where

$$k = (1 - z_v)\, l_1 \,, \tag{3.148}$$

up to subleading terms. In analogy to the real case the photon is soft as $z_v \to 1$. Of course we have already sliced the soft region out and so $z_v < 1 - \omega_s$. One may worry about the virtual photon having unbounded energy, however recall that it is actually cut off at $|\boldsymbol{k}| = \Lambda$, (3.57), by the θ function generated in the quark loop integral. Translated to the z_v variable this gives the bounds

$$\delta_H < z_v < 1 - \omega_s \,, \qquad \delta_H \equiv \frac{m_+^2}{p_B^2} \,, \tag{3.149}$$

where δ_H is the hard cut-off. Other energy parameterisations are available however this is the simplest choice[14]. We now derive the virtual phase space in $d = 4 - 2\epsilon$ dimensions (also retaining non-zero masses), though we only need the $d = 4$ case in this work.

Write the virtual photon momentum quite generally as

$$k^\mu = c_1\, l_1^\mu + c_2\, l_2^\mu + k_T^\mu \,, \tag{3.150}$$

where k_T^μ is a part transverse to the leptons and $c_{1,2}$ are coefficients. Collinearity is therefore the limit $k_T \to 0$ (and $m_\ell^2 \to 0$). Anticipating the result we may as well relabel $c_1 = 1 - z_v$ and enforcing $k^2 = 0$ gives

$$k^\mu = (1 - z_v)\, l_1^\mu + \frac{|\boldsymbol{k_T}|^2 - (1 - z_v)^2 m_\ell^2}{(m_B^2 - m_\ell^2)(1 - z_v)}\, l_2^\mu + k_T^\mu \,, \tag{3.151}$$

where $\boldsymbol{k_T}$ is a $d-2$ dimensional transverse vector, $k_T^2 = -|\boldsymbol{k_T}|^2$, and $k_T \cdot l_{1,2} = 0$. Working in the $p_B = (\sqrt{s}, \boldsymbol{0})$ rest frame one can give an explicit parameterisation,

[14] In general one could take any parameterisation $k = f(z) l_1$ (for sensible functions f) in the collinear region as this really is just a change of energy variables. Indeed one recovers the same results when taking $f(z) = (1 - z)/z$, the direct equivalent of (3.147). Note however that requiring $z \leq 1$ when taking (3.148) is only possible with certain kinematic choices. This is guaranteed for $l_2 \cdot r = 0$, but not for $l_1 \cdot r = 0$ at large s_0 for example.

cf. (3.18)

$$k^\mu \;=\; \frac{1}{2\sqrt{s}}\bigg(s(1-z_v)+\frac{|\boldsymbol{k_T}|^2}{1-z_v},\, 2\sqrt{s}\,\boldsymbol{k_T}\,,s(1-z_v)-\frac{|\boldsymbol{k_T}|^2}{1-z_v}\bigg), \tag{3.152}$$

where the leptons are aligned with the z-axis, $k_T^\mu = (0, \boldsymbol{k_T}, 0)$. Further we get

$$k\cdot l_1 \;=\; \tfrac{1}{2}(1-z_v)m_\ell^2+\frac{|\boldsymbol{k_T}|^2}{2(1-z_v)}\,, \tag{3.153}$$

showing how the lepton mass regulates the minimum value of $k\cdot l_1$ when $|\boldsymbol{k_T}|\to 0$. We define the upper boundary of the collinear region by $k\cdot l_1 < \omega_c\, p_B^2$ where following [156] the hierarchy $\omega_c/\omega_s \ll 1$ is required to properly resolve the overlap between the soft and collinear regions. The collinear photon phase space can be written in terms of a transverse part and a component in the z direction, i.e. in cylindrical coordinates

$$\int \mathrm{d}^{d-1}\boldsymbol{k} = \int \mathrm{d}\boldsymbol{k}_z\, |\boldsymbol{k_T}|^{d-3}\,\mathrm{d}|\boldsymbol{k_T}|\,\mathrm{d}\Omega_{d-2}\;. \tag{3.154}$$

Transforming to $\{z_v, k\cdot l_1\}$ variables with Jacobian

$$\left|\frac{\partial(\boldsymbol{k}_z,|\boldsymbol{k_T}|)}{\partial(z_v,k\cdot l_1)}\right| \;=\; \frac{\boldsymbol{k}_z}{|\boldsymbol{k_T}|}\Big[1+\mathcal{O}(|\boldsymbol{k_T}|,m_\ell^2)\Big]\,, \tag{3.155}$$

where in the collinear region we drop all subleading behaviour as this generates negligible $\mathcal{O}(\omega_c)$ terms. We finally get the hard-collinear phase space parameterisation

$$\int_{\mathrm{HC}}\frac{\mathrm{d}^{d-1}\boldsymbol{k}}{|\boldsymbol{k}|} \;=\; \Omega_{d-2}\int_{\delta_H}^{1-\omega_s}\mathrm{d}z_v\int_{\frac{1}{2}(1-z_v)m_\ell^2}^{\omega_c\,p_B^2}\mathrm{d}(k\cdot l_1)\,\left[2(1-z_v)k\cdot l_1\right]^{\frac{d-4}{2}}\,, \tag{3.156}$$

which is conveniently simple in $d=4$. Collinear divergences arise from $1/(l_1\cdot k)$ terms in the integrand and are regulated into $\ln m_\ell$ by the m_ℓ^2 in the lower integration limit.

3.4.2 Virtual Results

Now we give explicit results for the S-P and V-A cases.

The S-P case: The blue cuts are found to match scalar QED

$$\begin{aligned}\operatorname{Im}\Pi^{(2)}_{\text{S-P}}(p_B^2)\big|^{\text{HC}}_{\text{blue}} &= -\frac{\alpha}{\pi}Q_{\ell_1}(Q_b-Q_q)\operatorname{Im}\Pi^{(0)}_{\text{S-P}}(p_B^2)\ln m_\ell \\ &= -\frac{\alpha}{\pi}\operatorname{Im}\Pi^{(0)}_{\text{S-P}}(p_B^2)\ln m_\ell\,. \end{aligned} \tag{3.157}$$

Only the $b\,\ell_1$ and $q\,\ell_1$ diagrams contribute unlike in the red cuts where there is also the $\Phi\,\ell_1$ diagram. This extra diagram facilitates the cancellation by charge in the red cuts

$$\begin{aligned}\operatorname{Im}\Pi^{(2)}_{\text{S-P}}(p_B^2)\big|^{\text{HC}}_{\text{red}} &= \frac{\alpha}{\pi}Q_{\ell_1}Q_{\mathcal{J}_B}\ln m_\ell\int_{\delta_H}^{1-\omega_s}\mathrm{d}z_v\,\frac{z_v}{1-z_v}\operatorname{Im}\Pi^{(0)}_{\text{S-P}}(z_v p_B^2) \\ &= 0\,, \end{aligned} \tag{3.158}$$

as the three diagrams sum to $Q_{\mathcal{J}_B} = Q_\Phi - Q_b + Q_q = 0$. That is, there are no hard-collinear logs generated from the red cuts in the S-P case; there is perfect cancellation. Such a cancellation does not occur in the V-A case however.

In theory there could also be hard-collinear logs generated from the soft part of the red cuts in the manner of (3.138). However such terms also cancel by charge conservation, $Q_{\mathcal{J}_B} = 0$, as above and so we do not need to worry about them. Soft photons do not discriminate between S-P and V-A interactions meaning the same behaviour occurs in the V-A case.

There are also hard-collinear logs generated from the lepton renormalisation constants (3.70)

$$\operatorname{Im}\Pi^{(2)}_{\text{S-P}}(p_B^2)\big|^{\text{HC}}_{\text{SE}} = \frac{3\alpha}{4\pi}\operatorname{Im}\Pi^{(0)}_{\text{S-P}}(p_B^2)\ln m_\ell\,, \tag{3.159}$$

with an identical equation in the V-A case. To summarise, the virtual S-P logs match scalar QED exactly with no extra structure-dependence. The exact cancellation of the red cuts has additionally been shown in the toy model.

The V-A case: The extra freedom accorded by the helicity suppression means the explicit results are more involved. The blue cuts are found to be

$$\operatorname{Im}\Pi^{(2)}_{\text{V-A}}(p_B^2)\big|^{\text{HC}}_{\text{blue}} = \frac{m_+ g_{\text{eff}}\alpha Q_{\ell_1}N_c}{16\pi^2}\frac{m_\ell\bar{u}\Gamma v}{p_B^4}\cdot\mathbb{H}_{\text{blue}}\cdot\ln m_\ell\,, \tag{3.160}$$

where

$$\begin{aligned}\mathbb{H}_{\text{blue}} = &+ Q_b\Big[2m_+m_-^2\lambda^{\frac{1}{2}} + (m_+ + m_-)\big(p_B^2 - m_-(m_+ + m_-)\big)p_B^2 L^+\Big] \\ &- Q_q\Big[2m_-(m_+m_- - p_B^2)\lambda^{\frac{1}{2}} + m_-(m_+ - m_-)^2 p_B^2 L^-\Big],\end{aligned} \tag{3.161}$$

and we have logarithms

$$L^\pm = \ln\left(\frac{p_B^2 \pm m_+m_- + \lambda^{\frac{1}{2}}}{p_B^2 \pm m_+m_- - \lambda^{\frac{1}{2}}}\right). \tag{3.162}$$

The result need not be proportional to the tree level as these are not genuine collinear logs but $m_\ell \ln m_\ell$ of course. For the red cuts we get the same cancellation as in the S-P case (3.158) in the soft region, however there are now extra terms arising from non-soft virtual photons

$$\begin{aligned}\operatorname{Im}\Pi^{(2)}_{\text{V-A}}(p_B^2)\big|^{\text{HC}}_{\text{red}} &= \frac{\alpha}{\pi}Q_{\ell_1}Q_{\mathcal{J}_B}\ln m_\ell \int_{\delta_H}^{1-\omega_s}\frac{z_v}{1-z_v}\operatorname{Im}\Pi^{(0)}_{\text{V-A}}(z_v p_B^2)\,\mathrm{d}z_v \\ &\quad - \frac{m_+ g_{\text{eff}}\alpha Q_{\ell_1}N_c}{8\pi^2}m_\ell \ln m_\ell\, \bar{u}\Gamma v \int_{\delta_H}^{1-\omega_s}\mathbb{H}_{\text{red}}(z_v, p_B^2)\,\mathrm{d}z_v \\ &= - \frac{m_+ g_{\text{eff}}\alpha Q_{\ell_1}N_c}{8\pi^2}m_\ell \ln m_\ell\, \bar{u}\Gamma v \int_{\delta_H}^{1}\mathbb{H}_{\text{red}}(z_v, p_B^2)\,\mathrm{d}z_v\,,\end{aligned} \tag{3.163}$$

where

$$\begin{aligned}\mathbb{H}_{\text{red}}(z_v, p_B^2) \;= &+ Q_b(m_+ + m_-)(1-z_v)L_q^+ \\ &- \frac{m_-}{2p_B^2}\Big[Q_b(m_+ + m_-)^2 L_q^+ + Q_q(m_+ - m_-)^2 L_q^-\Big] \\ &+ \lambda_q^{\frac{1}{2}}\Big[(Q_b - Q_q)\frac{m_+m_-^2 - p_B^2(m_+ + m_-)}{p_B^4 z_v} + \frac{2Q_b m_- + (Q_b - Q_q)m_+}{p_B^2}\Big],\end{aligned} \tag{3.164}$$

and we define $L_q^\pm \equiv L^\pm|_{p_B^2 \to q^2}$. Note that in the collinear region $q^2 = z_v p_B^2$. As all soft terms cancel in (3.163) we may safely take $\omega_s \to 0$ in the integral. Neglecting m_q terms for simplicity (a negligible numerical effect) then this integral is easily performed. Combining the result with the blue cuts (3.160) gives the total V-A 1PI hard-collinear logs

$$\operatorname{Im}\Pi^{(2)}_{\text{V-A}}(p_B^2)\big|^{\text{HC}}_{\text{1PI}} = \frac{m_b^2 g_{\text{eff}}\alpha Q_{\ell_1}N_c}{16\pi^2}\frac{m_\ell \bar{u}\Gamma v}{p_B^4}\Big[2m_b^2(Q_b - Q_q)(m_b^2 - 2p_B^2)\ln\frac{p_B^2}{m_b^2}$$

$$+ (p_B^2 - m_b^2)\Big(p_B^2(4Q_b - Q_q) - m_b^2(2Q_b + Q_q)\Big)\Big] \ln m_\ell \,. \quad (3.165)$$

Finally, adding in the self-energy contributions and applying $Q_b = -1/3$ and $Q_q = 2/3$ one gets the total virtual V-A collinear logs

$$\mathrm{Im}\,\Pi^{(2)}_{\text{V-A}}(p_B^2)|_{\text{HC}} = \quad (3.166)$$
$$\frac{m_b^2 g_{\text{eff}}\,\alpha N_c}{32\pi^2}\frac{m_\ell \bar{u}\Gamma v}{p_B^4}\left((p_B^2 - m_b^2)(7p_B^2 - 3m_b^2) + 4m_b^2(m_b^2 - 2p_B^2)\ln\frac{p_B^2}{m_b^2}\right)\ln m_\ell \,.$$

Comparing to the scalar QED result, $\frac{5\alpha}{4\pi}\,\mathrm{Im}\,\Pi^{(0)}\ln m_\ell$ there is a clear structure-dependent effect. Structure-dependence gives a positive correction to the decay rate acting against the negative scalar QED contribution. We have thus demonstrated explicitly one of the important takeaways of this work – that structure-dependent logs can and do exist in helicity suppressed decays.

3.4.3 Real Contribution

Real collinear logs arise from the integration of powers of $k \cdot l_1 = \frac{1}{2}m_B^2(x + y - 1)$ over the Dalitz variable y in (3.142). To compare to the literature we will write results in terms of the traditional slicing variable $z = 1 - x$. Note that the form factors $V_{\parallel,\perp}$ depend on z.

The S-P case: For (pseudo)scalar interactions there are no structure-dependent form factors. The integration over y is easily performed and the hard-collinear behaviour is

$$\Big[|\mathcal{Z}_B|^2\Gamma_{B\to\ell\bar{\nu}\gamma}\Big]^{\text{S-P}}_{\text{HC}} = -\frac{m_B\tilde{g}^2Q_{\ell_1}^2}{16\pi^3}\Big(e^{\frac{m_B^2}{M^2}}\mathcal{B}_{M^2}\Pi^{\text{S-P}}_{f_B}(p_B^2)\Big)^2\int_{1-r_E}^{1-\omega_s^\gamma}\tilde{P}_{f\to f\gamma}(z)\,\mathrm{d}z\,\ln m_\ell\,, \quad (3.167)$$

which in the fully inclusive limit $r_E \to 1$ is

$$\Big[|\mathcal{Z}_B|^2\Gamma_{B\to\ell\bar{\nu}\gamma}\Big]^{\text{S-P}}_{\text{HC}} \xrightarrow{r_E\to 1}$$
$$\frac{m_B\tilde{g}^2Q_{\ell_1}^2}{16\pi^3}\Big(e^{\frac{m_B^2}{M^2}}\mathcal{B}_{M^2}\Pi^{\text{S-P}}_{f_B}(p_B^2)\Big)^2\left[\frac{3}{2} + 2\ln\omega_s^\gamma\right]\ln m_\ell \,+\, \mathcal{O}(\omega_s^\gamma)\,. \quad (3.168)$$

In the S-P case the real collinear emission part of the fermion splitting function, $\tilde{P}_{f\to f\gamma}(z)$ (2.80), appears and is easily integrated. To this we can add the hard-

collinear log from the real soft region (3.138) ("V-A = S-P" when soft) and the virtual S-P logs, (3.157) and (3.159), to give

$$\left[|\mathcal{Z}_B|^2\Gamma^{\text{S-P}}_{B\to\ell\bar{\nu}(\gamma)}\right]^{(2)}_{\text{HC}} = \frac{\alpha}{\pi}Q_{l_1}^2\left[|\mathcal{Z}_B|^2\Gamma^{\text{S-P}}_{B\to\ell\bar{\nu}}\right]^{(0)} \ln m_\ell \times \tag{3.169}$$
$$\left(\left[\frac{3}{2}+2\ln\omega_s^\gamma\right]_{\text{real (hard)}} + \left[-1-2\ln\omega_s^\gamma\right]_{\text{real (soft)}} + \left[\frac{3}{2}-2\right]_{\text{virt}}\right) = 0\,,$$

showing finally the complete cancellation (once fully inclusive) of the collinear logs in the S-P case! This of course is guaranteed by the KLN theorem and therefore matches the form found in [90]. The logarithmic dependence on the soft cut-off ω_s^γ cancels between the soft and hard regions as it must.

The V-A case: For the V-A case there are structure-dependent logs due to dependence on the form factors $V_{\perp,\parallel}(q^2)$, where $q^2 = z\,m_B^2$.

$$\left[|\mathcal{Z}_B|^2\Gamma_{B\to\ell\bar{\nu}\gamma}\right]^{\text{V-A}}_{\text{HC}} = -\frac{m_B\tilde{g}^2m_\ell^2Q_{\ell_1}}{16\pi^3}\,e^{\frac{m_B^2}{M^2}}\mathcal{B}_{M^2}\Pi_{f_B}(p_B^2)\,\ln m_\ell \times \tag{3.170}$$
$$\int_{1-r_E}^{1-\omega_s^\gamma}\mathrm{d}z\left[Q_{\ell_1}\tilde{P}_{f\to f\gamma}(z)\,e^{\frac{m_B^2}{M^2}}\mathcal{B}_{M^2}\Pi_{f_B}(p_B^2) + \frac{m_B}{m_+}(1-z)^2\left(V_\parallel(q^2)-V_\perp(q^2)\right)\mathcal{Z}_B\right]$$

The splitting function again appears as it must do to recover the scalar QED result for $V_{\perp,\parallel}\to 0$. Similarly in the soft limit the structure-dependent term vanishes. However it is important to remember that for hard photons the helicity suppression of the tree-level amplitude is lifted and so collinear logs are no longer important numerically (there are no helicity un-suppressed logs). That being said, for a sufficiently small photon energy cut the second term on the RHS can play an important role. Exactly how important such structure-dependent effects are is the subject of the next chapter: numerics.

Chapter 4

Numerical Results

In this chapter we give numerical results and plots for $\bar{B} \to \ell\bar{\nu}(\gamma)$, showing the importance of including structure-dependent corrections over just scalar QED. In Section 4.3 we discuss the relevance of this work for experimental searches while in Section 4.4 we give some concluding remarks.

4.1 Inputs and Uncertainties

Numerical inputs for the decay rate calculation consist of the usual particle masses and coupling constants (summarised in Table 4.1), the real form factors, and the sum-rule specific parameters, s_0 and M^2.

As explained in Section 2.1.2, we fix the continuum threshold s_0 through the Daughter Sum Rule consistency condition, (2.42). An intermediate Borel mass M^2 is then taken to simultaneously suppress higher dimensional operators and continuum contributions. While it is perhaps most elegant to take the same sum-rule parameters for both the numerator and denominator correlators, $\Pi^{(\gamma)}$ and C, this is not required and there is some tradition of treating them differently to achieve better convergence in the individual sum rules [41]. We have checked that the final results are unaffected by this choice: changing by $< 1\%$ upon taking the same parameters for $\Pi^{(\gamma)}$ and C. In our numerics we take

$$\begin{aligned} \Pi^{(\gamma)}(p_B^2, p_\Phi^2): &\qquad s_0 = 37.2(1.0)\,\mathrm{GeV}^2\,, &&\qquad M^2 = 7.9(5)\,\mathrm{GeV}^2\,, \\ C(p_B^2, p_\Phi^2): &\qquad s_0 = 36.9(1.0)\,\mathrm{GeV}^2\,, &&\qquad M^2 = 6.3(5)\,\mathrm{GeV}^2\,, \end{aligned} \tag{4.1}$$

Boson masses [37]		
m_{B^-}	M_W	M_Z
5.279 GeV	80.377 GeV	91.19 GeV
Lepton masses [37]		
m_τ	m_μ	m_e
1.777 GeV	105.7 MeV	0.511 MeV
Quark masses [37]		
$m_b^{kin}\vert_{1\text{GeV}}$	$\bar{m}_u\vert_{2\text{GeV}}$	
4.53(6) GeV	$2.16^{+0.49}_{-0.26}$ MeV	
Miscellaneous [37]		
τ_{B^-}	G_F	α^{-1}
$1.638(4) \times 10^{-12}$ s	$1.166 \times 10^{-5}\,\text{GeV}^{-2}$	137.036
$\langle\bar{q}q\rangle\vert_{2\text{GeV}}$ [44]	$\vert V_{ub}\vert$	
$-(269(2)\,\text{MeV})^3$	$3.82(20) \times 10^{-3}$	

Table 4.1 *Summary of input parameters. Note that the uncertainties in most particle masses are negligible and are ignored. We set the renormalisation scale $\mu = m_b$ following [207], although scale dependence upon varying $\mu^2 \to (1/2, 2)\,\mu^2$ is negligible since it is $\mathcal{O}(\alpha^2)$ and below numerical precision.*

where the brackets indicate the uncertainties we apply in the error calculations. Note that one *must* take the same parameter values for Π^γ and Π to ensure numerical cancellation of the soft poles between real and virtual. We take the same parameters for all channels $\ell = e, \mu, \tau$ which is acceptable on account of the smallness of the QED correction. These values lead to good flatness in the Borel window.

For the numerator sum-rule, using the values in (4.1) and requiring the DSR consistency condition to be obeyed to $< 0.1\%$, the quark condensate is suppressed to 35.8% of the perturbative ($\mathbb{1}$) contribution while continuum states above s_0 make up 35.6% of the total dispersive integral. For the denominator these figures are 34.4% and 34.7%. These values are slightly on the high side, though not unreasonable. However convergence gets much worse for lighter mesons and it is for this reason that we do not consider the $D_{d,s}$ decay.

For the slicing procedure we take $\omega_s = \omega_s^\gamma$ at $s = m_B^2$ and enforce the hierarchy $\omega_c/\omega_s \ll 1$ as far as possible. There is also the constraint $\omega_c \gtrsim \hat{m}_\ell^2$ that must be satisfied. All slicing parameters are chosen to be the same for both the numerator and denominator. We take $\omega_s^{(e)} = 10^{-3} = 100 \cdot \omega_c^{(e)}$ for the electron channel while the heavier muon constrains us to take $\omega_s^{(\mu)} = 5 \cdot 10^{-3} = 50 \cdot \omega_c^{(\mu)}$. We take

$\omega_s^{(\tau)} = \omega_s^{(\mu)}$ and of course no collinear slicing is performed in the tau channel. These choices give good stability under small $\omega_{s,c}$ variations and have a negligible impact on the final numerics.

The most relevant input parameter is the heavy quark mass m_b for which we take the kinetic[1] scheme value $m_b = 4.53(6)\,\text{GeV}$ at $\mu_{\text{kin}} = 1\,\text{GeV}$ (cf. $\overline{\text{MS}}$ conversion formulae in [211]). We choose this scheme due to its previous good convergence in QED-related sum rules computations, [195, 196] and in Chapter 5, and we have checked explicitly that it performs better than the pole or $\overline{\text{MS}}$ scheme. Further, we are actually forced to use this scheme to match the LCSR computation [195] whose form factors we use in our numerics. However in view that our computation is LO in α_s we take the m_b uncertainty as $\delta m_b = \pm 0.2\,\text{GeV}$ to accommodate the pole and $\overline{\text{MS}}$ schemes. The light quark mass on the other hand must be taken in $\overline{\text{MS}}$.

Uncertainties are computed in the standard way, varying the input parameters by their errors and adding the resulting uncertainties in quadrature[2]. For the virtual rate the dominant uncertainty arises from the b-quark mass, making up roughly three-quarters of the total error budget. The remaining uncertainty is equal parts due to the Borel parameters s_0 and M^2 with $< 5\%$ contributions coming from other quantities. On the real side, especially for hard photons, the largest source of uncertainty is the external form factors $V_{\parallel,\perp}$ (mainly the vector channel).

Before discussing results it is worthwhile to briefly mention some limitations of the above procedure that are rarely stressed in the sum-rules literature. While varying parameters and adding the results in quadrature is standard practise for computing uncertainties, the sum-rules procedure itself is essentially of unknown accuracy. The extractions (3.10) and (3.12) rely on suppressing unwanted contributions to the residue via a Borel procedure. While such contributions do enter as s_0 and M^2 uncertainties the correspondence is not wholly rigorous. Nevertheless sum-rules techniques have a long history of accurate predictions, thus validating the procedure to some extent.

[1]The kinetic scheme has its origins in HQET and can be defined [210] in terms of the pole mass, $\bar{\Lambda}$ and the kinetic operator (1.22).

[2]This assumes no correlation between the errors. When performing the m_b variation we duly should adjust the hadronic threshold s_0 appropriately. Doing this gives a negligible effect on the final quoted errors.

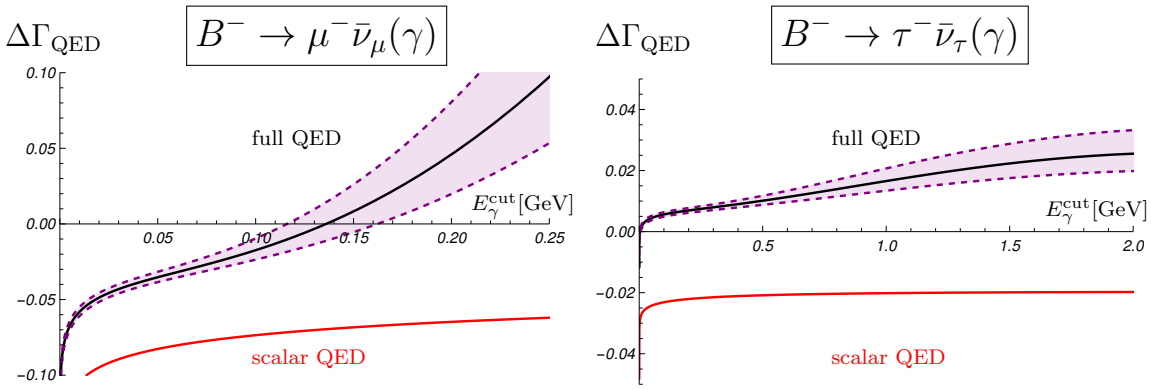

Figure 4.1 *The QED correction (black line, error in purple) as a function of the photon energy cut, E_γ^{cut}, as defined in* (4.2)*. (Left) The muon channel. (Right) The tau channel. For comparison, the red line is the scalar QED result which does not exhibit the same lifting of helicity suppression. Note the different scales in the two plots.*

4.2 Results

The main result we report is the relative QED correction to the LO decay rate, $\Delta\Gamma_{\rm QED}$, which is a function of the photon energy cut $E_\gamma^{\rm cut}$

$$1 + \Delta\Gamma_{\rm QED}(E_\gamma^{\rm cut}) \equiv \frac{1}{\Gamma^{(0)}}\left(\Gamma^{B\to\ell\bar{\nu}} + \Gamma^{B\to\ell\bar{\nu}\gamma}_{E_\gamma<E_\gamma^{\rm cut}}\right) + \mathcal{O}(\alpha^2)\,. \tag{4.2}$$

The corresponding plot is given in Figure 4.1 for the muon and tau channels. We plot our full structure-dependent computation (black line, error bands in purple) with the scalar QED result given in red for comparison.

The plot shows the significant effect of the lifting of helicity suppression in the muon case due to its small mass. For $E_\gamma^{\rm cut} \gtrsim 250\,\text{MeV}$ the real structure-dependent terms enhance the rate so much that $\Delta\Gamma_{\rm QED}$ becomes an irrelevant notion and one should consider the radiative decay as a decay in its own right. The relative QED correction vanishes for $E_\gamma^{\rm cut} = 136(23)\,\text{MeV}$, in line with the expectation that structure-dependent terms are dominant for $E_\gamma^{\rm cut} \gg m_\ell$.

The lifting of helicity suppression is taken to the extreme in the electron case. A plot in this channel is essentially meaningless as $E_\gamma^{\rm cut}$ would have to be restricted to less than 1 MeV. While there is essentially no prospect of the non-radiative decay being measured in the foreseeable future, we give some comments on structure-dependent effects below.

In the tau channel there is no great helicity suppression to begin with and so the

effect of real radiation is smaller. Over the range of $E_\gamma^{\rm cut} \in [0, 2.34\,{\rm GeV}]$ the QED correction is positive and rises slowly to +2.60(69)% at the endpoint. We note that this is markedly different to the scalar QED result which is negative. This is important as while scalar QED is clearly unsuitable for the light lepton channels (due to its lack of lifting of helicity suppression) one may have assumed it could describe the tau channel acceptably.

The other important result we report is the size of the *virtual* structure-dependent corrections. By structure-dependent we mean (infrared safe) contributions on top of scalar QED. As expected the $b\,\ell_1$, $q\,\ell_1$ and $\Phi\,\ell_1$ diagrams dominate numerically due to the presence of structure-dependent hard-collinear logs. The results are given in Table 4.2. The table shows the expected hierarchy, with the structure-

	τ	μ	e
$\Delta\Gamma_{\rm QED}\vert^{\rm virtual}_{\rm struc}$	+2.9(2)%	+4.6(6)%	+7.8(1.0)%†

Table 4.2 *Virtual structure-dependent QED corrections in $B^- \to \ell^-\bar\nu$ for $\ell = \tau, \mu, e$. †The electron case is based on an extrapolation to the physical mass.*

dependent effects being largest for the light leptons due to $\ln(m_\ell/m_B)$ terms. These large (positive) corrections show the peril of neglecting structure-dependent effects. Figure 4.2 shows the same plot as Figure 4.1 but now broken down to show real and virtual structure-dependent effects separately. The blue (dashed) curve gives the result upon setting the real structure-dependent form factors to zero. In other words, the difference between the blue line and red line gives the virtual structure-dependent contribution while real structure-dependence is the difference between the blue and black lines. These lines all converge to the scalar QED result in the ultrasoft region.

In Table 4.2, the tiny value of the electron mass causes numerical issues for $m_\ell \lesssim 50 m_e$ (a problem also encountered in [151]). We instead perform an extrapolation down to the physical point by using a range of values $m_\ell \in \{m_\tau, 400m_e, 200m_e, 150m_e, 100m_e, 50m_e\}$ and assuming a linear relationship in $\ln \hat{m}_\ell$. That is, assuming hard-collinear logs are the only important structure-dependent effects for small m_ℓ. The fit being extremely good justifies this procedure (though we account for it in the error estimate).

In general the results for the virtual structure-dependent contribution to $\Delta\Gamma_{\rm QED}$ are rather stable, displaying an $\mathcal{O}$(6-7%) uncertainty upon varying the input parameters. This can be traced back to a sizeable cancellation (due to a sign

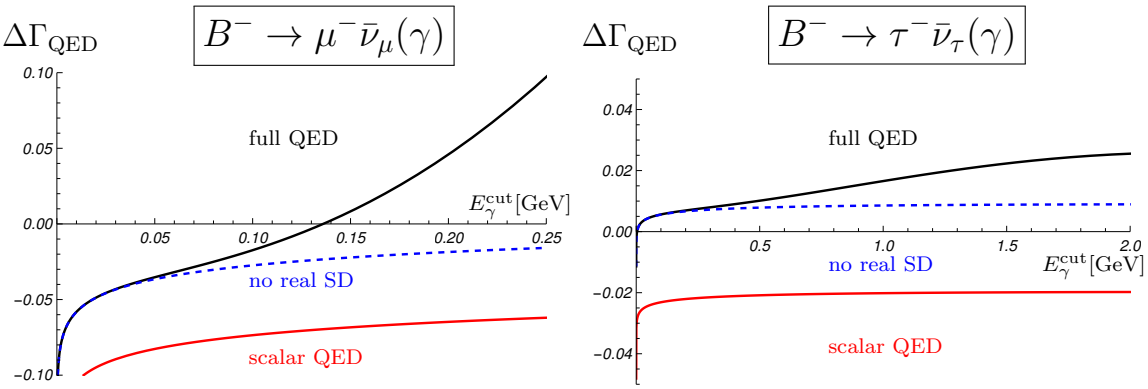

Figure 4.2 *The structure-dependent (SD) contributions to $\Delta\Gamma_{QED}$, cf. Figure 4.1, for muons (left) and taus (right). As well as the full result (black) and the scalar QED result (red), we give our calculation having set the real form factors $V_{\parallel,\perp}$ to zero (blue, dashed).*

change) in the m_b variation when integrated over s from m_b^2 to s_0 in the dispersion. In view that this is possibly accidental we double the original uncertainty to remain on the conservative side.

The generalised LSZ factor, $|\mathcal{Z}_B|^2$, is free of leptons and therefore does not contain large QED effects. Making the identification $|\mathcal{Z}_B^{(0)}|^2 = m_B^4 f_B^2$ our result is[3]

$$|\mathcal{Z}_B|^2 = m_B^4 f_B^2 \Big(1 - 1.28(19)\frac{\alpha}{\pi} + \mathcal{O}(\alpha^2)\Big)\,, \tag{4.3}$$

where again we are conservative and double the original uncertainty. This is a -0.3% correction, which in view of Table 4.2 is not particularly important numerically.

For the radiative rate we may work at the single or double differential level. The plots in Figure 4.3 show the differential branching ratio $\frac{\mathrm{d}B}{\mathrm{d}E_\gamma}$ over the full photon energy range. For the muon channel the plot shows the $E_\gamma^3(1 - \frac{2E_\gamma}{m_B})$ functional form of (3.143) as the muon mass is indeed small. The structure-dependent form factors dominate the plot with the soft divergence as $E_\gamma \to 0$ barely being visible. The soft divergence takes the form $\frac{\mathrm{d}B}{\mathrm{d}E_\gamma} \propto m_\ell^2 f_B^2/E_\gamma$ and so is much more prominent in the tau case due to its large mass.

For hard photons the form factor uncertainties are as much as $\mathcal{O}(20\,\text{-}\,30\%)$, though of course these already include m_b effects so there is likely some small over-

[3]Recall our scheme choices: the kinetic scheme for the b-mass renormalisation, the on-shell scheme for the external particles and $\overline{\rm MS}$ for all other poles. Strictly this result should only be used in conjunction with the same scheme choices in the numerator, to avoid introducing additional uncertainties that are otherwise cancelled.

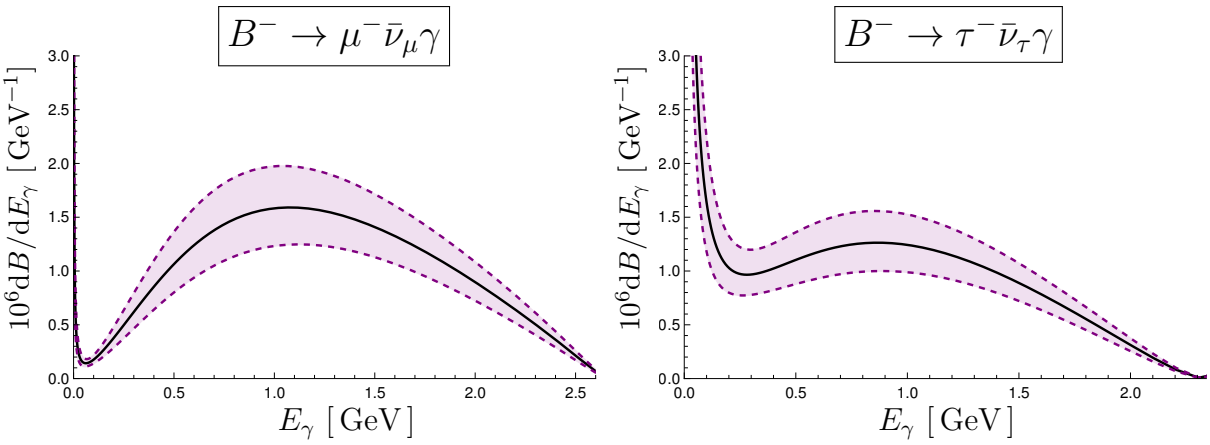

Figure 4.3 *The differential branching ratio* $10^6\,\mathrm{d}B(\bar{B} \to \ell\bar{\nu}\gamma)\,/\,\mathrm{d}E_\gamma$ *for* $\ell = \mu$ *(left) and* $\ell = \tau$ *(right) with the uncertainties in purple. As this plot is not relative to the LO there is also the (sizeable) uncertainty due to the CKM matrix element* V_{ub}.

counting. In the soft (though not ultrasoft) region the form factors are $\mathcal{O}(1/E_\gamma)$ in the heavy quark limit which softens the E_γ^3 dependence to E_γ^1 for $\bar{B} \to \mu\bar{\nu}\gamma$.

The conventional plot at the double differential level is the Dalitz plot in (x, y) variables. In Figure 4.4 we plot $\frac{1}{\Gamma^{(0)}}\frac{\mathrm{d}^2\Gamma}{\mathrm{d}x\mathrm{d}y}$ (top line) as well as $(\frac{\mathrm{d}^2\Gamma}{\mathrm{d}x\mathrm{d}y})/(\frac{\mathrm{d}^2\Gamma}{\mathrm{d}x\mathrm{d}y})_{\text{scalar QED}}$ (middle) and $\frac{1}{\Gamma^{(0)}}\frac{\mathrm{d}^2\Gamma}{\mathrm{d}x\mathrm{d}\cos\theta}$ (bottom). The Dalitz plots are not especially noteworthy and only really serve to show how much the structure-dependent terms enhance the real rate. The differential plot in $(x, \cos\theta)$, where θ is the angle between the photon and the lepton (in the $\bar{B}$ rest frame), also shows this enhancement. However in the muon channel collinear behaviour can additionally be seen as $\cos\theta \to 1$. The lifting of helicity suppression is less severe in this limit as the neutrino has maximum energy and a term of the form $(m_B - 2E_\nu)^2(V_\parallel + V_\perp)^2$ no longer contributes.

Finally we comment on the relative sizes of the structure-dependent corrections in the real and virtual cases. In the tau case the structure-dependent real radiation is always less important than the $+2.9\%$ virtual correction even when fully inclusive. Conversely for the muon case the real structure-dependent correction equals the virtual (4.6%) at $E_\gamma^{\mathrm{cut}} = 175(31)\,\mathrm{MeV}$ and then rapidly overwhelms it. For reference the QED correction is $\Delta\Gamma_{\mathrm{QED}} = +2.6(2.2)\%$ at this point, with the large error due to the poorly known form factors.

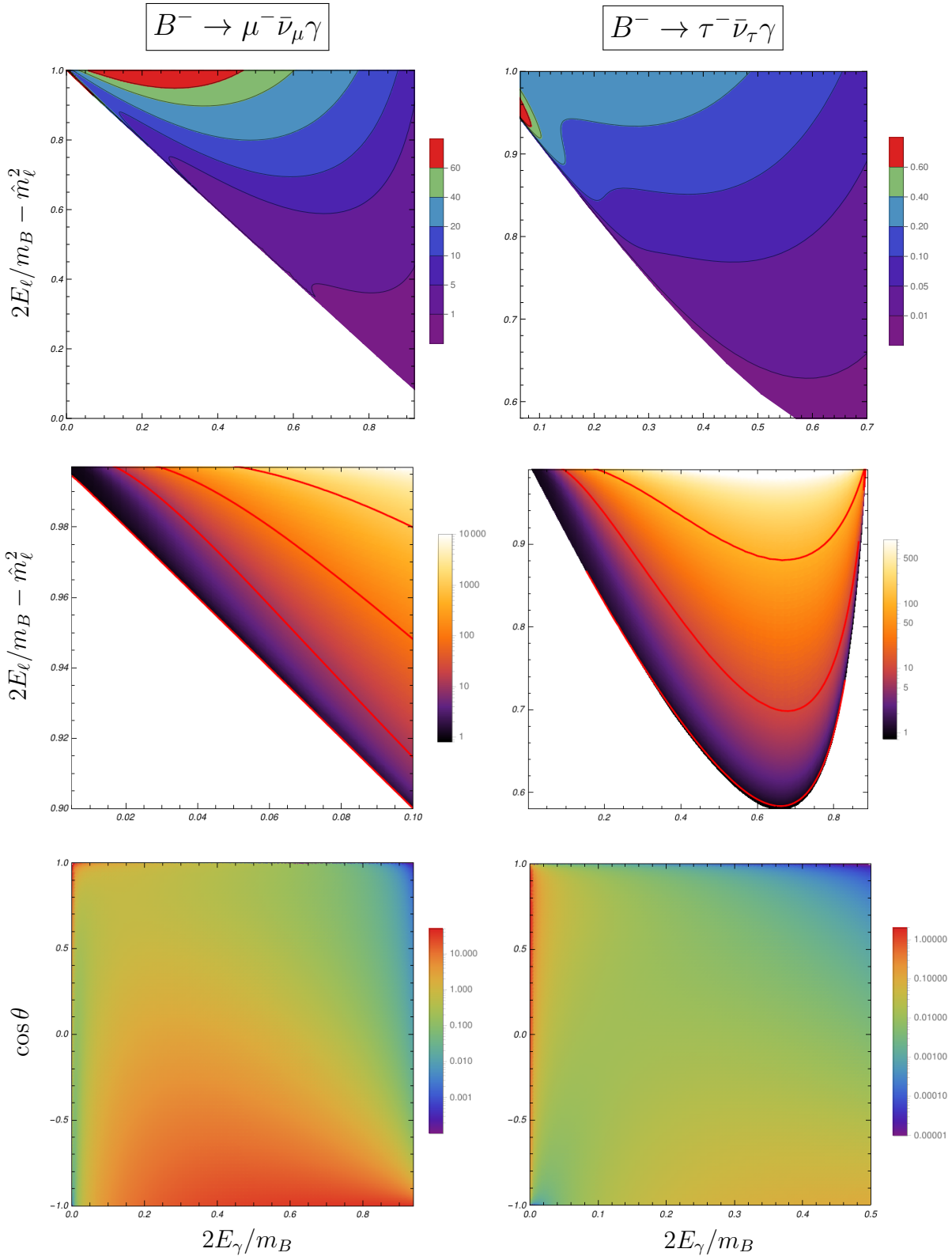

Figure 4.4 *Plots at the double differential level for muons (left) and taus (right). (Top line) The plot* $\frac{1}{\Gamma^{(0)}}\frac{\mathrm{d}^2\Gamma}{\mathrm{d}x\mathrm{d}y}$ *in the style of [179]. The contours show the number of radiative events relative to the non-radiative decay. (Middle) The plot* $(\frac{\mathrm{d}^2\Gamma}{\mathrm{d}x\mathrm{d}y})/(\frac{\mathrm{d}^2\Gamma}{\mathrm{d}x\mathrm{d}y})_{scalar\ QED}$*, i.e. the result relative to scalar QED. The red contours mark* $(1, 10, 100, (1000))$ *times enhancements. (Bottom) The plot* $\frac{1}{\Gamma^{(0)}}\frac{\mathrm{d}^2\Gamma}{\mathrm{d}x\mathrm{d}\cos\theta}$ *where* θ *is the photon-lepton angle in the meson rest frame. Note the different scales and colourbars in all these plots.*

$\mathcal{B}(\bar{B} \to \ell\bar{\nu})$	τ	μ	e
Theory [81]	$7.7(6) \cdot 10^{-5}$	$3.5(3) \cdot 10^{-7}$	$8.1(6) \cdot 10^{-12}$
Experiment [37]	$1.09(24) \cdot 10^{-4}$	$< 8.6 \cdot 10^{-7\,\dagger}$	$< 9.8 \cdot 10^{-7\,\dagger}$

Table 4.3 *Current theoretical predictions and experimental measurements for the branching ratio $\mathcal{B}(\bar{B} \to \ell\bar{\nu})$. †Only known as a 90% confidence limit.*

4.3 Phenomenology

In Table 4.3 we compare the current best theoretical and experimental predictions for the decay $\bar{B} \to \ell\bar{\nu}$, cf. (1.28) and (1.29). Due to the helicity suppression the electron and muon channels are not well measured experimentally and only upper 90% confidence limits exist. The tau channel has been measured at Belle [212–214] and BaBar [215, 216] and agrees with the SM prediction at the 2σ level.

On the experimental side, Belle II is expected to collect up to 50ab^{-1} of data over its run which should considerably improve statistical uncertainties. While the light decays are rarer they have a simpler experimental signature compared to the tau which itself subsequently decays into further leptons and neutrinos. For this reason the full Belle II dataset is expected to measure the branching fraction $\mathcal{B}(\bar{B} \to \mu\bar{\nu})$ to 7% uncertainty, only slightly worse than for the tau channel (5-6%) [81]. The electron rate is not expected to be measured; only if its rate is enhanced by the effects of new physics.

On the theoretical side, without QED, the dominant uncertainties arise from the $\bar{B}$-meson decay constant and the CKM matrix element. The former is now known to $\mathcal{O}(1\%)$ accuracy with the current $N_f = 2 + 1 + 1$ (isospin-symmetric) lattice average result $f_B = 190.0(1.3)\,\text{MeV}$ [40]. The main uncertainty however arises from the CKM matrix element $|V_{\text{ub}}| = 3.82(20) \times 10^{-3}$ [37] due to discrepancies between extractions using inclusive and exclusive decays. In fact one can actually use the lattice determination of f_B along with the measured τ branching ratio and $\bar{B}$ lifetime to determine $|V_{\text{ub}}| = 4.11(39) \times 10^{-3}$, in agreement with [37].

In light of these theory uncertainties it is attractive to consider ratios of branching fractions so that V_{ub} and f_B drop out. For example

$$R_{\text{ps}} \equiv \frac{\Gamma(B^- \to \tau^-\bar{\nu})}{\Gamma(\bar{B}^0 \to \pi^+\ell^-\bar{\nu})}\,, \qquad \ell = e, \mu \tag{4.4}$$

which does not depend on $V_{\rm ub}$ and

$$R_{\rm pl} \equiv \frac{\mathcal{B}(B^- \to \tau^- \bar{\nu})}{\mathcal{B}(B^- \to \mu^- \bar{\nu})}\,, \tag{4.5}$$

which only depends on the particle masses (neglecting QED) and therefore is extremely precisely known in the SM. Experimentally $\bar{B}^0 \to \pi^+ \ell^- \bar{\nu}$ is well-studied and these ratios are expected to be known to $\mathcal{O}(10\%)$ uncertainty by the end of the Belle II run [81] which should put constraints on BSM physics [217]. For the same reasons almost all of the results quoted in Section 4.2 are ratios[4].

In view of the expected 7% experimental uncertainty in the $\bar{B} \to \mu\bar{\nu}$ channel by the end of the decade the prediction of a +4.6% virtual structure-dependent QED effect is certainly relevant. While slightly smaller the +2.9% tau channel result will still be important, especially if used to weigh in on the $V_{\rm ub}$ uncertainty puzzle or in the ratios $R_{\rm ps}$, $R_{\rm pl}$. These two channels are in fact so-called 'Golden observables' in the Belle II experiment due to their sensitivity to new physics and the competitiveness of the Belle II measurement in comparison to LHCb. Once the $V_{\rm ub}$ uncertainty diminishes QED effects will become the largest source of theory error in leptonic decays.

For the radiative decay $\bar{B} \to \ell\bar{\nu}\gamma$ we have done nothing novel in the hard photon regime owing to the fact we use external form factors. Indeed predictions for the branching ratio $\mathcal{B}(\bar{B} \to \ell\bar{\nu}\gamma)$ integrated over various q^2 bins can be found in [195]. In the soft region however our Φ_B construction puts the calculation on a more solid theoretical footing. Our main plot, Figure 4.1, shows the importance of the photon energy cut, $E_\gamma^{\rm cut}$, when IR physics is handled in the traditional Bloch-Nordsieck sense. In modern experimental analyses QED effects are usually unfolded from the final state shape using Monte-Carlo simulations, for example PHOTOS. These are based on scalar QED results and so our work could be used in future to inform a purpose-built Monte-Carlo generator[5].

[4]Sum rules based calculations can no longer match the accuracy of lattice results and so ratios in which f_B drops out are preferable. Our results give $F_B = 192\,\text{MeV}$ (or 185 MeV from just $\mathcal{Z}_B^{(0)}$) which is actually remarkably accurate for a LO calculation.

[5]We make our results available in the form of a Mathematica notebook in the published work [1]. Note that typical photon energy cuts are effectively of the order $E_\gamma^{\rm cut} \sim 0.2\,\text{GeV}$, cf. [151].

4.4 Conclusions

To conclude, in Chapters 3 and 4 we have developed and applied a new explicitly gauge-invariant formalism in the concrete setting of leptonic B decays. Complete next-to-leading order QED corrections have been calculated with a reliable treatment of soft photons using the Φ_B construction.

We have paid particular attention to the role of helicity suppression, firstly demonstrating the cancellation of collinear logs for S-P type interactions and then showing the importance of structure-dependent logs in the V-A (SM) case. Numerically such terms lead to sizeable structure-dependent QED corrections of $+4.6(6)\%$ and $+2.9(2)\%$ in $\bar{B} \to \mu\bar{\nu}$ and $\bar{B} \to \tau\bar{\nu}$ respectively. Principal uncertainties arise from working at LO in QCD, neglecting $\mathcal{O}(\alpha\alpha_s)$ effects. Real radiation lifts the helicity suppression and structure-dependent corrections in the muon channel exceeds the virtual structure-dependence for $E_\gamma^{\text{cut}} > 0.18(3)\,\text{GeV}$. In the tau channel real structure-dependent terms are always subdominant.

This work is, to the best of our knowledge, the first computation of structure-dependent QED effects in the charged current decay $B^- \to \ell^-\bar{\nu}_\ell(\gamma)$. Note that the SCET analysis [178] awaits a further study (and is non-numerical). The natural direction of future work would be to analyse the *neutral current* decay $\bar{B}_{d,s} \to \ell^+\ell^-$ in a similar sum-rules framework. This decay has drawn considerable attention in recent years as it is additionally loop-suppressed and so again is an excellent candidate for probing new physics. In this case the Φ_B framework is unnecessary as the $\bar{B}$ is neutral. As well as kinematic changes, electroweak penguin diagrams would have to be included and the handling of the dispersion variable p_B^2 would need to be rethought. The motivation to study $\bar{B}_{d,s} \to \ell^+\ell^-$ is perhaps lessened by a preexisting SCET study describing structure-dependent QED effects analytically and numerically [176, 177]. However, as discussed in Section 2.4, the neutral current decay exhibits power enhanced electromagnetic corrections and so an analysis from a sum rules perspective would still be of interest.

Precision measurements in the Standard Model continue to be important, especially as hints of LFU violation subside. This work clearly demonstrates that QED effects are important and cannot be neglected. As experimental uncertainties decrease such effects will remain ever relevant.

Chapter 5

Mass Differences of Pseudoscalar Mesons

In this final chapter we consider the difference in mass between a charged pseudoscalar meson $P^{\pm}$ and its neutral counterpart P^0. This mass splitting is driven by electromagnetic effects and differences in the mass of the meson's light valence quark. While we are not the first to study this problem, we attack it for the first time using QCD sum rules and a double dispersion relation. We compute both the electromagnetic shift (Section 5.3) and the quark mass shift (Section 5.4) in a unified manner, using the same hadronic input and without introducing any model dependence.

Unlike the *single* dispersion relations used in previous chapters, *double* dispersion relations are on the whole less accurate. Compounding this, we also consider the lighter mesons, $P = D, K$ in addition to the B, whose sum rules converge less well. This work should therefore be viewed as a 'proof-of-principle' calculation, rather than a precision one, and correspondingly we always work at leading order in the relevant coupling. Nevertheless numerical results, summarised in Section 5.5, are fully consistent with experiment.

5.1 Introduction

The charged-neutral mass differences

$$\Delta m_P = m_{P^\pm} - m_{P^0}\,, \qquad P = B, D, K, \pi\,, \tag{5.1}$$

of pseudoscalar mesons are known experimentally to high precision [37]. Neutral B and K mesons are heavier than their charged counterparts, while the opposite is true for the D and the π. This sign difference fundamentally originates from the different light quark assignments in the two cases. While $B^\pm$ and $K^\pm$ contain an up quark, the B^0 and K^0 have instead a down quark and these masses are not the same, with $m_u < m_d$. For the D and π this is reversed. As quarks are non-perturbative objects this quark mass correction $\Delta m_P|_{m_q}$ is more than just the difference $\delta m_q \equiv m_u - m_d$, on account of strong force effects, though it is expected to be of roughly the same order.

The other isospin-breaking contribution is of electromagnetic origin and is of the same (positive) sign for all the mesons. It arises as photons probe differing quark charges in the charged and neutral case. We may decompose

$$\Delta m_B = \Delta m_B|_{\text{QED}} + \Delta m_B|_{m_q}\,, \tag{5.2}$$

where we take $P = B$ for definiteness. Effects due to the weak force are further $\mathcal{O}(\Lambda^2_{\text{QCD}}/M_W^2)$ suppressed and can be ignored. Strictly speaking the separation in (5.2) has a $\mathcal{O}(\alpha\, m_q)$ ambiguity in defining the renormalised quark masses, though again this is a higher order effect and can be ignored. Similarly, in the calculation of $\Delta m_B|_{\text{QED}}$ we may take $m_q = m_{\text{ud}}$ where $m_{\text{ud}} \equiv \frac{1}{2}(m_u + m_d)$ and we denote light quark masses taken in $\overline{\text{MS}}$ as $\bar{m}_q$.

Electromagnetic mass differences can be calculated in perturbation theory from the Compton forward scattering amplitude, known well before the advent of QCD [218, 219]. In 1963, Cottingham [220] rewrote this in Euclidean space in terms of an integral over structure functions for (in)elastic e-N scattering, $N = p, n$, to weigh in on the famous proton-neutron mass difference. Since then many phenomenological studies have attempted to apply this formula to both nucleon and meson systems. For example by using χPT for the light π and K [221, 222], HQET for B and D [223, 224] or by assuming vector meson dominance [225]. In general a calculation via the Cottingham method is a formidable task

as one requires knowledge of structure functions over a large energy range. While perturbative QCD can often be used for deep inelastic scattering, resonances at lower energies often require some experimental constraints.

We however do not follow Cottingham and instead stay in Minkowski space, using sum rules to link high energy and low energy regions. Non-perturbative effects enter through condensates as before. We also use sum rules to estimate the quark mass correction $\Delta m_B|_{m_q}$ which is attractive as we can thus use the same approach and inputs for both parts of Δm_B.

We work at tree level in our calculations and so cannot possibly compare with experimental measurements which are known in the pion case to 5 digits of precision for example. Our uncertainties are typically of order 30%, worsening for lighter mesons and indeed we do not quote results for the pion as we were not able to obtain stable sum rules. Recent lattice calculations quote uncertainties in the range 10-20% for the lighter pseudoscalar mesons [226] and hadrons [227] though of course these cannot simulate bottom quarks.

We set up the relevant theory and define appropriate correlators in the next section with the actual calculations for $\Delta m_B|_{\rm QED}$ and $\Delta m_B|_{m_q}$ given in Section 5.3 and 5.4 respectively. Closing remarks and a numerical summary is given in Section 5.5

5.2 Theory

Focusing first on the QED splitting, both the B^+ and B^0 masses receive (Feynman gauge) electromagnetic self-energy corrections [218, 219]

$\delta m_B|_{\rm QED} =$ 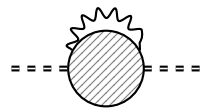

$$= \frac{i\alpha}{2m_B(2\pi)^3}\int \mathrm{d}^d q\, \frac{g^{\mu\nu}T_{\mu\nu}(q)}{q^2+i\varepsilon} + \mathcal{O}(\alpha^2)\,, \tag{5.3}$$

where

$$\Delta m_B|_{\rm QED} \equiv \delta m_{B^+}|_{\rm QED} - \delta m_{B^0}|_{\rm QED}\,. \tag{5.4}$$

This is written in terms of the Compton forward scattering tensor

$$T_{\mu\nu}(q) = i \int \mathrm{d}^d x \, e^{-iq\cdot x} \langle B | T j_\mu(x) j_\nu(0) | B \rangle \,, \tag{5.5}$$

where as before $j_\mu = \sum_q Q_q \, \bar{q} \gamma_\mu q$ is the electromagnetic current. On the other hand quark mass effects can be calculated via the Feynman-Hellmann theorem (FHT) [228, 229] - a technique often employed on the lattice. Given a Hamiltonian, wavefunction and energy level (H, Ψ_n, E_n), which all depend on some external parameter λ, the FHT states

$$\frac{\mathrm{d}E_n(\lambda)}{\mathrm{d}\lambda} \;=\; \langle \Psi_n(\lambda) | \frac{\mathrm{d}H(\lambda)}{\mathrm{d}\lambda} | \Psi_n(\lambda) \rangle \;. \tag{5.6}$$

Taking the parameter as the light quark mass, and $H_m = \sum_q m_q \bar{q} q$ then

$$\frac{\mathrm{d}m_B}{\mathrm{d}m_q} \;=\; \frac{1}{2m_B} \, \langle B | \bar{q} q | B \rangle \;, \tag{5.7}$$

which upon integration gives the classic result [224]

$$\Delta m_B|_{m_q} \;=\; \frac{m_u - m_d}{2m_B} \langle B | \bar{q} q | B \rangle + \mathcal{O}\big((m_u - m_d)^2 \big) \,, \tag{5.8}$$

where at LO one can assume the isospin limit $\langle B | \bar{u} u | B \rangle = \langle B | \bar{d} d | B \rangle$. We will shortly define correlators to extract $\delta m_B|_{\mathrm{QED}}$ and $\langle B | \bar{q} q | B \rangle$ as dispersion residues, like in Chapter 3. We make predictions for the B and the D though as discussed not for pions. For Kaons we are only able to make predictions for $\Delta m_K|_{\mathrm{QED}}$ and not for $\Delta m_K|_{m_q}$. In Section 5.2.3 we 'fill in the gaps' using some classic χPT and $SU(3)_F$ results.

As there are *two* $|B\rangle$ states in both (5.5) and (5.8) one needs *two* insertions of $|B\rangle\langle B|$ in an appropriate correlator in order to extract the required residues. This means using a *double* dispersion relation with two dispersion variables, s and $\tilde{s}$. The spectral density $\rho(s, \tilde{s})$ is correspondingly now given by the *double* discontinuity. By construction the s and $\tilde{s}$ channels do not overlap and so the spectral density can be non-zero by the Steinman relations [230].

Rather than a single integral over $s \in [m_+^2, s_0]$ the duality interval becomes a region in the s-$\tilde{s}$ plane. Exactly what shape this duality region should be (rectangular, triangular, a quarter-circle etc.) is a matter of some debate [231, 232]. We shall not worry with such discussions and work pragmatically,

following the recipe of [196][1]. We write our dispersions in the form

$$\int_{m_+^2}^{\bar{\delta}^{(a)}(m_+^2)} \mathrm{d}s \int_{m_+^2}^{\bar{\delta}^{(a)}(s)} \mathrm{d}\tilde{s}\; e^{-\frac{s}{M^2}} e^{-\frac{\tilde{s}}{M^2}} \rho(s,\tilde{s})\,, \tag{5.9}$$

after (double) Borel transformation, where

$$\bar{\delta}^{(a)}(s) = 2^{1/a}\sigma_0 \left[1 - \left(\frac{s}{2^{1/a}\sigma_0}\right)^a\right]^{1/a}. \tag{5.10}$$

The variable a parameterises the choice of duality region, with $a = 1$ being triangular, $a = 2$ being circular and $a \to \infty$ being rectangular. We calculate our results for a selection of different a with the spread being factored into the final uncertainty. The number σ_0 takes on the role of s_0 in single dispersion relations. That is, its value is $\approx 35\,\mathrm{GeV}^2$ and hereafter we shall notate $\sigma_0 \equiv s_0$ for reasons of familiarity. In theory one has the freedom to take different Borel masses $M_1^2 \neq M_2^2$ in (5.9), however as the two channels are to be treated identically we take $M_1^2 = M_2^2 = M^2 \equiv 2\hat{M}^2$.

5.2.1 Correlators for $\Delta m_B|_{\mathsf{QED}}$

To extract the QED mass shift $\delta m_X|_{\mathrm{QED}}$, with $X = \{B^\pm, \bar{B}^0\}$ we define the correlator

$$\begin{aligned} F^X(p_B^2, \tilde{p}_B^2) = \frac{\alpha}{(2\pi)^3} \int \mathrm{d}^d q\, \mathrm{d}^d x\, \mathrm{d}^d y\, \mathrm{d}^d z\, e^{-ip_B\cdot y} e^{+i\tilde{p}_B\cdot z} e^{-i(q+r)\cdot x} \\ \times \langle 0|T J_B^\dagger(z) j_\mu(x) j_\nu(0) J_B(y)|0\rangle \frac{1}{q^2 + i\varepsilon}\left(g^{\mu\nu} - (1-\xi)\frac{q^\mu q^\nu}{q^2}\right), \end{aligned} \tag{5.11}$$

where J_B is defined in (1.14) and we work in general gauge. In the B^- case this is evaluated for $q = u$ while one takes $q = d$ for $X = B^0$. We denote both the charged and neutral $\bar{B}$-mass by m_B as whether one takes m_{B^-} or $m_{\bar{B}^0}$ in the dispersion is immaterial. We calculate this correlator at $\mathcal{O}(\alpha\,\alpha_s^0)$, including the perturbative ($\mathbb{1}$) and quark condensate contributions.

In (5.11) the variable q labels the photon momentum and r is an auxiliary momentum used to distinguish the two channels, $\tilde{p}_B = p_B + r$. This is handled

[1] In their notation we have $\tilde{s}_0 = \tilde{t}_0 = 2^{1/a}\sigma_0$ as our channels are identical. For a double dispersion the Daughter Sum Rule takes the form $\int_{s\tilde{s}} \frac{1}{2}(s+\tilde{s})\rho(s,\tilde{s})$ in the numerator compared to $\int_s s\rho(s)$ for single dispersions.

like in Chapter 3, being suppressed under the dispersion relation where $p_B^2 \approx m_B^2$ and $\tilde{p}_B^2 \approx m_B^2$ is enforced. The two channels are identical and so we further require $p_B - \tilde{p}_B$ symmetry. This correlator can be represented through a double dispersion relation

$$\begin{aligned} F^X(p_B^2, \tilde{p}_B^2) &= \int \mathrm{d}s \int \mathrm{d}\tilde{s}\, \frac{\rho_{F_X}(s,\tilde{s})}{(s-p_B^2)(\tilde{s}-\tilde{p}_B^2)} + \cdots \\ &= \frac{Z_X^2 \cdot \delta m_X^2|_{\mathrm{QED}}}{(m_B^2-p_B^2)(m_B^2-\tilde{p}_B^2)} + \cdots , \end{aligned} \tag{5.12}$$

where $Z_X \equiv m_B^2 f_X$, $\delta m_X^2 = 2 m_B \delta m_X$ and

$$(2\pi i)^2 \rho_{F_X}(s,\tilde{s}) \;=\; \mathrm{disc}_{s,\tilde{s}}[F^X(s,\tilde{s})]_{\mathrm{blue}}\,. \tag{5.13}$$

Here $\rho_{F_X}(s,\tilde{s})$ is the specific double spectral density where we do not cut the photon propagator. In order to extract $\delta m_X|_{\mathrm{QED}}$ we require the cut structure

$$\underbrace{\langle 0|J_B^\dagger(z)|\bar{B}\rangle}_{Z_B^\dagger}\;\underbrace{\langle \bar{B}|T j_\mu(x) j_\nu(0)|\bar{B}\rangle}_{\sim T_{\mu\nu}}\;\underbrace{\langle \bar{B}|J_B(y)|0\rangle}_{Z_B}\,, \tag{5.14}$$

in other words the blue cuts in the language of Chapter 3. Other cuts either vanish or do not contribute to (5.3) and can be considered a QED correction to the $\bar{B}$-meson state itself. As the mass shift is already an $\mathcal{O}(e^2)$ observable we may safely take the remainder of the residue $Z_B = \langle \bar{B}|J_B|0\rangle$ at LO. That is we do not need to invoke the Φ_B construction, $\mathcal{Z}_B = \langle B^-|\mathcal{J}_B|\Phi_B\rangle$, as we do not probe the J_B operator beyond LO. Fundamentally no issues arise because the mass shift is an infrared safe quantity and we do not require an on-shell particle to reproduce soft logs. We have explicitly verified that all results are gauge-invariant[2]. The mass shift follows from a double Borel transform, as advertised in (5.9), specifically

$$2 m_B\, \delta m_X|_{\mathrm{QED}} = \frac{1}{Z_X^2} \int_{m_+^2}^{\bar{\delta}^{(a)}(m_+^2)} \mathrm{d}s\, e^{\frac{m_B^2 - s}{M^2}} \int_{m_+^2}^{\bar{\delta}^{(a)}(s)} \mathrm{d}\tilde{s}\; e^{\frac{m_B^2-\tilde{s}}{M^2}} \rho_{F_X}(s,\tilde{s})\,. \tag{5.15}$$

Evaluating this for $X = B^-$ and $X = \bar{B}^0$ and subtracting the two results one gets $\Delta m_B|_{\mathrm{QED}}$, à la (5.4). Note that we must also calculate the denominator Z_X^2 using a sum-rules method to allow necessary cancellations to occur.

For light mesons the above pseudoscalar correlator (5.11) is known to be

[2]As before, only the red cuts (that here are not included) require charge conservation at each vertex.

unsuitable due to so-called direct instanton effects [105, 110]. We therefore instead treat the Kaon case differently, using an axial correlator

$$F^K_{\alpha\beta}(p_B^2,\tilde{p}_B^2) = \frac{\alpha}{(2\pi)^3}\int \mathrm{d}^d q\,\mathrm{d}^d x\,\mathrm{d}^d y\,\mathrm{d}^d z\, e^{-ip_B\cdot y}e^{+i\tilde{p}_B\cdot z}e^{-i(q+r)\cdot x} \\ \times \langle 0|TA^\dagger_\alpha(z)j_\mu(x)j_\nu(0)A_\beta(y)|0\rangle \frac{1}{q^2+i\varepsilon}\left(g^{\mu\nu}-(1-\xi)\frac{q^\mu q^\nu}{q^2}\right), \quad (5.16)$$

where

$$A_\mu = \bar{s}\gamma_\mu\gamma_5 q\,, \qquad \langle K^-(p)|A_\mu|0\rangle = -ip_\mu f_K\,. \quad (5.17)$$

This can be decomposed as

$$F^K_{\alpha\beta}(p_B^2,\tilde{p}_B^2) = g_{\alpha\beta}F_1^K(p_B^2,\tilde{p}_B^2) + (p_B)_\alpha(p_B)_\beta F_2^K(p_B^2,\tilde{p}_B^2) + \mathcal{O}(r)\,, \quad (5.18)$$

where as before Lorentz structures involving r carry extra irrelevant information. The coefficient of $(p_B)_\alpha(p_B)_\beta$ has hadronic representation

$$F_2^K \;=\; \frac{f_K^2\cdot\delta m_K^2|_{\mathrm{QED}}}{(m_K^2-p_B^2)(m_K^2-\tilde{p}_B^2)} \;+\; \cdots\,, \quad (5.19)$$

which we extract via a projection[3]. Note that axial operators are unsuitable for heavy mesons as the axial resonance $m^2_{B^1}$ is too close to the continuum threshold, s_0. Again the mass shift follows from a double Borel transformation and the splitting follows from subtracting the $K = K^-$ and $K = \bar{K}^0$ results.

5.2.2 Correlators for $\Delta m_B|_{m_q}$

The quark mass correction $\Delta m_B|_{m_q}$ is determined from the matrix element $\langle\bar{B}|\bar{q}q|\bar{B}\rangle$ which we estimate for heavy mesons via a $\bar{q}q$ insertion in the pseudoscalar correlator

$$G(p_B^2,\tilde{p}_B^2) = i^2\int \mathrm{d}^d y\,\mathrm{d}^d z\, e^{-ip_B\cdot y}e^{+i\tilde{p}_B\cdot z}e^{-ix\cdot r}\langle 0|TJ_B^\dagger(z)(\bar{q}q)(x)J_B(y)|0\rangle \\ = \int\frac{\mathrm{d}s}{2\pi i}\int\frac{\mathrm{d}\tilde{s}}{2\pi i}\,\frac{\mathrm{disc}_{s,\tilde{s}}[G(s,\tilde{s})]}{(s-p_B^2)(\tilde{s}-\tilde{p}_B^2)}$$

[3]At $s=\tilde{s}$ one has $s^2(1-d)F_2^K(s,s) = sF^K_{\alpha\alpha}(s,s) - dF^K(s,s)$ via Ward identities. The generalisation to $s\neq\tilde{s}$ has a slight ambiguity due to p_B and $\tilde{p}_B$ being linearly dependent. This arises due to our choice $\boldsymbol{r}=0$ which is necessary to make the integrals tractable. We take the generalisation $s\tilde{s}(1-d)F_2^K(s,\tilde{s}) = \frac{1}{2}(s+\tilde{s})F^K_{\alpha\alpha}(s,\tilde{s}) - dF^K(s,\tilde{s})$ and we have checked that other (symmetric) choices have a negligible impact on the results, considering the large uncertainties in the Kaon case.

$$= \frac{Z_B^2 \langle \bar{B}|\bar{q}q|\bar{B}\rangle}{(m_B^2 - p_B^2)(m_B^2 - \tilde{p}_B^2)} + \cdots , \tag{5.20}$$

in the same manner as before. The result is thus

$$\langle \bar{B}|\bar{q}q|\bar{B}\rangle = \frac{1}{Z_B^2} \int_{m_+^2}^{\bar{\delta}^{(a)}(m_+^2)} \mathrm{d}s\, e^{\frac{m_B^2 - s}{M^2}} \int_{m_+^2}^{\bar{\delta}^{(a)}(s)} \mathrm{d}\tilde{s}\; e^{\frac{m_B^2 - \tilde{s}}{M^2}} \rho_G(s, \tilde{s})\,, \tag{5.21}$$

with $(2\pi i)^2 \rho_G(s,\tilde{s}) = \mathrm{disc}_{s,\tilde{s}}[G(s,\tilde{s})]$. We calculate this correlator at LO in QCD, however additionally include the mixed condensate $\langle \bar{q}\sigma_{\mu\nu}G^{\mu\nu}q\rangle$ as well as the quark condensate and perturbative contributions. We note that the $\bar{q}q$ insertion flips the chirality meaning the perturbative contribution is $\mathcal{O}(m_q)$ suppressed. The leading contribution therefore comes from the quark condensate, $\langle \bar{q}q\rangle$.

Note that in theory we could calculate the quark mass shift $\Delta m_B|_{m_q}$ directly using a QCD analogue of the correlator F^X in (5.11). One would calculate the QCD shift[4] by taking the difference between $\delta m_B|_{m_q = m_u}$ and $\delta m_B|_{m_q = m_d}$, having set the quark charges to 1 and taking $\alpha \to \alpha_s C_F$, with $C_F = 4/3$. This method gives results of the right order of magnitude, $\mathcal{O}(1\,\mathrm{MeV})$, however is not a practical method as the decay constants themselves have uncertainties of the same order.

5.2.3 Some Classic Results

Before giving the result of our sum rules calculations we review some classic estimates [222, 224] of $\Delta m_B|_{\mathrm{QED}}$ and $\Delta m_B|_{m_q}$, updating the latter results with modern input values (as these references are almost 30 years old).

Consider first the quark mass corrections. For the light Goldstones, π and K, we may expand the χPT Lagrangian (1.16) at linear order to give

$$\begin{aligned} m_\pi^2 &= B_0(m_u + m_d) \\ m_{K^\pm}^2 &= B_0(m_s + m_u) \\ m_{K^0}^2 &= B_0(m_s + m_d)\,, \end{aligned} \tag{5.22}$$

in terms of the low energy constant B_0. The pion mass splitting vanishes at this

[4]One would also require an $\mathcal{O}(g)$ variant of the Cottingham formula in QCD, due to contributions from the mixed condensate. With $D_\mu = \partial_\mu + i s_g g A_\mu$ then we derive the result $2m_B \delta m_B|_{\mathrm{QCD}} = g s_g \langle B|j \cdot A|B\rangle$ with $j_\mu = \sum_q \bar{q}\gamma_\mu q$ here and A_μ a gluon field.

order, however the Kaon mass difference is

$$\Delta m_K|_{m_q} = \frac{B_0(m_u - m_d)}{2m_K}\,, \tag{5.23}$$

which upon employing $2B_0 = m_\pi^2/m_{\rm ud}$ gives

$$\Delta m_K|_{m_q} = \frac{m_u - m_d}{2m_{\rm ud}}\frac{m_\pi^2}{2m_K} = -6.74^{+0.98}_{-1.21}\,\text{MeV}\,, \tag{5.24}$$

using the PDG values [37] in $\overline{\rm MS}$. Note that while quark masses are scale dependent, quark mass *ratios* are not. These ratios are on the whole better known than the individual quark masses and so we use them in the numerics where possible. In passing we note that the light quark masses run oppositely to the quark condensate as can be seen from the famous Gell-Mann-Oakes-Renner relation [233]

$$m_\pi^2 f_\pi^2 = -2(m_u + m_d)\langle\bar{q}q\rangle\,, \tag{5.25}$$

as the LHS is physical. Taking instead $B_0 = -2\langle\bar{q}q\rangle/f_\pi^2$ and using (5.23) directly gives the result $\Delta m_K|_{m_q} \approx -5.7\,\text{MeV}$. While within uncertainty this demonstrates that these predictions are all within the chiral $\text{SU}(3)_\text{F}$ framework. The pion quark mass correction on the other hand only enters at quadratic order in δm_q and is therefore quite small

$$\Delta m_\pi|_{m_q} = \frac{(m_u - m_d)^2}{m_s - m_{\rm ud}}\frac{m_\pi}{16m_{\rm ud}} = +0.16^{+0.06}_{-0.05}\,\text{MeV}\,. \tag{5.26}$$

For the heavy mesons we instead exploit $\text{SU}(3)_\text{F}$ flavour symmetry, $\langle B|\bar{q}q|B\rangle \approx \langle B_s|\bar{s}s|B_s\rangle$, which holds at the $\mathcal{O}(20\%)$ level. Further we assume that the B_s-B mass difference ($\sim 100\,\text{MeV}$) is entirely driven by the heavy strange quark and not by electromagnetic effects, which are $\mathcal{O}(1\,\text{MeV})$. By the FHT then

$$\begin{aligned} m_{B_s}^2 - m_{B^\pm}^2 &= (m_s - m_u)\langle B_s|\bar{s}s|B_s\rangle \\ m_{B_s}^2 - m_{B^0}^2 &= (m_s - m_d)\langle B_s|\bar{s}s|B_s\rangle\,, \end{aligned} \tag{5.27}$$

and at leading order we can take

$$m_{B_s}^2 - m_B^2 = (m_s - m_{\rm ud})\langle B_s|\bar{s}s|B_s\rangle\,. \tag{5.28}$$

Invoking flavour symmetry we can therefore write $\langle B|\bar{q}q|B\rangle$ in terms of the B_s-B

mass difference (taken experimentally). We get

$$\Delta m_B|_{m_q} = \frac{m_u - m_d}{m_s - m_{\rm ud}} \frac{m_{B_s}^2 - m_B^2}{2m_B}\,, \tag{5.29}$$

and similarly for $\Delta m_D|_{m_q}$. Using PDG values [37] this gives[5]

$$\begin{aligned} \Delta m_B|_{m_q} &= -2.37^{+0.35}_{-0.43} \pm 20\%_{SU_3}\,\text{MeV} \\ \Delta m_D|_{m_q} &= +2.81^{+0.51}_{-0.41} \pm 20\%_{SU_3}\,\text{MeV}\,, \end{aligned} \tag{5.30}$$

where we have added an explicit error due to $\text{SU}(3)_\text{F}$ violation. The relation $\Delta m_B|_{m_q} = -\Delta m_D|_{m_q}$, valid in the heavy quark limit, holds reasonably well.

Electromagnetic corrections in general are derived via the Cottingham method. For convenience we repeat the results of [222, 224]

$$\begin{aligned} \Delta m_B|_{\rm QED} &= +1.40 \pm 0.07\,\text{MeV} \\ \Delta m_D|_{\rm QED} &= +1.79 \pm 0.16\,\text{MeV} \\ \Delta m_K|_{\rm QED} &= +2.60 \pm 0.60\,\text{MeV} \\ \Delta m_\pi|_{\rm QED} &= +4.54 \pm 0.50\,\text{MeV}\,, \end{aligned} \tag{5.31}$$

which shows a $\sim 100\%$ violation of Dashen's theorem [235]. Dashen's theorem states that the electromagnetic differences of pions and kaons should follow

$$2m_\pi \Delta m_\pi|_{\rm QED} = 2m_K \Delta m_K|_{\rm QED}\,, \tag{5.32}$$

(or equivalently $\Delta m_\pi^2 = \Delta m_K^2$ in the $m_q \to 0$ limit) and arises from χPT+QED at $\mathcal{O}(E^0)$. These results are slightly larger than the rule of thumb estimate $\frac{\alpha}{\pi} Q^{\rm eff} \Lambda_{\rm QCD} \sim 0.5\,\text{MeV}$, especially for the pion.

5.3 Electromagnetic Mass Splittings

We now turn to the calculation of the correlator F^X, defined in (5.11). This involves the calculation of the diagrams given in Figure 5.1. The actual mass splitting arises from the diagram proportional to $Q_b Q_q$ as the bb and qq diagrams

[5] Alternatively the direct determination of the quark mass ratio from $\eta \to 3\pi$ decays in [234] gives the more precise result $\{\Delta m_B|_{m_q}, \Delta m_D|_{m_q}\} = \{-2.54(18)\,\text{MeV}, +3.01(21)\,\text{MeV}\}$, before adding the $\text{SU}(3)_\text{F}$ uncertainty.

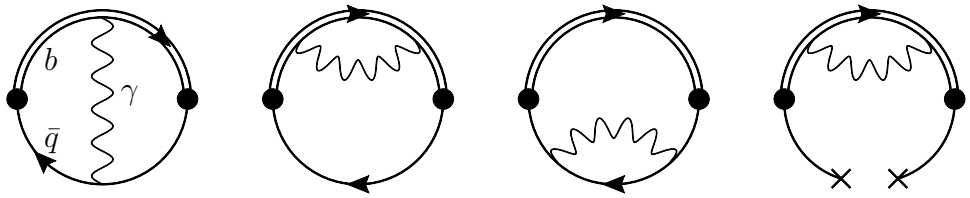

Figure 5.1 *The relevant diagrams for computing $\delta m_B|_{QED}$. The black circle represents the J_B operator (or the axial operator in the Kaon case) while the pair of crosses represents the quark condensate. For pions there would also be an extra disconnected diagram, though lattice results [236] have shown this to be a tiny ($\sim 1\%$) contribution.*

cancel in the subtraction (5.4). Nevertheless they are important to stabilise the individual sum rules for $\delta m_X|_{\text{QED}}$.

5.3.1 Calculation

The diagrams are evaluated using Cutkosky rules using the methods of Section 3.2.2. By choosing the $p_B = (\sqrt{s}, \mathbf{0})$ frame and $\boldsymbol{r} = \mathbf{0}$ for convenience the integrals are reasonably straightforward as there is minimal angular dependence. For example, for the $b\,q$ perturbative diagram the spectral density is

$$\rho_{F_X}(s,\tilde{s})_{bq} = -\frac{\alpha\, m_+^2 N_c Q_b Q_q}{32\pi^5}\int \mathrm{d}^d k\, \mathrm{d}^d l\, \frac{\mathrm{Tr}[\cdots]_{\mu\nu}}{q^2}\left(g^{\mu\nu} - (1-\xi)\frac{q^\mu q^\nu}{q^2}\right)\Bigg|_{q=k-l}$$
$$\times\, \delta^+(l^2 - m_q^2)\delta^+(k^2 - m_q^2)\delta^+((p_B - l)^2 - m_b^2)\delta^+((\tilde{p}_B - k)^2 - m_b^2)\,, \quad (5.33)$$

where k and l are the loop momenta flowing in the two halves of the diagram and we suppress the numerator trace structure. The delta functions fix the quark energies on both sides of the diagram while the angle between $\boldsymbol{k}$ and $\boldsymbol{l}$ generates a log term. The result is

$$\rho_{F_X}(s,\tilde{s})_{bq} = \frac{\alpha\, m_+^2 N_c Q_b Q_q}{16\pi^3}\cdot\frac{\sqrt{\lambda\tilde{\lambda}}}{s\tilde{s}}\left(A + \frac{B + B|_{b\leftrightarrow q}}{\mathtt{b}}\ln\left(\frac{\mathtt{a}+\mathtt{b}}{\mathtt{a}-\mathtt{b}}\right)\right), \quad (5.34)$$

where

$$\mathtt{a} = \frac{1}{2}\left[m_+^2 + m_-^2 - \frac{s\tilde{s} + m_+^2 m_-^2}{\sqrt{s\tilde{s}}}\right]$$
$$\mathtt{b} = \frac{1}{2}\sqrt{\frac{\lambda\tilde{\lambda}}{s\tilde{s}}}\,, \quad (5.35)$$

with $\lambda = \lambda(s, m_b^2, m_q^2)$, $\tilde{\lambda} = \lambda(\tilde{s}, m_b^2, m_q^2)$ and

$$\begin{aligned} A &= m_-^2 \\ B &= \frac{1}{8}\bigg[8s\mathbb{Y}\tilde{s}\tilde{\mathbb{Y}} + \big(m_+ - m_-\big)^2\big((\mathbb{Y}+\tilde{\mathbb{Y}})\sqrt{s\tilde{s}} - m_-^2\big) \\ &\qquad - 2m_-^2\big(s + \tilde{s} + m_+^2 - m_-^2\big) - 2m_+^2\sqrt{s\tilde{s}}\bigg], \end{aligned} \tag{5.36}$$

with $\mathbb{Y}$ defined in (3.47) and $\tilde{\mathbb{Y}} = \mathbb{Y}|_{s\to\tilde{s}}$. As usual $Q_b = -1/3$, $Q_u = +2/3$ and $m_\pm = m_b \pm m_q$. Note that we have dropped (suppressed) $\mathcal{O}(r)$ terms that break the $b - q$ symmetry which are regarded as unphysical. The gauge parameter disappears in the final result as it must. The corresponding result for the axial case is more complicated and is attached as an ancillary file to the published work [2].

Similarly, the perturbative bb graph has density

$$\rho_{F_X}(s,\tilde{s})_{bb} = \frac{\alpha\, m_+^2 N_c Q_b^2}{16\pi^3}\cdot\frac{\lambda^{\frac{1}{2}}(s-m_-^2)}{s+m_+m_-}\Big(f(m_b^2) + \frac{32\pi^2 m_b^2}{e^2}\delta Z_m\Big)\delta(\tilde{s}-s) \tag{5.37}$$

with

$$f(m^2) = 4m^2 B_0(m^2, 0, m^2) + (d-2)A_0(m^2)\,, \tag{5.38}$$

and δZ_m the usual one-loop mass renormalisation, e.g. $\delta Z_m = -(3\alpha/4\pi\hat{\epsilon})$ in $\overline{\text{MS}}$. Note that as the particles are forced on-shell in the cut then $\rho_{F_X}(s,\tilde{s})_{bb}$ vanishes in the pole scheme. The qq graph follows from the replacement $b \leftrightarrow q$ and is numerically negligible as it is $\mathcal{O}(m_q^2)$.

Neglecting the light quark mass the bb quark condensate diagram is

$$\begin{aligned} \rho_{F_X}(s,\tilde{s})_{bb}^{\langle\bar{q}q\rangle} = -\frac{\alpha\, m_b^2 Q_b^2}{4\pi} m_b\langle\bar{q}q\rangle\Big(f(m_b^2) + \frac{32\pi^2 m_b^2}{e^2}\delta Z_m\Big)\delta(s-m_b^2)\delta(\tilde{s}-m_b^2) \\ + \mathcal{O}(m_q)\,, \end{aligned} \tag{5.39}$$

which is good enough for practical purposes. Including light quark mass corrections, going beyond (2.27), involves the short distance expansion

$$\langle 0|\bar{q}_\alpha(x)q_\beta(0)|0\rangle = \langle 0|\bar{q}_\alpha(0)q_\beta(0)|0\rangle + x^\mu\langle 0|(\partial_\mu\bar{q}_\alpha(0))q_\beta(0)|0\rangle + \cdots\,, \tag{5.40}$$

where α, β are spinor indices and we suppress the colour indices. The partial derivative can be replaced by a covariant one by employing the Fock-Schwinger

gauge $x^\mu A_\mu = 0$ for the gluon field A_μ. Lorentz invariance implies the matrix element $\langle 0|(D_\mu \bar{q}_\alpha(0))\bar{q}_\beta(0)|0\rangle$ must be proportional to $(\gamma_\mu)_{\beta\alpha}$ and using the equation of motion gives the result [108]

$$\langle 0|\bar{q}_\alpha(x)q_\beta(0)|0\rangle \;=\; \frac{\langle\bar{q}q\rangle}{4N_c}\left(\delta_{\alpha\beta} + \frac{im_q}{4}x_\mu(\gamma^\mu)_{\beta\alpha} + \cdots\right). \tag{5.41}$$

Returning to the bb condensate, the Taylor expansion occurs in the variable $(z-y)_\mu$ which leads to the derivatives $\partial_{p_B^\mu}$ and $\partial_{\tilde{p}_B^\mu}$ in the $\mathcal{O}(m_q)$ correction. These can be performed using the helpful identity

$$\frac{\partial}{\partial p^\mu}S(p) = -S(p)\gamma_\mu S(p)\,, \qquad S(p) = \frac{\not{p}+m}{p^2-m^2}\,. \tag{5.42}$$

The spectral density therefore involves derivatives of delta functions and so it is easier to present the result post-Borel transformation. The analogue of (5.39), now including m_q corrections is

$$2m_B Z_B^2\,(\delta m_B|_{\rm QED})|_{bb}^{\langle\bar{q}q\rangle} = -\frac{\alpha\, m_+^2 Q_b^2}{4\pi}\langle\bar{q}q\rangle e^{\frac{2(m_B^2-m_b^2)}{M^2}}\left(f(m_b^2) + \frac{32\pi^2 m_b^2}{e^2}\delta Z_m\right) \times\left[m_b - \frac{m_q}{4}\left(1+\frac{4m_b^2}{M^2}\right)\right], \tag{5.43}$$

where notice that the derivative brings down a power of M^2 in the result. The other $\langle\bar{q}q\rangle$ condensate graph where the photon connects the b and the q quark is not of short distance type and is omitted. It leads to $1/m_q^2$ behaviour and exactly this graph was similarly ommited in the $B\to\gamma$ calculation [195].

Results for the axial correlator are derived in exactly the same fashion, just with different trace structures. We note that as the strange quark does form a condensate there is additionally a $Q_q^2\langle\bar{s}s\rangle$ diagram. However this is both m_q^2 suppressed and condensate suppressed so practically speaking can be ignored.

5.3.2 Results

The numerics and Borel transform are handled in the same way as in Chapter 4. We again make use of the Daughter Sum Rule to fix the hadronic threshold s_0 and set M^2 to suppress continuum and condensate contributions. Other input parameters are given in Table 5.1. The only novel parameter is a, (5.10), which parameterises the choice of duality region in the double dispersion. We take $a = 1$

and quantify this uncertainty by taking the standard deviation of the results with $a \in [\frac{1}{2}, 1, 2, \infty]$. This accounts for roughly a fifth of the final error budget.

As in the leptonic decay the most important parameter is the heavy quark mass $m_{b,c,s}$. For the Kaon (axial) case we can only take the $\overline{\text{MS}}$ mass (at $\mu = 2\,\text{GeV}$), however for $m_{b,c}$ we may also consider the kinetic mass. Again for the B-case the kinetic mass proves best at suppressing the condensates while for the D there is little difference. In view of [196], where the kinetic scheme proved unsuitable for $g_{DD^*\gamma}$ we take the $\overline{\text{MS}}$ mass $\bar{m}_c(\bar{m}_c)$. The heavy quark mass makes up 50% of the error budget for $\Delta m_B|_{\text{QED}}$ rising to 60% and 70% in the D and K case respectively. The total uncertainties are calculated as before by adding individual errors in quadrature. Apart from the previously mentioned m_b and a uncertainties the only other relevant uncertainty is from the Borel mass M^2, an approximately 20% contribution. The sum rules parameters are summarised in Table 5.2.

Unlike in Chapter 4, these sum rules are generically of poor quality on account of being a LO double dispersion. This is reflected by less stability in the (smaller) Borel windows and this leads to quite sizeable uncertainties. This is compounded in the result for $\Delta m_B|_{\text{QED}}$ due to cancellations when the sum rules for $\delta m_{B^\pm}|_{\text{QED}}$ and $\delta m_{\bar{B}^0}|_{\text{QED}}$ are subtracted. As is standard the sum rules perform better for heavier mesons, with the convergence best for the B, cf. Table 5.2. The Kaon sum rule is the worst and it struggles to satisfy the Daughter Sum Rule consistency constraint, presumably due to its light mass. As an improvement we use a weight function $\omega(s, \tilde{s}) = m_B^4/s\tilde{s}$ (cf. Section 2.1.2) to at least make the sum-rule consistent, even if not necessarily very accurate[6]. Even with a weight

[6]The weight function does not change the result as it is essentially equivalent to working with a subtracted dispersion relation, and disappears after Borel transformation. Indeed $\omega \to 1$ in the limit of perfect quark-hadron duality. Concretely for a sum-rule

$$\Pi(p^2) = \int \frac{\rho(s)}{s - p^2}\,\mathrm{d}s = \frac{f^2}{m^2 - p^2} + \cdots\,, \tag{5.44}$$

by subtracting off $\Pi(0) = f^2/m^2$ we get

$$\int \frac{\rho(s)}{s(s - p^2)}\,\mathrm{d}s + C = \frac{f^2}{m^2(m^2 - p^2)} + \cdots\,, \tag{5.45}$$

where $C = \Pi'(0) - \int_s \rho(s)/s^2$ is a subtraction constant that is killed by the Borel procedure. Thus we can recover the original sum rule with the modification $\rho(s) \to (m^2/s)\rho(s)$. Other powers $(m^2/s)^n$, $n > 1$ (i.e. higher moments) in theory would also work though quark-hadron duality requires some level of smoothness. The other requirement is that $\Pi(0)$ can still be calculated in perturbation theory, i.e. that $p^2 = 0$ is not too close to the Kaon resonance at $p^2 = m_K^2$ in our scenario. We have checked for the well-known f_K sum rules that using a weight function makes little difference to the final result, providing at least a partial justification for our procedure.

$J^P = 0^-$ Meson masses [37]

m_B	m_{B_s}	m_D	m_{D_s}	m_K	m_π
5.280 GeV	5.367 GeV	1.867 GeV	1.968 GeV	0.496 GeV	0.137 GeV

$J^P = 0^-$ Mass Differences [37]

Δm_B	Δm_D	Δm_K	Δm_π		
$-0.32(5)$ MeV	$+4.822(15)$ MeV	$-3.934(20)$ MeV	$+4.5936(5)$ MeV		

Quark masses [37]

$\bar{m}_b(\bar{m}_b)$	$\bar{m}_c(\bar{m}_c)$	m_b^{pole}	m_c^{pole}	$m_b^{kin}\vert_{1\text{GeV}}$	$m_c^{kin}\vert_{1\text{GeV}}$
$4.18^{+0.03}_{-0.02}$ GeV	1.27(2) GeV	4.78(6) GeV	1.67(7) GeV	4.53(6) GeV	1.13(5) GeV
$\bar{m}_s\vert_{2\text{GeV}}$	$\bar{m}_d\vert_{2\text{GeV}}$	$\bar{m}_u\vert_{2\text{GeV}}$	$\bar{m}_{ud}\vert_{2\text{GeV}}$	$\frac{\bar{m}_u}{\bar{m}_d}$	$\frac{\bar{m}_s}{\bar{m}_{ud}}$
$93.4^{+8.6}_{-3.4}$ MeV	$4.67^{+0.48}_{-0.17}$ MeV	$2.16^{+0.49}_{-0.26}$ MeV	$3.45^{+0.35}_{-0.15}$ MeV	$0.474^{+0.056}_{-0.074}$	$27.33^{+0.67}_{-0.77}$

Condensates

$\langle\bar{q}q\rangle\vert_{2\text{GeV}}$ [44]	$\langle\bar{s}s\rangle\vert_{2\text{GeV}}$ [237]	m_0^2 [238]	$\langle 0\vert\frac{\alpha_s}{\pi}G^2\vert 0\rangle$ [27]		
$-(269(2)\,\text{MeV})^3$	1.08(16) $\langle\bar{q}q\rangle$	$0.8(2)\,\text{GeV}^2$	$0.012(4)\,\text{GeV}^4$		

Table 5.1 *Summary of input parameters and other numerical quantities relevant for the calculation of Δm_P. Note as inputs into the sum rules we use $m_{P^0} = m_{P^-}$ which has a completely negligible impact. The quantity $m_{ud} \equiv \frac{1}{2}(m_u + m_d)$ is the light quark average. The mixed condensate is parameterised as $\langle\bar{q}\sigma gGq\rangle = m_0^2\langle\bar{q}q\rangle$, with $m_0^2 > 0$, as is standard in the literature, though note its sizeable uncertainty. For the charm quark mass we take an error of $\delta m_c = \pm 0.1\,\text{GeV}$, cf. Section 4.1.*

P	$s_0\,[\,\text{GeV}^2]$	$\hat{M}^2\,[\,\text{GeV}^2]$	$f_P\,[\,\text{GeV}]$	DSR	Cond.	Cont.	$\Delta m_P\vert_{\text{QED}}$
B	35.2(1.0)	2.6(0.5)	0.16	$< 0.1\%$	15.6%	29.6%	$+1.58\,\text{MeV}$
D	5.5(0.1)	1.00(0.25)	0.16	$< 0.1\%$	23.2%	30.0%	$+2.25\,\text{MeV}$
K	0.7(0.1)	0.95(0.50)	0.15	$\sim 0.1\%$	–	27.0%	$+1.85\,\text{MeV}$

Table 5.2 *The sum rules parameters used in the calculation of $\Delta m_P\vert_{QED}$, with the applied errors in brackets. Additionally we give the suppression of the continuum (Cont.) states above s_0 as well as how well the condensates (Cond.) are suppressed. Both of these contributions should ideally be kept below 30%. The Daughter Sum Rule (DSR) is used to set s_0 as far as possible (i.e. without affecting convergence). This column shows to what precision level this can be performed. Note that in the axial case the bb condensate graph vanishes identically which is one reason why the K sum rule is of poor quality. In this case the Borel window is chosen simply as the region around the Borel minimum that exhibits some level of flatness. The 'denominator' factor Z_B^2 must also be included via a sum rules method to reduce some of the m_b instability. The expressions for $f_{B,D,K}$ are well known (e.g. [107, 239]) and we use the $(s_0, M^2)^{f_P}$ values $(33.6, 6.0)\,\text{GeV}^2$, $(5.7, 2.0)\,\text{GeV}^2$ and $(1.1, 1.5)\,\text{GeV}^2$ for B, D, K respectively. Our values are correspondingly lower as we must work at LO for consistency with the numerator. Note that the f_K sum rule introduces an $\langle\bar{s}s\rangle$ dependence into the result.*

function the pion case cannot be salvaged (likely due to its extremely low mass) and so we do not consider this channel.

With these inputs and choices our final results are

$$\begin{aligned}\Delta m_B|_{\text{QED}} &= +1.58^{+0.26}_{-0.23}\,\text{MeV}\,,\\ \Delta m_D|_{\text{QED}} &= +2.25^{+0.89}_{-0.52}\,\text{MeV}\,,\\ \Delta m_K|_{\text{QED}} &= +1.85^{+0.42}_{-0.66}\,\text{MeV}\,,\end{aligned} \tag{5.46}$$

which we will compare to previous work in Section 5.5.

5.4 Quark Mass Corrections

The linear quark mass correction $\Delta m_B|_{m_q}$, or more specifically the matrix element $\langle \bar{B}|\bar{q}q|\bar{B}\rangle$, is calculated from the correlator $G(p_B^2, \tilde{p}_B^2)$ defined in (5.20). We give results for the B and the D as for the light mesons the sum rules are far inferior to the χPT results of Section 5.2.3.

5.4.1 Calculation

We calculate $G(p_B^2, \tilde{p}_B^2)$ in QCD at leading order in α_s, however include condensate contributions up to dimension 5. The relevant graphs are drawn in Figure 5.2. As well as the quark condensate we must also include the mixed condensate $\langle q\sigma\cdot Gq\rangle$ as this is the second most important contribution (owing to the perturbative graph being numerically very small). The mixed condensate is also necessary to stabilise the sum rule.

Proceeding as before by cutting rules, the perturbative spectral density is

$$\rho_G(s,\tilde{s})_{\mathbb{1}} = \frac{m_+^2 N_c}{2\pi^2}\cdot\frac{m_q(s-m_-^2)}{s-m_+m_-}\lambda^{\frac{1}{2}}\delta(\tilde{s}-s)\,, \tag{5.47}$$

which exhibits the advertised $\mathcal{O}(m_q)$ suppression and is numerically negligible. Indeed the perturbative contribution must vanish in the massless limit as the QCD Lagrangian has chiral symmetry which is only spontaneously broken by exactly $\langle\bar{q}q\rangle \neq 0$. The same suppression also affects the gluon condensate, $\langle G^2\rangle$, and so this contribution can be ignored.

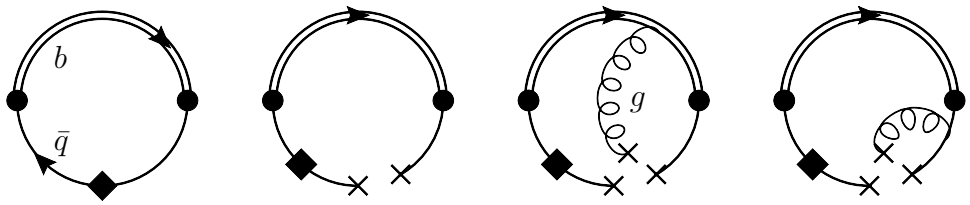

Figure 5.2 *Diagrams contributing to the matrix element $\langle \bar{B}|\bar{q}q|\bar{B}\rangle$. The solid black diamond denotes the insertion of the $\bar{q}q$ operator. As the perturbative diagram is suppressed the main contribution comes from the quark condensate (diagram 2). There are two mixed condensate diagrams: $b-q$ type (third) and $q-q$ type (fourth). There are also analogous diagrams with the $\bar{q}q$ operator on the RHS of the condensates.*

The dominant contribution therefore arises from the quark condensate graph. The result is

$$\langle \bar{B}|\bar{q}q|\bar{B}\rangle_{\langle\bar{q}q\rangle} = -\frac{4m_+^2 m_b^2\langle\bar{q}q\rangle}{Z_B^2} e^{\frac{2(m_B^2-m_b^2)}{M^2}}\,, \tag{5.48}$$

where for simplicity we neglect light quark mass effects. For higher dimensional condensates diagrammatic representations become unreliable and one should work directly from Wick contractions and short distance expansions like (5.40). For the mixed condensate we use the general results from [108, 240, 241]

$$\begin{aligned}\langle 0|\bar{q}_\alpha(x_1)q_\beta(x_2)|0\rangle \;=\; & \\ & \frac{1}{4N_c}\bigg[\Big(1-\frac{m_q^2}{2d}x_{12}^2\Big)\delta_{\alpha\beta}+\frac{im_q}{d}(\not{x}_{12})_{\beta\alpha}\Big(1-\frac{m_q^2}{2(d+2)}x_{12}^2\Big)\bigg]\langle\bar{q}q\rangle \\ & +\frac{x_{12}^2}{16N_c\,d}\Big(\delta_{\alpha\beta}+\frac{im_q}{d+2}(\not{x}_{12})_{\beta\alpha}\Big)\langle q\sigma gGq\rangle \;+\;\cdots\,,\end{aligned} \tag{5.49}$$

and

$$\begin{aligned}\langle 0|\bar{q}_\alpha(x_1)G^{\mu\nu}(z)q_\beta(x_2)|0\rangle \;=\; & \\ & \frac{\langle q\sigma\cdot Gq\rangle}{4d(d-1)(d-2)N_c}\bigg[(d-2)\sigma^{\mu\nu}+m_q\Big(\gamma^\mu x_{12}^\nu-\gamma^\nu x_{12}^\mu+i\sigma^{\mu\nu}\not{x}_{12}\Big)\bigg]_{\beta\alpha}+\cdots\,,\end{aligned} \tag{5.50}$$

where $x_{12}=x_1-x_2$ and '$+\cdots$' denotes four-quark condensate and higher terms. One should only expand in genuine short distance parameters and we neglect higher dimensional (longer distance) effects. Ignoring light quark corrections again this gives

$$\langle B|\bar{q}q|\bar{B}\rangle_{\langle\bar{q}\sigma gGq\rangle} = -\frac{m_+^2\langle\bar{q}\sigma gGq\rangle}{Z_B^2} e^{\frac{2(m_B^2-m_b^2)}{M^2}}\left(\frac{13}{8}-\frac{m_b^2}{M^2}-\frac{4m_b^2}{M^4}\right). \tag{5.51}$$

In passing we also give the result

$$\int_{m_+^2}^{\bar{\delta}^{(a)}(m_+^2)} \int_{m_+^2}^{\bar{\delta}^{(a)}(s)} \mathrm{d}s\,\mathrm{d}\tilde{s}\; e^{-\frac{s+\tilde{s}}{M^2}}\,(s+\tilde{s})\,\rho_G(s,\tilde{s})_{\langle\bar{q}\sigma gGq\rangle} = \\ -\,m_+^2\langle\bar{q}\sigma gGq\rangle e^{\frac{-2m_b^2}{M^2}} m_b^2\left(\frac{17}{4}+\frac{6m_b^2}{M^2}-\frac{8m_b^2}{M^4}\right), \quad (5.52)$$

useful for the Daughter Sum Rule, as this is non-trivial due to the various derivatives.

5.4.2 Results

The numerics are performed as in the QED case, using the input values of Table 5.1. There are however some important differences. As the perturbative contribution is negligible the parameters s_0 and a do not enter the sum rule. This also means the result depends strongly on the choice of Borel mass M^2. While previously we have used the Daughter Sum Rule consistency condition to fix s_0, here we can use it instead to fix M^2.

Again we take the b quark mass in the kinetic scheme and the charm quark in $\overline{\mathrm{MS}}$. The main uncertainties in this case arise from setting M^2 and the heavy quark mass. Really however almost all uncertainties can be traced back, one way or another, to the fact this is a $\mathcal{O}(\alpha_s^0)$ calculation. For the Borel parameters we take

$$(s_0,\hat{M}^2)_B = (35.0, 4.0)\,\mathrm{GeV}^2 \qquad \text{and} \qquad (s_0,\hat{M}^2)_D = (6.0, 0.75)\,, \quad (5.53)$$

and the mixed condensate is 27% (52%) of the quark condensate in the B (D) case. Again the D sum rule is poorer quality than the B sum rule and in the D case the mixed condensate is not very well suppressed at all. That being said, the next relevant condensate is the 4-quark condensate which, in the factorisation approximation, is $\sim\langle\bar{q}q\rangle^2$ and should be a $\mathcal{O}(1\%)$ effect. This provides at least partial reassurance though really this is just a highly non-standard sum rule. Again the factor of Z_B in the denominator is computed via the f_B sum rule [107], cf. Table 5.2. Our results for the matrix elements are

$$\begin{aligned} \langle\bar{B}|\bar{q}q|\bar{B}\rangle|_{\,\mu=1\,\mathrm{GeV}} &= +5.99^{+1.99}_{-1.41}\,\mathrm{GeV}\,, \\ \langle\bar{D}|\bar{q}q|\bar{D}\rangle|_{\,\mu=\bar{m}_c} &= +3.40^{+1.78}_{-1.71}\,\mathrm{GeV}\,, \end{aligned} \quad (5.54)$$

which via (5.8) gives the quark mass shifts

$$\begin{aligned} \Delta m_B|_{m_q} &= -1.88^{+0.49}_{-0.71}\,\text{MeV}\,, \\ \Delta m_D|_{m_q} &= +2.68^{+1.48}_{-1.38}\,\text{MeV}\,. \end{aligned} \tag{5.55}$$

5.5 Summary and Conclusions

In this chapter we have computed electromagnetic and quark mass corrections to the pseudoscalar meson masses. Our predictions for the mass differences between charged and neutral mesons are summarised in Table 5.3 along with the experimental values for comparison.

P	$\Delta m_P\|_{\text{QED}}$	$\Delta m_P\|_{m_q}$	Δm_P	$\Delta m_P\|_{\text{PDG}}$
B	+1.58(24) MeV	−1.88(60) MeV	−0.30(65) MeV	−0.32(5) MeV
D	+2.25(70) MeV	+2.7(1.4) MeV	+4.9(1.6) MeV	+4.822(15) MeV
K	+1.85(54) MeV	−6.7(1.1) MeV[a]	−4.9(1.2) MeV	−3.934(20) MeV
π	+4.54(50) MeV[a]	+0.16(5) MeV[a]	+5.0(1.2) MeV	+4.5936(5) MeV

Table 5.3 *Summary of our results (with errors symmetrised) for the pseudoscalar mass differences, broken down into QED and quark mass contributions. The measured experimental values [37] are given in the rightmost column. Note that entries marked [a] are not predictions of this work, they come from low energy theorems.*

Our results for Δm_P are consistent with the experimental values, though with large uncertainties. This is to be expected from a double dispersion calculation at leading order which certainly cannot match the precision of the results in Section 5.2.3. As noted before, our sum rules perform best for the B and worsen for the lighter mesons. For $\Delta m_P|_{\text{QED}}$ our results for the B and D are in good agreement with [224], though our prediction for the Kaon is roughly 30% smaller than [222]. For the linear quark mass shift, via the Feynman-Hellmann theorem, we again are in rough agreement with the classic results though note the considerable ($\sim 50\%$) errors involved in the D case.

Accurate numerical estimates however are not really the aim of this work. Its main purpose was to show that one can obtain isospin breaking mass differences from QCD sum rules without having to follow the traditional Cottingham

procedure. The electromagnetic shift via a double dispersion may be regarded as the central part of this chapter, with the calculation of $\langle P|\bar{q}q|P\rangle$ *also* via a dispersion being a pleasing addition. The quality of the sum rules could be improved by including higher order strong force corrections, though this would be a formidable task. Perhaps more interestingly the method could be modified to consider higher spin hadrons like baryons and could even be applied to the fabled proton-neutron mass difference.

Chapter 6

Conclusions

In this thesis we have calculated electromagnetic corrections in two areas of b physics, both using a sum rules framework. The main work is a complete next-to-leading order QED calculation of the decay rate $\bar{B} \to \ell\bar{\nu}(\gamma)$ using a new explicitly gauge-invariant formalism. This is one of the first truly structure-dependent QED calculations for B decays and certainly the first via a dispersive sum rules technique. A second project considered the mass difference, Δm_P, between charged and neutral pseudoscalar mesons, $P = B, D, K, \pi$ and demonstrated that this can also be extracted using similar sum rule ideas.

In Chapter 3 we discussed the calculation of the leptonic decay $\bar{B} \to \ell\bar{\nu}(\gamma)$ in detail, paying careful attention to its cut structure. We use a new construction, involving an auxiliary Φ_B particle, to allow for proper treatment of soft photons. This particle plays the role of the long distance $\bar{B}$-meson and renders our interpolating operators gauge-invariant. We also devoted considerable attention to the helicity suppressed nature of the V-A decay and how this is lifted in the real rate by structure-dependent terms. The helicity suppression in $\bar{B} \to \ell\bar{\nu}$ allows for structure-dependent hard-collinear logs to exist and we have shown this explicitly to be the case. As a check of our methodology we demonstrate the complete cancellation of hard-collinear logs for S-P (non-SM) type interactions once fully inclusive in the photon.

In Chapter 4 we follow this up with a numerical study. We show that virtual structure-dependence gives a $+4.6(6)\%$ ($\ell = \mu$) and $+2.9(2)\%$ ($\ell = \tau$) correction on top of scalar QED, driven mainly by the extra hard-collinear logs. Such effects are certainly important, in view of the sub-1% precision

(isospin symmetric) lattice results for f_B, and relevant, considering the reduced experimental uncertainties by the end of the Belle II run. The total relative QED correction also depends strongly on the choice of photon energy cut-off, showing the importance of the $\bar{B} \to \gamma$ form factors in the real rate (which we take externally).

This leptonic decay is an important channel phenomenologically as it may be considerably enhanced by new physics. Our work complements existing SCET analysis [177] of the neutral current decay $\bar{B}_{d,s} \to \mu^+\mu^-$, as a full analysis of $\bar{B} \to \mu\bar{\nu}$ has yet to appear. We note that our results are equally valid for all three channels $\ell = \tau, \mu, e$, unlike SCET techniques which heavily depend on the lepton mass scale.

Finally in Chapter 5 we calculate isospin-breaking corrections to the pseudoscalar meson masses. We extract both electromagnetic and quark mass effects via a double dispersion using the same hadronic inputs and without introducing any model dependence. Our results, which we give for the B, D and K, are consistent with classic estimates and experimental values, though exhibit large uncertainties.

The work we have presented in this thesis adds to the growing body of evidence that QED effects are now too important to be neglected. Experimental analyses must move beyond point-like approximations and theorists must be careful not to always assume that QED corrections are small. With the wealth of experimental data being generated, accurate theoretical predictions will continue to be vital in the search for new physics. This thesis helps contribute to that search, even if only in a small way.

Appendix A

Notation and Conventions

We take the QED covariant derivative as

$$D_\mu = \partial_\mu + ies_e Q_f A_\mu \,, \tag{A.1}$$

where $e > 0$ and retaining $s_e = \pm 1$ allows us to work with both frequently chosen conventions. Here the charges are $(Q_\Phi, Q_{\ell_1}, Q_b, Q_q) = (-1, -1, -1/3, +2/3)$ and we note that the hatted charge notation of Section 2.2.2 is not particularly useful in Chapter 3 as there are now two vertices. The quarks flow out of $\mathcal{J}_B$ and into $\mathcal{L}_W$. We work in $d = 4 - 2\epsilon$ dimensions and use the mostly-minus metric. The Clifford algebra is the usual

$$\{\gamma^\mu, \gamma^\nu\} \,=\, 2g^{\mu\nu} \,, \qquad i[\gamma^\mu, \gamma^\nu] \,=\, 2\sigma^{\mu\nu} \,, \tag{A.2}$$

with $\gamma_5 = i\gamma^0\gamma^1\gamma^2\gamma^3$ in $d = 4$. The treatment of γ_5 in dimensional regularisation is in general a thorny issue though does not cause too many problems in our case. Where necessary the Larin scheme [242] is employed to deal with any single γ_5. The Levi-Civita symbol is taken with 'Bjorken and Drell' conventions $\epsilon_{0123} = +1$. We work with the amplitude phase convention $\mathcal{A} = \langle f| - \mathcal{L}|i\rangle$.

The only place we work directly with QCD is in Section 5.4.1 with the convention $D_\mu = \partial_\mu + igs_g \frac{\lambda^a}{2} A^a_\mu$ and $g > 0$. Otherwise, conventions are as in the papers [1, 2] with the only exception being a missing factor of $e^{\frac{m_B^2}{M^2}}$ in the definition of $\mathcal{B}_{M^2}$.

A.1 Passarino-Veltman Functions

The Passarino-Veltman functions $A_0, B_0, C_0, \ldots$ [119] form a complete basis for the one-loop scalar integrals. We define them with the normalisation

$$\frac{(2\pi\mu)^{2\epsilon}}{i\pi^2}\int \mathrm{d}^d k \tag{A.3}$$

and the conventions of FeynCalc [117, 118], FeynHelpers [204] and Package X [203]. The simplest integral is the tadpole function A_0 which has one propagator

$$A_0(m^2) \equiv \frac{(2\pi\mu)^{2\epsilon}}{i\pi^2}\int \frac{\mathrm{d}^d k}{k^2-m^2} = m^2\left(\frac{1}{\hat{\epsilon}_{\mathrm{UV}}}+1+\ln\frac{\mu^2}{m^2}\right)+\mathcal{O}(\epsilon)\,, \tag{A.4}$$

where $1/\hat{\epsilon} = 1/\epsilon - \gamma_E + \ln 4\pi$ and the $+i\varepsilon$ in the denominator is left implicit. In the limit $m \to 0$ the result vanishes. This can be considered as a $\epsilon_{\mathrm{UV}}^{-1} - \epsilon_{\mathrm{IR}}^{-1} = 0$ cancellation as scaleless integrals are zero in dimensional regularisation. The bubble integral in its most general form is

$$\begin{aligned} B_0(p^2, m_0^2, m_1^2) &\equiv \frac{(2\pi\mu)^{2\epsilon}}{i\pi^2}\int \frac{\mathrm{d}^d k}{(k^2-m_0^2)((k+p)^2-m_1^2)} \\ &= \frac{1}{\hat{\epsilon}_{\mathrm{UV}}} + 2 + \frac{m_0^2-m_1^2}{2p^2}\ln\frac{m_1^2}{m_0^2} - \ln\frac{m_0 m_1}{\mu^2} \\ &\quad + \frac{\lambda^{\frac{1}{2}}(p^2,m_0^2,m_1^2)}{p^2}\ln\left(\frac{2m_0m_1}{m_0^2+m_1^2-p^2-\lambda^{\frac{1}{2}}(p^2,m_0^2,m_1^2)}+i\varepsilon\right)+\mathcal{O}(\epsilon), \end{aligned} \tag{A.5}$$

where λ is the Källeń function. This becomes imaginary for $p^2 \geq (m_0+m_1)^2$ taking the value $\mathrm{Im}\, B_0(p^2, m_0^2, m_1^2) = (\pi/p^2)\lambda^{\frac{1}{2}} + \mathcal{O}(\epsilon)$, agreeing with (3.38) as a nice check. When one of the propagators is massless then

$$B_0(p^2, 0, m^2) = \frac{1}{\hat{\epsilon}_{\mathrm{UV}}} + 2 + \ln\frac{\mu^2}{m^2} + \frac{m^2-p^2}{p^2}\ln\frac{m^2-p^2-i\varepsilon}{m^2} + \mathcal{O}(\epsilon)\,, \tag{A.6}$$

and for $p^2 = m^2$ one gets $m^2 B_0(m^2, 0, m^2) = m^2 + A_0(m^2)$. The derivative of the bubble integral with respect to p^2 is denoted by $\mathrm{D}B_0(p^2, m_0^2, m_1^2)$ and this is IR divergent in the limit $p^2 \to (m_0+m_1)^2$. We require the result

$$\mathrm{D}B_0(m^2, 0, m^2) \equiv \frac{\mathrm{d}}{\mathrm{d}p^2} B_0(p^2, 0, m^2)\bigg|_{p^2=m^2}$$

$$= \frac{-1}{2m^2}\left(\frac{1}{\hat{\epsilon}_{\rm IR}} + 2 + \ln\frac{\mu^2}{m^2}\right) + \mathcal{O}(\epsilon)\,, \tag{A.7}$$

in the calculation of blue cuts in bb and qq diagrams. Higher point functions C_0, D_0, etc., become too complicated to give explicitly. They are defined as

$$C_0\big(p_1^2,(p_1-p_2)^2,p_2^2,m_0^2,m_1^2,m_2^2\big) = \frac{(2\pi\mu)^{2\epsilon}}{i\pi^2}\int\frac{\mathrm{d}^d k}{(k^2-m_0^2)((k+p_1)^2-m_1^2)((k+p_2)^2-m_2^2)}\,, \tag{A.8}$$

and

$$D_0\big(p_1^2,(p_1-p_2)^2,(p_2-p_3)^2,p_3^2,p_2^2,(p_1-p_3)^2,m_0^2,m_1^2,m_2^2,m_3^2\big) = \frac{(2\pi\mu)^{2\epsilon}}{i\pi^2}\int\frac{\mathrm{d}^d k}{(k^2-m_0^2)((k+p_1)^2-m_1^2)((k+p_2)^2-m_2^2)((k+p_3)^2-m_3^2)}\,, \tag{A.9}$$

and so on with a considerable number of useful results collected in the QCDloop repository [243].

Bibliography

[1] M. Rowe and R. Zwicky, "Structure-dependent QED in $B^- \to \ell^- \overline{\nu}\,(\gamma)$," *JHEP* **07** (2024) 249, arXiv:2404.07648 [hep-ph].

[2] M. Rowe and R. Zwicky, "Isospin mass differences of the B, D and K," *JHEP* **06** (2023) 089, arXiv:2301.04972 [hep-ph].

[3] M. Gell-Mann, "Symmetries of baryons and mesons," *Phys. Rev.* **125** (1962) 1067–1084.

[4] Y. Ne'eman, "Derivation of strong interactions from a gauge invariance," *Nucl. Phys.* **26** (1961) 222–229.

[5] M. Gell-Mann, "A Schematic Model of Baryons and Mesons," *Phys. Lett.* **8** (1964) 214–215.

[6] G. Zweig, "An SU(3) model for strong interaction symmetry and its breaking. Version 1,".

[7] G. Zweig, *An SU(3) model for strong interaction symmetry and its breaking. Version 2*, pp. 22–101. Hadronic Press, 2, 1964.

[8] J. S. Schwinger, "Quantum electrodynamics. I A covariant formulation," *Phys. Rev.* **74** (1948) 1439.

[9] J. S. Schwinger, "On Quantum electrodynamics and the magnetic moment of the electron," *Phys. Rev.* **73** (1948) 416–417.

[10] F. J. Dyson, "The Radiation theories of Tomonaga, Schwinger, and Feynman," *Phys. Rev.* **75** (1949) 486–502.

[11] S. Tomonaga, "On a relativistically invariant formulation of the quantum theory of wave fields," *Prog. Theor. Phys.* **1** (1946) 27–42.

[12] R. P. Feynman, "Space - time approach to quantum electrodynamics," *Phys. Rev.* **76** (1949) 769–789.

[13] R. P. Feynman, "The Theory of positrons," *Phys. Rev.* **76** (1949) 749–759.

[14] R. P. Feynman, "Mathematical formulation of the quantum theory of electromagnetic interaction," *Phys. Rev.* **80** (1950) 440–457.

[15] W. Heisenberg, "Die 'beobachtbaren Grössen' in der Theorie der Elemetarteilchenphysik," *Z. Phys.* **120** (1943) 513–538.

[16] N. G. van Kampen, "S-Matrix and Causality Condition. I. Maxwell Field," *Phys. Rev.* **89** (Mar, 1953) 1072–1079.

[17] N. G. van Kampen, "S Matrix and Causality Condition. II. Nonrelativistic Particles," *Phys. Rev.* **91** (Sep, 1953) 1267–1276.

[18] T. Regge, "Introduction to complex orbital momenta," *Nuovo Cim.* **14** (1959) 951.

[19] D. J. Gross and F. Wilczek, "Ultraviolet Behavior of Nonabelian Gauge Theories," *Phys. Rev. Lett.* **30** (1973) 1343–1346.

[20] H. D. Politzer, "Reliable Perturbative Results for Strong Interactions?," *Phys. Rev. Lett.* **30** (1973) 1346–1349.

[21] J. D. Bjorken, "Asymptotic Sum Rules at Infinite Momentum," *Phys. Rev.* **179** (1969) 1547–1553.

[22] C.-N. Yang and R. L. Mills, "Conservation of Isotopic Spin and Isotopic Gauge Invariance," *Phys. Rev.* **96** (1954) 191–195.

[23] P. W. Higgs, "Broken Symmetries and the Masses of Gauge Bosons," *Phys. Rev. Lett.* **13** (1964) 508–509.

[24] F. Englert and R. Brout, "Broken Symmetry and the Mass of Gauge Vector Mesons," *Phys. Rev. Lett.* **13** (1964) 321–323.

[25] G. S. Guralnik, C. R. Hagen, and T. W. B. Kibble, "Global Conservation Laws and Massless Particles," *Phys. Rev. Lett.* **13** (1964) 585–587.

[26] G. 't Hooft, "The Evolution of Quantum Field Theory, From QED to Grand Unification," *Adv. Ser. Direct. High Energy Phys.* **26** (2016) 1–27, `arXiv:1503.05007 [hep-th]`.

[27] M. A. Shifman, A. I. Vainshtein, and V. I. Zakharov, "QCD and Resonance Physics. Theoretical Foundations," *Nucl. Phys.* **B147** (1979) 385–447.

[28] M. A. Shifman, A. I. Vainshtein, and V. I. Zakharov, "QCD and Resonance Physics: Applications," *Nucl. Phys.* **B147** (1979) 448–518.

[29] M. E. Peskin and D. V. Schroeder, *An Introduction to quantum field theory*. Addison-Wesley, Reading, USA, 1995.

[30] M. D. Schwartz, *Quantum Field Theory and the Standard Model*. Cambridge University Press, 3, 2014.

[31] C. Itzykson and J. B. Zuber, *Quantum Field Theory*. International Series In Pure and Applied Physics. McGraw-Hill, New York, 1980.

[32] J. C. Collins, *Renormalization*, vol. 26 of *Cambridge Monographs on Mathematical Physics*. Cambridge University Press, Cambridge, 7, 2023.

[33] J. F. Donoghue, E. Golowich, and B. R. Holstein, *Dynamics of the Standard Model: Second edition*. Cambridge University Press, 11, 2022.

[34] L. D. Faddeev and V. N. Popov, "Feynman Diagrams for the Yang-Mills Field," *Phys. Lett. B* **25** (1967) 29–30.

[35] J. C. Ward, "An Identity in Quantum Electrodynamics," *Phys. Rev.* **78** (1950) 182.

[36] Y. Takahashi, "On the generalized Ward identity," *Nuovo Cim.* **6** (1957) 371.

[37] **Particle Data Group** Collaboration, R. L. Workman *et al.*, "Review of Particle Physics," *PTEP* **2022** (2022) 083C01.

[38] R. Assmann, M. Lamont, and S. Myers, "A brief history of the LEP collider," *Nucl. Phys. B Proc. Suppl.* **109** (2002) 17–31.

[39] G. Apollinari, O. Brüning, T. Nakamoto, and L. Rossi, "High Luminosity Large Hadron Collider HL-LHC," *CERN Yellow Rep.* no. 5, (2015) 1–19, arXiv:1705.08830 [physics.acc-ph].

[40] **Flavour Lattice Averaging Group (FLAG)** Collaboration, Y. Aoki *et al.*, "FLAG Review 2021," *Eur. Phys. J. C* **82** no. 10, (2022) 869, arXiv:2111.09849 [hep-lat].

[41] P. Ball and R. Zwicky, "New results on $B \to \pi, K, \eta$ decay formfactors from light-cone sum rules," *Phys. Rev. D* **71** (2005) 014015, arXiv:hep-ph/0406232.

[42] J. Gasser and H. Leutwyler, "Chiral Perturbation Theory to One Loop," *Annals Phys.* **158** (1984) 142.

[43] J. Gasser and H. Leutwyler, "Chiral Perturbation Theory: Expansions in the Mass of the Strange Quark," *Nucl. Phys. B* **250** (1985) 465–516.

[44] G. S. Bali, F. Bruckmann, M. Constantinou, M. Costa, G. Endrodi, S. D. Katz, H. Panagopoulos, and A. Schafer, "Magnetic susceptibility of QCD at zero and at finite temperature from the lattice," *Phys. Rev. D* **86** (2012) 094512, arXiv:1209.6015 [hep-lat].

[45] J. Bijnens, N. Hermansson-Truedsson, and S. Wang, "The order p^8 mesonic chiral Lagrangian," *JHEP* **01** (2019) 102, arXiv:1810.06834 [hep-ph].

[46] J. Bijnens, N. Hermansson-Truedsson, and J. Ruiz-Vidal, "The anomalous chiral Lagrangian at order p^8," *JHEP* **01** (2024) 009, arXiv:2310.20547 [hep-ph].

[47] H. Georgi, "An Effective Field Theory for Heavy Quarks at Low-energies," *Phys. Lett. B* **240** (1990) 447–450.

[48] E. Eichten and B. R. Hill, "Static Effective Field Theory: 1/m Corrections," *Phys. Lett. B* **243** (1990) 427–431.

[49] M. E. Luke, "Effects of subleading operators in the heavy quark effective theory," *Phys. Lett. B* **252** (1990) 447–455.

[50] H. Georgi, B. Grinstein, and M. B. Wise, "$\Lambda_{(b)}$ semileptonic decay form-factors for m_c does not equal infinity," *Phys. Lett. B* **252** (1990) 456–460.

[51] C. W. Bauer, S. Fleming, and M. E. Luke, "Summing Sudakov logarithms in $B \to X_s\gamma$ in effective field theory.," *Phys. Rev. D* **63** (2000) 014006, arXiv:hep-ph/0005275.

[52] C. W. Bauer, S. Fleming, D. Pirjol, and I. W. Stewart, "An Effective field theory for collinear and soft gluons: Heavy to light decays," *Phys. Rev. D* **63** (2001) 114020, arXiv:hep-ph/0011336.

[53] C. W. Bauer and I. W. Stewart, "Invariant operators in collinear effective theory," *Phys. Lett. B* **516** (2001) 134–142, arXiv:hep-ph/0107001.

[54] C. W. Bauer, D. Pirjol, and I. W. Stewart, "Soft collinear factorization in effective field theory," *Phys. Rev. D* **65** (2002) 054022, arXiv:hep-ph/0109045.

[55] M. Beneke, A. P. Chapovsky, M. Diehl, and T. Feldmann, "Soft collinear effective theory and heavy to light currents beyond leading power," *Nucl. Phys. B* **643** (2002) 431–476, arXiv:hep-ph/0206152.

[56] M. Beneke and T. Feldmann, "Multipole expanded soft collinear effective theory with non Abelian gauge symmetry," *Phys. Lett. B* **553** (2003) 267–276, arXiv:hep-ph/0211358.

[57] R. J. Hill and M. Neubert, "Spectator interactions in soft collinear effective theory," *Nucl. Phys. B* **657** (2003) 229–256, arXiv:hep-ph/0211018.

[58] K. G. Wilson, "Nonlagrangian models of current algebra," *Phys. Rev.* **179** (1969) 1499–1512.

[59] G. 't Hooft, "A Planar Diagram Theory for Strong Interactions," *Nucl. Phys. B* **72** (1974) 461.

[60] W. Lucha, F. F. Schoberl, and D. Gromes, "Bound states of quarks," *Phys. Rept.* **200** (1991) 127–240.

[61] K. G. Wilson, "Confinement of Quarks," *Phys. Rev. D* **10** (1974) 2445–2459.

[62] M. Creutz, "Monte Carlo Study of Quantized SU(2) Gauge Theory," *Phys. Rev. D* **21** (1980) 2308–2315.

[63] M. Creutz, "Asymptotic Freedom Scales," *Phys. Rev. Lett.* **45** (1980) 313.

[64] M. Creutz, *Quarks, Gluons and Lattices*. Oxford University Press, 1983.

[65] A. J. Buras, J. Girrbach, D. Guadagnoli, and G. Isidori, "On the Standard Model prediction for BR($B_{s,d} \to \mu^+\mu^-$)," *Eur. Phys. J. C* **72** (2012) 2172, arXiv:1208.0934 [hep-ph].

[66] K. De Bruyn, R. Fleischer, R. Knegjens, P. Koppenburg, M. Merk, A. Pellegrino, and N. Tuning, "Probing New Physics via the $B^0_s \to \mu^+\mu^-$ Effective Lifetime," *Phys. Rev. Lett.* **109** (2012) 041801, arXiv:1204.1737 [hep-ph].

[67] C. Bobeth, M. Gorbahn, T. Hermann, M. Misiak, E. Stamou, and M. Steinhauser, "$B_{s,d} \to l^+l^-$ in the Standard Model with Reduced Theoretical Uncertainty," *Phys. Rev. Lett.* **112** (2014) 101801, arXiv:1311.0903 [hep-ph].

[68] M. Beneke, T. Feldmann, and D. Seidel, "Exclusive radiative and electroweak $b \to d$ and $b \to s$ penguin decays at NLO," *Eur. Phys. J. C* **41** (2005) 173–188, arXiv:hep-ph/0412400.

[69] M. Beneke, T. Feldmann, and D. Seidel, "Systematic approach to exclusive $B \to Vl^+l^-$, $V\gamma$ decays," *Nucl. Phys. B* **612** (2001) 25–58, arXiv:hep-ph/0106067.

[70] G. Hiller and M. Schmaltz, "R_K and future $b \to s\ell\ell$ physics beyond the standard model opportunities," *Phys. Rev. D* **90** (2014) 054014, arXiv:1408.1627 [hep-ph].

[71] A. Lenz and U. Nierste, "Theoretical update of $B_s - \bar{B}_s$ mixing," *JHEP* **06** (2007) 072, arXiv:hep-ph/0612167.

[72] A. Lenz and U. Nierste, "Numerical Updates of Lifetimes and Mixing Parameters of B Mesons," in *6th International Workshop on the CKM Unitarity Triangle*. 2, 2011. arXiv:1102.4274 [hep-ph].

[73] M. Bordone, G. Isidori, and A. Pattori, "On the Standard Model predictions for R_K and R_{K^*}," *Eur. Phys. J. C* **76** no. 8, (2016) 440, arXiv:1605.07633 [hep-ph].

[74] G. Hiller and F. Kruger, "More model-independent analysis of $b \to s$ processes," *Phys. Rev. D* **69** (2004) 074020, arXiv:hep-ph/0310219.

[75] **LHCb** Collaboration, R. Aaij *et al.*, "Test of lepton universality using $B^+ \to K^+\ell^+\ell^-$ decays," *Phys. Rev. Lett.* **113** (2014) 151601, arXiv:1406.6482 [hep-ex].

[76] **LHCb** Collaboration, R. Aaij *et al.*, "Test of lepton universality with $B^0 \to K^{*0}\ell^+\ell^-$ decays," *JHEP* **08** (2017) 055, arXiv:1705.05802 [hep-ex].

[77] **LHCb** Collaboration, R. Aaij *et al.*, "Search for lepton-universality violation in $B^+ \to K^+\ell^+\ell^-$ decays," *Phys. Rev. Lett.* **122** no. 19, (2019) 191801, arXiv:1903.09252 [hep-ex].

[78] **LHCb** Collaboration, R. Aaij *et al.*, "Test of lepton universality in beauty-quark decays," *Nature Phys.* **18** no. 3, (2022) 277–282, arXiv:2103.11769 [hep-ex]. [Addendum: Nature Phys. 19, (2023)].

[79] **LHCb** Collaboration, R. Aaij *et al.*, "Test of lepton universality in $b \to s\ell^+\ell^-$ decays," *Phys. Rev. Lett.* **131** no. 5, (2023) 051803, arXiv:2212.09152 [hep-ex].

[80] **LHCb** Collaboration, R. Aaij *et al.*, "Measurement of lepton universality parameters in $B^+ \to K^+\ell^+\ell^-$ and $B^0 \to K^{*0}\ell^+\ell^-$ decays," *Phys. Rev. D* **108** no. 3, (2023) 032002, arXiv:2212.09153 [hep-ex].

[81] **Belle-II** Collaboration, W. Altmannshofer *et al.*, "The Belle II Physics Book," *PTEP* **2019** no. 12, (2019) 123C01, arXiv:1808.10567 [hep-ex]. [Erratum: PTEP 2020, 029201 (2020)].

[82] **RBC, UKQCD** Collaboration, T. Blum *et al.*, "Domain wall QCD with physical quark masses," *Phys. Rev. D* **93** no. 7, (2016) 074505, arXiv:1411.7017 [hep-lat].

[83] **HPQCD, UKQCD** Collaboration, E. Follana, C. T. H. Davies, G. P. Lepage, and J. Shigemitsu, "High Precision determination of the π, K, D and $D_{(s)}$ decay constants from lattice QCD," *Phys. Rev. Lett.* **100** (2008) 062002, arXiv:0706.1726 [hep-lat].

[84] **MILC** Collaboration, A. Bazavov *et al.*, "Results for light pseudoscalar mesons," *PoS* **LATTICE2010** (2010) 074, arXiv:1012.0868 [hep-lat].

[85] **Fermilab Lattice, MILC** Collaboration, A. Bazavov *et al.*, "Charmed and Light Pseudoscalar Meson Decay Constants from Four-Flavor Lattice QCD with Physical Light Quarks," *Phys. Rev. D* **90** no. 7, (2014) 074509, arXiv:1407.3772 [hep-lat].

[86] R. J. Dowdall, C. T. H. Davies, G. P. Lepage, and C. McNeile, "$V_{\rm us}$ from π and K decay constants in full lattice QCD with physical u, d, s and c quarks," *Phys. Rev. D* **88** (2013) 074504, arXiv:1303.1670 [hep-lat].

[87] N. Carrasco *et al.*, "Leptonic decay constants f_K, f_D, and f_{D_s} with $N_f = 2 + 1 + 1$ twisted-mass lattice QCD," *Phys. Rev. D* **91** no. 5, (2015) 054507, arXiv:1411.7908 [hep-lat].

[88] J. F. Donoghue and L. F. Li, "Properties of Charged Higgs Bosons," *Phys. Rev. D* **19** (1979) 945.

[89] E. Golowich and T. C. Yang, "Charged Higgs Bosons and Decays of Heavy Flavored Mesons," *Phys. Lett. B* **80** (1979) 245–248.

[90] G. Isidori, S. Nabeebaccus, and R. Zwicky, "QED corrections in $\overline{B} \to \overline{K}\ell^+\ell^-$ at the double-differential level," *JHEP* **12** (2020) 104, arXiv:2009.00929 [hep-ph].

[91] R. J. Eden, P. V. Landshoff, D. I. Olive, and J. C. Polkinghorne, *The analytic S-matrix*. Cambridge Univ. Press, Cambridge, 1966.

[92] R. Zwicky, "A brief Introduction to Dispersion Relations and Analyticity," in *Quantum Field Theory at the Limits: from Strong Fields to Heavy Quarks*, pp. 93–120. 2017. arXiv:1610.06090 [hep-ph].

[93] S. Mizera, "Physics of the analytic S-matrix," *Phys. Rept.* **1047** (2024) 1–92, arXiv:2306.05395 [hep-th].

[94] H. Lehmann, K. Symanzik, and W. Zimmermann, "On the formulation of quantized field theories," *Nuovo Cim.* **1** (1955) 205–225.

[95] H. A. Kramers, "La diffusion de la lumière par les atomes," *Atti Cong. Intern. Fisici, (Transactions of Volta Centenary Congress) Como* **2** (1927) 545–557.

[96] R. de L. Kronig, "On the theory of the dispersion of X-rays," *J. Opt. Soc. Am.* **12** no. 6, (1926) 547–557.

[97] E. C. Titchmarsh, *Introduction to the theory of Fourier integrals*. Oxford University Press, Oxford, 1937.

[98] H. Cartan, *Elementary Theory of Analytic Functions of One or Several Complex Variables*. Addison-Wesley, 1963.

[99] R. E. Cutkosky, "Singularities and discontinuities of Feynman amplitudes," *J. Math. Phys.* **1** (1960) 429–433.

[100] G. Kallen, "On the definition of the Renormalization Constants in Quantum Electrodynamics," *Helv. Phys. Acta* **25** no. 4, (1952) 417.

[101] L. D. Landau, "On analytic properties of vertex parts in quantum field theory," *Nucl. Phys.* **13** no. 1, (1959) 181–192.

[102] S. Mandelstam, "Determination of the pion - nucleon scattering amplitude from dispersion relations and unitarity. General theory," *Phys. Rev.* **112** (1958) 1344–1360.

[103] S. Mandelstam, "Analytic properties of transition amplitudes in perturbation theory," *Phys. Rev.* **115** (1959) 1741–1751.

[104] L. J. Reinders, S. Yazaki, and H. R. Rubinstein, "Masses and Couplings of Open Beauty States in QCD," *Phys. Lett. B* **104** (1981) 305–310.

[105] M. Shifman and B. Ioffe, eds., *At the frontier of particle physics. Handbook of QCD. Vol. 1-3*. World Scientific, Singapore, Singapore, 2001.

[106] P. Colangelo and A. Khodjamirian, "QCD sum rules, a modern perspective," arXiv:hep-ph/0010175.

[107] M. Jamin and B. O. Lange, "f_B and f_{B_s} from QCD sum rules," *Phys. Rev. D* **65** (2002) 056005, arXiv:hep-ph/0108135.

[108] P. Pascual and R. Tarrach, *QCD: Renormalization for the Practitioner*, vol. 194. Springer Berlin, Heidelberg, 1984.

[109] L. J. Reinders, "QCD Sum Rules: An Introduction and Some Applications," *Acta Phys. Polon. B* **15** (1984) 329.

[110] E. V. Shuryak, "Pseudoscalar Mesons and Instantons," *Nucl. Phys. B* **214** (1983) 237–252.

[111] E. Di Salvo, "Instantons and the QCD Sum Rule for the Pion," *Nuovo Cim. A* **104** (1991) 1–12.

[112] I. I. Balitsky, V. M. Braun, and A. V. Kolesnichenko, "$\Sigma^+ \to P\gamma$ Decay in QCD. (In Russian)," *Sov. J. Nucl. Phys.* **44** (1986) 1028.

[113] I. I. Balitsky, V. M. Braun, and A. V. Kolesnichenko, "Radiative Decay $\Sigma^+ \to p\gamma$ in Quantum Chromodynamics," *Nucl. Phys. B* **312** (1989) 509–550.

[114] V. L. Chernyak and I. R. Zhitnitsky, "B meson exclusive decays into baryons," *Nucl. Phys. B* **345** (1990) 137–172.

[115] P. Ball, V. M. Braun, and H. G. Dosch, "Form-factors of semileptonic D decays from QCD sum rules," *Phys. Rev. D* **44** (1991) 3567–3581.

[116] V. M. Braun, "Light cone sum rules," in *4th International Workshop on Progress in Heavy Quark Physics*, pp. 105–118. 9, 1997. arXiv:hep-ph/9801222.

[117] R. Mertig, M. Bohm, and A. Denner, "FEYN CALC: Computer algebraic calculation of Feynman amplitudes," *Comput. Phys. Commun.* **64** (1991) 345–359.

[118] V. Shtabovenko, R. Mertig, and F. Orellana, "FeynCalc 9.3: New features and improvements," *Comput. Phys. Commun.* **256** (2020) 107478, arXiv:2001.04407 [hep-ph].

[119] G. 't Hooft and M. J. G. Veltman, "Scalar One Loop Integrals," *Nucl. Phys. B* **153** (1979) 365–401.

[120] S. Dittmaier, "Separation of soft and collinear singularities from one loop N point integrals," *Nucl. Phys. B* **675** (2003) 447–466, arXiv:hep-ph/0308246.

[121] W. E. F. Pauli and M. Fierz, "Zur theorie der emission langwelliger lichtquanten," *Il Nuovo Cimento (1924-1942)* **15** (1938) 167–188.

[122] J.-M. Jauch and F. Rohrlich, "The infrared divergence," *Helv. Phys. Acta* **27** no. 7, (1954) 613–636.

[123] D. R. Yennie, S. C. Frautschi, and H. Suura, "The infrared divergence phenomena and high-energy processes," *Annals Phys.* **13** (1961) 379–452.

[124] F. Bloch and A. Nordsieck, "Note on the Radiation Field of the electron," *Phys. Rev.* **52** (1937) 54–59.

[125] T. Muta, *Foundations of Quantum Chromodynamics: An Introduction to Perturbative Methods in Gauge Theories, (3rd ed.)*, vol. 78 of *World scientific Lecture Notes in Physics*. World Scientific, Hackensack, N.J., 3rd ed., 2010.

[126] V. Chung, "Infrared Divergence in Quantum Electrodynamics," *Phys. Rev.* **140** (1965) B1110–B1122.

[127] T. W. B. Kibble, "Coherent soft-photon states and infrared divergences. ii. Mass-shell singularities of green's functions," *Phys. Rev.* **173** (1968) 1527–1535.

[128] T. W. B. Kibble, "Coherent soft-photon states and infrared divergences. iii. Asymptotic states and reduction formulas," *Phys. Rev.* **174** (1968) 1882–1901.

[129] T. W. B. Kibble, "Coherent soft-photon states and infrared divergences. iv. The scattering operator," *Phys. Rev.* **175** (1968) 1624–1640.

[130] P. P. Kulish and L. D. Faddeev, "Asymptotic conditions and infrared divergences in quantum electrodynamics," *Theor. Math. Phys.* **4** (1970) 745.

[131] V. N. Gribov and L. N. Lipatov, "Deep inelastic $e\,p$ scattering in perturbation theory," *Sov. J. Nucl. Phys.* **15** (1972) 438–450.

[132] Y. L. Dokshitzer, "Calculation of the Structure Functions for Deep Inelastic Scattering and $e^+\,e^-$ Annihilation by Perturbation Theory in Quantum Chromodynamics.," *Sov. Phys. JETP* **46** (1977) 641–653.

[133] G. Altarelli and G. Parisi, "Asymptotic Freedom in Parton Language," *Nucl. Phys. B* **126** (1977) 298–318.

[134] C. F. von Weizsacker, "Radiation emitted in collisions of very fast electrons," *Z. Phys.* **88** (1934) 612–625.

[135] E. J. Williams, "Correlation of certain collision problems with radiation theory," *Kong. Dan. Vid. Sel. Mat. Fys. Med.* **13N4** no. 4, (1935) 1–50.

[136] T. Kinoshita, "Mass singularities of Feynman amplitudes," *J. Math. Phys.* **3** (1962) 650–677.

[137] T. D. Lee and M. Nauenberg, "Degenerate Systems and Mass Singularities," *Phys. Rev.* **133** (1964) B1549–B1562.

[138] R. Zwicky, "Notes on QED Corrections in Weak Decays," *Symmetry* **13** no. 11, (2021) 2036, arXiv:2205.06194 [hep-ph].

[139] F. E. Low, "Scattering of light of very low frequency by systems of spin 1/2," *Phys. Rev.* **96** (1954) 1428–1432.

[140] F. E. Low, "Bremsstrahlung of very low-energy quanta in elementary particle collisions," *Phys. Rev.* **110** (1958) 974–977.

[141] T. H. Burnett and N. M. Kroll, "Extension of the Low soft photon theorem," *Phys. Rev. Lett.* **20** (1968) 86.

[142] M. Gell-Mann and M. L. Goldberger, "Scattering of low-energy photons by particles of spin 1/2," *Phys. Rev.* **96** (1954) 1433–1438.

[143] Z. Bern, S. Davies, P. Di Vecchia, and J. Nohle, "Low-Energy Behavior of Gluons and Gravitons from Gauge Invariance," *Phys. Rev. D* **90** no. 8, (2014) 084035, arXiv:1406.6987 [hep-th].

[144] S. Weinberg, "Infrared photons and gravitons," *Phys. Rev.* **140** (1965) B516–B524.

[145] E. Barberio, B. van Eijk, and Z. Was, "PHOTOS: A Universal Monte Carlo for QED radiative corrections in decays," *Comput. Phys. Commun.* **66** (1991) 115–128.

[146] E. Barberio and Z. Was, "PHOTOS: A Universal Monte Carlo for QED radiative corrections. Version 2.0," *Comput. Phys. Commun.* **79** (1994) 291–308.

[147] P. Golonka and Z. Was, "PHOTOS Monte Carlo: A Precision tool for QED corrections in Z and W decays," *Eur. Phys. J. C* **45** (2006) 97–107, arXiv:hep-ph/0506026.

[148] N. Davidson, T. Przedzinski, and Z. Was, "PHOTOS interface in C++: Technical and Physics Documentation," *Comput. Phys. Commun.* **199** (2016) 86–101, arXiv:1011.0937 [hep-ph].

[149] M. Schonherr and F. Krauss, "Soft Photon Radiation in Particle Decays in SHERPA," *JHEP* **12** (2008) 018, arXiv:0810.5071 [hep-ph].

[150] **Sherpa** Collaboration, E. Bothmann *et al.*, "Event Generation with Sherpa 2.2," *SciPost Phys.* **7** no. 3, (2019) 034, arXiv:1905.09127 [hep-ph].

[151] G. Isidori, D. Lancierini, S. Nabeebaccus, and R. Zwicky, "QED in $\bar{B} \to \bar{K}\ell^+\ell^-$ LFU ratios: theory versus experiment, a Monte Carlo study," *JHEP* **10** (2022) 146, arXiv:2205.08635 [hep-ph].

[152] T. Huber, E. Lunghi, M. Misiak, and D. Wyler, "Electromagnetic logarithms in $\bar{B} \to X_s l^+ l^-$," *Nucl. Phys. B* **740** (2006) 105–137, arXiv:hep-ph/0512066.

[153] T. Huber, T. Hurth, and E. Lunghi, "Inclusive $\overline{B} \to X_s \ell^+ \ell^-$: complete angular analysis and a thorough study of collinear photons," *JHEP* **06** (2015) 176, arXiv:1503.04849 [hep-ph].

[154] G. Isidori, "Soft-photon corrections in multi-body meson decays," *Eur. Phys. J. C* **53** (2008) 567–571, arXiv:0709.2439 [hep-ph].

[155] R. K. Ellis, D. A. Ross, and A. E. Terrano, "The Perturbative Calculation of Jet Structure in $e^+ e^-$ Annihilation," *Nucl. Phys. B* **178** (1981) 421–456.

[156] B. W. Harris and J. F. Owens, "The Two cutoff phase space slicing method," *Phys. Rev. D* **65** (2002) 094032, arXiv:hep-ph/0102128.

[157] J. Lyon and R. Zwicky, "Isospin asymmetries in $B \to (K^*, \rho)\gamma / l^+ l^-$ and $B \to K l^+ l^-$ in and beyond the standard model," *Phys. Rev. D* **88** no. 9, (2013) 094004, arXiv:1305.4797 [hep-ph].

[158] A. Bharucha, D. M. Straub, and R. Zwicky, "$B \to V \ell^+ \ell^-$ in the Standard Model from light-cone sum rules," *JHEP* **08** (2016) 098, arXiv:1503.05534 [hep-ph].

[159] A. Khodjamirian and D. Wyler, "Counting contact terms in $B \to V\gamma$ decays," arXiv:hep-ph/0111249.

[160] S. M. Berman, "Radiative corrections to pion beta decay," *Phys. Rev. Lett.* **1** (1958) 468.

[161] T. Kinoshita, "Radiative corrections to $\pi - e$ decay," *Phys. Rev. Lett.* **2** (1959) 477.

[162] S. M. Berman, "Radiative corrections to muon and neutron decay," *Phys. Rev.* **112** (1958) 267–270.

[163] T. Kinoshita and A. Sirlin, "Radiative corrections to Fermi interactions," *Phys. Rev.* **113** (1959) 1652–1660.

[164] N. Carrasco, V. Lubicz, G. Martinelli, C. T. Sachrajda, N. Tantalo, C. Tarantino, and M. Testa, "QED Corrections to Hadronic Processes in Lattice QCD," *Phys. Rev. D* **91** no. 7, (2015) 074506, arXiv:1502.00257 [hep-lat].

[165] A. Sirlin, "Radiative Corrections in the $SU(2)_L \times U(1)$ Theory: A Simple Renormalization Framework," *Phys. Rev. D* **22** (1980) 971–981.

[166] A. Sirlin, "Large m_W, m_Z Behavior of the $\mathcal{O}(\alpha)$ Corrections to Semileptonic Processes Mediated by W," *Nucl. Phys. B* **196** (1982) 83–92.

[167] T. Kinoshita, "Everyone makes mistakes: Including Feynman," *J. Phys. G* **29** (2003) 9–22, arXiv:hep-ph/0101197.

[168] R. Gatto and M. Ruderman, "A suggestion on the theory of the $\pi \to e + \nu$ to $\pi \to \mu + \nu$ ratio," *Nuovo Cim* **8** (1958) 775–777.

[169] M. Knecht, H. Neufeld, H. Rupertsberger, and P. Talavera, "Chiral perturbation theory with virtual photons and leptons," *Eur. Phys. J. C* **12** (2000) 469–478, arXiv:hep-ph/9909284.

[170] V. Cirigliano and I. Rosell, "$\pi/K \to e\bar{\nu}_e$ branching ratios to $\mathcal{O}(e^2p^4)$ in Chiral Perturbation Theory," *JHEP* **10** (2007) 005, arXiv:0707.4464 [hep-ph].

[171] V. Cirigliano, M. Knecht, H. Neufeld, H. Rupertsberger, and P. Talavera, "Radiative corrections to $K_{(l3)}$ decays," *Eur. Phys. J. C* **23** (2002) 121–133, arXiv:hep-ph/0110153.

[172] V. Cirigliano, M. Giannotti, and H. Neufeld, "Electromagnetic effects in $K_{(l3)}$ decays," *JHEP* **11** (2008) 006, arXiv:0807.4507 [hep-ph].

[173] V. Cirigliano, M. Knecht, H. Neufeld, and H. Pichl, "The Pionic beta decay in chiral perturbation theory," *Eur. Phys. J. C* **27** (2003) 255–262, arXiv:hep-ph/0209226.

[174] V. Cirigliano, A. Pich, G. Ecker, and H. Neufeld, "Isospin violation in epsilon-prime," *Phys. Rev. Lett.* **91** (2003) 162001, arXiv:hep-ph/0307030.

[175] J. Bijnens and F. Borg, "Isospin breaking in $K \to 3\pi$ decays. II. Radiative corrections," *Eur. Phys. J. C* **39** (2005) 347–357, arXiv:hep-ph/0410333.

[176] M. Beneke, C. Bobeth, and R. Szafron, "Enhanced electromagnetic correction to the rare B-meson decay $B_{s,d} \to \mu^+\mu^-$," *Phys. Rev. Lett.* **120** no. 1, (2018) 011801, arXiv:1708.09152 [hep-ph].

[177] M. Beneke, C. Bobeth, and R. Szafron, "Power-enhanced leading-logarithmic QED corrections to $B_q \to \mu^+\mu^-$," *JHEP* **10** (2019) 232, arXiv:1908.07011 [hep-ph]. [Erratum: JHEP 11, 099 (2022)].

[178] C. Cornella, M. König, and M. Neubert, "Structure-dependent QED effects in exclusive B decays at subleading power," *Phys. Rev. D* **108** no. 3, (2023) L031502, arXiv:2212.14430 [hep-ph].

[179] D. Becirevic, B. Haas, and E. Kou, "Soft Photon Problem in Leptonic B-decays," *Phys. Lett. B* **681** (2009) 257–263, arXiv:0907.1845 [hep-ph].

[180] M. Beneke and J. Rohrwild, "B meson distribution amplitude from $B \to \gamma l \nu$," *Eur. Phys. J. C* **71** (2011) 1818, arXiv:1110.3228 [hep-ph].

[181] B. Lucini, A. Patella, A. Ramos, and N. Tantalo, "Charged hadrons in local finite-volume QED+QCD with C^* boundary conditions," *JHEP* **02** (2016) 076, arXiv:1509.01636 [hep-th].

[182] M. G. Endres, A. Shindler, B. C. Tiburzi, and A. Walker-Loud, "Massive photons: an infrared regularization scheme for lattice QCD+QED," *Phys. Rev. Lett.* **117** no. 7, (2016) 072002, arXiv:1507.08916 [hep-lat].

[183] M. Hayakawa and S. Uno, "QED in finite volume and finite size scaling effect on electromagnetic properties of hadrons," *Prog. Theor. Phys.* **120** (2008) 413–441, arXiv:0804.2044 [hep-ph].

[184] X. Feng and L. Jin, "QED self energies from lattice QCD without power-law finite-volume errors," *Phys. Rev. D* **100** no. 9, (2019) 094509, arXiv:1812.09817 [hep-lat].

[185] Z. Davoudi and M. J. Savage, "Finite-Volume Electromagnetic Corrections to the Masses of Mesons, Baryons and Nuclei," *Phys. Rev. D* **90** no. 5, (2014) 054503, arXiv:1402.6741 [hep-lat].

[186] D. Giusti, V. Lubicz, G. Martinelli, C. T. Sachrajda, F. Sanfilippo, S. Simula, N. Tantalo, and C. Tarantino, "First lattice calculation of the QED corrections to leptonic decay rates," *Phys. Rev. Lett.* **120** no. 7, (2018) 072001, arXiv:1711.06537 [hep-lat].

[187] M. Di Carlo, D. Giusti, V. Lubicz, G. Martinelli, C. T. Sachrajda, F. Sanfilippo, S. Simula, and N. Tantalo, "Light-meson leptonic decay rates in lattice QCD+QED," *Phys. Rev. D* **100** no. 3, (2019) 034514, arXiv:1904.08731 [hep-lat].

[188] A. Desiderio *et al.*, "First lattice calculation of radiative leptonic decay rates of pseudoscalar mesons," *Phys. Rev. D* **103** no. 1, (2021) 014502, arXiv:2006.05358 [hep-lat].

[189] C. Kane, C. Lehner, S. Meinel, and A. Soni, "Radiative leptonic decays on the lattice," *PoS* **LATTICE2019** (2019) 134, arXiv:1907.00279 [hep-lat].

[190] R. Frezzotti, N. Tantalo, G. Gagliardi, F. Sanfilippo, S. Simula, V. Lubicz, F. Mazzetti, G. Martinelli, and C. T. Sachrajda, "Lattice calculation of the D_s meson radiative form factors over the full kinematical range," *Phys. Rev. D* **108** no. 7, (2023) 074505, arXiv:2306.05904 [hep-lat].

[191] R. Frezzotti, N. Tantalo, G. Gagliardi, F. Sanfilippo, S. Simula, V. Lubicz, G. Martinelli, and C. T. Sachrajda, "$B_s \to \mu^+\mu^-\gamma$ decay rate at large q^2 from lattice QCD," *Phys. Rev. D* **109** no. 11, (2024) 114506, arXiv:2402.03262 [hep-lat].

[192] P. A. M. Dirac, "Gauge invariant formulation of quantum electrodynamics," *Can. J. Phys.* **33** (1955) 650.

[193] M. Hansen, B. Lucini, A. Patella, and N. Tantalo, "Gauge invariant determination of charged hadron masses," *JHEP* **05** (2018) 146, arXiv:1802.05474 [hep-lat].

[194] S. Nabeebaccus and R. Zwicky, "Resolving charged hadrons in QED — gauge invariant interpolating operators," *JHEP* **11** (2022) 101, arXiv:2209.06925 [hep-ph].

[195] T. Janowski, B. Pullin, and R. Zwicky, "Charged and neutral $\overline{B}_{u,d,s} \to \gamma$ form factors from light cone sum rules at NLO," *JHEP* **12** (2021) 008, arXiv:2106.13616 [hep-ph].

[196] B. Pullin and R. Zwicky, "Radiative decays of heavy-light mesons and the $f^{(T)}_{H,H^*,H_1}$ decay constants," *JHEP* **09** (2021) 023, arXiv:2106.13617 [hep-ph].

[197] S. Borowka, G. Heinrich, S. Jahn, S. P. Jones, M. Kerner, J. Schlenk, and T. Zirke, "pySecDec: a toolbox for the numerical evaluation of multi-scale integrals," *Comput. Phys. Commun.* **222** (2018) 313–326, arXiv:1703.09692 [hep-ph].

[198] V. E. Lyubovitskij, F. Wunder, and A. S. Zhevlakov, "New ideas for handling of loop and angular integrals in D-dimensions in QCD," *JHEP* **06** (2021) 066, arXiv:2102.08943 [hep-ph].

[199] V. A. Smirnov and F. Wunder, "Expansion by regions meets angular integrals," arXiv:2405.13120 [hep-ph].

[200] B. W. Harris and J. Smith, "Heavy quark correlations in deep inelastic electroproduction," *Nucl. Phys. B* **452** (1995) 109–160, arXiv:hep-ph/9503484.

[201] W. Beenakker, H. Kuijf, W. L. van Neerven, and J. Smith, "QCD Corrections to Heavy Quark Production in p anti-p Collisions," *Phys. Rev. D* **40** (1989) 54–82.

[202] G. Somogyi, "Angular integrals in d dimensions," *J. Math. Phys.* **52** (2011) 083501, arXiv:1101.3557 [hep-ph].

[203] H. H. Patel, "Package-X 2.0: A Mathematica package for the analytic calculation of one-loop integrals," *Comput. Phys. Commun.* **218** (2017) 66–70, arXiv:1612.00009 [hep-ph].

[204] V. Shtabovenko, "FeynHelpers: Connecting FeynCalc to FIRE and Package-X," *Comput. Phys. Commun.* **218** (2017) 48–65, arXiv:1611.06793 [physics.comp-ph].

[205] J. Brod and M. Gorbahn, "Electroweak Corrections to the Charm Quark Contribution to $K^+ \to \pi^+ \nu\bar{\nu}$," *Phys. Rev. D* **78** (2008) 034006, arXiv:0805.4119 [hep-ph].

[206] M. Gorbahn, S. Jäger, F. Moretti, and E. van der Merwe, "Semileptonic weak Hamiltonian to $\mathcal{O}(\alpha\alpha_s)$ in momentum-space subtraction schemes," *JHEP* **01** (2023) 159, arXiv:2209.05289 [hep-ph].

[207] D. Bigi, M. Bordone, P. Gambino, U. Haisch, and A. Piccione, "QED effects in inclusive semi-leptonic B decays," *JHEP* **11** (2023) 163, arXiv:2309.02849 [hep-ph].

[208] Z.-G. Wang, "Analysis of heavy mesons in nuclear matter with a QCD sum rule approach," *Phys. Rev. C* **92** no. 6, (2015) 065205, arXiv:1501.05093 [hep-ph].

[209] P. Gelhausen, A. Khodjamirian, A. A. Pivovarov, and D. Rosenthal, "Decay constants of heavy-light vector mesons from QCD sum rules," *Phys. Rev. D* **88** (2013) 014015, arXiv:1305.5432 [hep-ph]. [Erratum: Phys.Rev.D 89, 099901 (2014), Erratum: Phys.Rev.D 91, 099901 (2015)].

[210] D. Benson, I. I. Bigi, T. Mannel, and N. Uraltsev, "Imprecated, yet impeccable: On the theoretical evaluation of $\Gamma(B \to X_c l\nu)$," *Nucl. Phys. B* **665** (2003) 367–401, arXiv:hep-ph/0302262.

[211] M. Fael, K. Schönwald, and M. Steinhauser, "Relation between the $\overline{\text{MS}}$ and the kinetic mass of heavy quarks," *Phys. Rev. D* **103** no. 1, (2021) 014005, arXiv:2011.11655 [hep-ph].

[212] **Belle** Collaboration, K. Ikado *et al.*, "Evidence of the Purely Leptonic Decay $B^- \to \tau^- \bar{\nu}_\tau$," *Phys. Rev. Lett.* **97** (2006) 251802, arXiv:hep-ex/0604018.

[213] **Belle** Collaboration, I. Adachi *et al.*, "Evidence for $B^- \to \tau^- \bar{\nu}_\tau$ with a Hadronic Tagging Method Using the Full Data Sample of Belle," *Phys. Rev. Lett.* **110** no. 13, (2013) 131801, arXiv:1208.4678 [hep-ex].

[214] **Belle** Collaboration, B. Kronenbitter *et al.*, "Measurement of the branching fraction of $B^+ \to \tau^+ \nu_\tau$ decays with the semileptonic tagging method," *Phys. Rev. D* **92** no. 5, (2015) 051102, arXiv:1503.05613 [hep-ex].

[215] **BaBar** Collaboration, B. Aubert *et al.*, "A Search for $B^+ \to \ell^+ \nu_\ell$ Recoiling Against $B^- \to D^0 \ell^- \bar{\nu} X$," *Phys. Rev. D* **81** (2010) 051101, arXiv:0912.2453 [hep-ex].

[216] **BaBar** Collaboration, J. P. Lees *et al.*, "Evidence of $B^+ \to \tau^+\nu$ decays with hadronic B tags," *Phys. Rev. D* **88** no. 3, (2013) 031102, arXiv:1207.0698 [hep-ex].

[217] M. Tanaka and R. Watanabe, "New physics contributions in $B \to \pi\tau\bar{\nu}$ and $B \to \tau\bar{\nu}$," *PTEP* **2017** no. 1, (2017) 013B05, arXiv:1608.05207 [hep-ph].

[218] R. P. Feynman and G. Speisman, "Proton-Neutron Mass Difference," *Phys. Rev.* **94** no. 2, (1954) 500.

[219] M. Cini, E. Ferrari, and R. Gatto, "Neutron-Proton Mass Difference by Dispersion Theory," *Phys. Rev. Lett.* **2** no. 1, (1959) 7–9.

[220] W. N. Cottingham, "The neutron proton mass difference and electron scattering experiments," *Annals Phys.* **25** (1963) 424–432.

[221] W. A. Bardeen, J. Bijnens, and J. M. Gerard, "Hadronic Matrix Elements and the π^+ π^0 Mass Difference," *Phys. Rev. Lett.* **62** (1989) 1343.

[222] J. F. Donoghue and A. F. Perez, "The Electromagnetic mass differences of pions and kaons," *Phys. Rev. D* **55** (1997) 7075–7092, arXiv:hep-ph/9611331.

[223] J. L. Goity, "Electromagnetic mass splittings in heavy mesons," *Phys. Lett. B* **303** (1993) 337–344, arXiv:hep-ph/9212230.

[224] P. Colangelo, M. Ladisa, G. Nardulli, and T. N. Pham, "Electromagnetic mass difference of heavy mesons," *Phys. Lett. B* **416** (1998) 208–215, arXiv:hep-ph/9709201.

[225] T. Hambye, "A Unified treatment of mass differences for light and heavy pseudoscalars," *Phys. Lett. B* **319** (1993) 300–306.

[226] D. Giusti, V. Lubicz, C. Tarantino, G. Martinelli, F. Sanfilippo, S. Simula, and N. Tantalo, "Leading isospin-breaking corrections to pion, kaon and charmed-meson masses with Twisted-Mass fermions," *Phys. Rev. D* **95** no. 11, (2017) 114504, arXiv:1704.06561 [hep-lat].

[227] **BMW** Collaboration, S. Borsanyi *et al.*, "Ab initio calculation of the neutron-proton mass difference," *Science* **347** (2015) 1452–1455, arXiv:1406.4088 [hep-lat].

[228] R. P. Feynman, "Forces in Molecules," *Phys. Rev.* **56** (1939) 340–343.

[229] H. Hellmann, *Einführung in die Quantenchemie*. Franz Deuticke, Leipzig, 1937.

[230] O. Steinmann, "Über den Zusammenhang zwischen den Wightmanfunktionen und den retardierten Kommutatoren," *Helv. Physica Acta* **33** (1960) 257.

[231] M. Neubert, "Heavy meson form-factors from QCD sum rules," *Phys. Rev. D* **45** (1992) 2451–2466.

[232] B. Blok and M. A. Shifman, "The Isgur-Wise function in the small velocity limit," *Phys. Rev. D* **47** (1993) 2949–2964, arXiv:hep-ph/9207217.

[233] M. Gell-Mann, R. J. Oakes, and B. Renner, "Behavior of current divergences under SU(3) x SU(3)," *Phys. Rev.* **175** (1968) 2195–2199.

[234] G. Colangelo, S. Lanz, H. Leutwyler, and E. Passemar, "Dispersive analysis of $\eta \to 3\pi$," *Eur. Phys. J. C* **78** no. 11, (2018) 947, arXiv:1807.11937 [hep-ph].

[235] R. F. Dashen, "Chiral SU(3) x SU(3) as a symmetry of the strong interactions," *Phys. Rev.* **183** (1969) 1245–1260.

[236] X. Feng, L. Jin, and M. J. Riberdy, "Lattice QCD Calculation of the Pion Mass Splitting," *Phys. Rev. Lett.* **128** no. 5, (2022) 052003, arXiv:2108.05311 [hep-lat].

[237] C. McNeile, A. Bazavov, C. T. H. Davies, R. J. Dowdall, K. Hornbostel, G. P. Lepage, and H. D. Trottier, "Direct determination of the strange and light quark condensates from full lattice QCD," *Phys. Rev. D* **87** no. 3, (2013) 034503, arXiv:1211.6577 [hep-lat].

[238] B. L. Ioffe, "Condensates in quantum chromodynamics," *Phys. Atom. Nucl.* **66** (2003) 30–43, arXiv:hep-ph/0207191.

[239] P. Ball and R. Zwicky, "SU(3) breaking of leading-twist K and K* distribution amplitudes: A Reprise," *Phys. Lett. B* **633** (2006) 289–297, arXiv:hep-ph/0510338.

[240] J. Gratrex and R. Zwicky, "Parity Doubling as a Tool for Right-handed Current Searches," *JHEP* **08** (2018) 178, arXiv:1804.09006 [hep-ph].

[241] J. Gratrex, *Rare radiative and semileptonic B meson decays*. PhD thesis, Edinburgh U., 2018.

[242] S. A. Larin, "The Renormalization of the axial anomaly in dimensional regularization," *Phys. Lett. B* **303** (1993) 113–118, arXiv:hep-ph/9302240.

[243] R. K. Ellis and G. Zanderighi, "Scalar one-loop integrals for QCD," *JHEP* **02** (2008) 002, arXiv:0712.1851 [hep-ph].

'*For now we see in a mirror dimly,*'
1 Corinthians 13.